Mineralogie

„Chondrule formation in the early Solar System: A combined ICP-MS, ICP-OES and petrological study"

Inaugural-Dissertation
zur Erlangung des Doktorgrades der Naturwissenschaften
im Fachbereich Geowissenschaften
der Mathematisch-Naturwissenschaftlichen Fakultät
der Westfälischen Wilhelms-Universität Münster

vorgelegt von
Madelein Gerber
Johannesburg, South Africa

– 2012 –

Dekanin/Dekan: Prof. Dr. Hans Kerp

Erstgutachter/-in: Prof. Klaus Mezger (Bern Universität)

Zweitgutachter/-in: Prof. Erik Scherer (WWU Münster)

Tag der mündlichen Prüfung: 13.05.2015

Tag der Promotion: .....

Abstract

This work focuses on the formation and evolution of chondrules in the CR, CV, CK and EH chondrites, as well as the analytical tools and methods required for such an investigation. The project first looks at the chemical fingerprinting of individual chondrules to allow for intra- and intermeteorite comparison. To this end, a novel combination of freeze-thaw disaggregation, table-top digestion of individual chondrules and ICP-MS and -OES measurements of trace and major elements, respectively, were tested for applicability to such small samples (average ~1 mg). Chemical classification of chondrules using the whole chondrule data collected in this study is compared to existing single mineral phase classifications and new schemes are proposed. Suggestions are put forward regarding the evolution of different chondrule types within a single chondrite and their relationships to similar types of chondrules in other chondrites. In addition, the link between chondrules and the bulk composition of their host meteorite is investigated. Whole chondrule data collected in this study are also compared to available values for the Solar System and CI chondrites, ordinary chondrite chondrules and CAI. Potential source material for the chondrules is identified and the type and number of processes that are likely to have operated in the chondrule formation region are evaluated, including metal-sulfide fractionation, mineral condensation and magmatic evolution. Based on this, assignation of a nebular or planetary formation setting is made for the studied chondrules and a likely formation mechanism and timeframe for the formation is suggested.

Acknowledgements

To my family, Eugene, Gilbert, and Ma. This thesis represents the end of many long years of study that started off with simply being made curious about how things work. Thank you for supplying the fuel for my initial curiosity and for your boundless love and support over the years. And to my extended family, Helen and Manuel. Of all the extras that came along with doing a doctorate, you're definitely the most surprising and by far the most wonderful. To all of you, thank you from the bottom of my heart, since this thesis wouldn't have gotten this far if you hadn't been behind me all the way. I'm looking forward to celebrating this with you...

To Klaus, Dewashish, Claudia, Andrew, Christine, Erik, Michael Bröcker, Heidi, Michael Feldhaus and Frank. Assigning specific thanks is bit difficult since your roles often overlapped, but I'll give it a go... To Klaus, thank you for the chance to come to Germany. It was a privilege working in Münster. To Dewashish, thank you for taking me under you wing and helping to get my project going. To Claudia, thank you for helping me get to Münster in the first place (!) and all the millions of other things you've helped me organise during my stay there. To Heidi, Michael Feldhaus and Frank, thank you for teaching me, helping to put my ideas into practice and keeping the Triton alive! To Andrew, Christine, Erik and Michael Bröcker, thank you for jumping in when I needed it most. And to Andrew and Christine, thank you for many delicious dinners!

A big thanks to Dieter Garbe-Schönberg and Ulrike Westernströer at Kiel Uni for allowing me to use their facilities and their support with the method development.

I would also like to thank the following institutions for kindly provinding me with samples:

- Karoonda CK4 – The South Australian Museum

- Allendé CV3 and Acfer 311 CR2 – Institut für Planetologie, WWU Münster
- Indarch EH4 – The Smithsonian Nuseum of Natural History (USNM 3482)

(I hope I haven't forgotten anyone…)

"Von den Sternen kommen wir,

zu den Sternen gehen wir.

Das Leben ist nur eine Reise in die Fremde."

(From the stars we came,

and to the stars we'll return.

Life is merely a journey in the Unknown.)

Walter Moers, *Die Stadt der träumenden Bücher*

- For Dad -

Contents

List of Figures

List of Tables

Abbreviations, Symbols and Mineral Formulæ

(Abbreviations are given in standard font; symbols are given in *italics*; mineral formulæ are given in ***bold italics***)

2D	Two dimensional
3D	Three dimensional
a	Year *(Annum)*
ap	Apatite $\boldsymbol{Ca_5(PO_4)_3(OH,Cl,F)}$
AU	Astronomical unit
BM	Bulk meteorite
BO	Barred olivine (chondrule)
CAI	Calcium Aluminium-rich Inclusion
CB_b	Bencubbin-type carbonaceous chondrite, subgroup 'b'
CC	Cryptocrystalline (chondrule)
CCh	Carbonaceous chondrite
CCAM	Carbonaceous chondrite anhydrous mineral mixing (line)
chr	Chromite $\boldsymbol{FeCr_2O_4}$
CH	'High-Iron'-type Carbonaceous chondrite
CI	Ivuna-type carbonaceous chondrite
CK	Karoonda-type carbonaceous chondrite
CM	Murchison-type carbonaceous chondrite
Co#	*Cobalt number*
CO	Ornans-type carbonaceous chondrite
cp	Chalcopyrite $\boldsymbol{CuFeS_2}$
CPM	Chondrule Precursor Material
cpx	Clinopyroxene $\boldsymbol{Ca(Fe^{2+},Mg)Si_2O_6}$
CR	Renazzo-type carbonaceous chondrite
CV	Vigarano-type carbonaceous chondrite
Δ OR Δ%	*Range OR difference*
D	Deuterium
E_K	*Kinetic energy*
EC	Enstatite chondrite
EH	High Fe, high metal enstatite chondrite
EMP(A)	Electron Microprobe (Analysis)
EtOH	*Ethanol*
fO_2	*Oxygen fugacity*
Fo	Forsterite $\boldsymbol{Mg_2SiO_4}$

H (e.g. H3)	High Fe, high metal ordinary chondrite
HED	Howardite-Eucrite-Diogenite group (Martian meteorites)
hbld	Hornblende $Ca_2[(Mg,Fe^{2+})_4(Al,Fe^{3+})]Si_7AlO_{22}(OH)_2$
HFSE	High Field Strength Element
hib	Hibonite $(Ca,Ce)(Al,Ti,Mg)_{12}O_{19}$
hmt	Hematite Fe_2O_3
HREE	Heavy Rare Earth Element
ICP	Inductively Coupled Plasma
ilm	Ilmenite $FeTiO_3$
IR	Infrared
ISM	InterStellar Medium
K	Kelvin
K_d	Distribution (partition) coefficient
LREE	Light Rare Earth Element
m	*Meter OR Mass*
M	*Molar*
$M_\odot$	*Solar mass*
Ma	*Million year(s)*
mel	Melilite $(Ca,Na)_2(Al,Mg,Fe^{2+})(Si,Al)_2O_7$
Mg#	*Magnesium number*
mgt	Magnetite $Fe^{2+}Fe_2^{3+}O_4$
min	Minute
MS	Mass Spectrometer
M-S	Metal-Sulfide (melt)
msts	Mesostasis
mQ	18Ω ultrapure water
n	*Number of samples*
n/o	Not observed
OC	Ordinary chondrite
ol	Olivine $(Mg,Fe)_2SiO_4$
OES	Optical Emission Spectrometer
old	Oldhamite CaS
opx	Orthopyroxene $(Mg,Fe)Si_2O_6$
ox	Oxide(s)
PGE	Platinum Group Element(s)
PGM	Platinum Group Mineral(s)

phyl	Phyllosilicate(s)
plag	Plagioclase $\boldsymbol{CaAl_2Si_2O_8 - NaAlSi_3O_8}$
PO	Porphyritic olivine (chondrule)
POP	Porphyritic olivine pyroxene (chondrule)
PP	Porphyritic pyroxene (chondrule)
ppl	*Plain polarized light*
ppm	*Parts per million or microgram per gram*
prt	Pyrrhotite $\boldsymbol{Fe_{1-x}S}$
PSG	PreSolar Grain
pyx	Pyroxene $\boldsymbol{(Mg,Fe)SiO_3}$
R (chondrite)	Rumuruti-type carbonaceous chondrite
REE	Rare Earth Element
rfl	*Reflected light*
RLE	Refractory Lithophile Elements
RP	Radial pyroxene (chondrule)
RSD%	*Percent Relative Standard Deviation*
SD	*Standard deviation*
SEM	Scanning Electron Microscope
serp	Serpentine $\boldsymbol{Mg_3Si_2O_5(OH)_4}$
SMOW	Standard Mean Ocean Water
sp	Spinel $\boldsymbol{MgAl_2O_4}$
sph	Sphalerite $\boldsymbol{ZnS}$
sulf	Sulfide(s)
$T_{C50\%}$	*50% condensation temperature*
TFL	Terrestrial Fractionation Line
tlc	Talc $\boldsymbol{Mg_3(Si_4O_{10})OH_2}$
U_G	*Gravitational potential*
UOC	Unequilibrated Ordinary Chondrite
wt%	*Percentage determined as weight by weight*
xpl	*Crossed polarized light*

1 Introduction

Carbonaceous and Enstatite Chondrites (CCh and EC, respectively) have escaped the extensive homogenisation of planet building processes affecting the achondrite meteorites. They therefore record information about conditions in the young planetary nebula, including composition of the nebular dust, its thermal, physical and compositional evolution, and even preserve small parts of the interstellar medium in the form of PreSolar Grains (PSGs). The more refractory components in chondrite meteorites, namely chondrules and Calcium-Aluminium-rich Inclusions (CAIs), record high temperature (>1750 *K*) events that occurred early on in our own Solar System. But while the formation of CAIs by high temperature condensation processes is fairly widely accepted (Blander & Fuchs, 1975; Wood, 2004; Toppani *et al.*, 2006) the origin of chondrules and their exact role in the evolution of the Solar System remains somewhat enigmatic (Hewins, 1997; Zanda, 2004; Connolly & Desch, 2004)

1.1 Chondrules

Chondrules are spherical or rounded objects that are usually ≤1mm and most commonly dominated by Mg-rich silicates, but may contain a significant proportion Ca,Na-silicate glass or plagioclase, as well as metal, sulfides and oxides (Figure 1.1). The current classification scheme for chondrules is two-part (Table 1.1) and is based on both their texture (either porphyritic or fine grained/skeletal) and chemical/mineralogical composition (e.g. Fe-rich, Si-poor, Al-rich) (McSween, 1977; Gooding & Keil, 1981; Bischoff et al., 1989; Jones, 1994). Except in the CH, CB_b and E chondrites, the porphyritic olivine chondrules (PO) (Figure 1.1a) are the dominant chondrule type, followed by the porphyritic olivine-pyroxene chondrules (POP). Fine grained chondrule types such as the Barred Olivine (BO), Radial Pyroxene (RP) and CryptoCrystalline (CC) (Figure 1.1c & d) chondrules are usually an order of magnitude less abundant (Scott & Krot, 2007). Enstatite chondrites, as the name implies, are dominated by the Mg-rich pyroxene and both typical porphyritic and fine

grained/skeletal chondrule types are present with enstatite instead of olivine (Figure 1.1b). The CH and CB_b chondrules, however, are dominated by the fine grained chondrules types (Scott & Krot, 2007).

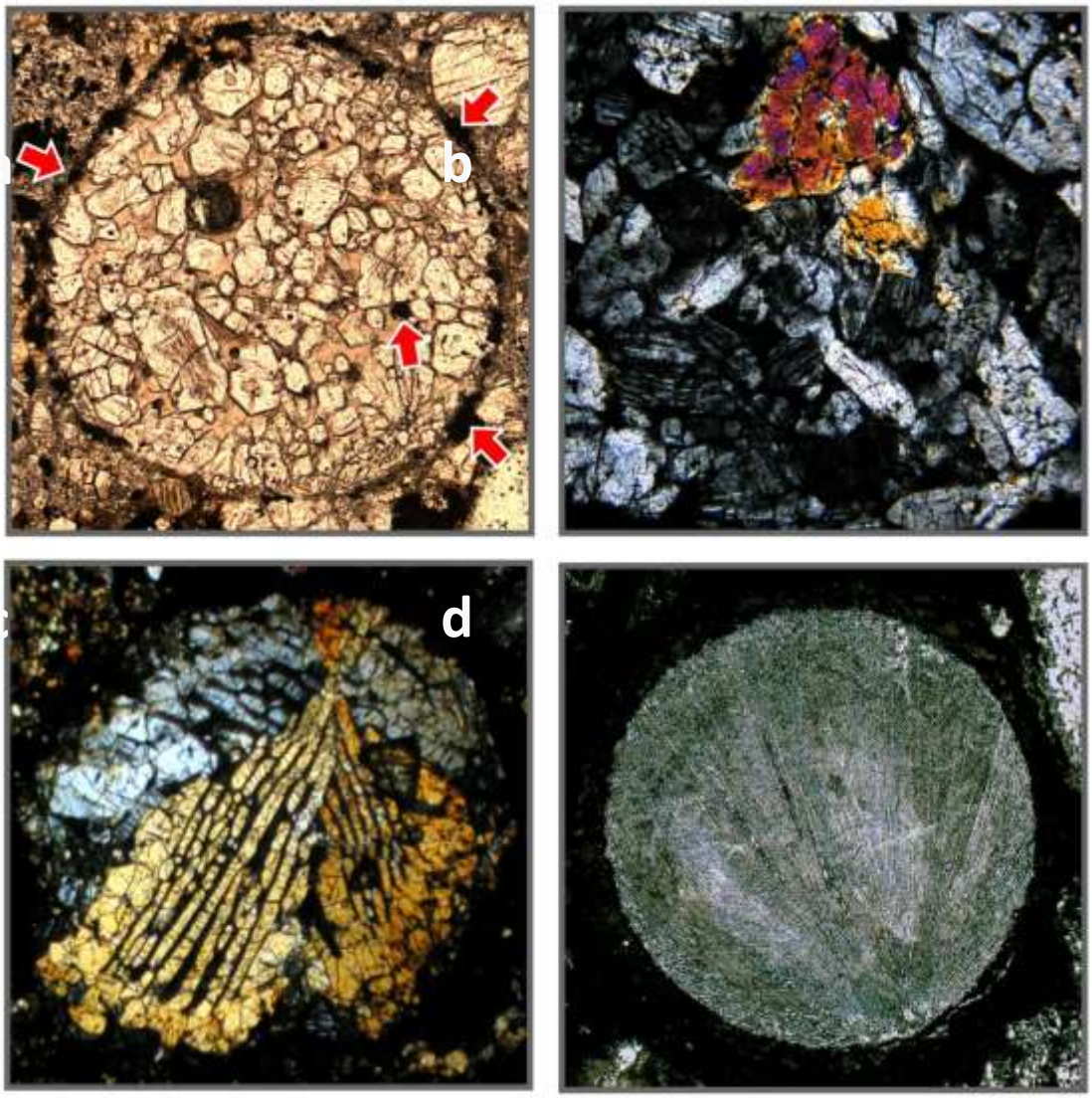

Figure 1.1 Photomicrographs of some basic chondrule types and textures. a) Type I PO chondrule, H3 chondrite (ppl). Porphyrocrysts are magnesian olivine and occasionally pyroxene. The pinkish mesostasis is essentially quenched liquid, usually with compositions ranging from bytownitic to anorthitic. Opaques occurring interstitially to the olivine and pyroxene and in the rim (red arrows) are metal. b) Type I PP chondrule, EH3 chondrite (xpl). The chondrule is dominated by pure enstatite phenocrysts (gray), but rare remnant FeO-rich olivine crystals occur (pink and orange). c) Type I BO chondrule with multiple growth zones, CR2 chondrite (xpl). d) Very fine grained RP chondrule, $CV3_{OXA}$ chondrite (ppl).

Experimental work has elucidated several aspects of chondrule genesis. Chondrules must necessarily have been partially or totally molten at some point in their history in

order to produce the observed textures (Tsuchiyama *et al.*, 1980; Connolly Jr. & Hewins, 1991; Jones & Lofgren, 1993; Hewins & Fox, 2004). Porphyritic textures can only be produced if a chondrule is partially molten since seed crystals within a melt are required for growth of large phenocrysts (Hewins & Fox, 2004). Coarse grained textures also require that the chondrule be cooled slowly, at <100 $K.h^{-1}$ (Tsuchiyama *et al.*, 1980; Whattam & Hewins, 2009). This constrains the melting temperatures to <1900 K (Hewins & Fox, 2004) to maintain unmelted mineral grains. Evaporation of a CI precursor over several hours (Cohen *et al.,* 2004) or rapid (several minutes) heating of a mafic-ultramafic precursor (Tsuchiyama *et al.*, 1980) have both experimentally reproduced chondrule textures. Fine grained textures (BO, RP) are a strong indication that the chondrules were completely molten and may or may not have been externally seeded by small amounts of fine grained minerals (Lofgren & Russell, 1986; Connolly Jr. & Hewins, 1991). Extreme undercooling can be achieved by totally molten chondrules if they do not encounter minerals to act as nucleation sites on their surfaces (Lofgren & Russell, 1986; Lofgren, 1989). Barred olivine are products of higher degrees of melting and very rapid cooling (>1000 $K.hr^{-1}$, Tsuchiyama *et al.*, 1980; Lofgren, 1989). The unusually high alkali content of chondrules, despite their high melting temperatures, has been found to be reproducible either through flash heating (Yu & Hewins, 1998) or gas-solid interaction at high dust:gas ratios (Yu & Hewins, 1998; Cohen *et al.*, 2004; Libourel *et al.*, 2006).

Table 1.1 Chondrule classification

Chemical classification	Textural type	Type A/B (SiO_2)
Type I - Mg#>0.9 (FeO-poor)	PO, BO (ol>80 vol%)	A
Type II - Mg#<0.9 (FeO-rich)	POP (20<ol<80 vol%)	AB
Al-rich Al_2O_3 >10 wt%	PP, RP (ol<20 vol%)	B

On a three O-isotope plot, chondrules of C, O and E chondrites plot in three separate regions (Figure 1.2; Clayton, 1993; Clayton & Mayeda, 1999; Rubin, 2000). The CCh chondrules largely overlap with each other and generally fall along the Carbonaceous Chondrite Anhydrous Mineral mixing (CCAM) line with a slope of ~1. This is distinct from the OC and EC chondrules that plot above and along the TFL respectively. Of all the meteorites only the EC chondrules overlap with the Terrestrial Fractionation Line (TFL) making the E chondrites favourite candidates for estimating the composition of the Earth (e.g. Berthet *et al.*, 2009). Figure 1.2 also shows the general compositional range for CAIs along the CCAM line, highlighting the tendency of chondrules to be more enriched in ^{17}O and ^{18}O compared to CAIs.

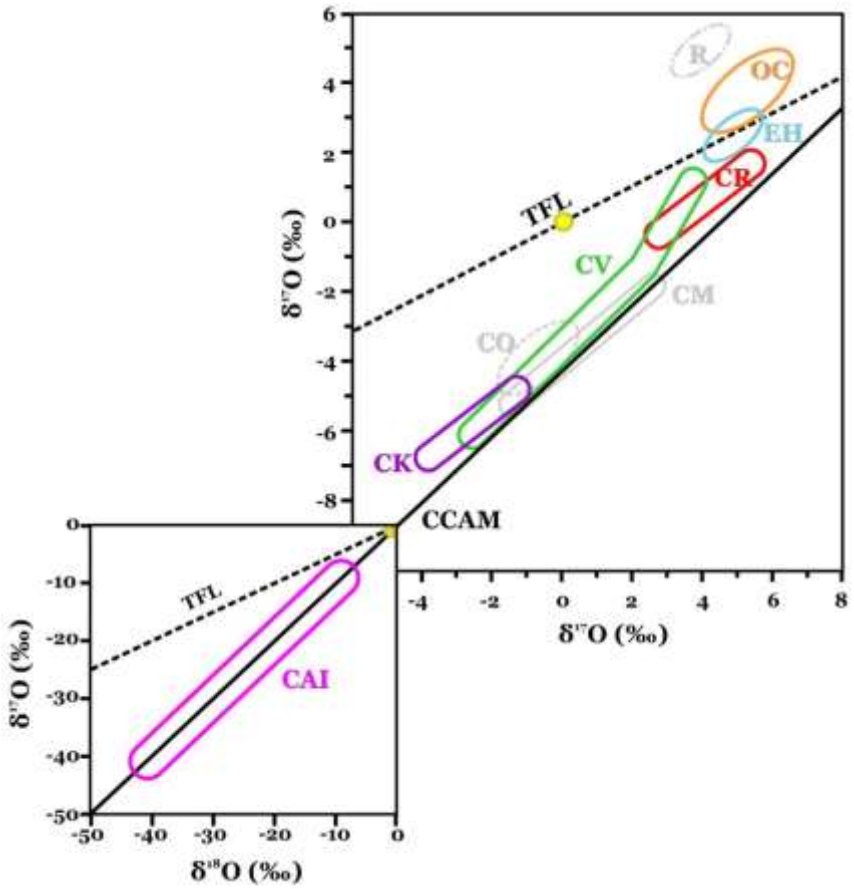

Figure 1.2 Three O-isotope plot for chondrules (upper right) and CAIs (lower left) from chondrite meteorites. The Terrestrial Fractionation line (TFL) is plotted with SMOW (Standard Mean Ocean Water) indicated as a yellow circle. Most carbonaceous chondrite chondrules plot close to the CCAM (Carbonaceous Chondrite Anhydrous Mixing) line, although not necessarily with slopes of 1. In contrast, chondrules from the E, O and R chondrite groups plot along or above the TFL. The CAIs plot in a much more ^{16}O-rich field along the CCAM line and show essentialy no overlap with chondrules (note change in scale). (Clayton, 1993; Clayton & Mayeda, 1999; Rubin, 2000).

1.2 Placing Chondrules in context

1.2.1 Overview of the early Solar System

The solar nebula started off as a cold molecular cloud composed of 'universal' gases such as H and He as well as material ejected from surrounding stars into the local interstellar medium (Ciesla & Charnley, 2006; Tolstikhin & Kramers, 2008). The types of stellar ejecta include phases such as SiC, diamond, graphite, ferromagnesian-amorphous and crystalline silicate phases (olivine and pyroxene), metal oxides, and native Fe-Ni metal (Day, 1976; Waters *et al.*, 1996; Zinner, 2007). Collapse of the molecular cloud will commence if the gravitational potential (U_G) outweighs the thermal support produced by kinetic energy (E_K) of the particles (Tolstikhin & Kramers, 2008):

$$2E_K < U_G$$

or

$$2\left(\frac{3MkT}{2m}\right) < \left(\frac{GM^2}{R}\right)$$

where E_K = Kinetic energy

U_G = Gravitational potential energy

M = Mass of the cloud

R = Radius of the cloud

m= mass of a particle

G = Gravitational constant (6.67×10^{-11} $m^3.kg^{-1}.s^{-2}$)

k = Boltzmann constant (1.38×10^{-23} $J.K^{-1}$)

Figure 1.3 compares the history of the Solar System based on astronomical observations and models, and isotope systematics. Modeling of Solar System mass nebulæ shows that matter will fall towards the center of the cloud at an average rate of 10^{-5} $M_{\odot}.a^{-1}$ after collapse is initiated (Tolstikhin & Kramers, 2008; Ciesla, 2009).

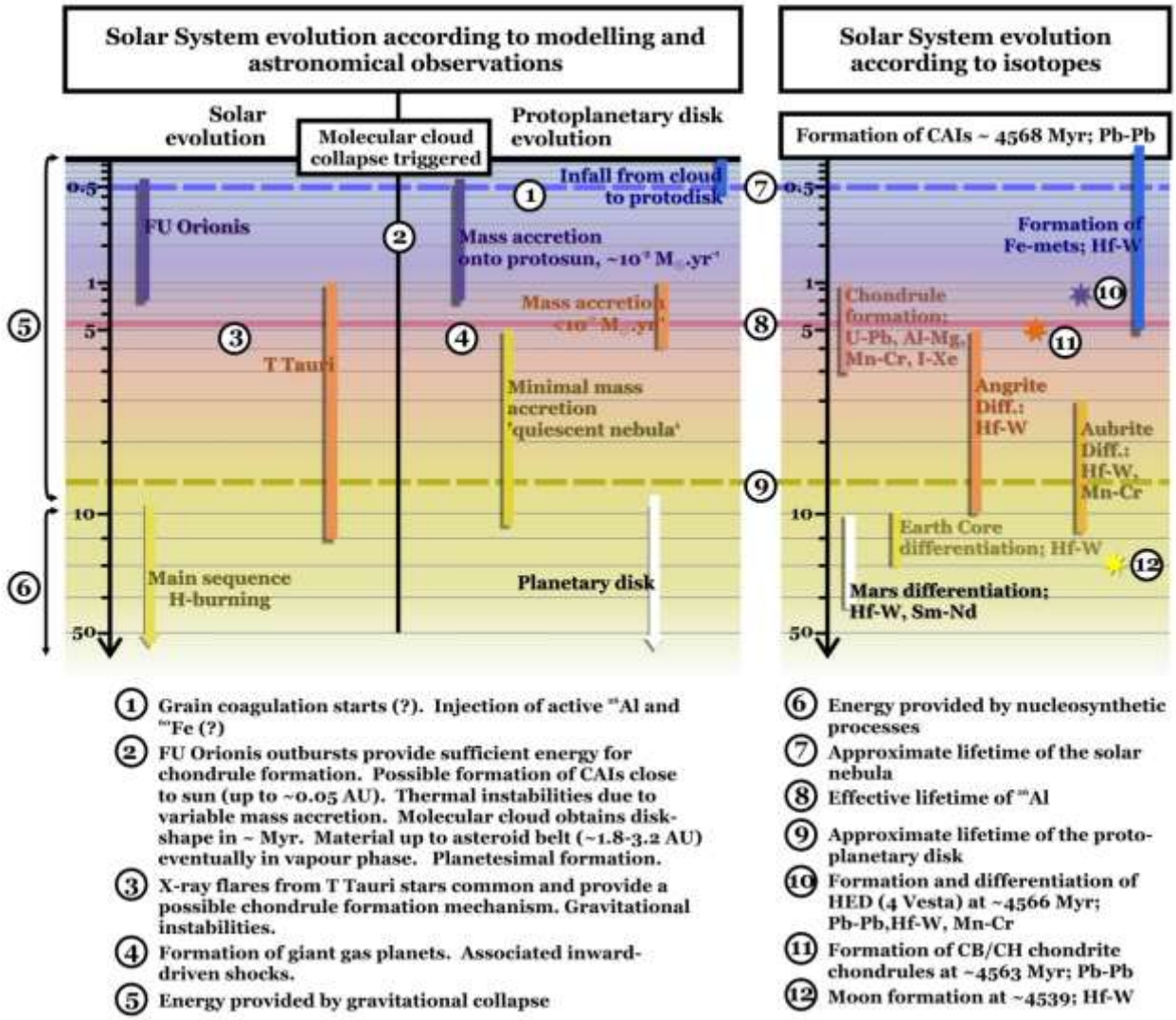

Figure 1.3 Timelines of Solar System evolution based on astronomical observations and modelling (left) vs. geochronology (right). The left schematic also compares the simultaneous evolution of the Sun and the solar disk. Timescale is in *Ma*. The 'solar nebula' is defined as the molecular cloud from which the Solar System was derived. Formation of the protodisk lasted approximately 0.5 *Ma*. The trigger for the collapse is thought to be the same supernova event that injected live ^{26}Al into the Solar System. If CAI formation is taken as the start of the Solar System then it raises questions about the source of heat for CAI formation since conditions would have been too cold for at least the lifetime of the nebular cloud until the start of the FU Orionis phase. Regardless, grain coagulation and therefore planetesimal formation would have started as soon as grains came within sticking range of each other during infall from the molecular cloud. By the time ^{26}Al was no longer a viable heat source (~5 *Ma*) most of the mass of the solar nebula would have been accreted onto the Sun and at least some planetesimals (e.g. 4 Vesta) would have been sufficiently large to undergo core formation and silicate differentiation. Chondrule formation overlaps with both the T Tauri phase of the Sun, the early phase of planetary formation and evolution, and formation of the giant gas planets, but does not extend beyond ~7 *Ma* after CAI. By the time that H-burning is ignited in the Sun the disk has mostly achieved its current configuration. (Desch *et al.* , 2005, Tolstikhin & Kramers, 2008; Ciesla & Charnley, 2006; Amelin *et al.*, 2002, Markowski *et al.*, 2006; Bouvier *et al.*, 2006; Connolly & Bizarro, 2009; Yurimoto & Wasson, 2002, Villeneuve *et al.*, 2011; Rudraswami *et al.*, 2008; Whitby *et al.*, 2002; Touboul *et al.*, 2008; Yin *et al.*, 2002; Krot *et al.*, 2005; Foley *et al.*, 2005; Cassen, 1996; O'Brian *et al.*, 2006; Scott, 2006; Petitat *et al.*, 2008; Shukolyukov & Lugmair, 2004; Kleine *et al.*, 2006).

Movement of dust to the midplane and grain coagulation occur rapidly, potentially

forming up to km-sized 'particles' in 10^4 *a* (Scott, 2006 and refs. therein). Turbulence from convection and gravitational instabilities in the early Solar System (e.g. Boss, 2004; Alexander, 2008) will transport grains radially and vertically and potentially also concentrate them. Boss & Durisen (2005) suggested that turbulent concentration of small particles (<cm) will stop them from falling into the Sun as predicted by gas-drag theory. A thermal gradient is created due to release of energy from the infalling material, heating the dust closest to the nascent star to ≥2000 K. (Cuzzi *et al.*, 2003). This would be sufficiently hot to evaporate all except the most refractory material (CAI-type) closest to the sun while silicates would be stable a little further out. Modeling by Cuzzi *et al.* (2003 and references therein) shows that the boundaries of these zones would migrate inwards as the nebula cools, so that the boundary CAI_{stable} at 0.01 *Ma* would be at ~0.3 AU and at 0.1 *Ma* at 0.01 AU. For silicates, the stability boundary would be at 2-3 AU at 0.01 *Ma* and at ~0.3 AU at 0.1 *Ma*. A protodisk is established approximately 0.5 *Ma* after cloud collapse and can persist for several million years (Ciesla & Charnley, 2006). The collapsing proto-sun passes through the FU Orionis and T Tauri stages that are both associated with energetic outburst of either thermal or magnetic natures respectively (Desch *et al.*, 2005; Ciesla & Charnley, 2006). The major phase of planet building is thought to occur during the T Tauri phase when most of the Solar System mass has already been accreted onto the protosun (e.g. Kominami & Ida, 2004). This period is also associated with major gravitational instabilities due to the formation of the giant gas planets at 5-10 AU that can drive shocks towards the inner disk (Desch *et al.*, 2005). Formation of the terrestrial planets is thought to occur prior to full formation of Jupiter since the latter has dramatic effects on the number and sizes of planetesimals inside of 5 AU (e.g. Kominami & Ida, 2004; Raymond *et al.*, 2009). Increasing density in the core of the collapsing cloud causes the temperature to approach 10^6 K at which point D-burning is started. This is followed by H-burning at 10^7 K, which heralds the birth of a star (Tolstikhin & Kramers, 2008). By this point all remaining mass in the protodisk has been accumulated into the planets.

In contrast to stellar observations and modeling, time zero according to isotope systematics of the Solar System is defined by the formation ages of CAIs at 4568.3 ± 0.7 *Ma* (Burkhardt *et al.*, 2008). Ages for the formation of magmatic Fe-meteorites (Figure 1.3) indicate that their formation may have started simultaneously with or even predated the CAIs, although it is generally accepted that they started differentiating within <1 *Ma after* CAI formation (Kleine *et al.*, 2005; Markowski *et al.,* 2006). By 2 *Ma* after CAI at least some of the asteroids such as 4 Vesta (parent body for the HED meteorites) had formed and differentiated (Kleine *et al.*, 2002). Formation of the CB/CH chondrites, which are thought to be the result of the collision between two totally molten bodies (e.g. Krot *et al.*, 2005b, 2007), occurred approximately 5 *Ma* after CAI formation. By 5 and 10 *Ma* respectively after CAI formation the angrite and aubrite parent bodies were sufficiently differentiated to experience core creation (Shukolyukov & Lugmair, 2004; Markowski *et al.*, 2007; Petitat *et al.*, 2008). Although the initial phase of 'planet' melting is probably related to the presence of live ^{26}Al early on in the Solar System, by ~5 *Ma* at the latest it would have lost its efficacy as heat source for self-insulating bodies (i.e. larger than 100 km). Chondrule formation coincided with this early period of planetary evolution, starting approximately 1 *Ma* after CAI and lasting another 6 *Ma* (e.g. Amelin *et al.*, 2002; Whitby *et al.*, 2002). A second major period of planetary differentiation is marked by the metal-silicate differentiation on the Earth and Mars starting approximately 10 *Ma* after CAI and is highlighted by the Moon-forming event at ~30 *Ma* after CAI (Yin *et al.*, 2002; Kleine *et al.*, 2002). Heat sources for later differentiation in the Earth and Mars are most likely the long-lived radioisotopes of U and Th (e.g. O'Neill & Palme, 1998).

Although the exact phase boundaries of the astronomical models are not well constrained and may show a large amount of overlap (Ciesla & Charnley, 2006), the general timescales seem to broadly agree with those constrained by isotopes. Detailed discussions about the exact timing of Solar System processes are beyond the scope of

this thesis, but Figure 1.3 provides the general framework for discussion of chondrule processes.

1.2.2 Chondrule ages

Despite the distinct O-isotope signatures, ages for chondrule formation show a large degree of overlap (Figure 1.4; see figure for references). With the exception of the CB and EH chondrules, the CCh and the OC chondrules have formation dates between 1-3 *Ma* after CAI formation. Data from the UOC chondrules (Rudraswami *et al.*, 2008) suggest a relatively short formation period of ~1.5 *Ma* overprinted by later metamorphism. In contrast, traces of ^{26}Mg are not uniformly present in chondrules from CCh meteorites, implying that chondrule formation took place over a period of several *Ma* both during and after the effective lifetime of ^{26}Al (e.g. Hutcheon *et al.* 2010). Data of Bizzarro *et al.* (2004) as well as textural evidence from Itoh & Yurimoto

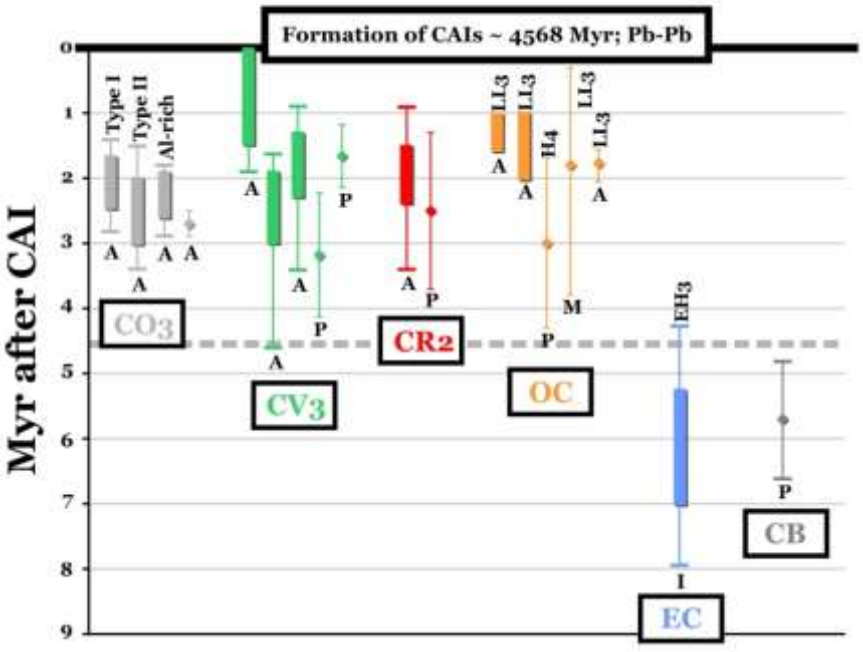

Figure 1.4 Summary of chondrule ages. A = Al-Mg, P = Pb-Pb, M = Mn-Cr, I = I-Xe. Bars represent ranges in ages, diamonds are individual chondrule ages. Most carbonaceous and ordinary chondrite ages fall within the first ~3 *Ma* after CAI formation with spreading mostly due to metamorphic overprint. The EC and CB chondrules are the only chondrule suites to plot at distinctly younger ages between ~5-7 *Ma* after CAI. The effective lifetime of ^{26}Al is indicated as a dashed gray line. (Kurahashi *et al.*, 2008; Kunihiro *et al.*, 2004; Connolly Jr. & Bizarro, 2009; Kita *et al.*, 2000; Bouvier *et al.*, 2007; Yin *et al.*, 2007; Kita *et al.*, 2000; Krot *et al.*, 2005b).

(2003) suggest that some CV chondrules may have formed contemporaneously with CAI, although this interpretation has been called into question by several authors (e.g. Krot *et al.* 2005a). The distinctly younger ages of the EC and CB chondrules postdate the effective lifetime of ^{26}Al. Iodine-Xe data for the EC show a range of chondrule formation ages between 5-7 *Ma* after CAI (Whitby *et al.* 2002) and a single Pb-Pb formation age of 4562.8 ± 0.9 *Ma* was determined for the CB chondrites (Krot *et al.* 2005b).

1.2.3 Chondrule formation mechanisms

Formation mechanisms for chondrules are generally labeled as either *nebular* or *planetary*. Table 1.2 lists some of the more common suggestions for chondrule formation. Nebular mechanisms can generally be divided into Shock heating, Direct condensation of a liquid, Flare heating or Current sheets. Sources for shock waves occur throughout most of the early history of the Solar System, starting with accretion shocks as gas falls from the remainder of the molecular cloud onto the protodisk (e.g. Ruzmaikina & Ip, 1994). Once planetesimals with radii of >1km exist the possibility of bow shocks (e.g. Miura *et al.*, 2010) and shocks due to gravitational instabilities from the formation of giant gas planets (Boss & Durisen, 2005) become important. Planetesimal bow shocks require that the body travels at essentially supersonic speeds on a slightly eccentric orbit (Miura *et al.*, 2010). Propagation of shock waves through the formation of the giant gas planets at 5-10 AU can provide the inner solar system with sufficient energy to melt solids in the region of the asteroid belt (Boss & Durison, 2005). Direct condensation of a silicate liquid is thought to be possible in a highly dust enriched environment (dust:gas >50x CI; e.g. Krot *et al.*, 2001; Engler *et al.*, 2007), which are likely to be the result of turbulent concentration (e.g. Hewins & Herzberg, 1996; Cuzzi & Alexander, 2006). As mentioned in Section 1.2.1, flares from the nascent Sun are likely to be mostly associated with the FU Orionis and T Tauri phases. Magnetic reconnection/X-ray flares from T Tauri stars as well as thermal flares driven

Table 1.2 Chondrule formation mechanisms

Nebular

	Author	Description	Details
Shock fronts	Boss & Durisen (2005)	Shock heating	Formation of material clumps in outer SS (linked to formation of Jupiter) drive shock waves into inner regions capable of heating material; creation of temporary spiral arms and ring structures with high densities (>10g/m^3)
	Ruzmaikina & Ip (1994)	Accretion shocks	Shocks produced by gas falling from the molecular cloud onto the evolving protodisk. Grains are heated by a combination of frictional heating and UV radiation from the shock front.
	Miura *et al*. (2010)	Planetesimal bow shocks	A planetesimal orbiting at supersonic speeds creates bow shocks that heat and melt (or vaporise) the surrounding dust. Upon cooling crystallisation (or condensation) takes place.
Direct condensation of liquids	Engler et al. (2007)	Open-system direct condensation	Chondrules from by direct condensation of a nebular gas. Requires highly dust-enriched region (800x CI and 10^{-3} atm) to stabilise liquids. For formation of pyroxene dominated chondrules, large silica enrichment is necessary, possibly through the depletion of Mg through olivine crystallisation. Suggest that BO and CC (pyx dominated) can potentially be formed in the same region.
	Krot *et al*. (2001)	Closed-system direct condensation	Highly enriched dust cloud (~10-50x solar). Slightly oxidized conditions. Chondrule condensation took place ahead of condensation of metal alloys. Coarser grained chondrules form earlier than but in chemical continuum with cryptocrystalline chondrules. Chondrules are isolated in order to preserve volatility controlled characteristics.
Flare heating	Shu *et al*. (1996, 1997, 2001)	Flare heating	Nebular material in the inner disk (<0.1 AU) is melted by short-lived flares created by magnetic instabilities in the young sun and cools to form either CAIs or chondrules. These are transported to ~2-3 AU by bipolar solar outflows.
	Boley *et al*. (2008)	Thermal flares driven by gravitational instabilities	FU Orionis events provide short-lived high temperature events. Temperature increases are expected within 1AU. Leads to instabilities that transfer mass outwards.
Current sheets	Joung *et al.* (2004)	Electrical current produced by induction	Ionised particles concentrate along magnetic nulls to form a current sheet. Dust moving through the sheet are heated to melting point.

Planetary

	Author	Description	Details
Planetesimal collision	Asphaug *et al*. (2011)	Chondrules = splash droplets	Collision between two partially or totally molten bodies. Creates dense, thermally insulating cloud that allows molten droplets to cool slowly. Some chondrules are re-accreted while other escape to the surrounding space.
	Krot et al. (2005, 2007)		Vapor-plume origin from the collision between two planetesimals.
Ablation	Genge (2000)	Chondrules = ablation melt droplets	Shocks in the nebula (> Mach 2) ablate the surface of small bodies (1 mm-500 m) and chondrule-sized droplets are created by gas drag.

by rapid accretion onto FU Orionis objects both operate early on during the history of the Solar System (e.g. Shu *et al.*, 2001; Ciesla & Charnley, 2006; Boley & Durisen, 2008). Electrical current sheets (e.g. Joung *et al.*, 2004) were suggested as a chondrule formation mechanism for a slightly more evolved disk when the dust and gas have been sufficiently separated from each other to create large dust:gas ratios. This formation method counts on magnetic activity from the sun and the presence of charged particles to create localised currents capable of heating dust grains.

Planetary models, i.e. methods of formation where the melt or solid precursor is derived from a planet or planetesimal, mostly focus on impact (e.g. Krot *et al.*, 2005, 2007; Asphaug *et al.*, 2011) or ablation scenarios (e.g. Genge, 2000). The most recent candidates for impact scenarios involve the collision of molten or partially molten bodies (Krot *et al.,* 2005, 2007; Asphaug *et al.* 2011). The impacts create dense atmospheres of molten and gaseous material. Droplets from the impact crystallise as chondrules and either escape the planetesimal if they have sufficient escape velocity or rain back onto the planetesimal surface (see figures in Asphaug *et al.*, 2011). Surface melting and ablation of small planetesimals is thought to be possible in the presence of high speed shocks (>Mach 2; Genge, 2000). Melting occurs on the 'bow end' of the body while the molten particles are swept away behind the planetesimal.

1.3 The Chondrule Problem

Table 1.3 lists some characteristics of chondrules and chondrites that constrain the conditions of chondrule formation theories. An important attribute is that Refractory Lithophile Elements (RLE) in chondrules and chondrites usually maintain their CI relationships to each other. This limits the amount of chemical fractionation in the chondrule precursor material, particularly in models that require planetary formation scenarios. Changes in fO_2 in chondrule forming regions as indicated by disequilibrium between MgO-rich chondrule olivine and FeO-rich rim olivine, relict grains with different compositions and the presence of both Type I (FeO-poor olivine/pyroxene)

Table 1.3 Chondrule and chondrite characteristics

1. Refractory Lithophile Elements in chondrules mostly maintain CI proportions to each other.

2. The range in element concentrations for chondrules is larger than for bulk meteorite or matrix.

2. Both Mg-rich and Fe-rich chondrules occur in a single meteorite.

4. Disequilibrium exists amongst silicates within a single chondrule e.g. CO type II FeO-rich chondrules containing FeO-poor relict grains (e.g. Wasson & Rubin, 2003) or EC enstatite chondrules with relict olivine (see fig. 1.1) or cores of high Fe-pyx in low Fe-pyx (e.g. Weisberg *et al.*, 1994, Berlin *et al.*, 2007).

5. Metal in chondrules is associated with high Mg-content of olivine and pyroxene, and may be associated with sulphides, whereas low Mg-content chondrules do not contain metal but often contain sulphides, e.g. CR chondrules.

6. In PO or POP chondrules pyroxene most often occurs as a late phase that increases towards chondrule rims and often poikilitically encloses olivine.

7. Both slow cooled, porphyritic chondrules and rapidly cooled, RP/CC chondrules occur in a single meteorite.

8. Non-porphyritic chondrules sometimes show perfectly spherical indentations not usually observed in porphyritic chondrules, e.g. RP chondrules in E chondrites

9. Presence of CAI relicts in chondrules (e.g.Krot *et al.*, 2002) and rarely of chondrules in CAI (e.g.Krot et al., 2005).

10. Coarse grained or 'igneous' rims present around some chondrules, which are assumed to indicate multiple heating events (e.g. Rubin, 1984).

11. Coarse grained rims do not necessarily occur on all chondrules of similar types in a meteorite.

12. Presence of coarse grained, high temperature and fine grained, low temperature rims can occur around single chondrules.

13. Large disequilibrium exists between rim and chondrule olivines (rim olivine is mostly more Fe-rich).

14. Low temperature rims are commonly close to or equivalent in composition to the surrounding matrix (e.g. Rubin, 1984; Cosarinsky *et al.*, 2008).

15. Apparent complementarity of chondrules and matrix, generally with the high temperature elements in the chondrules and volatile elements in the matrix (e.g. Hezel & Palme, 2008).

16. Chondrules may have a high volatile content e.g. Na, S, especially in the EC and CV chondrites, which is contrary to a high temperature formation in a canonical solar nebula. Sodium measured in oxide form is present up to hundreds of ppm in chondrule olivine with zoning patterns similar to that of Cr, Mn and Ca(Alexander et al., 2008).

17. Chondrules are commonly more ^{16}O rich than the matrix and bulk rock but less so than CAI (e.g. Scott & Krot, 2007).

18. Chondrules from the C, O and E chondrites plot on different areas on a three O-isotope plot (e.g. Rubin, 2000).

19. Porphyritic and BO chondrules from the same meteorite appear to have different O-isotope characteristics, e.g. Allendé, where the BO chondrules are heavier and lie along a different slope (Rubin *et al.* 1990)

20. Systematic variation of chondrules sizes in different types of meteorites implies some form of sorting mechanism (Wurm & Krauss, 2007).

21. Chondrules with a radial or CC texture are almost exclusively pyroxene.

and II (FeO-rich olivine/pyroxene) chondrules in a single meteorite still need to be adequately explained. Suggested mechanisms involve either reactions between reservoirs of different compositions (e.g. Cosarinsky *et al.*, 2008) or somehow varying the fO_2 conditions in the formation region (e.g. Kurahashi *et al.*, 2008), although specific mechanisms are often poorly constrained. Many chondrules are also anomalously enriched in Na and other relatively volatile elements despite the fact that chondrules are almost certainly high temperature objects. This is generally attributed to formation in regions with high dust enrichment (e.g. Ebel & Grossman, 2000) or

flash heating (e.g. Yu & Hewins, 1998). The exact relationship between chondrules and the accompanying matrix is also still a matter of debate. Average chondrule compositions for some elements (notably the bulk elements Mg/Si) appear to be complementary to the matrix (e.g. Bland *et al.*, 2005; Hezel & Palme, 2010) while the compositional range for chondrules is much larger than for either the bulk meteorite or matrix. There is also a tendency for chondrules to have lighter O-isotopes than the matrix (Scott & Krot, 2007) and for BO chondrules to be slightly heavier than PO(P) chondrules (Rubin *et al.*, 1990). Then there are still the general questions relating to the existence (or non-existence) of genetic links between the different chondrite types (Clayton *et al.*, 1976). Physical characteristics, such as the co-existence of quenched and slowly cooled chondrules in a single meteorite, chondrule indentations, systematic size variations in specific meteorite types and non-uniform presence of coarse-grained/igneous mantles, have been investigated individually or not at all (see Table 1.3 for references) but have not been brought together in a unified theory. To date there is also no unified theory capable of bringing together all physical, chemical and isotopic characteristics into a coherent model without contradictions. Considering the sheer number, complexity and sometimes contradictory nature of the chondrule and chondrite characteristics, this is perhaps not surprising.

1.4 Solving the Problem

The problem concerning chondrule and chondrite formation can be summed up simply as finding the correct astronomical setting to reproduce all the characteristics satisfactorily. This is no simple task since, as pointed out in Section 1.2.3, several scenarios have been proposed that are capable of reproducing multiple chondrule attributes. To this end the current study seeks to address some of the issues surrounding chondrule formation, particularly focusing on potential evidence for astronomical setting, mechanisms for producing the observed chemical compositions and relationships amongst the different chondrule and chondrite types. In this study

the author combines modern ICP-MS and –OES technology with an experimental chondrule liberation technique to obtain a wide range of chemical information for whole chondrules. Although whole chondrule measurements (in contrast to beam-based analysis) have the advantage of representing the 'droplet' composition, it should be supported by traditional thin section analysis, microscope studies of chondrules and results from beam-methods as shown in this study. Obtaining high quality chemical and petrological data on chondrules (and other Solar System objects) is of paramount importance since most models for chondrule formation are ultimately based on chemical analysis and petrology. Furthermore, the outcome of mathematical models are required to duplicate these chemical/mineralogical characteristics in order to gain acceptance. A necessity, therefore, for the testing of any model is the existence of a large and detailed database of chemical analyses on which to base its parameters. The author attempts to provide an effective method for obtaining such analyses on whole chondrules, which, to date, represent only a small fraction of the available data for Solar System object. A further aspect of this work is the advancement of the current chemical methods of chondrule classification. The meteorites selected for this study include Acfer 311 (CR2; find, S2[1], W2[2]), Allendé (CV3; fall, S1, W0), Karoonda (CK4; fall, S1, W0), Sahara 97158 (EH3; find, S2, W1) and Indarch (EH4; fall, S4, W0). The selection criteria were based on size and abundance of chondrules, availability of the meteorite, chemical diversity (ranging from highly reduced (Indarch) to highly oxidized (Karoonda)), differing friability to test the efficacy of the freeze-thaw method (Karoonda = highly friable, Indarch = highly resilient) and varying mineralogy.

[1] S = Shock stage (1 = unshocked – 6 = highly shocked, presence of e.g. ringwoodite; Stöffler *et al.*, 1991)

[2] W = Weathering stage (0 = unweathered - 6 = highly weathered, most silicates altered, Wlotzka, 1993)

2 Method

2.1 Sample preparation

2.1.1 Cleaning

Samples were abraded with corundum paper to remove loose surface contamination. This was followed by an ultrasonic bath in a mQ/ethanol mixture for approximately 15 min and then a thorough rinse with mQ and lastly acetone. The surfaces were further cleaned in dilute (~0.5M) HCl for 10-15 minutes. Stronger acids and longer submersion-times were avoided to minimise extensive dissolution and leaching of metal and sulfides (evidenced by the production of H_2S during the cleaning). This was followed by a last rinse in mQ and then acetone after which the samples were oven dried.

2.1.2 Freeze-thaw

Isolation of whole chondrules has been employed successfully in several areas of meteorite studies, including Pb-Pb dating and the duration of chondrule formation (e.g. Amelin *et al.*, 2002; Krot *et al.*, 2005), Eu-isotopic variations and mass-dependent fractionation in the Solar System (Moynier *et al.*, 2006) and major and trace element studies of chondrules (Grossman, *et al.* (1985). In some cases the meteorites are sufficiently loosely compacted or the matrix sufficiently friable that the chondrules are freed with little problem, except possibly some adhering matrix material, but in most cases the meteorites require more robust mechanical disaggregation. The normal method for liberating the chondrules has mostly been coarsely crushing the sample and then freeing any exposed chondrules with dentists tools (e.g. Grossman *et al.*, 1985). Potential problems with using dental tools, however, include contamination and incomplete removal of the surrounding matrix material. Also depending on the relationship between the matrix and non-matrix components, it is possible that crushing will rather break the chondrules than expose them, as well as breaking other

more fragile components such as CAIs and PSGs. Acid dissolution of matrix material composed largely of metal and sulfide in enstatite chondrites has also been successfully applied to isolate chondrules (e.g. Leitch *et al.*, 1982). This has the obvious drawbacks of not allowing the mechanical separation of metal and sulfide components and potentially leaching these components from the chondrules. In contrast to these techniques, Tizard *et al.* (2005) applied a freeze-thaw method to gently separate out PSGs from a small sample of Murchison (CM2) meteorite, maintaining both the structural integrity and preserving the often fragile and non-refractory coating on the grains. It was anticipated that chondrules separated using a freeze-thaw method would both remain intact and have sufficiently little matrix adhering to the surface to show the mineralogy and mineral textures of the chondrules while maintaining any original layered structuring. Assuming sufficient material could be separated, the different textural groups (e.g. PO, PP, CC) could then be analysed both for comparison with each other and between different meteorites. Part of this project therefore aimed to test the application of such a freeze-thaw method to the disaggregation of chondrites, particularly noting whether or not: a) it efficiently separated out chondrules and other potentially fragile phases of interest (e.g. CAIs), b) maintained textural associations (such as complex rim structures), c) achieved clean separation of matrix from the non-matrix components, d) the method could be applied to a wide variety of chondrite compositions and e) the method could be applied to relatively large sample sizes (~10g).

Chondrites were coarsely crushed to increase surface area in an agate mortar pre-cleaned with quartz sand. Chondrite chunks were transferred into capped 50ml centrifuge tubes (Figure 2.1a) that were pre-cleaned in 0.2M HCl over a period of weeks. Approximately 1ml of a 50/50 EtOH/mQ mixture (called the freezing solution hereafter) was added to the samples. The tubes were alternately submersed in liquid nitrogen (Figure 2.1b, c) and boiling water with a 10 minute ultrasonic bath after every

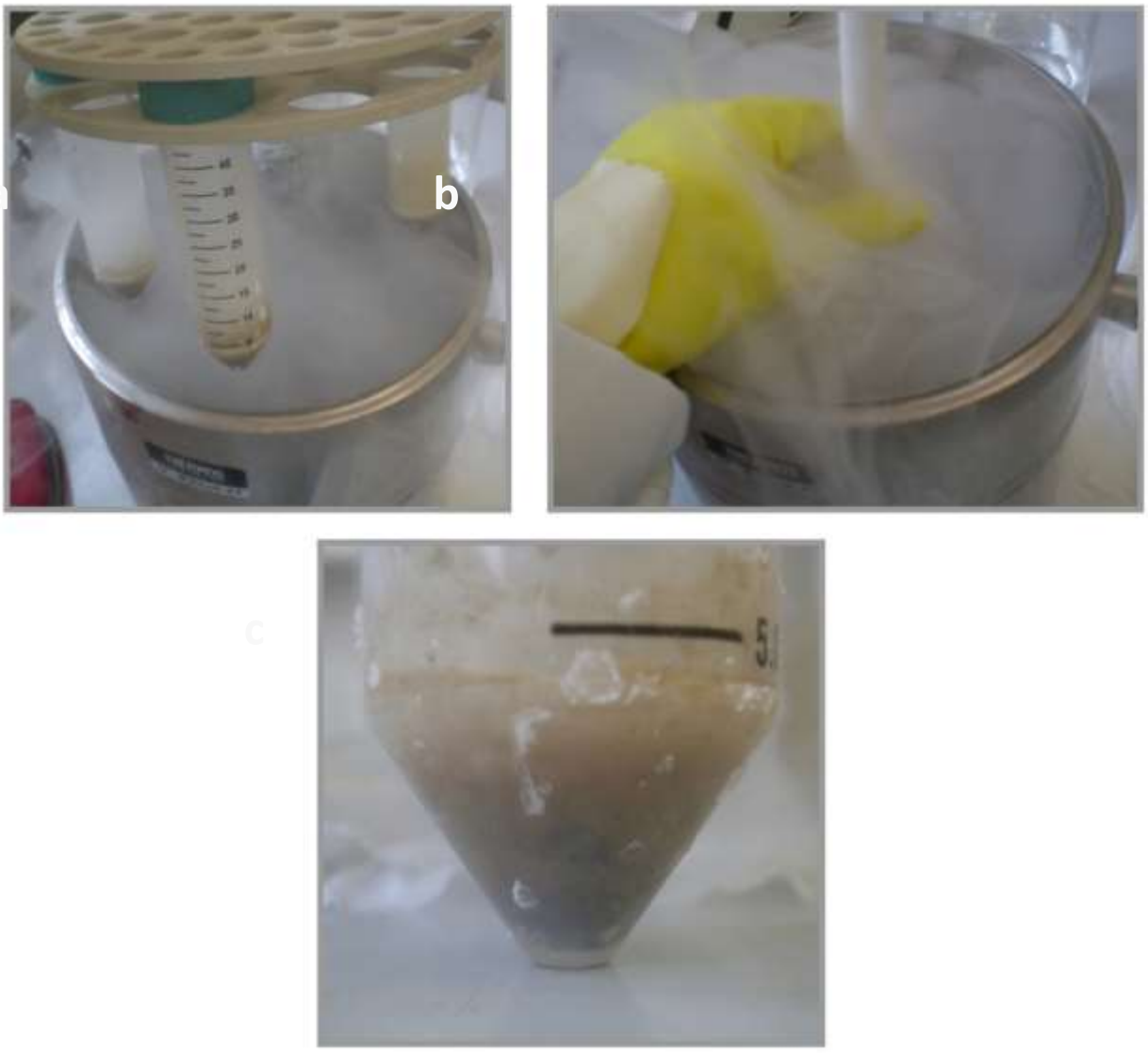

Figure 2.1 Freeze-thaw setup. a) Meteorite chunks are placed in pre-cleaned and capped 50 ml centrifuge tubes and the freezing solution added (see text for details). b) The tubes are dipped in liquid nitrogen, allowing the solution to freeze completely (c). Afterwards the frozen sample+solution is thawed in a bath of boiling water (not shown) but not brought to boiling point.

tenth cycle. Each hot-cold cycle (i.e. submersion in liquid nitrogen followed by boiling water) lasted approximately 5 minutes, which was largely determined by the rate at which the solution froze in the liquid nitrogen. Care was taken not to allow the freezing solution to boil. The process was repeated until the sample was sufficiently disaggregated, which required more than 200 cycles of the freeze-thaw process. In addition, samples were dried at the end of the day and gently rolled with a pestle in an agate mortar to aid in loosening the sample. Inspection of the samples after 50 cycles

during testing showed that the freezing solution avoided oxidation of metal and sulfide components but still allowed effective disaggregation of the sample, and that chondrules were being liberated with little or no adherence of matrix except for a loose coating of fine material that was effectively removed by washing the chondrules in distilled acetone in an ultrasonic bath. Inspection of chondrules from Allendé, which are known from thin section commonly to have fine grained rims surrounding coarse central chondrules, showed that the fine rims were preserved during freeze-thaw. Acfer 311 and Indarch chondrules had small amounts of fine grained surficial dust unrelated to fine grained rims that could not be completely removed despite multiple cycles of ultrasonic cleaning or attempting to scrape the surfaces. This was therefore assumed to be an integral part of the chondrules.

Petrography was performed on whole-meteorite thin sections prior to freeze-thaw to compare the matrices between the samples as an estimate of how easily the freeze-thaw might separate components. However, in several cases the samples behaved in totally different fashion compared to what was expected. Good examples of this are the E chondrites Sahara 97158 (EH3) and Indarch (EH4). Both EC have similar matrix composition and textures, but whereas chondrules in Indarch separated cleanly, Sahara separated poorly with only few chondrules being liberated and was therefore not used for further study. In general, however, Sahara behaved as a homogeneous lithology. This is surprising since an increase in metamorphic grade in chondrites leads to a coarsening of textures so that chondrules and matrix minerals eventually intergrow (Van Schmuss & Wood, 1967). It was therefore suspected that Sahara would separate with reasonably more success than Indarch. The degree of success of the freeze-thaw disaggregation also did not show any correlation with chondrule size.

The separates were sieved using nylon mesh to produce four size fractions of: >200μm (larger chondrules and mineral/clastic fragments), 100-200 μm (chondrules and separate minerals), 100-40 μm (very small chondrules and separate minerals) and <40

μm (fine grained matrix components). Components of interest from the >200 μm were hand-picked under a binocular microscope. Photos and descriptions of all analysed chondrules are given in Appendix A.

2.2 Analyses of major (ICP-OES) and trace (ICP-MS) elements

All ICP-MS and ICP-OES element determinations were done at the Institut für Geowissenschaften, Kiel University, under the supervision of Dr. Dieter Garbe-Schönberg.

2.2.1 Sample digestion

2.2.1.1 Digestion tests

Chondrules separated by freeze-thaw were cleaned in a two-step ultrasonic cleaning, first in EtOH and then in distilled acetone. This removed most of the surficial fine grained material. The digestions were done in 3 ml Savillex® vials. The small size of the chondrules excluded powdering them beforehand, but also made it hopeful that a multistep table top digestion would effectively dissolve them. Several terrestrial standards were selected as proxies for sample size and mineralogy and included: a pyroxenite (NIM-P), dunite (NIM-D), basalt (BIR-1), peridotite (PCC-1) and serpentinite (UB-N) (Table 2.1). Certain potentially problematic mineralogical features of the chondrules (such as the possible presence of PSGs and corundum) could not be exactly replicated. However, potentially tough phases in certain standards (such as chromite, magnetite and ilmenite) would test the rigour of the method to a large extent.

Table 2.1 Terrestrial standards for ICP-MS/OES concentration determination

Standard	BIR-1	UB-N	NIM-D	NIM-P	PCC-1
Description	basalt powder	serpentinite powder	dunite powder	pyroxenite powder	peridotite powder
Common phases	plag, cpx, opx, ilm, mgt, sp, ap, hbld	serp, mgt, tlc	ol, chr	cpx, opx, ilm, mgt, ol	ol, opx, cpx, sp

The digestion procedure is based on Garbe-Schönberg (1993) and summarised schematically in Figures 2.2 and 2.3. A series of test digestions (Figure 2.2) including five chondrules were performed to evaluate the efficiency of dissolving whole chondrules, to check the acid mixtures, gauge the necessity of pressure dissolution and estimate blanks. The chondrules (from Acfer 311 CR2) were fairly heterogeneous in composition, ranging from roughly mafic to ultramafic in composition with varying amounts of native and/or altered metal, sulfides and oxides. The sizes of the chondrules varied from ~3 mm (ca. 7 mg) to ~1 mm (ca. 0.8 mg). The first test started

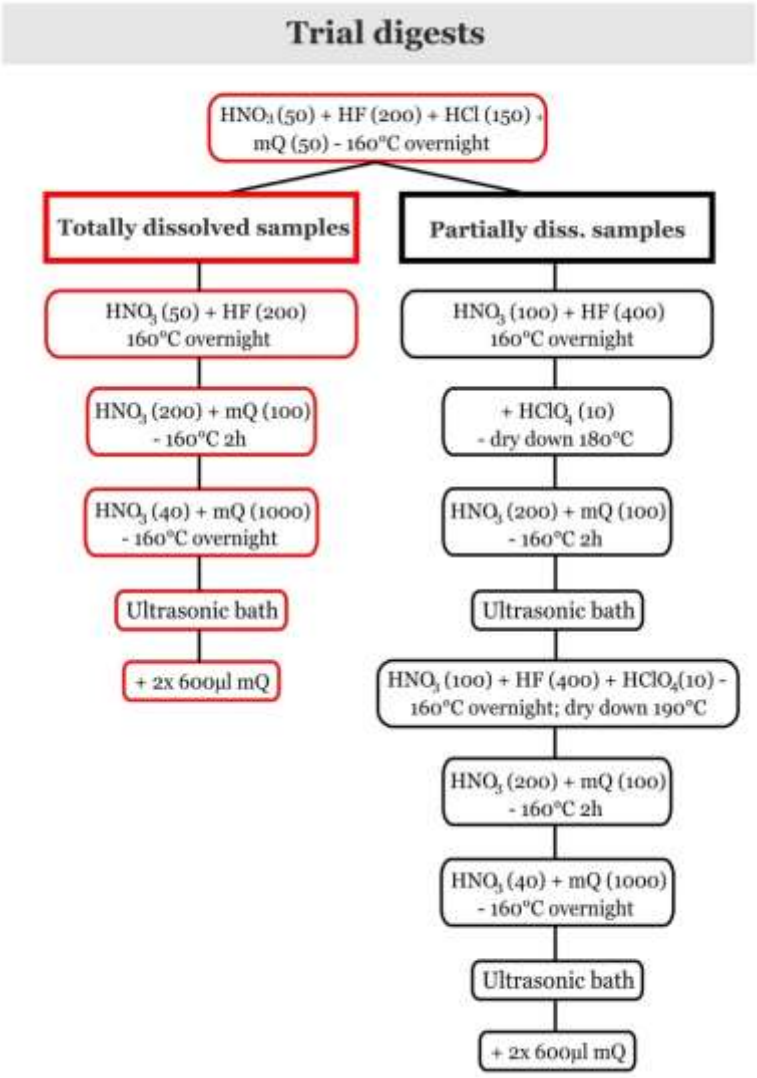

Figure 2.2 Schematic summary of the general dissolution procedure used at Kiel Univeristy (left, red) based on Garbe-Schönberg (1993) that was used for easily dissolved samples. The modified dissolution procedure for both larger and tougher samples is shown on the right. Both digestion procedures were tested on five Acfer type I PO chondrules and the terrestrial standards BIR-1, UB-N, PCC-1, NIM-D and NIM-P (see Table 2.1 for description).

with an overnight digestion in HNO_3-HCl-HF-MQ, which was dried down and followed by another overnight HNO_3-HF step. Inspection of the samples after the first step showed that the chondrules larger than ca. 1mg (AC-1, AC-2, AC-4 and AC-5) and the peridotite standard (NIM-P) were only partially dissolved while the smallest sample (AC-3; ~0.8 mg) and all other standards were totally dissolved. For the second step AC-1 and AC-4 and the NIM-P standard were given double the regular HNO_3-HF acid volumes and allowed to cook overnight with the regular samples. Inspection of the partially dissolved samples/standard the following morning showed that they had not dissolved to any greater degree. Ten milliliter of $HClO_4$ was added to these samples just prior to drying them down at 180°C. Following this, the partially dissolved chondrules were covered by a brown layer (peroxides) typical of a successful $HClO_4$ attack but retained a mostly spherical structure. The NIM-P standard had similarly turned a shade of brown. Addition of a 2:1 HNO_3 mixture to dissolve the surface peroxides immediately revealed that only an outer layer had been converted leaving behind a pale green core in the largest examples. The NIM-P standard was also still not totally dissolved, with small amounts of a black mineral (possibly chromite or ilmenite) remaining. The undigested samples were cooked overnight in an additional HNO_3-HF-$HClO_4$ step, followed by another 2:1 HNO_3 digestion. After the latter step, no residues were observed in these samples (except NIM-P). In NIM-P small black grains were still visible at the base of the beaker, although the amount was drastically reduced by the second $HClO_4$ attack. It was decided that the eluant of the semi-digested standard would be measured to gauge the effect of element partitioning in the remaining phases by comparison with the published data.

The final step prior to diluting the samples for measurement is overnight digestion in 40 µl HNO_3 + 1000 µl mQ. Samples are then transferred to the dilution bottles and 1ml mQ added. The solutions are precisely weighed for determination of the dilution factors and made up to a minimum of 2500 µl.

This series of tests largely validated table top digestion as a viable method for the dissolution of whole chondrules. Even in the case of potentially difficult samples, such as NIM-P, the use of repeated steps of highly oxidizing acid mixtures were sufficient to dissolve the tougher phases, thus avoiding the necessity of bomb digestion. This is advantageous since it both saves time (bomb digestion takes at least one week per 32 samples) and keeps the blanks at the sufficiently low levels required for measuring such small samples.

2.2.1.2 Sample dissolution

As a result of the difficulties observed in dissolving the largest of the chondrules as whole units, all remaining chondrules larger than ~1.5 mm in size were gently broken apart (but not powdered) with an agate mortar and pestle. The pieces were weighed in as a single sample and dissolved together. A slightly modified digestion procedure (Figure 2.3) was followed for the remaining samples and standard digestions. All samples heavier than 1.5 mg were dissolved in double volumes of acid. For the sample digestions the first step was performed without the addition of 50 µl mQ allowing the acids to work at full strength. Although all except the smallest samples still retained solid particles after the overnight digestion, fewer whole chondrules remained and particles were generally fewer and smaller. Perchloric acid was added to the second digestion step of all samples. After an overnight digest at 160°C the samples were dried down at 190°C as opposed to the normal 180°C.

2.2.2 Measurement

Procedures for the ICP-MS measurements are based on Garbe-Schönberg (1993) and the notes for the ICP-OES method description was provided by D. Garbe-Schönberg (pers. comm.)

2.2.2.1 *ICP-MS*

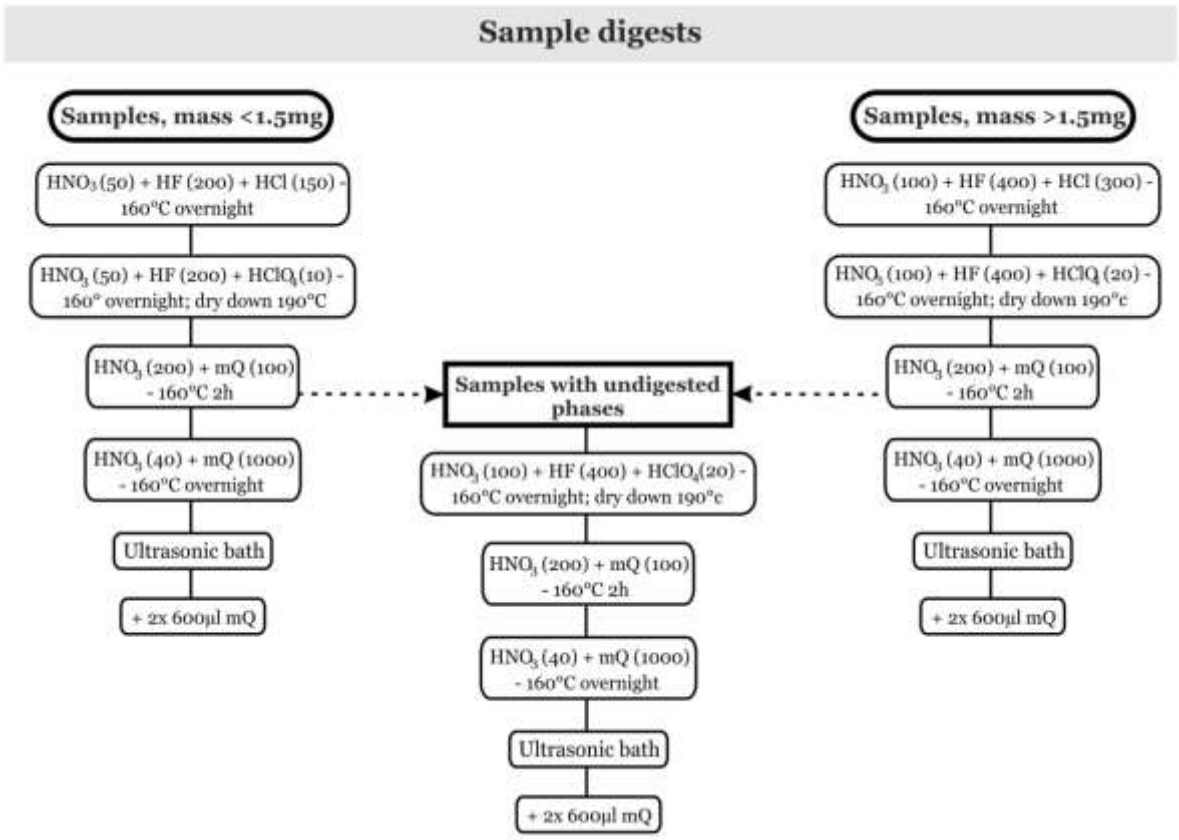

Figure 2.3 Schematic summary of the digestion procedures for the remaining chondrules. The amount of acid in the first two steps is deteremined by the chondrule weight, with samples >1.5 mg getting double the amount of acids. Samples that have undigested phases after the third step are treated with an additional oxidizing step before continuing from the third step of the regular digestion

Measurements were done by Ulrike Westernströer (Kiel Uni.) on an Agilent 7500cs in standard mode, equipped with an autosampler. Very small sample volumes, however, were introduced by hand. A PFA micro-nebulizer with 100 μl sample uptake was used in self-aspiration mode. The cyclonic spray chamber was cooled to 6°C with a Peltier cooler to increase long term stability of the signal and decrease formation of oxides and other polyatomic ions. Calibration solutions were prepared at two concentrations bracketing the expected sample range. Five ppb Re, In and Be were added as internal standards to correct for physical interferences. Laboratory blanks (acid blanks and instrument background), replicate measurements, and international rock standards were analyzed along with the unknown samples for analytical quality control. Reported analytical results are (laboratory) blank-subtracted averages of 3 runs. For more

details of the procedure see Garbe-Schönberg (1993). All work was done in a clean room environment.

2.2.2.2 ICP-OES

ICP-OES measurements were performed by Karin Kissling (Kiel Uni.) using a simultaneous, radially viewing Spectro Ciros CCD SOP instrument equipped with a cyclonic spraychamber and a microconcentric nebulizer with 200 μl/min sample uptake. Small sample volumes were introduced manually. Samples were spiked with 10 $\mu g/ml$ Y as internal standard. A matrix-matched calibration was applied using digest solutions of the international rock standards UB-N, BIR-1, and PCC-1, which covered the expected sample range. All samples were measured five times and the laboratory blank subtracted from the average. AQC schemes were the same as with ICP-MS measurements. All sample preparation work was done under a class 100 clean bench.

2.2.3 Blanks and reproducibility

Blanks obtained for the different digestion sequences are listed in Appendix B, Table B-1, including two previous ICP-MS blanks following the normal digestion procedures of Garbe-Schönberg (1993). With the exception of the REE, the modified digestion procedures have more blank for all trace elements, particularly the blanks that received double the normal acid volume. The source of the contamination is suspected to be the $HClO_4$ since this is the only acid that is not distilled in-house and has not previously been used in the digestion sequence. However, despite the increase in blank levels they mostly remain below 10% of the smallest measured sample or below the L.O.D. Exceptions are listed in Table 2.2. Tantalum is a potentially problematic element in more than half of the chondrules and abundances are therefore interpreted with caution. Similarly, W is a problem in Indarch chondrules due to generally small concentrations. In contrast to the trace elements, the major element blank levels are

Table 2.2 Summary of potential problem samples based on estimated max. blank

ICP-MS	W - all Ind, except Ind-8 U - Ind-3 Mo - Ind-5 Ta - all except, Ac-3; All-1, 2, 3, 5, 6, 7, 10, 8; Kar-2, 3, 7, 14 Sr - Ind-3 Zn - Ac-3
ICP-OES	Na_2O - Ac-1, 2, 4 K_2O - Ac-1, 4; All-9, 13; all Ind, except Ind-8; Kar-2, 4, 8, 12-14 P_2O_5 - Ind-5

generally consistent regardless of the digestion procedure. The only exceptions are elevated levels of Na_2O, K_2O and P_2O_5 during the trial digestions. However, since only Acfer chondrules were digested during the trials the increased contaminants should not pose a problem for the other chondrules as the blank levels were consistently low during the main digestion procedures. Although K_2O is highlighted as a potential blank problem in several chondrules, this is due to the low abundance of K in these chondrules rather than overabundance of the blank, as well as Na_2O in the Acfer chondrules.

Figure 2.4 shows volatility arranged CI-normalised plots for the terrestrial standards. Repeat measurements are plotted in colours, previous analyses in grey and GeoReM preferred values are shown in black. References for the preferred published values are given in Table 2.3. Measured values for the standards and deviations from the preferred values (as % Difference) are given in Appendix C, Table C-1. Values for CI are taken from Lodders (2003) (Appendix D, Table D-1). Previous analyses from Kiel University are only available for the BIR-1 Basalt and UB-N Serpentinite, which are run as routine standards. Standards NIM-P, NIM-D and PCC-1 were measured three times each during the course of the study. The three BIR-1 and one UB-N standards show good agreement with each other and with previous analyses and also, with few exceptions, the preferred values. Most elements have a %RSD of less than 10%, except

Table 2.3 References for preferred values

BIR-1	
(general)	Govindaraju, K. (1989)
Mo	Eggins *et al.* (1997)
P_2O_5	Smith, D.B. (1998)

UB-N	
(general)	Govindaraju, K. (1989)
Ir (compiled)	Meisel, T. & Moser, J. (2004), Yang, J.-S., Jiang, S.Y. & Brügmann, G. (2001), Puchtel, I.S., Humayun, M. & Walker, R.J. (2007), Puchtel *et al.* (2008), Becker *et al.* (2006), Kogiso *et al.* (2008)

NIM-D	
(general)	Govindaraju, K. (1994)
Zr, Ba, Th, Pb Hf, Y, U, Rb, REE	Dulski, P (2001)
Ir	Plessen, H.G. & Erzinger, J. (1998)

NIM-P	
(general)	Govindaraju, K. (1994)
Hf	Korotev, R.L. (1996)
REE, Zr, Pb, Rb, Th, U, Ba	Dulski, P. (2001)
Ir	Plessen, H.G. & Erzinger, J. (1998)

PCC-1	
(general)	Govindaraju, K. (1994)
REE, Zr, Hf, Ba, Y	Dulski, P. (2001)

for elements that are known to be analytically challenging (e.g. Ir, Mo). The large %RSD for La in BIR-1 is due to a contaminant encountered during the trial digestions. However, Figure 4.10 of the REE in Acfer chondrules shows that no appreciable enrichment of La over the other REE is present in the sample, suggesting no contamination. Blank values for La (Table A-1) are also normal, suggesting that the contaminant was only sampled by the standard. For NIM-P most elements still have %RSDs of below 10%, while for NIM-D and PCC-1 most lie well above 10%. This is somewhat surprising since the aliquot of NIM-P run during the trial digestions had an undissolved residue (noted in Section 2.2.1.1) while the test aliquots of both NIM-D and PCC-1 were completely dissolved. Considering that most of the variation in NIM-P and PCC-1 appear to be for the HFSE elements and that NIM-P, NIM-D and PCC-1 originate from coarse-grained plutonic rocks (in contrast to BIR-1 and UB-N) with variable HFSE-bearing phases, it should perhaps be considered that the standards are not homogenous on a mg level. This might also account for at least some of the variability between the preferred values and the measured data (Figure 2.4). Incomplete sample dissolution is a possibility, but thought unlikely since NIM-P did not show any significant partitioning effects from having a small amount of undissolved phases. The agreement amongst the standard analyses supports the internal reproducibility of the method. However, more analyses are required to resolve

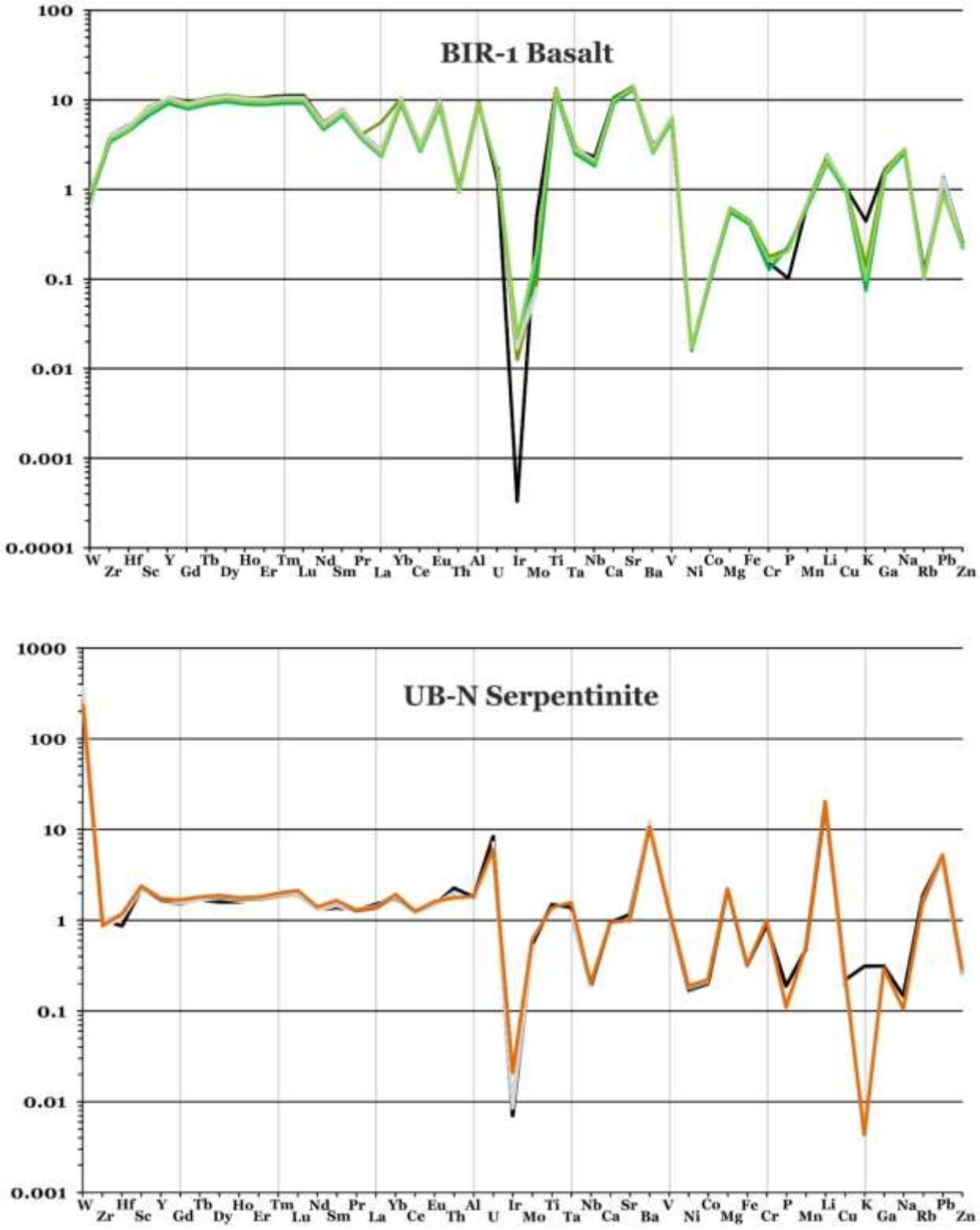

Figure 2.4 CI-normalised plots for the terrestrial standards sorted by decreasing $T_{C50\%}$ condensation temperatures. Normalisation values and condensation temperatures are from Lodders (2003) (see Appendix D, Table D-1).

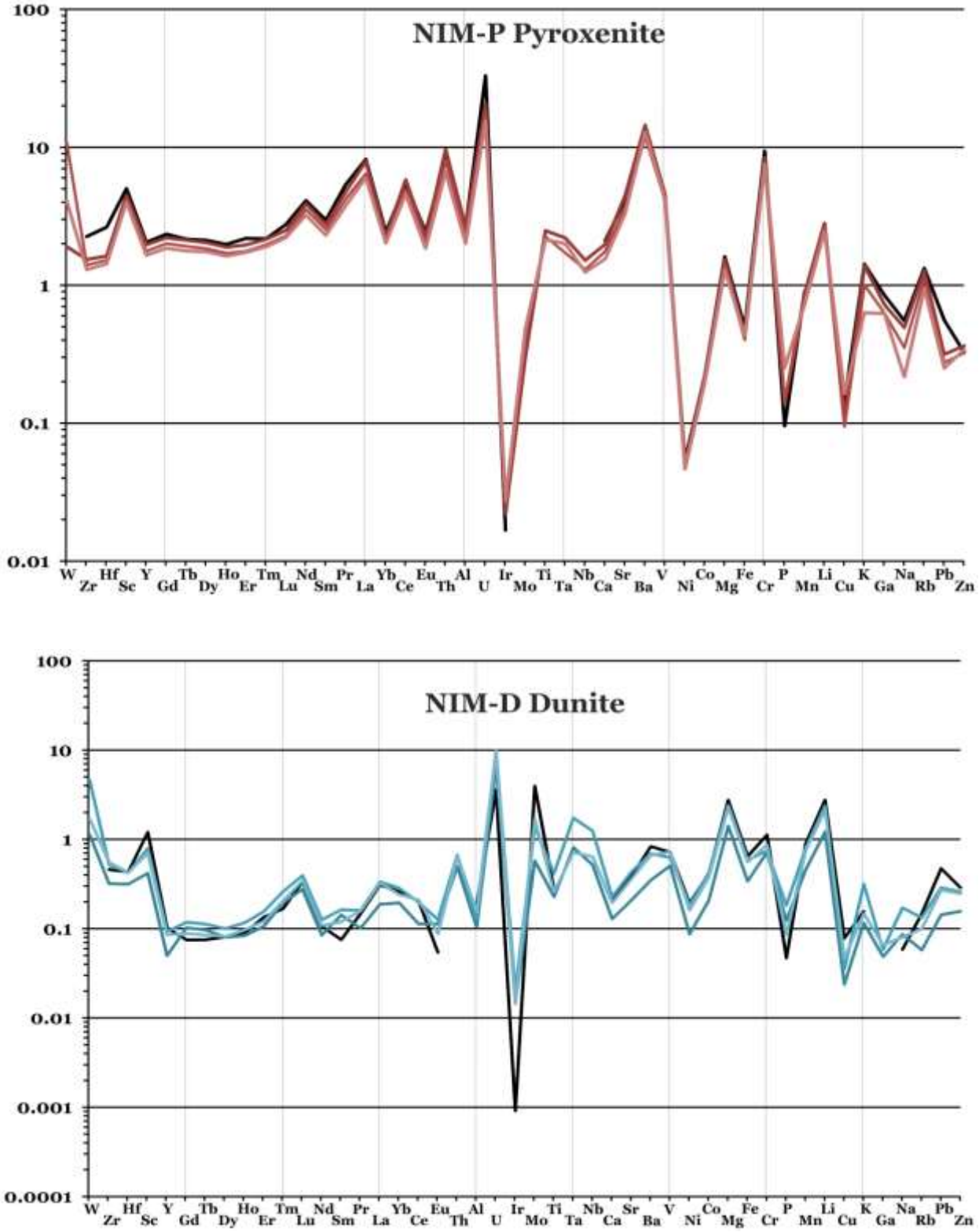

Figure 2.4 (continued) CI-normalised plots for the terrestrial standards sorted by decreasing $T_{C50\%}$ condensation temperatures. Normalisation values and condensation temperatures are from Lodders (2003) (see Appendix D, Table D-1).

the large discrepancies between published values and the data acquired in this study for NIM-D, NIM-P and PCC-1.

Repeat analysis of three solutions (standard BIR-1 and samples All-12 POP and Kar-6 PO) showed internal precision of better than 5% for most elements at 1SD (Table 2.4). Reproducibilities for the terrestrial standard and chondrule samples are mostly comparable, with the exception of Rb, Ba and Pb. Since the tendency is for the chondrules to have the slightly larger reproducibilities, it is suggested to be a matrix effect.

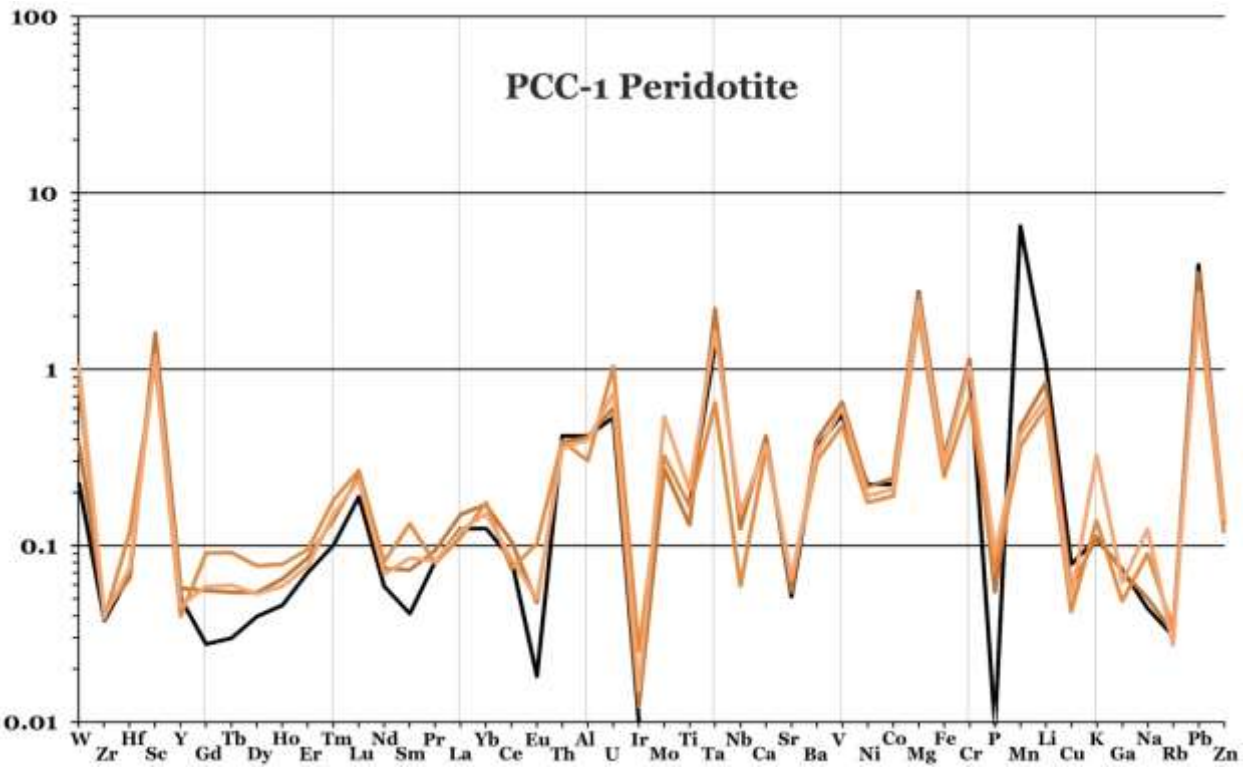

Figure 2.4 (continued) CI-normalised plots for the terrestrial standards sorted by decreasing $T_{C50\%}$ condensation temperatures. Normalisation values and condensation temperatures are from Lodders (2003) (see Appendix D, Table D-1).

Table 2.4 Internal reproducibility (RSD %)

		BIR-1	All-12	Kar-6
ICP-MS	W	2.8	2.8	0.8
	Zr	0.3	0.8	0.2
	Hf	0.3	1.1	2.1
	Sc	0.4	3.7	2.7
	Y	0.5	1.0	0.2
	Gd	0.4	0.8	1.5
	Tb	0.3	1.1	1.4
	Dy	0.3	0.4	1.0
	Ho	0.3	0.4	0.8
	Er	0.3	0.4	0.4
	Tm	0.5	0.3	0.9
	Lu	0.6	1.2	0.4
	Nd	0.1	0.4	0.3
	Sm	0.6	0.4	1.0
	Pr	0.4	0.5	0.8
	La	0.5	0.6	1.6
	Yb	0.2	0.3	0.5
	Ce	0.2	0.4	0.5
	Eu	0.2	0.6	1.4
	Th	2.3	0.6	2.9
	U	1.2	1.2	4.5
	Ir	2.7	0.6	0.2
	Mo	4.6	2.0	4.2
	Ta	0.3	0.5	2.3
	Nb	0.1	1.2	0.4
	Sr	0.4	0.4	3.2
	Ba	0.3	0.6	7.2
	V	0.2	3.3	3.3
	Ni	0.8	3.7	2.8
	Co	1.1	3.6	2.9
	Cr	0.2	3.4	3.0
	Li	0.1	1.5	0.9
	Cu	0.9	3.6	2.5
	Ga	0.2	2.1	1.5
	Rb	0.3	2.5	6.5
	Pb	1.3	5.4	25.2
	Zn	3.2	3.9	2.8

		UB-N	All-12 PO	Ac-4 PO	Ac-1 PO
ICP-OES	Al_2O_3	1.02	0.66	0.96	0.26
	Fe_2O_3T	0.84	0.84	0.47	0.30
	MnO	0.79	0.75	1.03	0.10
	MgO	1.23	0.19	1.87	0.18
	CaO	0.95	0.70	0.91	0.14
	Na_2O	9.30	0.88	1.76	0.40
	K_2O	57.53	31.77	5.78	6.53
	TiO_2	1.01	0.91	1.28	0.28
	P_2O_5	30.81	0.59	1.51	0.32

3 Results

3.1 PO(P) chondrules (Carbonaceous chondrites)

Major elements - Magnesium numbers (Mg#) for the PO(P) chondrules and WC (Whole Chondrules) span a wide range from 0.46 to 0.92 (Figure 3.1; Appendix D, Table D-2). Acfer 311 PO chondrules show the largest range (0.46-0.81) most likely reflecting varying amounts of metal, whereas Allendé PO chondrules have a slightly narrower range (0.70-0.92) likely related to the observed presence or absence of oxides

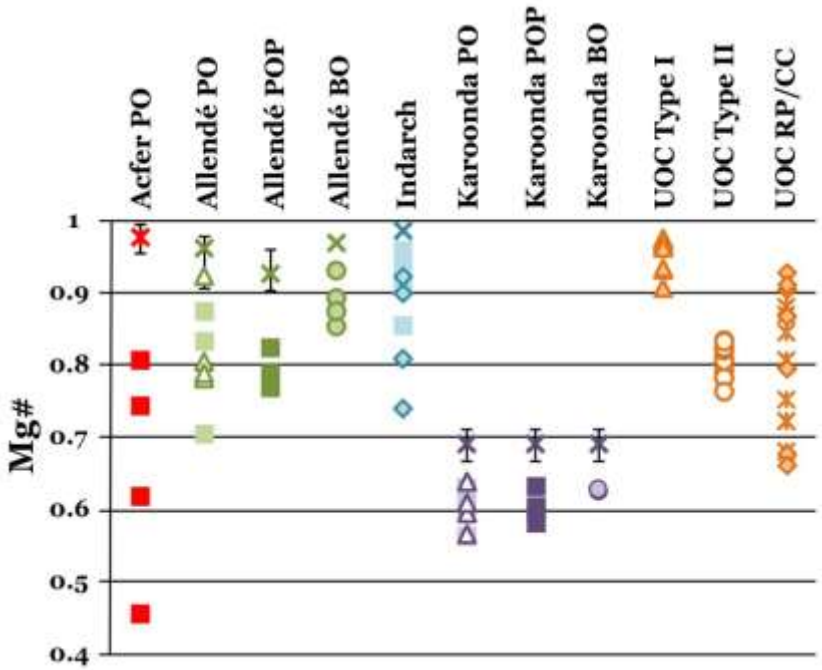

Figure 3.1 Magnesium numbers for analysed samples and UOC chondrule literature values. Crosses are published values for pure chondrule olivine with error bars representing ranges in Mg#. Error bars on published Indarch Mg# are smaller than the symbol.

(magnetite or chromite) and sulfides (troilite or pentlandite). Karoonda PO/WC chondrules have the narrowest range of Mg# for all the meteorites studied – 0.56-0.64. Allendé chondrules generally have the largest ranges in element concentrations of the chondrules in this study, and its WC chondrules are more enriched in the RLE compared to the PO(P). [RLE = W, Zr, Hf, Sc, REE, Th, Al, U, Ti, Ta, Nb, Ca, Sr, Ba, V]. In Karoonda, however, the RLE patterns in the WC and PO(P) chondrules are very similar and Karoonda chondrules in general have narrower ranges than those observed

in Allendé. Ranges in Acfer 311 are similar to those of Allendé. Plots of the major oxides versus Al_2O_3 (Figure 3.2) indicate that only CaO and TiO_2 correlate with Al_2O_3 in approximately solar (CI) proportions in all three meteorites, although the CaO/Al_2O_3 correlation is less well developed in Karoonda. On average Karoonda PO(P)/WC chondrules have the lowest measured Al_2O_3 concentrations while Allendé chondrules have the largest range and highest concentrations. Sodium oxide correlates with Al_2O_3 in non-CI proportions in Karoonda and to some extent in Allendé, but in the former the relationship is 1:4 and the latter is closer to 1:1.5. Potassium mostly does not correlate with Al_2O_3, except for a weak positive correlation in Allendé and is below the detection limit in most Karoonda PO(P)/WC chondrules. Iron(III)oxide, MnO and MgO have fairly narrow ranges for each meteorite and show no correlation with Al_2O_3, except for MgO in Acfer PO (slope=0.67, R^2=0.96). All chondrules (including the BO and Indarch chondrules) are enriched in MgO relative to CI and most are enriched in Al_2O_3, CaO and TiO_2. Karoonda and half the Acfer PO chondrules are the only samples with enrichment in Fe_2O_3 relative to CI. All PO(P)/WC (with the exception of Ac-1 PO) are depleted in MnO compared to solar values. Potassium oxide and Na_2O correlate only in Allendé WC and POP chondrules (slope=1.08, R^2=0.96 and slope=1.45, R^2=1.00 respectively) although the BO and PO chondrules trend roughly parallel to this.

Trace elements - Volatility patterns for the PO(P)/WC chondrule averages normalised to CI (Figure 3.3, 3.4 and 3.5; Appendix D, Table D-2) broadly follow the $T_{C50\%}$ pattern of the elements (Figure 3.6) and each meteorite is characterised by specific anomalies. The refractory elements are enriched relative to CI with mostly flat patterns, while moderately volatile and volatile elements become progressively depleted in an apparently erratic step-wise fashion roughly proportional to condensation temperature (Figure 3.6). Tungsten shows more variation than the other

Figure 3.2 (adjoining page) CI normalised major element oxides for studied samples. Black diagonal lines are 1:1 with CI.

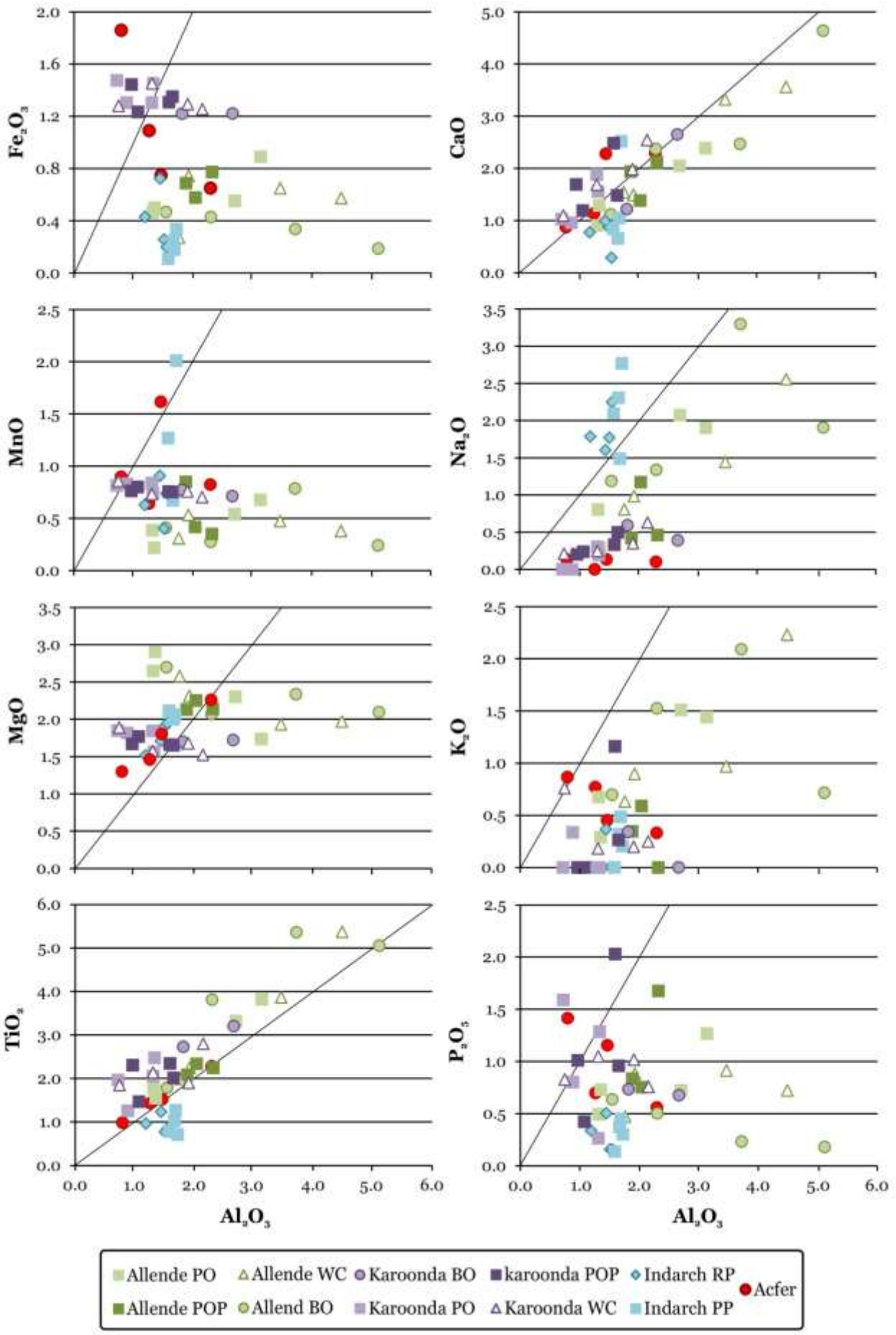
Fe2O3
CaO
MnO
Na2O
MgO
K2O
TiO2
P2O5
Al2O3
Al2O3
Allende PO
Allende WC
Karoonda BO
karoonda POP
Indarch RP
Acfer
Allende POP
Allend BO
Karoonda PO
Karoonda WC
Indarch PP

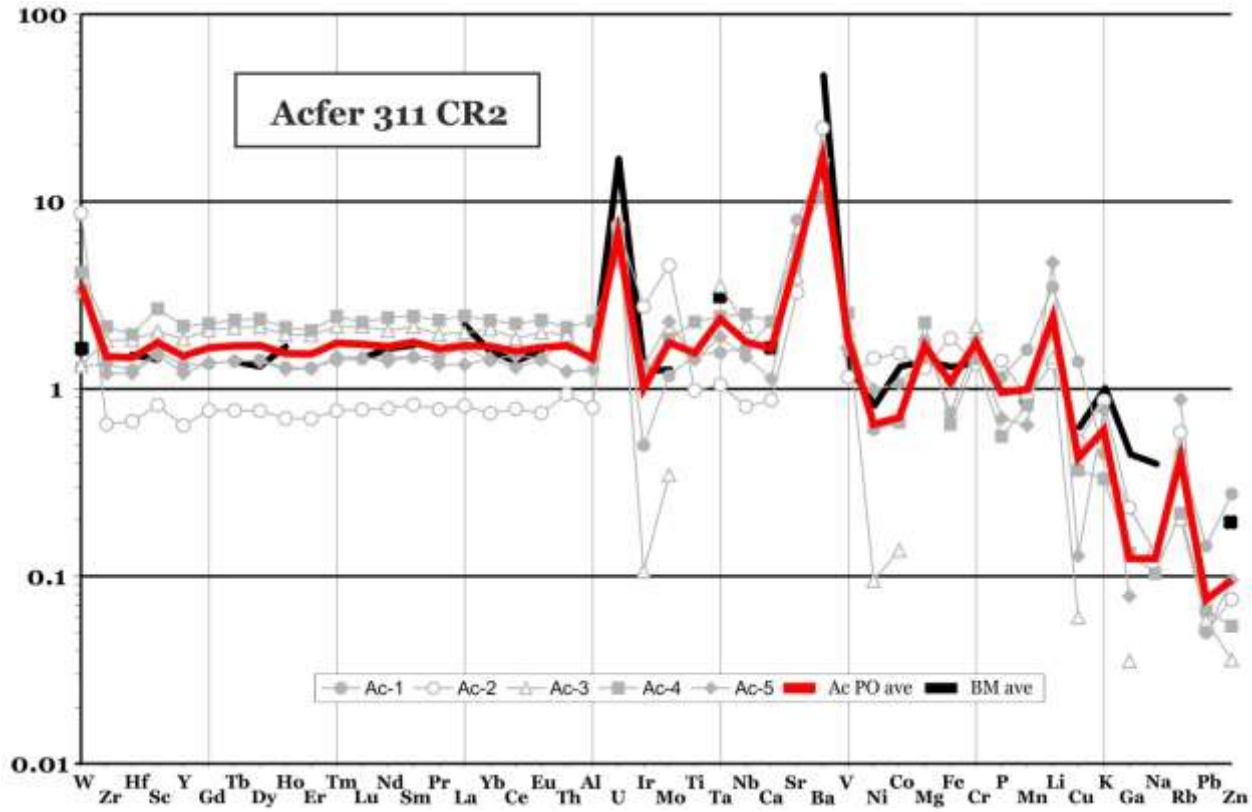

Figure 3.3 CI-normalised plots for analysed whole chondrules from Acfer 311 CR2 sorted by decreasing $T_{C50\%}$ condensation temperatures. Normalisation values and condensation temperatures are from Lodders (2003)

RLE and several chondrules show enrichment of W relative to Zr. The RLE in Acfer 311 are characterised by large positive U, Sr and Ba anomalies from aqueous alteration (Bischoff *et al.*, 1992), but otherwise have typically smooth and flat RLE patterns similar to those of Allendé. In contrast to this, Karoonda has more uneven RLE patterns that slope gently from Zr to Mn. The volatile lithophile patterns vary between chondrule types and meteorites, and to a smaller extent amongst individual chondrules. Acfer PO and Indarch chondrules show the only truly consistent volatile lithophile patterns, but in the former case this is most likely due to the aqueous alteration that also caused the large Ba and U anomalies. The volatile lithophile elements, however, show variable enrichment or depletion within a group of chondrules with no apparent volatility control. The siderophile and chalcophile elements are usually more depleted relative to the lithophile elements. The siderophile

elements show a rough correlation with decreasing condensation temperature. Negative anomalies in Ir, Co and also Ni and Fe are commonly observed. Zinc is almost always enriched relative to Pb. In Acfer 311 the samples with the largest RLE concentrations have the lowest siderophile element concentrations and *vice versa*, which is not observed in the other meteorites. Some elements show only small variation in concentration ranges, creating constriction nodes in the graphs. With the exception of Mg, these elements vary amongst the meteorites and less commonly amongst chondrule types. In Allendé, Mg is the only element that consistently shows a small concentration range in all of the chondrule types (Δ = ≤1.17), but others include: in the PO chondrules V; in the POP chondrules most of the RLE and Ir, and in the WC chondrules, Cr. In Karoonda, Mg, Mn, Fe and Zn create bottle necks in all the chondrule types (Δ=≤0.36, ≤0.15, <0.25 and <0.07 respectively), with W showing a small range in the WC. This effect is not appreciable in Acfer 311, besides U and Na that are probably homogenised due to aqueous effects (Kallemeyn & Wasson, 1982; Bischoff *et al.*, 1992).

Bulk meteorite values compiled from the literature (Appendix D, Table D-3) have patterns that generally show smoother trends than chondrules and narrower ranges in concentrations. These bulk rock data mostly fall within the ranges for the majority of the RLE data, but less so for the siderophile, chalcophile and volatile lithophile elements. Average bulk meteorite data and chondrule averages have very similar patterns for all chondrule types, including the BO and EC chondrules.

3.2 BO chondrules (Carbonaceous chondrites)

Major elements - Barred olivine chondrules of both Allendé and Karoonda show narrower ranges in Mg# than their corresponding PO(P)/WC chondrules – 0.85-0.93 in the former and 0.63 in the latter (Figure 3.1; Appendix D, Table D-2). Variations in Mg# are probably caused by differing proportions of Fe-sulfides. Major oxides for the BO chondrules overlap with those of their respective PO(P)/WC chondrules and fall on

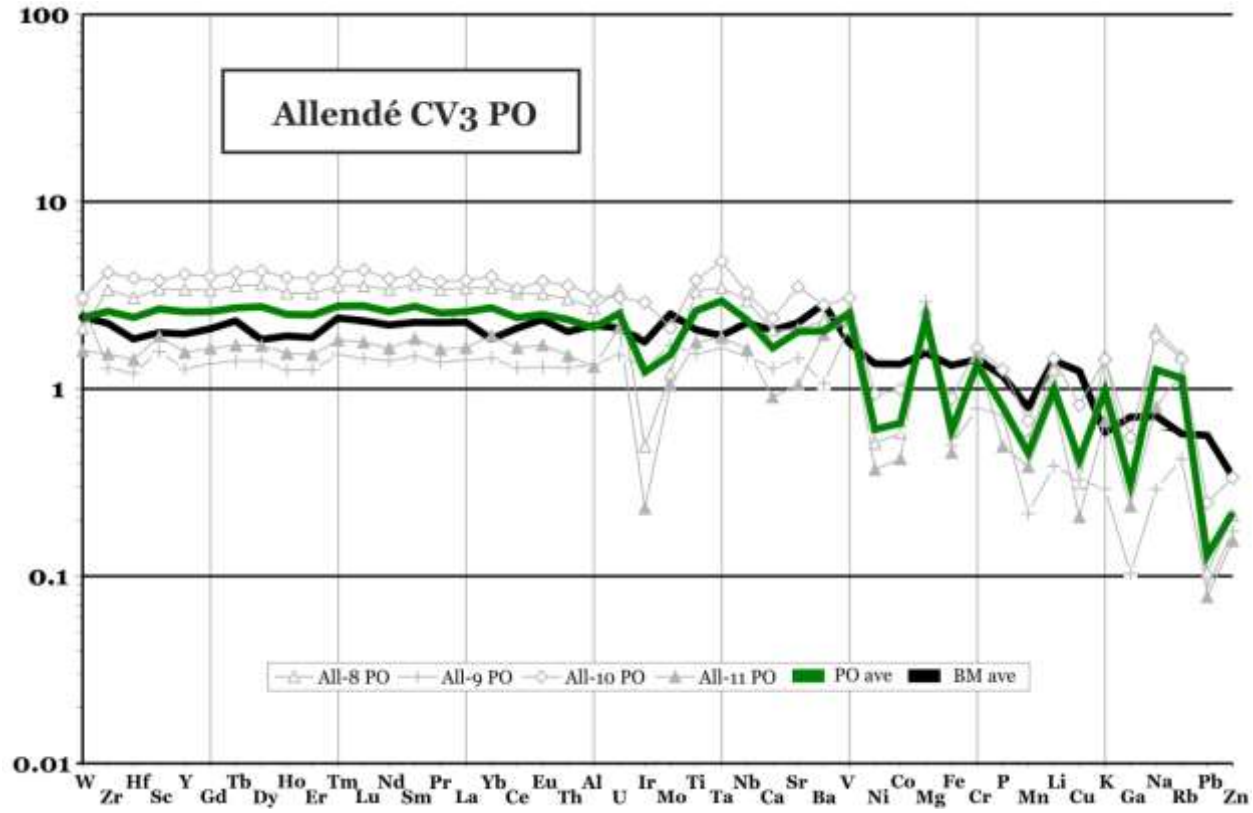

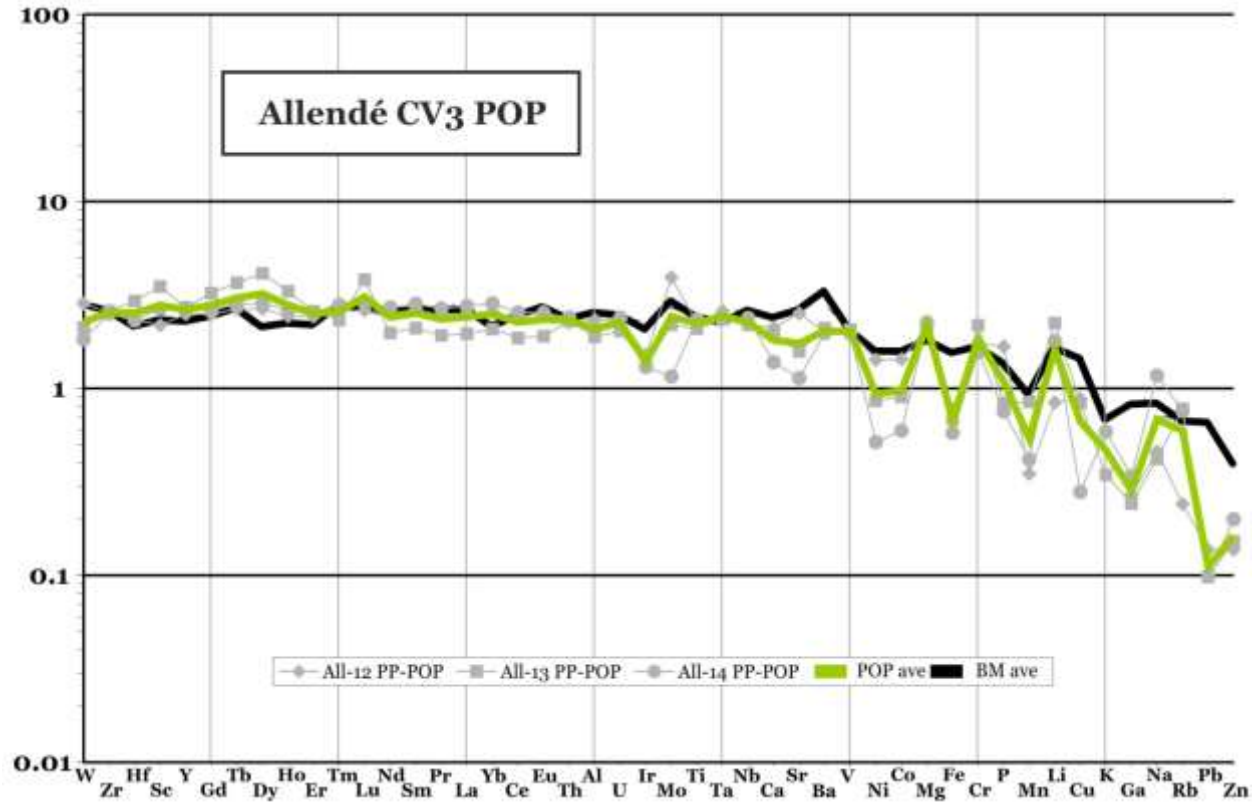

Figure 3.4 CI-normalised plots for analysed whole chondrules from Allendé CV3 sorted by decreasing $T_{C50\%}$ condensation temperatures. Normalisation values and condensation temperatures are from Lodders (2003)

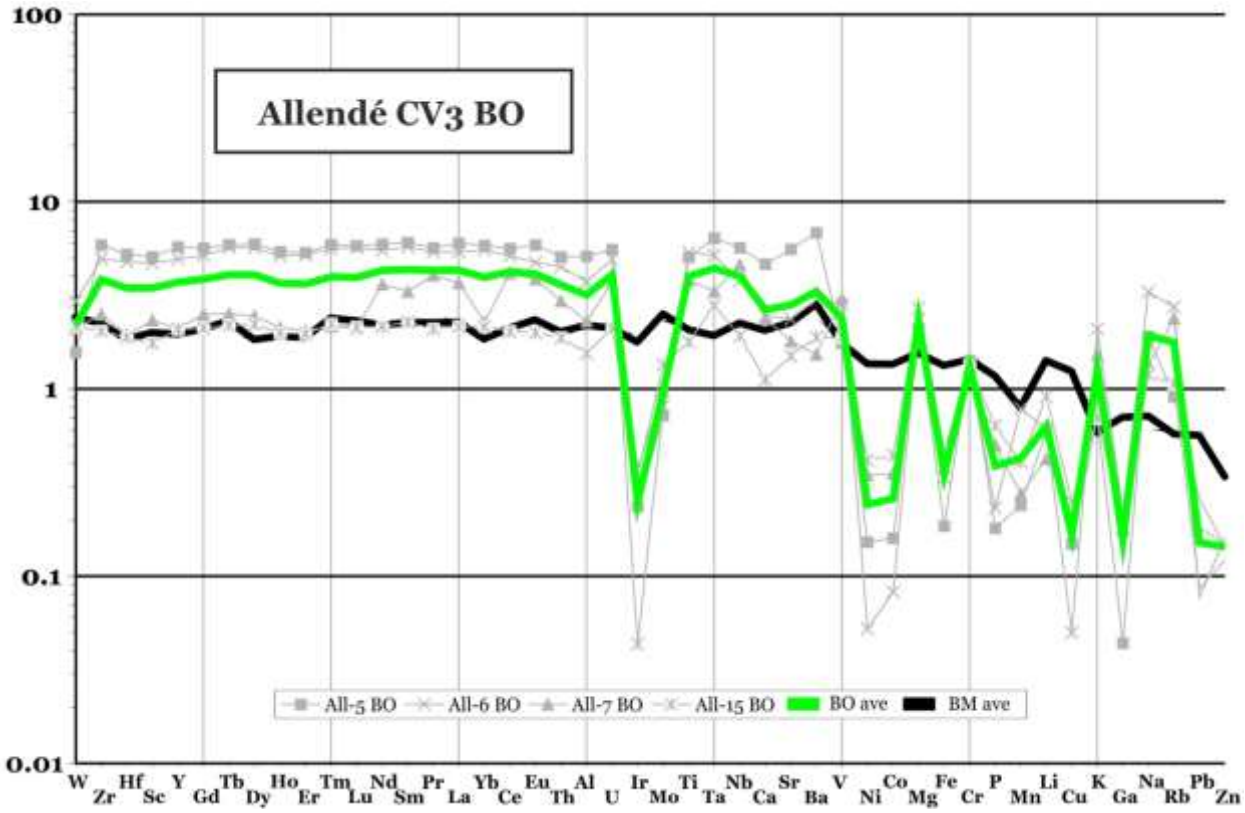

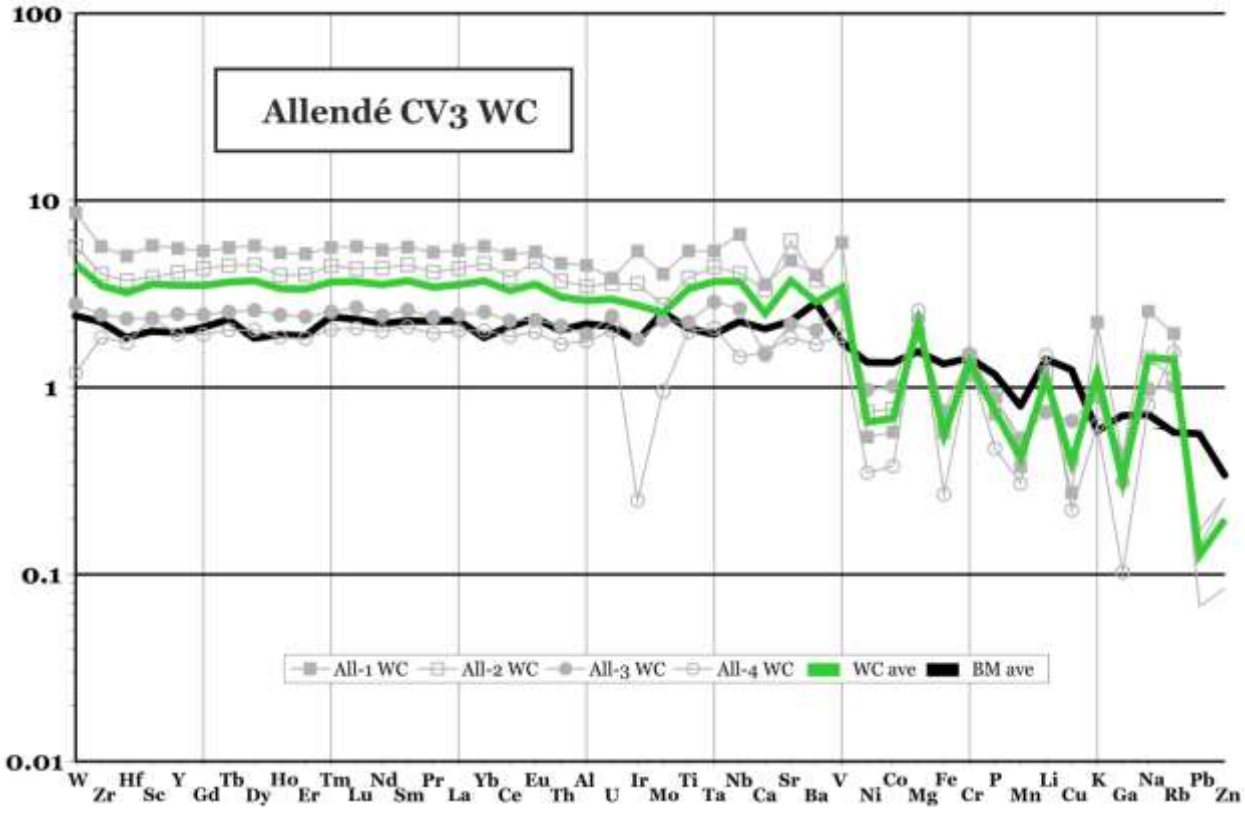

Figure 3.4 (continued) CI-normalised plots for analysed whole chondrules from Allendé CV3 sorted by decreasing $T_{C50\%}$ condensation temperatures. Normalisation values and condensation temperatures are from Lodders (2003)

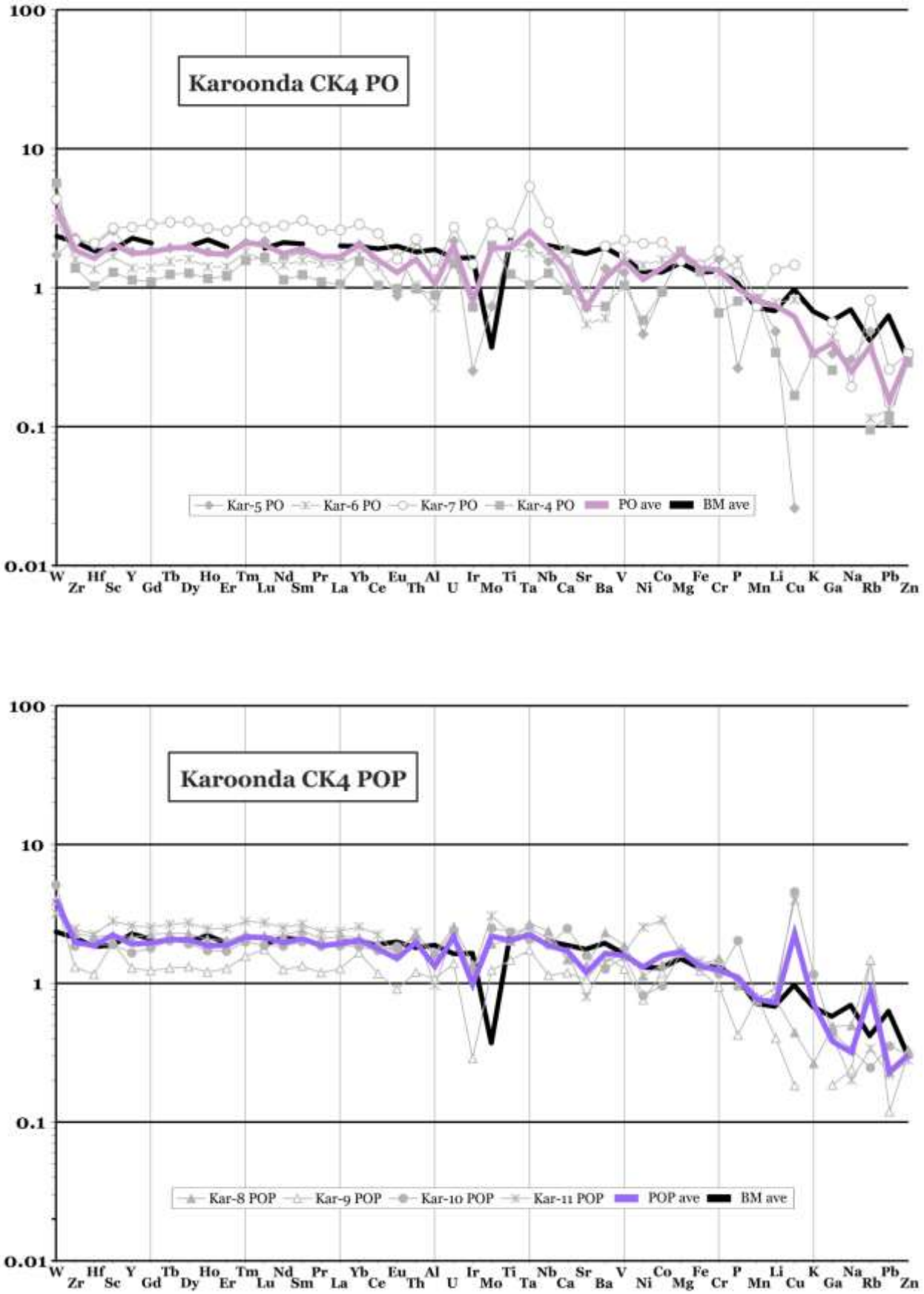

Figure 3.5 CI-normalised plots for analysed whole chondrules from Karoonda CK4 sorted by decreasing $T_{C50\%}$ condensation temperatures. Normalisation values and condensation temperatures are from Lodders (2003)

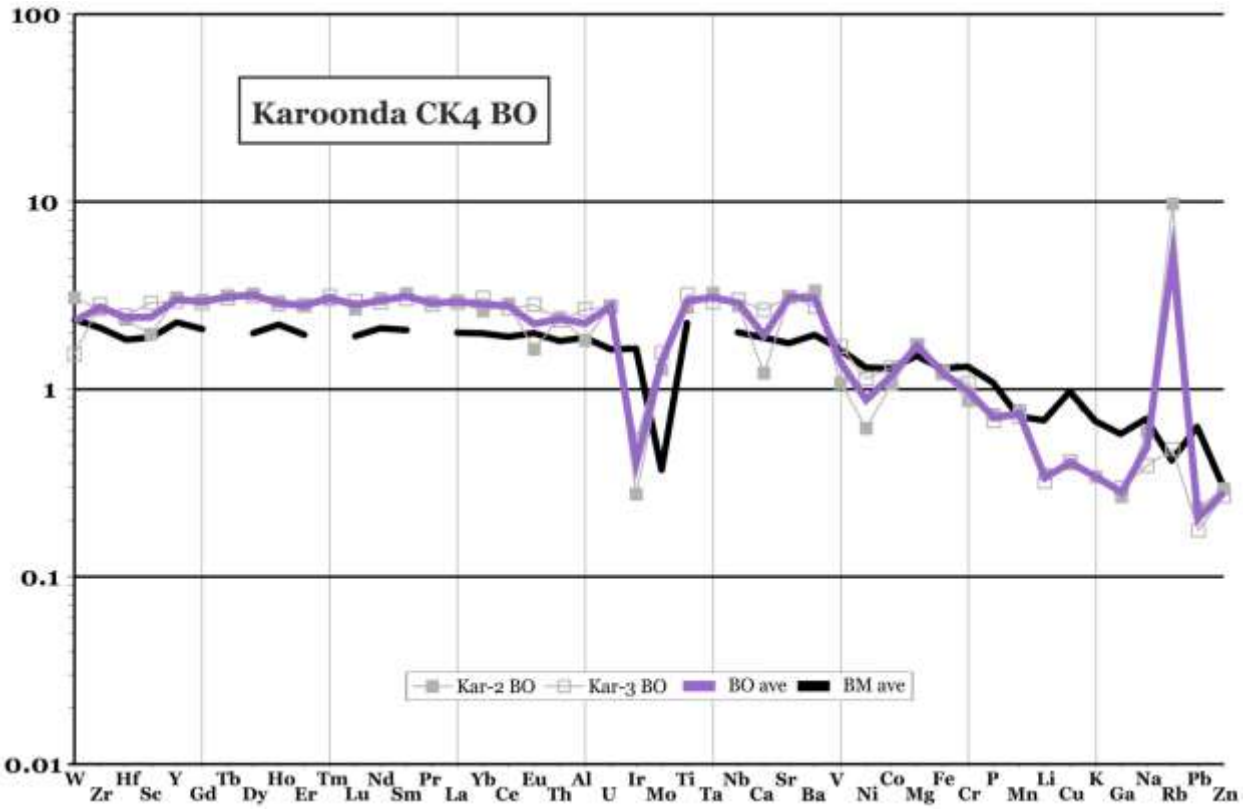

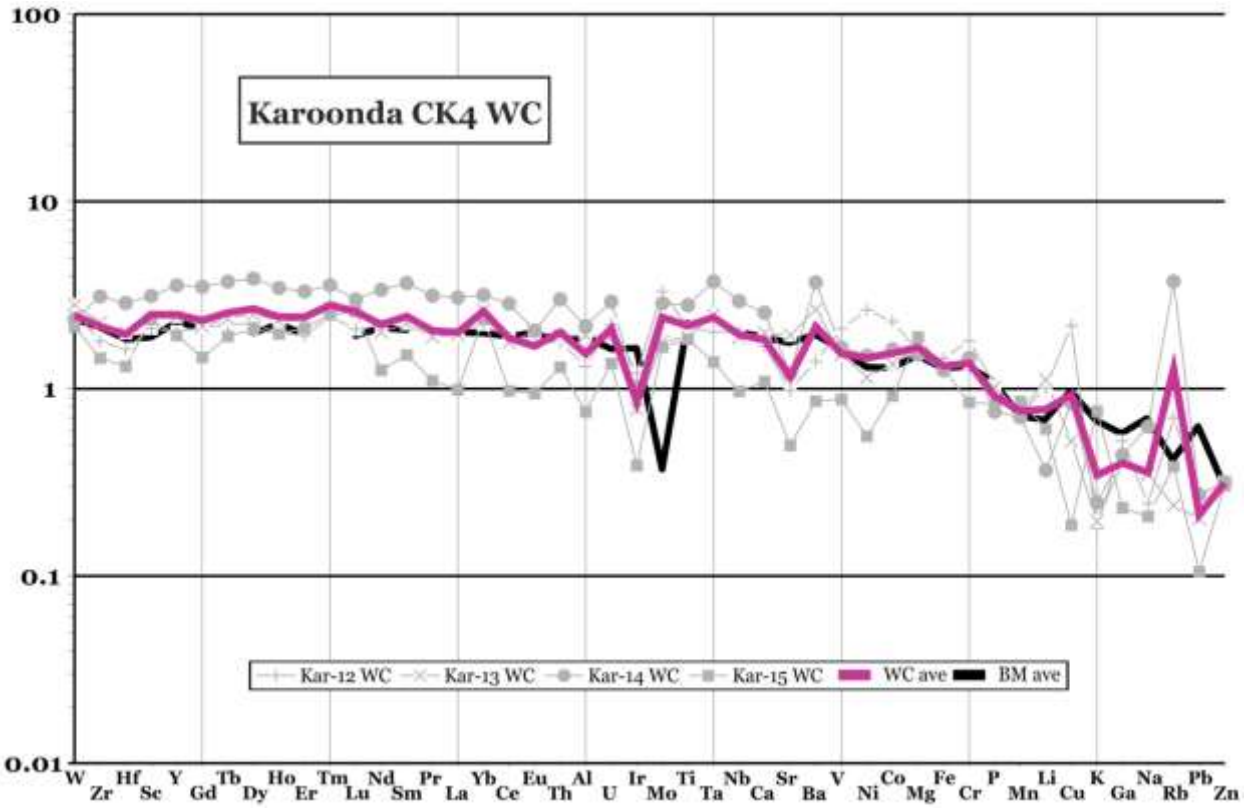

Figure 3.5 (contined) CI-normalised plots for analysed whole chondrules from Karoonda CK4 sorted by decreasing $T_{C50\%}$ condensation temperatures. Normalisation values and condensation temperatures are from Lodders (2003)

similar trends. The BO tend to be slightly more enriched in Al_2O_3 than the porphyritic olivine chondrules. Karoonda BO are also on average slightly enriched in TiO_2, Na_2O and slightly depleted in Fe_2O_3 compared to the PO(P)/WC (Figure 3.2).

Trace elements – Allendé and Karoonda BO chondrules show similar RLE pattern to their corresponding PO(P)/WC chondrules (Figure 3.4, 3.5; Appendix D, Table D-2) but are notably more depleted in siderophile elements compared to the PO(P)/WC chondrules. In Allendé BO chondrules, Mg, Cr and Zn create constrictions. The two Karoonda BO chondrules, however, have identical concentration for most elements, except Sc, Eu, Al, Ca, V, W, Ir, Ni, Na and Rb.

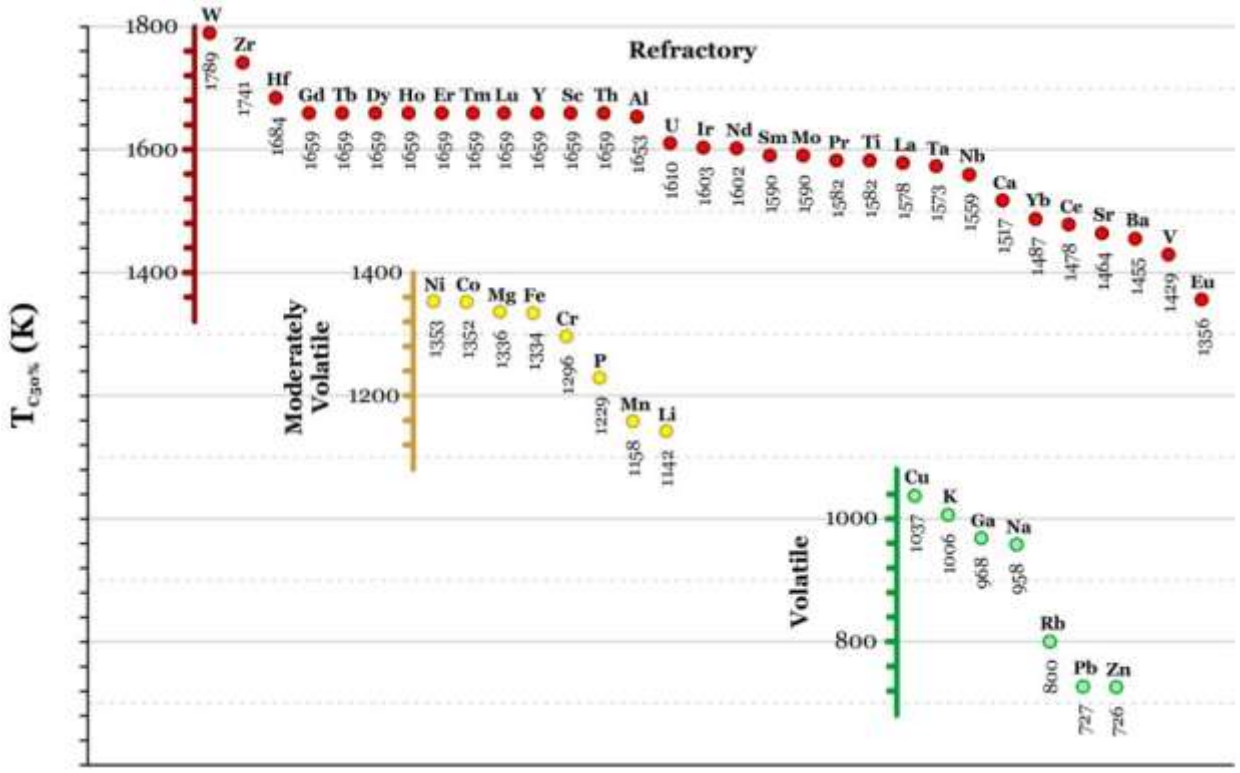

Figure 3.6 Elements sorted by decreasing $T_{C50\%}$. Refractory elements = red. Moderately volatile elements = yellow. Volatile elements = green. Condensation temperatures from Lodders (2003).

3.3 Pyroxene chondrules (Indarch EH4)

Major elements - Chondrules from Indarch have similar ranges in Mg# as observed in Allendé (0.96-0.74), although the RP have a notably larger range (0.72-

0.94) than the PP (0.86-0.96) (Figure 3.1; Appendix D, Table D-2). In terms of major element oxides Indarch chondrules mostly overlap with the CCh chondrules but have some of the lowest measured values for Fe_2O_3, CaO, TiO_2 and P_2O_5 and some of the highest Na_2O of all chondrules in this study. However, they are the only chondrules for which neither CaO nor TiO_2 show a solar relationship to Al_2O_3 probably due to their small range in Al_2O_3 (Δ_{Al2O3}=0.53 wt% compared to Allendé Δ_{Al2O3}=3.80 wt%). In the Indarch PP, MgO correlates to Al_2O_3 (slope=1.16, R^2=0.92) but not in the RP. All Indarch chondrules are enriched in Na_2O and depleted in Fe_2O_3, P_2O_5 and K_2O relative to CI, the latter which is below detection in three out of four RP and one PP chondrule. Sodium oxide and K_2O in the PP correlate negatively in non-CI proportions (slope=-4.57, R^2=1.00). Some Indarch PP chondrules are also enriched in MnO.

Trace elements - Indarch chondrules (and bulk meteorite) resemble CI more than any other studied objects, although significant variation occurs for some elements in the chondrules, particularly the lithophile and chalcophile elements (Figure 3.7; Appendix D, Table D-2). In contrast to chondrules from the Carbonaceous chondrites for which Mn (moderately volatile) is usually depleted relative to Zr (highly refractory), both these elements are roughly equally abundant in the EC chondrules. Tungsten, Hf and Zr and Sc are commonly depleted relative to Y, which is not observed in any of the CCh chondrules. For Ti to Mn the RLE have no obvious systematic variation, although the average pattern remains at 1 xCI. Magnesium and Al are the only major constricting RLE, along with Sc in the RP. The siderophile and chalcophile element patterns appear to be fairly similar for the RP and PP, but can be distinguished easily by their Mo/W (>0.5 and <0.4 respectively) and Fe/P ratios (>1 and <1 respectively). The siderophile and chalcophile elements in Indarch chondrules do not show the general decrease with decreasing condensation temperature observed in the CCh chondrules. With the exception of Cu (and in some samples W and Pb in the PP) the siderophile and chalcophile elements are all depleted relative to CI and to most of the

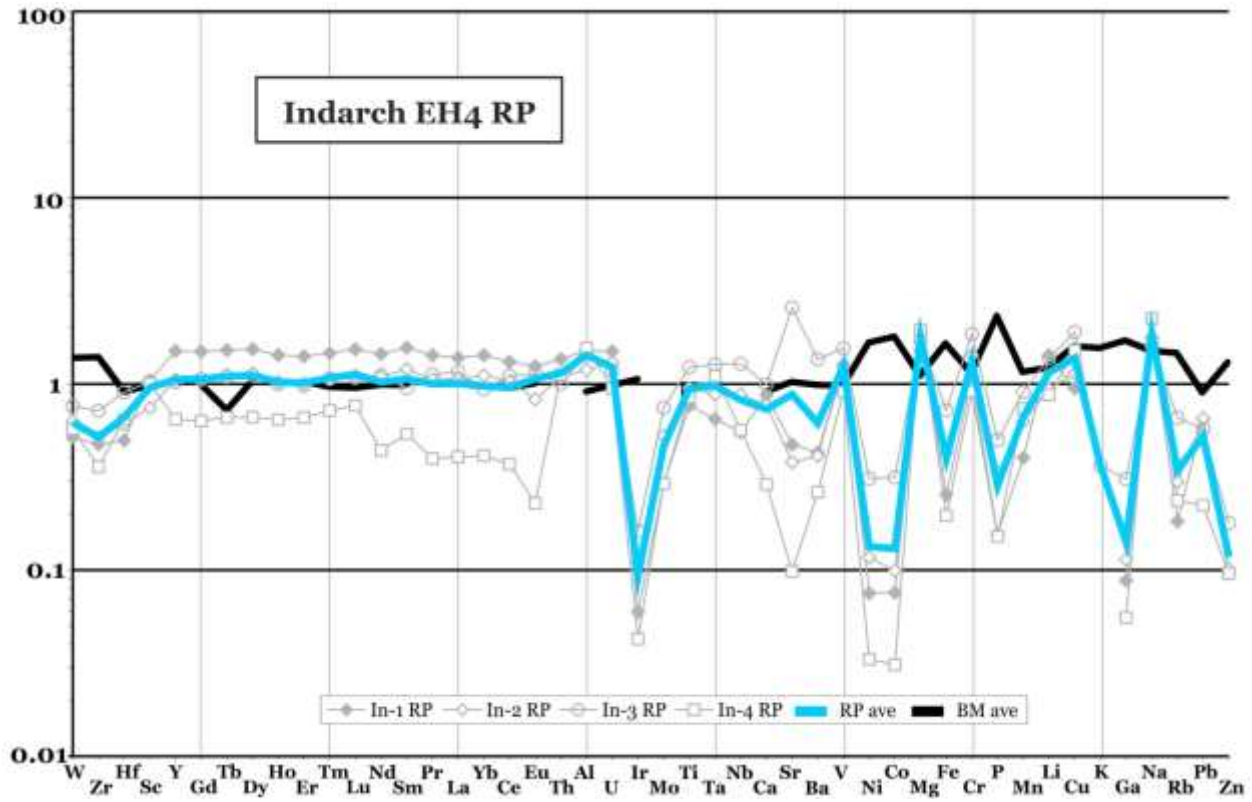

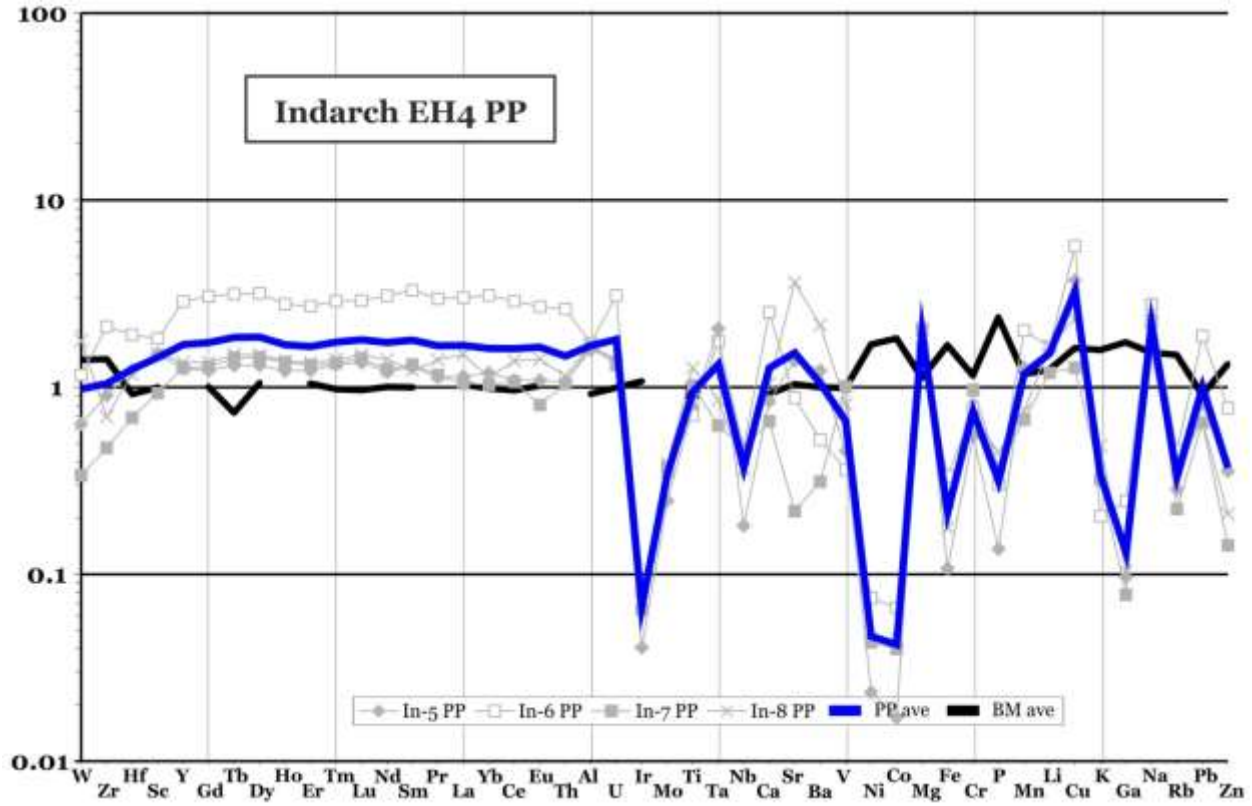

Figure 3.7 CI-normalised plots for analysed whole chondrules from Indarch EH4 sorted by decreasing $T_{c50\%}$ condensation temperatures. Normalisation values and condensation temperatures are from Lodders (2003)

RLE. Chalcophile elements on average are almost at equal levels or slightly enriched relative to the lithophile elements, which is also not observed in any of the CCh chondrules. Volatile lithophile elements in the Indarch RP and PP chondrules are essentially identical, showing enrichment in Li and Na relative to CI. Sodium is also slightly enriched relative to the bulk meteorite. A positive correlation is observed between Ca (as proxy for sulfides) and the amount of REE, and an inverse correlation between the amount of REE and size of the negative Eu and Yb anomalies.

In contrast to the chondrules, the bulk meteorite pattern for Indarch does not deviate considerably from 1 xCI for all elements (Figure 3.7; Appendix D, Table D-3).

4 Constraints from comparisons to known components

4.1 Conformation and deviation from solar elemental relationships

A distinctive feature of the CCh and EC chondrules is the largely unfractionated compositions for the RLE ratios relative to CI. In particular the major oxides CaO, TiO_2 and Al_2O_3 of the measured chondrules strongly suggest a relatively primitive nature for the precursor materials of the CCh and EC chondrules since they maintain their close to solar abundances. The CR chondrites have already been described as the most primitive chondrite group by authors such as Kong & Palme (1999) based on solar Cr/Mg ratios. This is further highlighted by the correlation of MgO and Al_2O_3 in Acfer 311 chondrules, which is not observed in the other CCh. Some of the scatter of the major element oxides along the 1:1 slopes is likely due to minor differences in the minerals sampled by the precursor materials, similar to the effect observed for CAIs (Sylvester *et al.*, 1993). The variation in the precursor materials would have to be limited, however, since a wide range in compositions would lead to more scatter in the data. The even stronger 1:1 correlations for CI normalised data of Ni:Co and Lu:Hf (Figure 4.1) present further evidence of a lack of extreme processing. Nickel and Co will remain together in a single-phase metal (e.g. Wasson & Rubin, 2010) under reducing conditions, but can fractionate from each other in silicate and sulfide phases under more oxidizing conditions (e.g. Ehlers *et al.*, 1992; Hirschmann & Ghiorso, 1994). The obvious exceptions from the Solar Ni:Co trend are the Karoonda chondrules. The CK meteorites are amongst the most oxidized chondrites known and contain almost no metal (Righter & Neff, 2007; Hutchison, 2004). The subsequent high concentration of Fe in olivine has a significant control on the compatibility of Ni and Co (Hirschmann & Ghiorso, 1994), the former preferentially partitioning into the olivine structure at higher Fe content. The additional presence of sulfides such as pentlandite and pyrrhotite helps to further fractionate these elements since Co is slightly more compatible in pyrite than in pentlandite (e.g. Geiger & Bischoff, 1995). However,

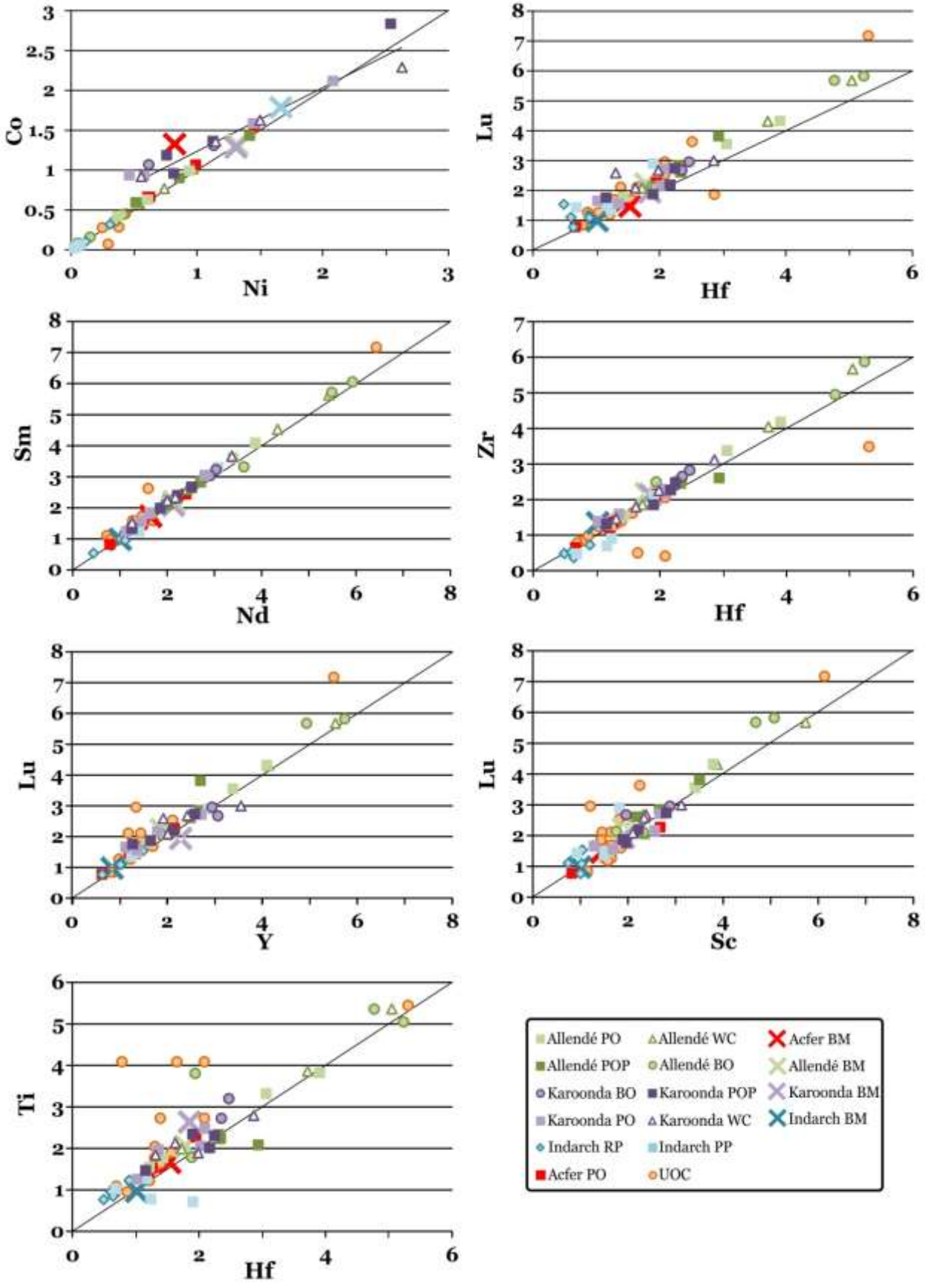

Figure 4.1 CI normalised trace element plots for analysed samples and published UOC whole chondrule and bulk meteorite data (for references see Appendices, Tables D-3 and E-1). Black diagonal lines are 1:1 with CI.

despite the non-solar relationship between Ni and Co in the CK chondrules, the bulk meteorite still plots on a solar slope and is identical to the Ni:Co ratio for the Allendé bulk. Lutetium:Hf data for the chondrules produce a similar tight correlation, although the Karoonda WC, Allendé POP and Indarch chondrules have Lu:Hf ratios deviate slightly from solar. It should be noted, though, that they still plot within close proximity of the main 1:1 trend of chondrules. Despite the variation observed amongst the chondrules, bulk meteorite Lu:Hf values for all the samples plot along the solar trend. Other element ratios that closely follow the Solar compositions are Sm:Nd, Hf:Zr, Y:Lu, Sc:Lu and Hf:Ti (Figure 4.1). Deviations from the relative solar element abundances amongst the refractory elements are mostly observed for W, Ir, Mo, Ta, Nb, Sr, Ba and V.

4.2 Comparison to UOC chondrules and chondrule discrimination plots

The UOC chondrules, both porphyritic and non-porphyritic show similar enrichments in the RLE relative to CI observed in the CCh and EC chondrules analysed in this study (Figure 4.2; Appendix E, Table E-1). The porphyritic UOC chondrules mostly appear to have similar volatility patterns to the CCh chondrules (i.e. relatively flat RLE decreasing through the more volatile elements), while the RP/CC chondrules have patterns similar to those of the EC chondrules, which are flat on average. The resemblance between the EC and fine grained UOC chondrules is furthered by the relative depletion of W and in some cases Zr and Hf relative to the other RLE. Furthermore, all UOC chondrule data for Ir, Ni, Co and Fe show similar roughly correlating depletions in these elements relative to the lithophile elements as observed in the CCh and EC chondrules. Plots of major element oxides plotted against Al_2O_3 for the UOC chondrules indicate similarly narrow ranges in MgO abundances (1.64-2.48 xCI; Figure 4.3) that span the same compositional range as the analysed samples (1.30-2.91 xCI). Differences include the total lack of correlation between MgO, FeO and Al_2O_3, and the sub-chondritic correlation of CaO, TiO_2 and Al_2O_3. Phosphorous is

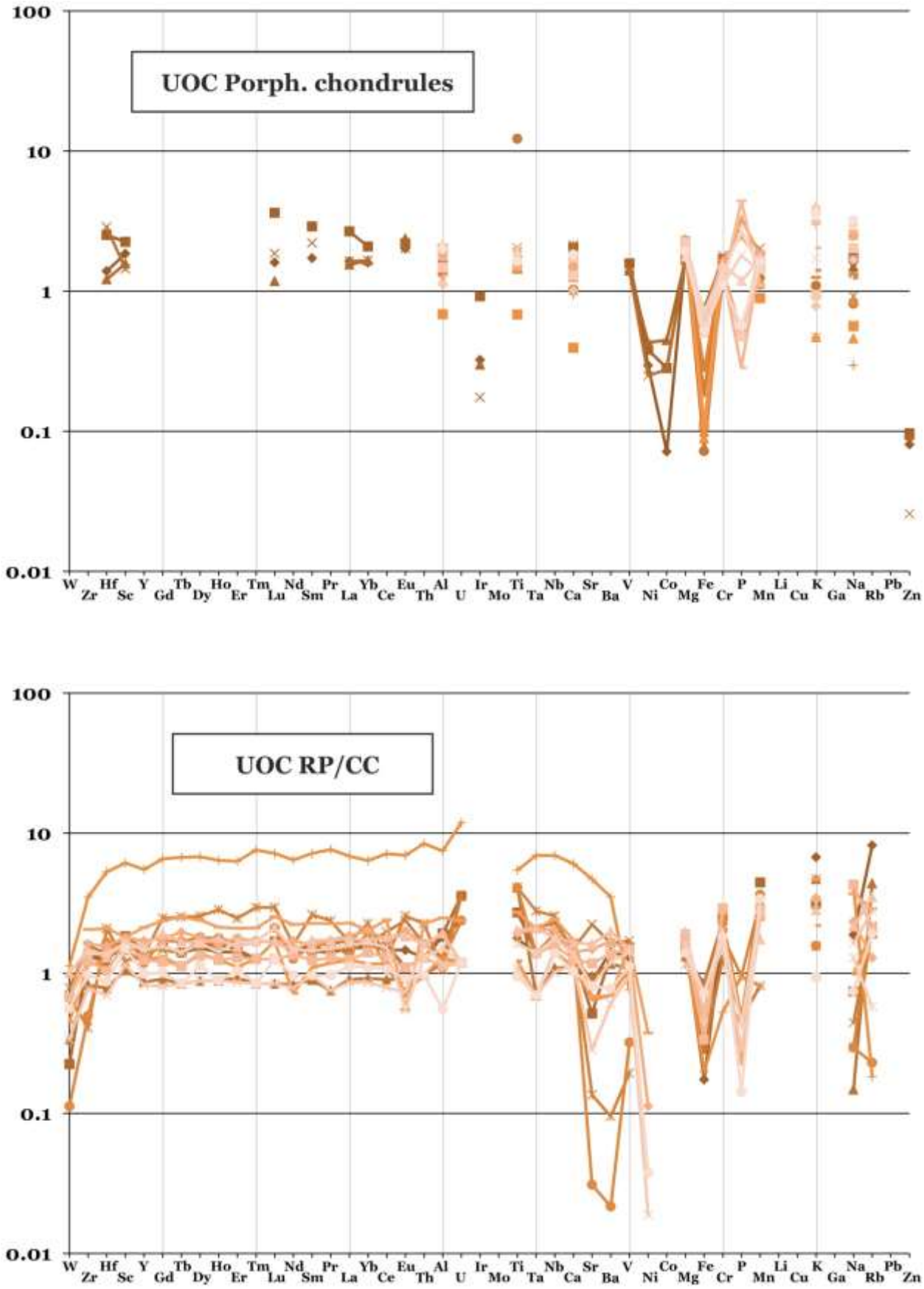

Figure 4.2 CI-normalised plots for published data of whole porphyritic (top) and non-porphyritic (bottom) chondrules from UOC sorted by decreasing $T_{C50\%}$ condensation temperatures. Normalisation values and condensation temperatures are from Lodders (2003)

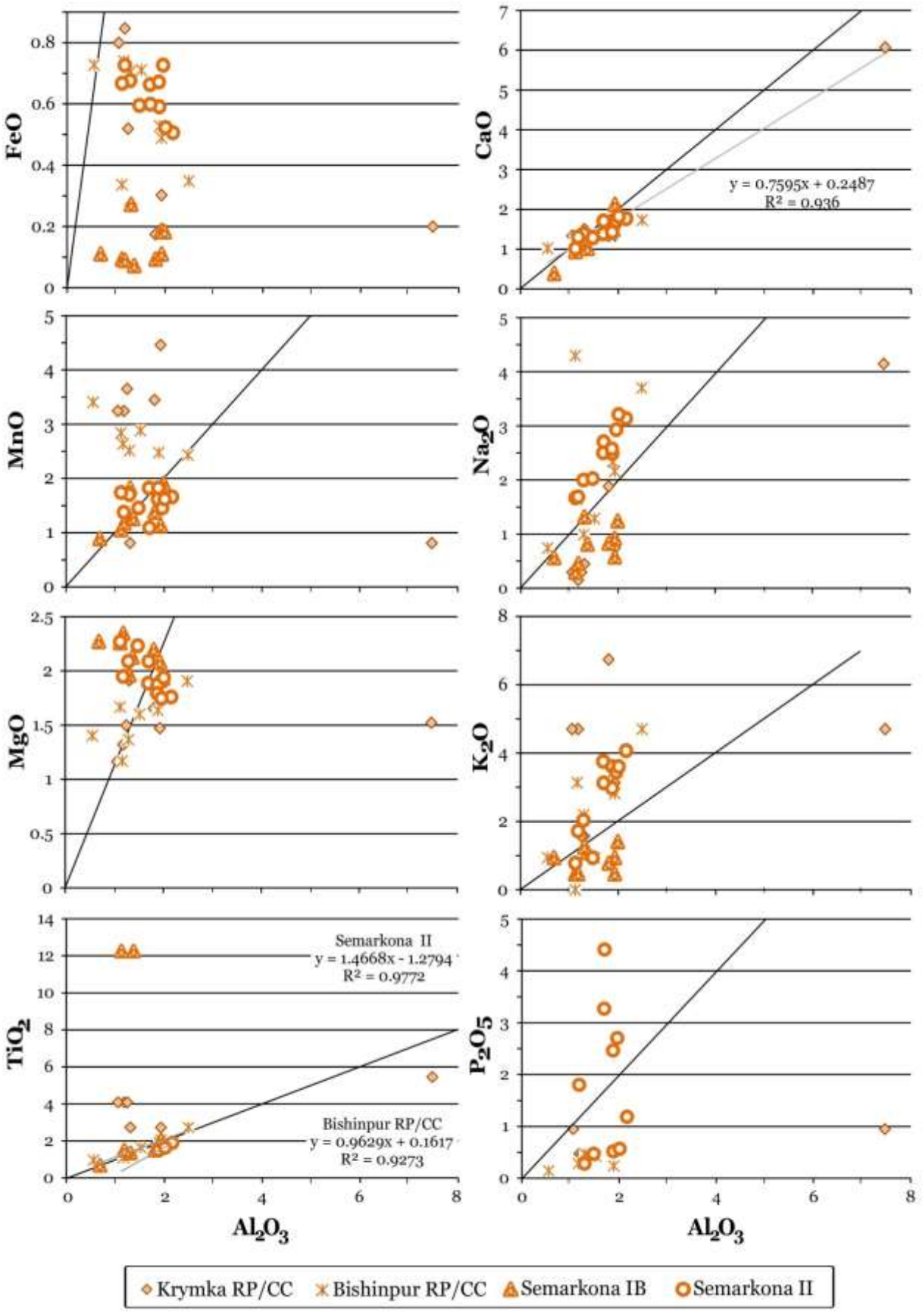

Figure 4.3 CI normalised major element oxides for published UOC chondrule data. Black diagonal lines are 1:1 with CI. Gray diagonals are regression lines.

mostly enriched in the UOC chondrules relative to Cr and shows no correlation to Fe - this is contrary to the CCh/EC chondrules, except for a few Karoonda chondrules.

Sears *et al.* (1992) proposed a purely chemical classification of chondrules based on the *in situ* measurement of CaO and FeO content of chondrule olivine (Figure 4.4a). Although this classification scheme is based on single mineral chemistry and designed to act as a thermometer, the applicability of CaO vs. FeO plots for whole chondrule data was tested given that whole chondrule CaO and FeO will vary based on mineralogy e.g. the presence of metal or mesostasis/feldspar. Distinct groupings of chondrule types within CaO-FeO-space might imply different source material leading to different major mineralogies, whereas correlations of FeO-CaO could highlight evolution of the chondrule/source material or mixing of components. Figure 4.4b plots CaO vs. FeO whole chondrule data for a variety of UOC ferromagnesian chondrules from Semarkona LL3.0 (see Appendix E, Table E-1 for references). Good distinction is made between Semarkona type I and II chondrules, suggesting that they may have had distinct source material with no common composition (the two groups do not appear to converge to a common point) or were produced at distinct points in time from the same reservoir. The low FeO values and narrow range in the type I chondrules likely reflect the general lack of metal in the LL3.0 chondrites. The type II chondrules, in contrast, show a weak negative correlation between CaO and FeO, which may be the result of 'dilution' of the mesostasis by troilite and chromite (Jones, 1990). The Semarkona RP/CC chondrules overlap with both type I and II chondrules making additional textural identification essential. Based on Figure 4.4b, the precursor material for Semarkona RP/CC chondrules appears to be similar to that of both the type I and II chondrules and they apparently have not undergone any mixing/fractionation. Application of the CaO vs. FeO plot to the samples analysed in this work provides mixed results. From Figure 4.4c it is obvious that a large amount of overlap exists for chondrules from several types of meteorite when plotted together. Despite this overlap between the CCh and

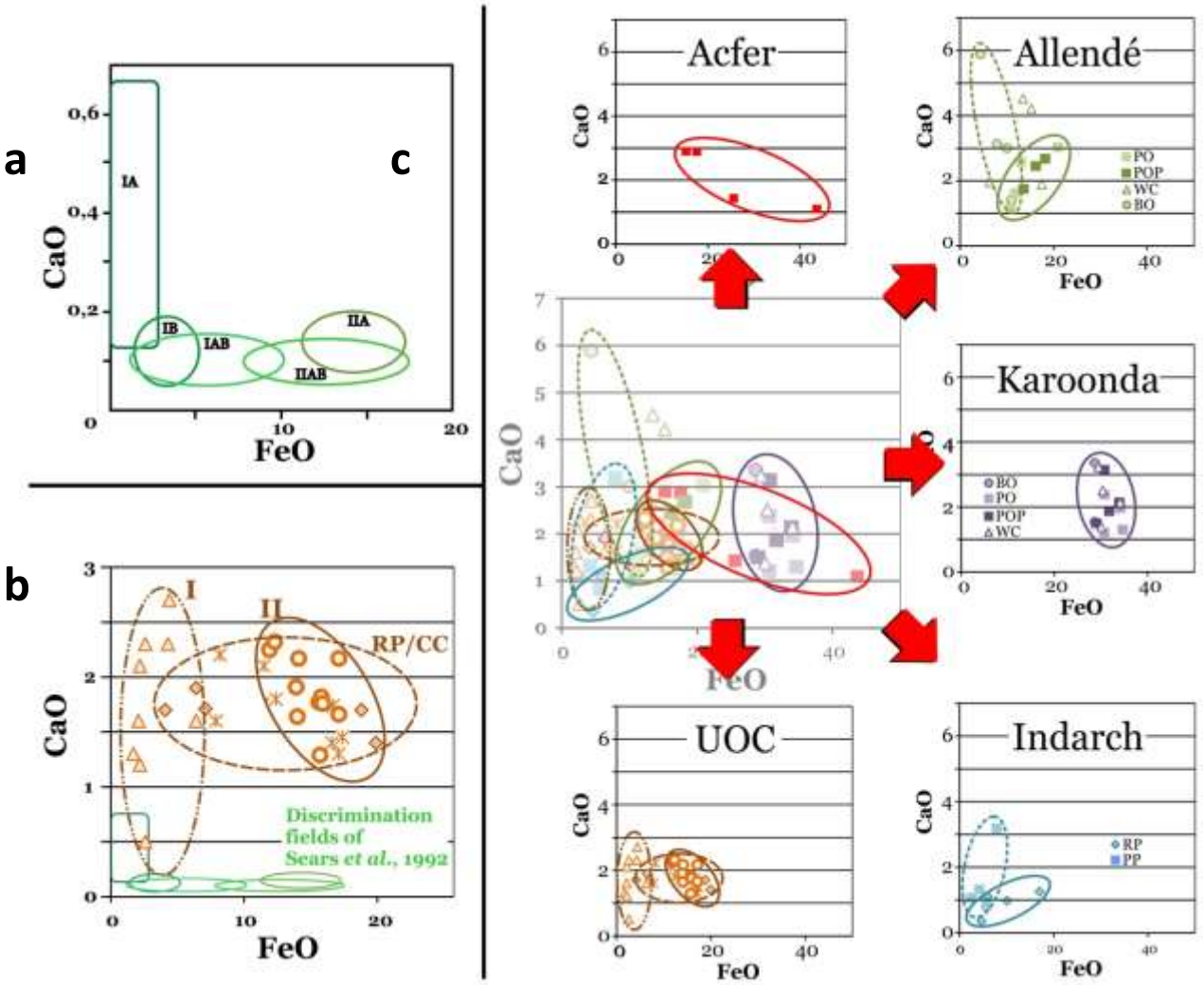

Figure 4.4 Chemical classification of chondrules based on raw CaO vs. FeO values. a) Original discrimination fields of Sears *et al.* (1992) based on CaO and FeO in *chondrule olivine only* determined by EMPA. b) Plotting CaO vs. FeO for whole chondrule UOC data shows that the original fields of Sears *et al.* (1992) are obviously not applicable to whole chondrule data. However, the plot itself still proves to be useful and new discrimination fields can be defined to distinguish between type I and type II UOC chondrules based on whole chondrule data. c). Central plot – Data from the studied samples and the UOC data show a large amount of overlap. However, plotting the meteorites individually shows that the plot distinguishes between trends in the Allendé BO and PO(P) (top right) and Indarch RP and PP (bottom right). Karoonda chondrules plot distinctly from all meteorites except Acfer, but no internal distinction is possible.

UOC chondrules, particularly between the CV (Allendé), EH (Indarch) and UOC (Semarkona), individual CaO vs. FeO plots for the different meteorites suggests that they all have distinct starting compositions for their chondrules. Chondrules from Karoonda are easily distinguished from all other groups, except Acfer PO, although no distinction is possible amongst different types of Karoonda chondrules. Karoonda chondrules have the narrowest ranges for FeO observed in any of the CCh meteorites in

this study and show no correlations between FeO and CaO. Most chondrules cluster around FeO ~30 wt% and CaO ~1 wt%. In contrast, Allendé, Indarch and UOC chondrules overlap significantly. Allendé PO(P) and BO chondrules plot in two well-defined group with distinctive trends that converge to a single point (FeO ~10 wt%, CaO ~1 wt%), suggesting a common precursor. The Allendé WC chondrules show a significant amount of scatter suggested to be a result of the fine grained and mineralogically variable rims that are volumetrically more abundant in these samples. Negative trends in the BO chondrules are likely to reflect differing proportions of sulfides while the positively trending PO(P) chondrules show increases in the amounts of opx and plagioclase. Indarch RP and PP chondrules also plot in two distinct but converging fields suggesting a common origin (FeO ~3 wt%, CaO ~0.3 wt%). Differences in the trends most likely reflect the larger proportion of mesostasis and sulfides in the PP chondrules compared to the RP. Since CaO and FeO are both located in sulfides in the E chondrites, relationship between the two elements will be positive in contrast to that of the Allendé BO chondrules where CaO is located in the silicates and FeO in the sulfides. The negative trend in the Acfer PO chondrules reflects differing amounts of metal diluting the CaO bearing components. Assuming that CaO is only present in silicates in Acfer PO chondrules, then the data suggest a rough upper estimate of ~4 wt% CaO in the silicate starting component. Addition of olivine to Acfer PO chondrules (Mg# ~0.98) would merely move the chondrule array closer to the origin and *vice versa*. Of all the CCh chondrules analysed in this study and presented in CaO vs. FeO space, only Allendé shows distinct chemical and textural evidence for the evolution of its source region over time as opposed to mixing of different components observed in Acfer, Karoonda and Indarch. It also appears that the history of the UOC chondrules may differ strongly from that of the CCh chondrules, potentially involving separate sources for the type I and type II UOC chondrules as opposed to common origins for the different types of CCh chondrules from a single meteorite. Plotting CaO vs. FeO therefore has potential application not only in the identification

of different chondrule types, but is also useful as a first order petrological tool in studying the evolution of chondrules provided that the data are supported by petrography. More whole chondrule data are necessary to rigorously test the applicability of the CaO vs. FeO plot to whole chondrule data across a wide spectrum of meteorite types.

Due to the large amount of overlap present in the major elements, additional means of discrimination are also investigated using trace and major element data. Initial observations of the volatility graphs highlight several elements that appear to differ consistently relative to each other and the RLE amongst the different types of chondrules: Ir, Mo, Ni, Co, Fe and to some extent Cu, Ga, Pb and Zn. Using the refractory lithophile elements to discriminate between the CCh chondrules is not as useful since the ranges in concentrations and ratios overlap significantly between meteorites and chondrule types (Figure 4.1). For Indarch, however, the differences in the refractory elements between the RP and PP can be characteristic and is discussed later. The lithophile elements Li, K, Rb and Na have proved to be of little use in discriminating between the chondrule types since there appears to be little or no correlation or trends amongst themselves or with other elements, most likely due to their volatility and metasomatic overprints. Figure 4.5 shows a selection of discrimination diagrams that best resolve the different meteorite groups. Acfer 311 overlaps with both Allendé and Karoonda in all plots but can be easily distinguished from Indarch. Allendé and Karoonda can be readily distinguished from each other and also from Indarch. The UOC chondrules are not included in this section since concentration data for the necessary elements are mostly not available. Plots of Fe vs. Ir (a), Co# [$=Co_{mol}/(Co_{mol}+ Fe_{mol})$] vs. Mg# [$=Mg_{mol}/(Mg_{mol}+ Fe_{mol})$] (b) and Zn vs. Pb (c) highlight the constrained compositional field for Karoonda chondrules. In these plots Indarch chondrules fall well apart from Karoonda and with only a small amount of overlap with the Allendé BO chondrules. With the exception of Zn vs. Pb (c) there is

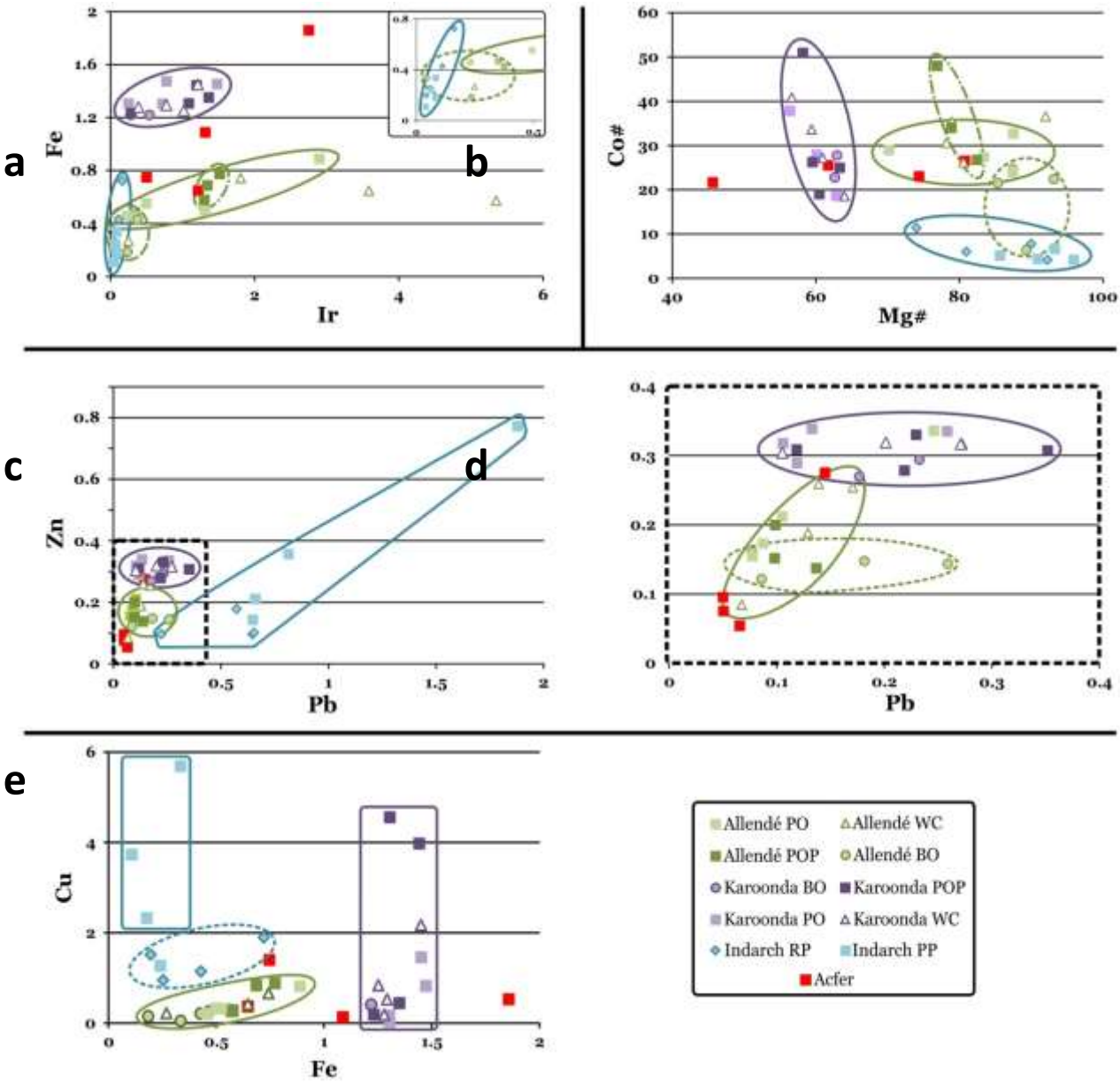

Figure 4.5 Chondrule discrimination diagrams based on CI normalised siderophile and chalcophile abundances. a) Fe vs. Ir, b) Co# vs. Mg#, c) Zn vs. Pb (black box highlighted in lower left corner of c is enlarged in d), e) Cu vs. Fe. See text for details.

always a distinct hiatus between Karoonda and Allendé chondrules. Although the Allendé BO chondrules overlap to some extent with the PO(P) chondrules, they either plot towards the 'lower end' of the Allendé field (Figure 4.6a and b) or with a distinct trend (Figure 4.6c). Allendé PO and POP chondrules mostly overlap, but the POP chondrules appear to plot in a narrowly defined field in Fe vs. Ir, and with a distinct slope in Co# vs. Mg#. No distinction is possible between the different Karoonda

chondrule classes regardless of the type of plot. In a plot of Cu vs. Fe (Figure 4.6e) Allendé, Karoonda and Indarch fall in three distinct fields. In addition it is also possible to distinguish between Indarch RP and PP chondrules. Interestingly, Ind-7, which is classified as a PP chondrule based on textural observations plots in the field of the RP chondrules. This association is further emphasised in Figure 4.6a and b, which shows clear distinction of the Indarch PP and RP chondrules with Ind-7 always plotting as an RP component. It is common for the PP and RP fields to plot with differing slopes but with a common intercept, e.g. Figure 4.6b. The CCh chondrules cannot be distinguished by plots of W/Nb vs. Cr/Ti and W vs. Mo.

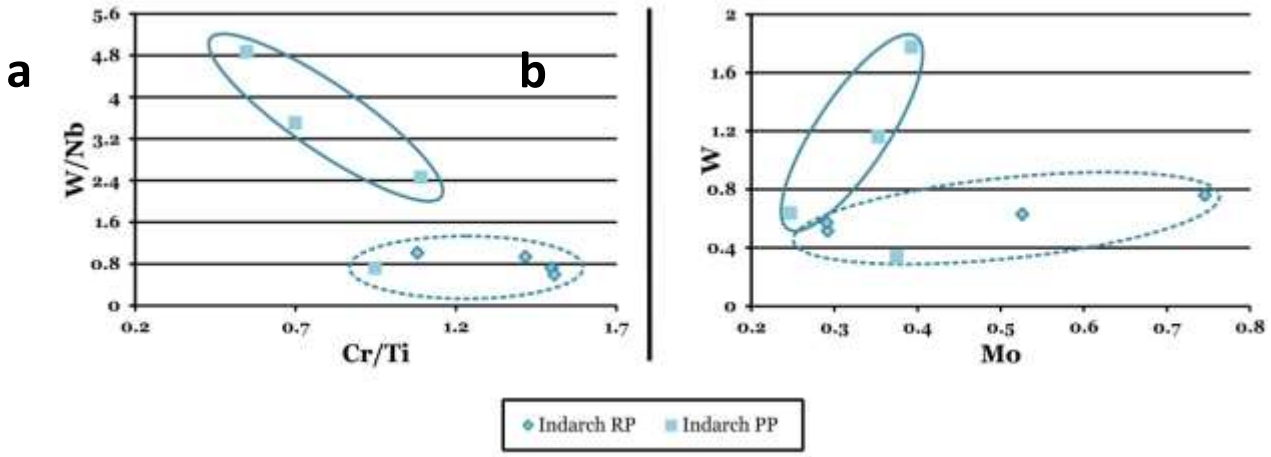

Figure 4.6 Chondrule discrimination diagrams for Indarch RP and PP chondrules based on CI normalised abundances. The sample Ind-7 PP dominantly plots with the RP samples despite its textural similarity to the PP group.

More data are required to rigorously test these discrimination diagrams, especially since only limited numbers and types of chondrules were analysed. This is particularly important for the Karoonda BO, of which only a pair was analysed, and Acfer 311, where subtle distinction between different types of porphyritic chondrules was not possible due to surface coatings. Since distinguishing between high MgO and high FeO chondrules while hand picking is also not always possible, combining the ICP element determinations with a first step of e.g. SEM textural and compositional analysis would

confirm whether or not the type I/II classification observed in the UOC whole chondrules is possible in other meteorites.

4.3 Relationship between chondrules and bulk meteorite

The observation that a large degree of similarity exists between the composition of the bulk meteorite and that of the chondrules (Section 3.1) is of key importance. To illustrate this Figure 4.7 compares the CI normalised chondrule values to the CI and bulk meteorite normalised values. Since, like the chondrules, the bulk meteorites are also enriched in refractory elements and progressively depleted in the more volatile elements, the general effect of the normalisation is for the volatility patterns to become flat on average and lie closer to 1. This hints at a strong control of the local formation region on chondrule composition. However, depletion of the siderophile and chalcophile elements and extreme enrichment or depletion of the volatile elements remain, requiring that most likely some form of silicate-metal/sulfide separation took place within the chondrule formation region to create the former (discussed in Chapter 5) and local temperature effects or metasomatism controlled the latter. Also, considering the agreement between the trace element patterns for chondrules from a particular meteorite, it would require that any chemical heterogeneities present early on in the formation region be largely homogenised prior to both chondrite and chondrule formation. Although radial mixing is known to have occurred in the early solar system (Bockelée-Morvan *et al.*, 2002; Gail, 2004), the chemical evidence seems to suggest that mixing between the different formation regions was minimal if not totally absent after a specific point in time. Any chemical fractionation amongst the different types of chondrules within a single meteorite may therefore largely have been closed-system on the scale of the formation region.

Figure 4.7 (adjoining page) Comparison of CI normalised (left) and CI + bulk meteorite (right) normalised chondrule volatility plots. CI and bulk meteorite (BM) normalised data plot scatter symmetrically around 1 for most of the elements, suggesting a strong control of the bulk meteorite over the chondrule composition.

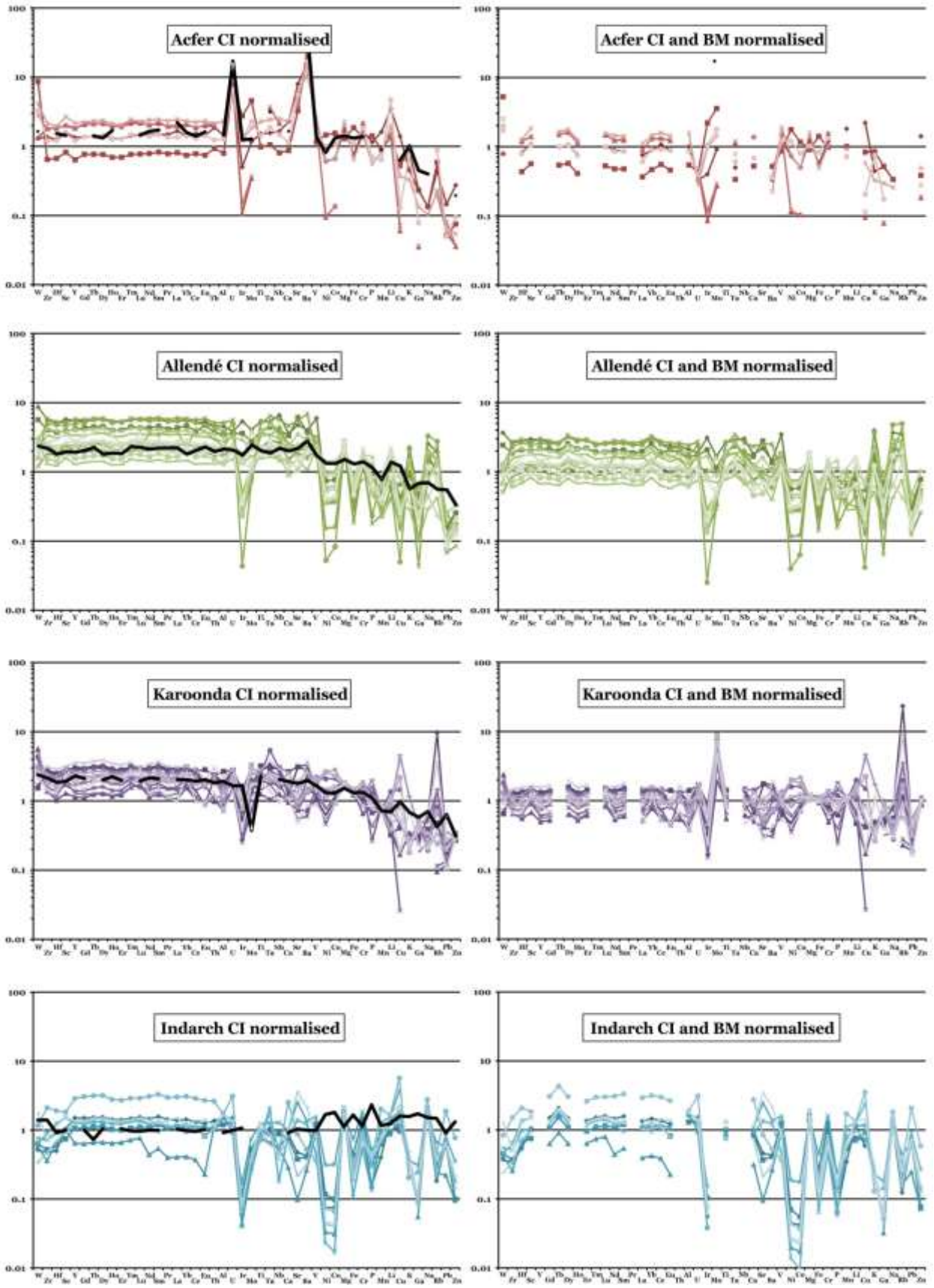
Acfer CI normalised
Acfer CI and BM normalised
Allendé CI normalised
Allendé CI and BM normalised
Karoonda CI normalised
Karoonda CI and BM normalised
Indarch CI normalised
Indarch CI and BM normalised

4.4 Constraints on precursor materials

Textures for porphyritic chondrules require pre-existing solid crystals (Hewins & Fox, 2004), although the exact nature of their origin is unspecified. Regardless of the favoured heating mechanism for chondrule formation or the presence of recycled grains, the crystalline Chondrule Precursor Materials (CPMs) ultimately either had to have a nebular/condensation or planetary/crystallisation origin. Forsterite, the dominant phase in the chondrule suite in this study, is calculated to condense after the CAIs as the first major silicate (e.g. Lodders, 2003) but will also be amongst the first phases to crystallise from an (ultra)mafic melt. The challenge is therefore to deduce from chondrule chemistry whether the CPMs originated in a condensation/nebular environment or crystallisation/planetary setting.

Calcium Aluminium Inclusions (CAIs) are generally favoured as the first condensates from the cooling solar nebula (Ireland & Fegley, 2000; Ebel & Grossman, 2000; Simon *et al.,* 2002) and are extremely enriched in the refractory elements (up to 100 xCI). For general overviews the reader is referred to Scot & Krott (2007), Hutchison (2004) and Tolstikhin & Kramers (2008). The first order control on trace element composition of condensates is directly linked to the crystal structure so that partitioning is based on ion radius and valence i.e. the only influence on the elements is the type of mineral present (e.g. Grossman & Ganapathy, 1975; El Goresy *et al.*, 2002). Compositional differences in the RLE amongst individual CAIs are thought to be the result of sampling of different amounts of the primary condensate phases such as melilite, perovskite and spinel (Sylvester *et al.*, 1993). The consequence of random sampling of condensed phases is to create uncorrelated scatter amongst the major elements when plotted against Al_2O_3 (e.g. TiO_2 and CaO; Figure 4.8; Appendix E, Table E-2). Scatter is also observed in such RLE as Hf and Lu, which are fractionated in high temperature condensates. In contrast, geochemical twins, such as Ni and Co or Sm and Nd correlate with each other and the solar composition. Rare Earth Element (REE)

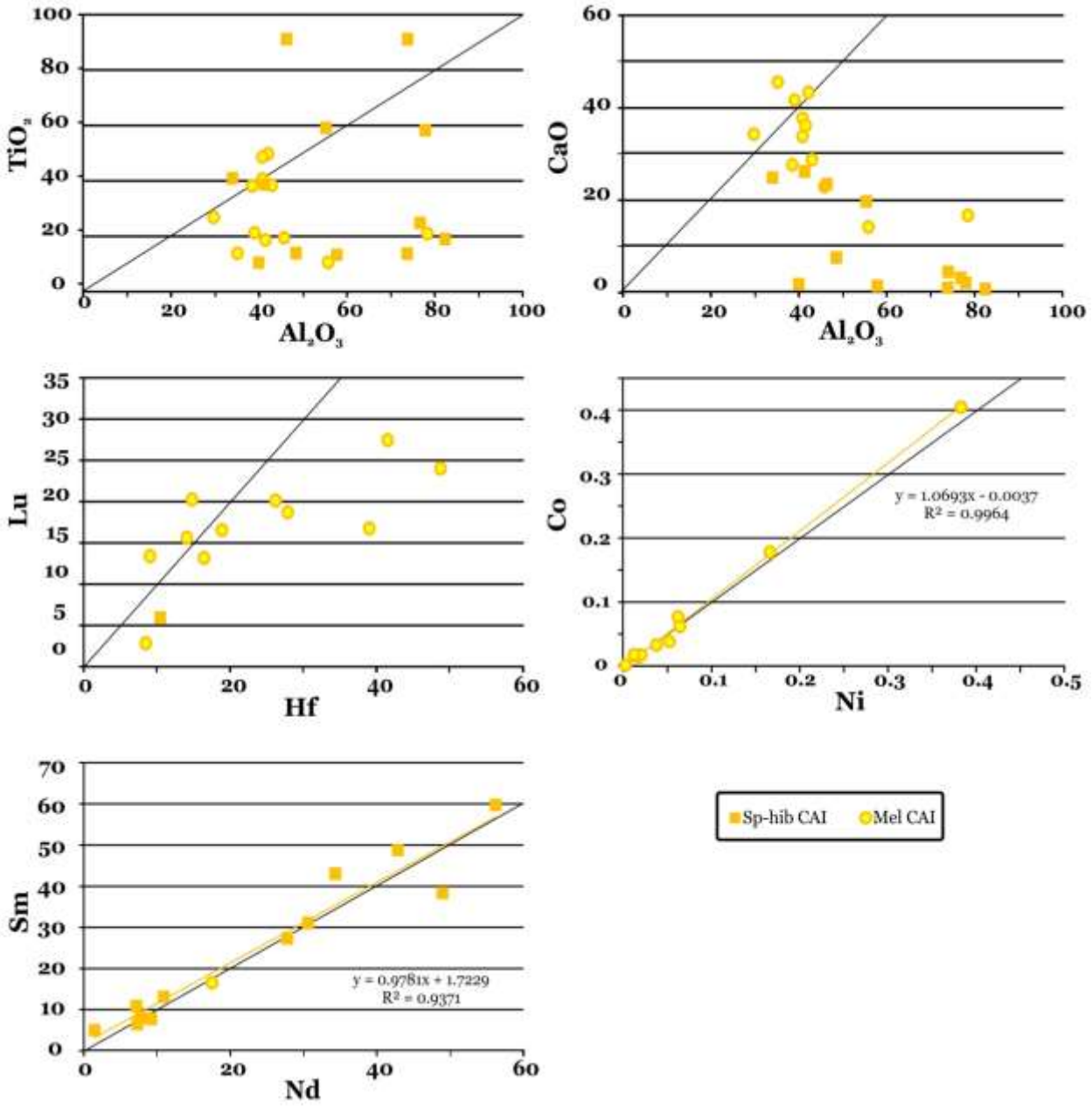

Figure 4.8 CI normalised trace element plots for published CAI data (for references see Appendices, Table E-2). Black diagonal lines are 1:1 with CI, yellow diagonals are regression lines.

fractionations in CAIs may have strong volatility controlled characteristics resulting in large depletions in the more volatile REEs Ce, Eu and Yb (e.g. MacPherson & Davis, 1994). A secondary effect that controls the trace element compositions in CAI is the duration of contact between the condensing mineral phases and the surrounding gases. Phases that are allowed to equilibrate with the surrounding gas for a longer period will have flatter trace element patterns, while minerals that are removed at an early stage

are more likely to have large fractionation effects (e.g. Boynton, 1975; Mao *et al.*, 1990; Lodders & Fegley, 1993; Campbell *et al.*, 2003). Olivine condensing from a solar gas that has already produced refractory minerals is likely to show smaller enrichment or even depletion in the RLE elements relative to CI. If a sufficiently large volume of CAIs was produced then later phases may also show inherited scatter in the major elements Ca, Ti, Al and Mg. In contrast, trace minerals such as Li, Mn and Zn that are commonly depleted in the CAI are likely to partition into forsterite (Lodders, 2003) and should show some enrichment. The REE in such olivines should be fractionated based on the exact nature of the pre-condensed refractory phases and may show enrichment in the more volatile Ce, Eu and Yb.

In contrast, olivines crystallising from igneous (ultra)mafic melts are depleted in the REE (K_d «1) and show a distinct preference for the HREE over the LREE (e.g. Rollinson, 1993; Bédard, 2005). This also holds for olivine (and pyroxene) crystallising from a typical MgO-rich chondrule melts (Kennedy *et al.*, 1993). The study of Kennedy *et al.* (1993) additionally indicates significant depletion in the +4 trace elements as well as the +2 Ba, Sr and Ca. Fractionation of e.g. Lu to Hf is therefore expected.

As shown in Section 3.1, the refractory elements (Zr to V) from both Acfer and Allendé chondrules in this study are usually enriched relative to CI (normally minus Ir and Mo) and show flat patterns. High temperature major elements MgO, TiO_2, CaO and Al_2O_3 mostly trend along a Solar line and in addition to very strongly correlating Sm:Nd and Co:Ni, most of the HFSE correlate with Lu in solar proportions. These characteristics put the chondrules in stark contrast to both the CAIs or olivine crystallised from a melt. The lack of preference of the HREE over the LREE in the Acfer and Allendé chondrules (Figure 4.9) and the solar Lu:Hf give the impression that the precursor material was not formed by fractional crystallisation. Formation of CPMs by disruption of a planetesimal that has undergone extensive silicate fractionation is therefore unlikely. However, the solar correlation amongst both the refractory major

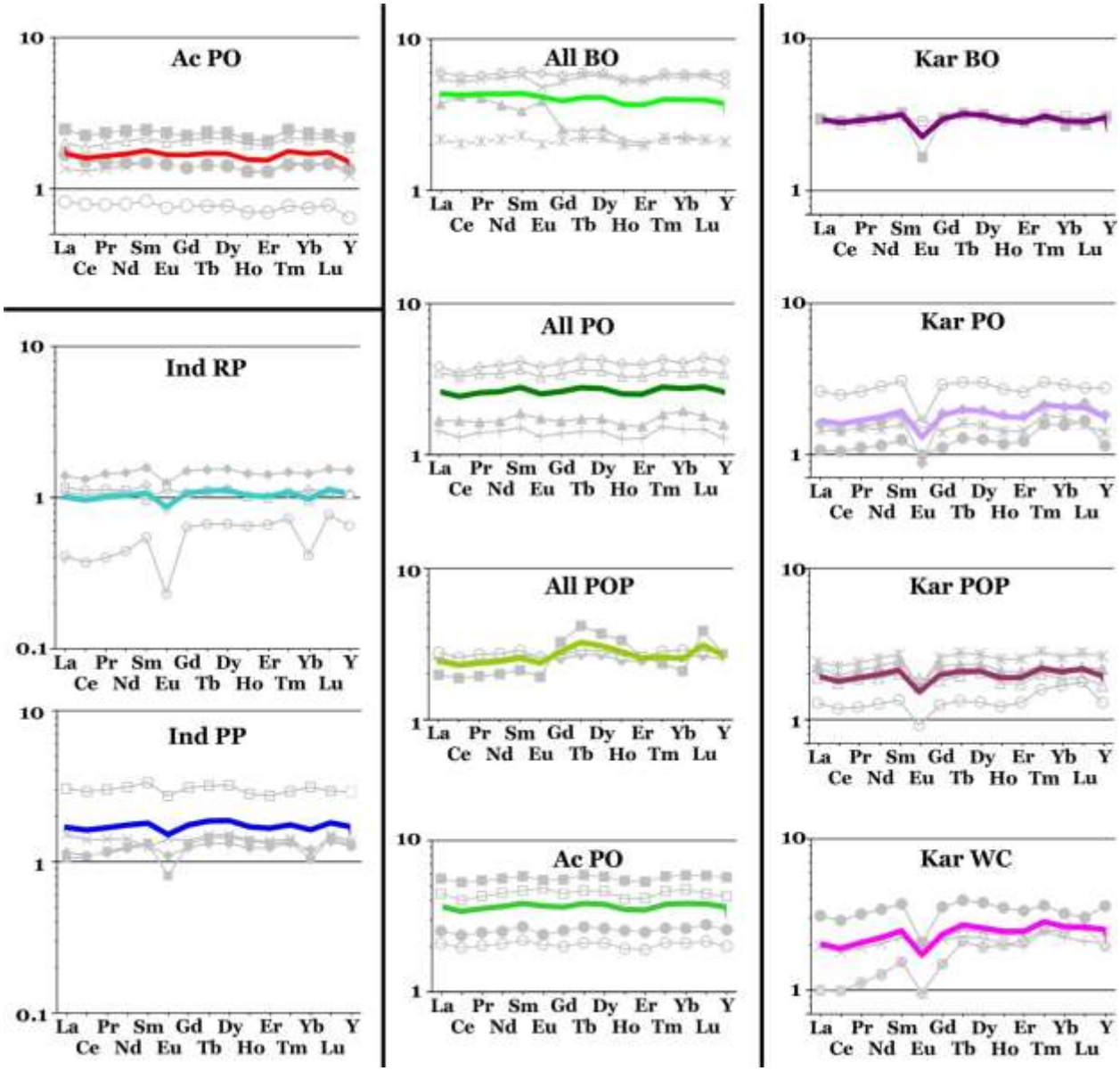

Figure 4.9 CI normalised REE patterns for studied chondrules. Red = Acfer 311 CR2; Blue = Indarch EH4; Green = Allendé CV3OXA; Purple = Karoonda CK4 (keys for the individual samples – gray plots – are similar to figures 3.3-5 and 3.7). Normalisation values are from Lodders (2003).

and trace elements also argue against a condensation origin similar to the high temperature origins of the CAIs. It is furthermore unlikely that the chondrule precursor material formed as a condensate from an already fractionated reservoir (e.g. after CAI formation) since this would lead to non-solar relationships amongst the RLE in particular.

An alternative origin for CPM comes from the formation of ferromagnesian material in the outer shells of stars and resulting composition of the InterStellar Medium (ISM). As mentioned in Section 1.2.1, stellar ejecta contain a range of minerals, including both crystalline and amorphous ferromagnesian material as well as metal oxides and native Fe-Ni metal (e.g. Day, 1976; Waters *et al.*, 1996; Zinner, 2007). Non-organic solid matter in IR spectra of planetary nebulæ, which is derived from the ISM (Gail, 2004; van Boekel *et al.*, 2004), consists dominantly of olivine, pyroxene and amorphous Mg-Fe-phases with little or no detectable CAI-like material (Waters *et al.*, 1998; Meixner, 2002; Rietmeijer, 2002). If such ferromagnesian silicate material and not CAI-like material is therefore the dominant condensation phase in the stellar environment, it is plausible that the refractory elements would condense into the Fe-Mg-silicates with little or no fractionation since there would be no other host phase. The large volume of Fe-Mg-silicate relative to the refractory elements would lead to less enrichment compared to the CAIs. The resulting volatility patterns are theorised to be similar to those of the refractory lithophile elements of the Acfer and Allendé chondrules. The depletions of Ir and Mo are suggested to be a function of solar system processes rather than from the source of the interstellar material in the O-rich shells of evolved stars (Waters *et al.,* 1996) since bulk meteorites are not depleted in these elements. Since the proportions of relatively FeO-rich amorphous Fe-Mg silicate to forsterite and enstatite in the young Solar System will initially be larger (Gail, 2004; van Boekel *et al.*, 2004) it could be speculated that the Karoonda chondrules formed from such an early FeO-rich non-equilibrium assemblage. The evidence that the EC chondrules might originally have been more oxidized and FeO-rich (this study; Weisberg *et al.,* 1994; Fagan *et al.*, 1999; Berlin *et al.*, 2007) makes a similar, more oxidized precursor material plausible.

4.5 Summary Chapter 4

The solar nebula would have contained sufficient crystalline and amorphous ferromagnesian silicate material to act as chondrule precursors. The chemical composition of these silicates was determined by their condensation conditions in the stellar environment. Since silicates are the dominant phase in spectra of AGB stars and not CAI-like material, it follows that the RLE elements would have to condense into the silicates as the dominant phase. This would most likely lead to flat REE patterns and 1:1 CI normalised RLE patterns since these elements would not have another major phase to sequester into. The solar nebula would have been composed of such stellar material potentially from several stars, some or all of which would not have been in equilibrium with the conditions in the evolving Solar System. Re-equilibration of the raw stellar material under solar system conditions would most likely have had the effect of reducing the FeO content in the silicates and creating minerals such as olivine and pyroxene, as well as native metals. Or, in regions where temperatures were sufficiently high, total evaporation followed by condensation would lead to formation of CAIs. The latter process most likely operated in restricted zones close to the sun and did not affect the chemistry of most of the Solar System. The compositions of the formation zones of the different meteorites (i.e. the bulk meteorite compositions) were established prior to chondrule formation and determined the constitution of the chondrules. The depletion in volatile elements in the bulk meteorites is not easily explained since the enstatite chondrites, which supposedly formed much closer to the Sun than the carbonaceous chondrites (Anders, 1971; Baedecker & Wasson, 1975; Shukolyukov & Lugmair, 2004), show no depletion in volatiles. Separation of metal and sulfides from silicates occurred only after the bulk meteorite composition was established. The very primitive (solar-like) nature of the RLE element signatures in Acfer and Allendé chondrules suggest that the reworking of the precursor material did not involve extensive fractional crystallisation of any kind of silicates. A degree of devolatilisation may be necessary to account for depletion of such elements as Ba

relative to the bulk meteorite. In Karoonda and Indarch, on the other hand, an amount of 'igneous' reworking could explain e.g. the HREE enriched, Eu-depleted patterns. An igneous environment would also account for the lack of differences in volatile element concentrations between the chondrules and bulk meteorites in Karoonda and Indarch, since the control on element partitioning would no longer be volatility controlled. And ideal setting would perhaps be a mostly molten planetesimal that has undergone a degree of fractional crystallisation (see also Sections 5.4, 6.1 and 8)

5 Metal-sulfide formation

5.1 Mineral textures and associations

Thin section and binocular observations show that free metal is only observed in the Acfer and Indarch chondrules. In the former metal occurs as rounded blebs interstitial to olivine, as smaller blebs closer to the rims or as dispersed blebs in the surrounding rims (Figure 5.1). Sulfides were not observed in the separates, although thin section observations show that they commonly occur as small disseminated blebs associated with silicates and oxides in the chondrule rims (Figure 5.1a). Magnetite is a common accessory mineral both inside the chondrules and in the rims. Mesostasis in the Acfer chondrules can be dotted with a multitude of small black inclusions, presumably magnetite (Appendix A, Acfer-3 PO). Metal commonly has a thin coating of a black mineral, possibly magnetite or carbon (Figure 5.1b). Schrader *et al.* (2008) point out that metal is mostly absent from type II chondrules in CR meteorites. Allendé chondrules do not contain any visible metal, but are always associated with sulfides. In the PO and POP chondrules sulfides are commonly found as large blebs interstitial to the dominant phenocrysts (Figure 5.2a, b). These may be associated with oxides (presumably either magnetite or chromite; Clarke *et* al., 1971) that are dispersed in the mesostasis of some chondrules. In the fine grained rims, however, sulfides are mostly disseminated with scattered small blebs (Figure 5.2c). There is also a distinct increase in the amount of sulfides related to an increase in pyroxene and fine grained silicates. Olivine and pyroxene crystals may have dusty appearance due to small sulfide or oxide inclusions (Figure 5.2d). The BO chondrules have only minor amounts of sulfides that are mostly linked to the presence of a fine grained rim (Appendix A). Rarely small sulfide blebs are observed in the mesostasis between the olivine bars, and thin section observations show that larger blebs may occur on the edge of the barred section (Figure 5.2e, f). Sulfides in Karoonda chondrules have similar textures to those found in Allendé (Appendix A). Silicates are commonly riddled with abundant very fine grained

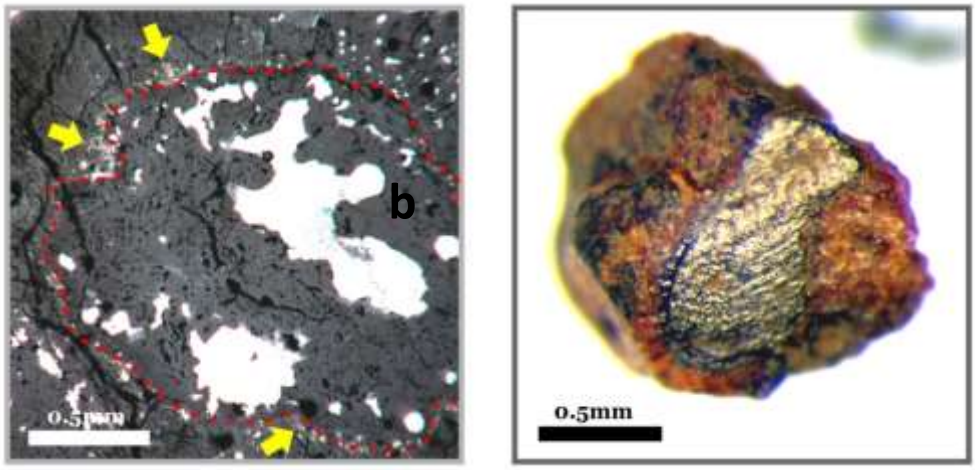

Figure 5.1 a) Photomicrograph (rfl) of a type I chondrule from Acfer 311. The chondrule contains only Fe-Ni metal as non-silicatephase while the rim contains finely dispersed sulfides (yellow arrows) and metal. b) Photo of separated Acfer 311 type I chondrule showing a large metal bleb surrounded by a black mantle of either magnetite or graphite.

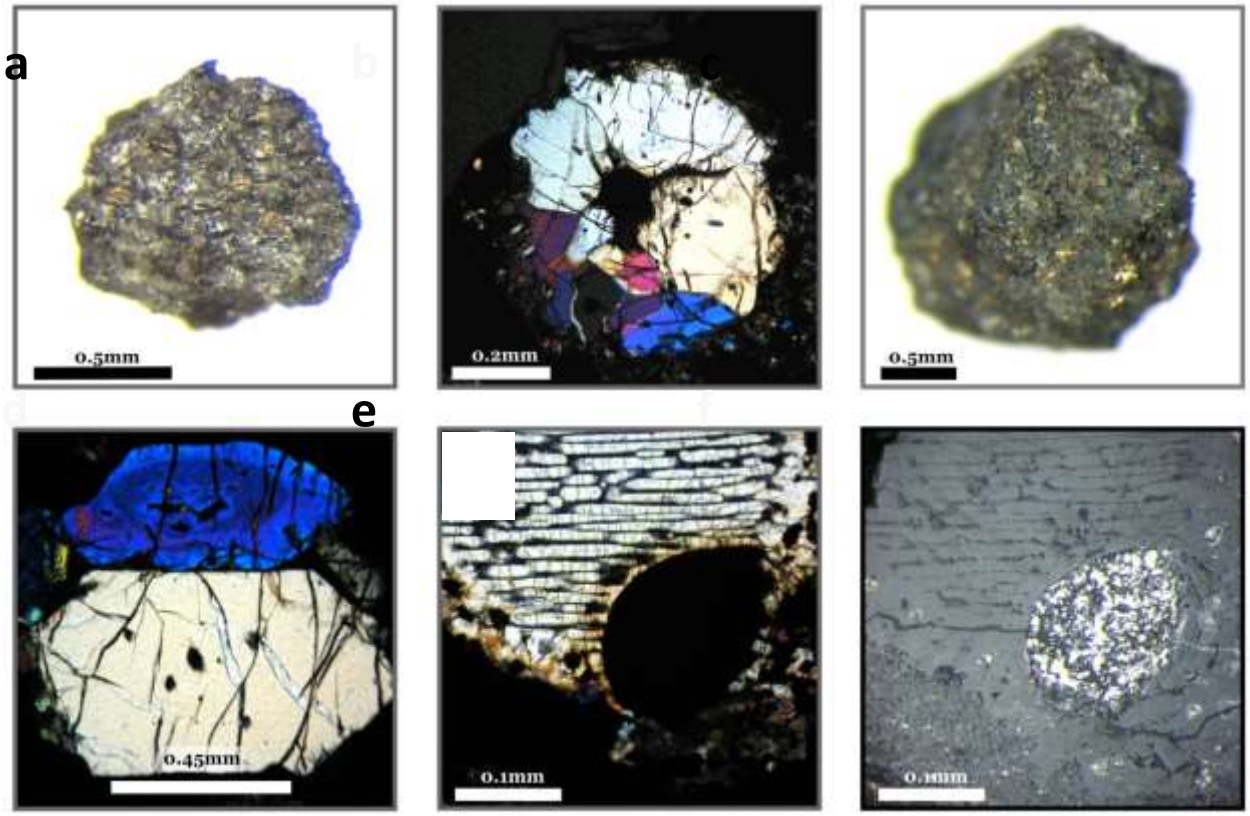

Figure 5.2 Examples of sulfide textures from Allendé CV3. a) Separated type IA PO chondrule. Sulfide blebs occur in the mesostasis, interstitial to olivine phenocrysts. b) Photomicrograph (xpl) of a type IA PO chondrule with large sulfide bleb (black) in the center of the chondrule. c) Type IAB POP chondrule with fine grained rim. Sulfides are finely disseminated along the surface or form small blebs. d) Photomicrograph (xpl) of an olivine crystal (upper) showing evidence of in situ redox reactions. Inner zone of olivine crystal is cloudy with small opaque inclusions but has the same olivine composition as the clear outer rim. e) Photomicrograph (xpl) of a BO chondrule showing a large sulphide bleb bottom right. f) Same BO chondrules as in (e), but in rfl.

magnetite inclusions (Figure 5.3a, b; Scott & Taylor, 1985) but may either have a completely clear outer zone of the same composition. Some olivine grains have no magnetite inclusions at all. Clear olivine appears to be associated with larger sulfide and oxide blebs and 'melt inclusions'. Sulfides are also more common in the Karoonda BO chondrules than in their cousins from Allendé (Figure 5.3c). Also important is the general greater abundance of magnetite associated with the sulfides in Karoonda (Figure 5.3d) and the presence of sulfide-magnetite chondrules (Figure 5.3e, f).

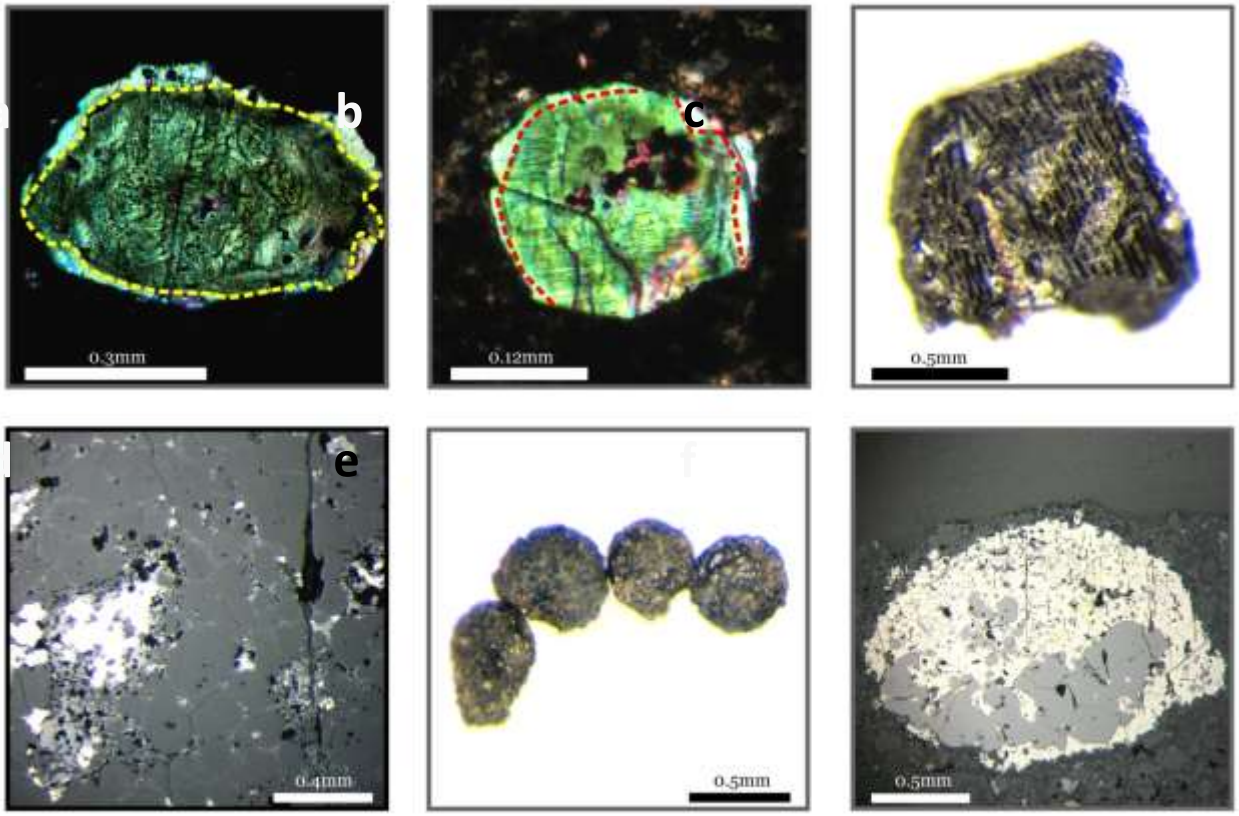

Figure 5.3 Examples of sulfide textures in Acfer 311 CR2. a and b) Photomicrographs (xpl) of olivine showing cores clouded with crystallographically controlled magnetite inclusions surrounded by a rim of clear olivine. Both the inner and outer olivines have the same composition. c) Separated BO chondrule showing large central sulfide bleb and smaller dispersed sulphides interstitial to the olivine bars. d) Photomicrograph (rfl) of a type II PO chondrule with interstitial sulfides (pale yellow) and magnetite (pale gray). e) Separated magnetite-sulfide±olivine chondrules. The chondrules are magnetically stuck to each other. f) Photomicrograph (rfl) of a sulfide-magnetite chondrule.

Indarch RP and PP chondrules commonly have minor amounts of disseminated sulfides and metal interstitial to the pyroxene laths (Figure 5.4a). Sulfide is more common than metal inside the chondrules. In thin section some pyroxene crystals have a dusty appearance due to an abundance of small sulfide and metal inclusions. Occasionally a

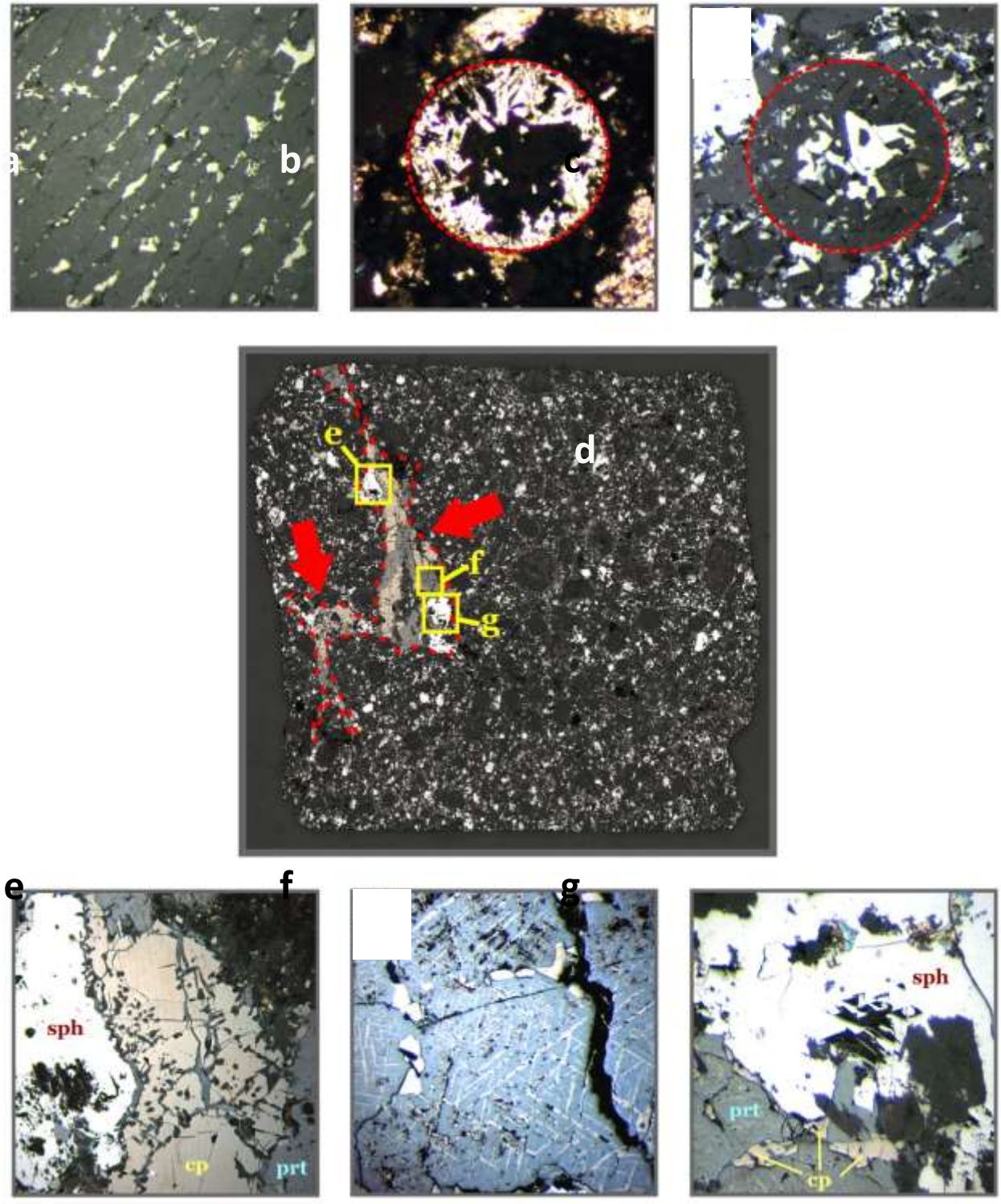

Figure 5.4 Photomicrographs of metal and sulfide textures in Indarch EH4. a) Barred pyroxene crystal with interstitial sulfide and metal (rfl). b) PP chondrule with interstitial sulfides and metal (ppl). c) Same PP chondrules as in (b) in rfl. d) Location of a sulfide-oxide-metal shock vein highlighted in red. e, f, g) Common sulfides in the shock vein include sphalerite (e and g), pyrrhotite with pentlandite flame exsolution (e, f, g) and chalcopyrite (e and g).

PP chondrule may contain large volumes of sulfide located centrally, with pyroxene

crystals growing into the sulfide (Figure 5.4b, c). Indarch also has shock veins dominantly composed of sulfides (Figure 5.4d, e, f, g) and accompanying oxides.

The textural evidence from the chondrules suggests an origin of the metal and sulfides by the coexistence of immiscible liquids. The shapes of the metal and sulfide blebs that occur in the chondrules are always dictated by the surrounding silicates and occur either interstitially or are enclosed by a host crystal. Similar textures are observed in terrestrial magmatic sulfide deposits (e.g. Bushveld Igneous Complex) whose origins are directly linked to sulfide immiscibility and have been reproduced experimentally (e.g. Holzheid, 2010). *In situ* reduction/oxidation (or exsolution) that occurs well below the liquidus of the host phase is likely to produce textures similar to those in Figures 5.2d and 5.3a and b, i.e. a multitude crystallographically controlled small opaque minerals scattered throughout the host. The chondrule textures would also be very difficult if not impossible to produce by trying to add liquid metal/sulfide to liquid silicate. Both metal and sulfide melts are significantly denser than silicate melts and would probably remain close to or on the surface of the silicate melt due to surface tension effects (Grossman & Wasson, 1985). Connolly *et al.* (2001) have also suggested liquid immiscibility and the expulsion of metal melt as the origin for the silicate-metal textures in CR meteorites (Planner, 1986; Connolly et al., 1994). Alternatively the presence of metal or sulfides on the outer edges of chondrules has also been suggested to be the result of centrifugal forces produced by a spinning chondrule (Kong & Palme, 1999). The relative positioning of the metal and sulfide (henceforward referred to as M-S) blebs may yield additional clues to the timing of the saturation event. In order for M-S blebs to migrate to the outer surface of a chondrule, its interior has to be at least partially molten. Therefore, saturation in an M-S melt that occurs only towards the end of the crystallisation sequence of a chondrule is likely to be trapped in its interior. If the chondrule melt reaches saturation early on, then the M-S melt has the option either to migrate outwards when possible, or to be penetrated by rapidly

growing crystals of e.g. a barred olivine or radial pyroxene crystal. The exact composition of the immiscible melt will be determined by the local conditions.

5.2 Siderophile elements

Figure 5.5 plots the volatility arranged siderophile and chalcophile elements (collectively called the 'core elements') for the studied chondrule suites. Distinctive features of the siderophile elements are summarised as follows: the siderophile elements have a general tendency to decrease in abundance with decreasing $T_{C50\%}$ (except Indarch); W is commonly more enriched than the neighbouring RLE in the CCh chondrules (see Figures 3.3-5); W and Mo are more enriched than Ir, all three of which are refractory; Ni and Co are the most depleted siderophile elements along with Ir; Mo and Ir do not correlate; Ni:Co is solar (except Karoonda). An important consideration for the interpretation of the core element patterns is the susceptibility of the elements to change their geochemical behaviour. Except under very oxidizing conditions like those found in Karoonda, the PGEs are essentially siderophile. Iridium is therefore used as a proxy for the metal component. The elements Mo and W are highly sensitive to changes in fO_2 conditions and will readily partition into silicates and form sulfides or oxides (Campbell *et al.*, 2003). Since Ir is almost exclusively siderophile, a plot of Mo/Ir vs. W/Ir is an indicator of oxidation control on the distribution of Mo and W (Campbell *et al.*, 2002). Positive correlations between the two elements indicate oxidation, which are both sensitive to redox conditions in comparison to Ir, which is not. Tungsten is more sensitive to oxidation than Mo (Campbell *et al.*, 2002) and will develop a larger spread with increasing/continuing oxidation. Negative correlations between Mo/Ir and W/Ir are an indication of normal siderophile behaviour for all three elements. When the CI normalised data are plotted for the chondrule suite studied here (Figure 5.6), Acfer is the only meteorite for which the chondrules show a negative trend suggesting the siderophile behaviour of W and Mo. Allendé and Karoonda

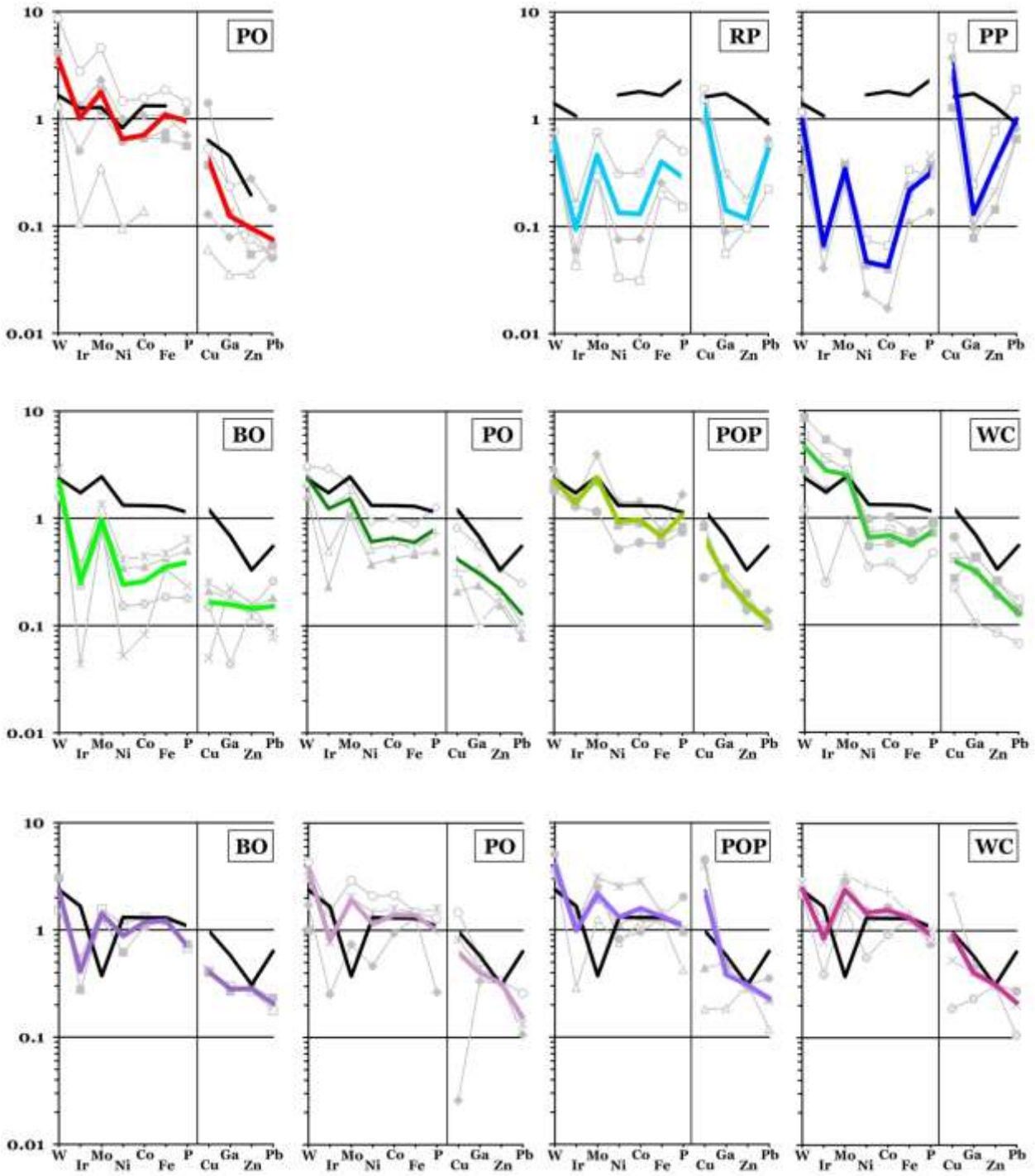

Figure 5.5 CI normalised abundances of siderophile and chalcophile elements. Red = Acfer 311 CR2; Blue = Indarch EH4; Green = Allendé CV3OXA; Purple = Karoonda CK4 (keys for the individual samples – gray plots – are similar to figures 3.3-5 and 3.7). Normalisation values from Lodders (2003).

chondrules all show positive correlations between Mo and W. In Karoonda the slopes are slightly shallower with a broader range in W/Ir compositions than in Allendé, which is in good agreement with the more oxidized nature of Karoonda. It is

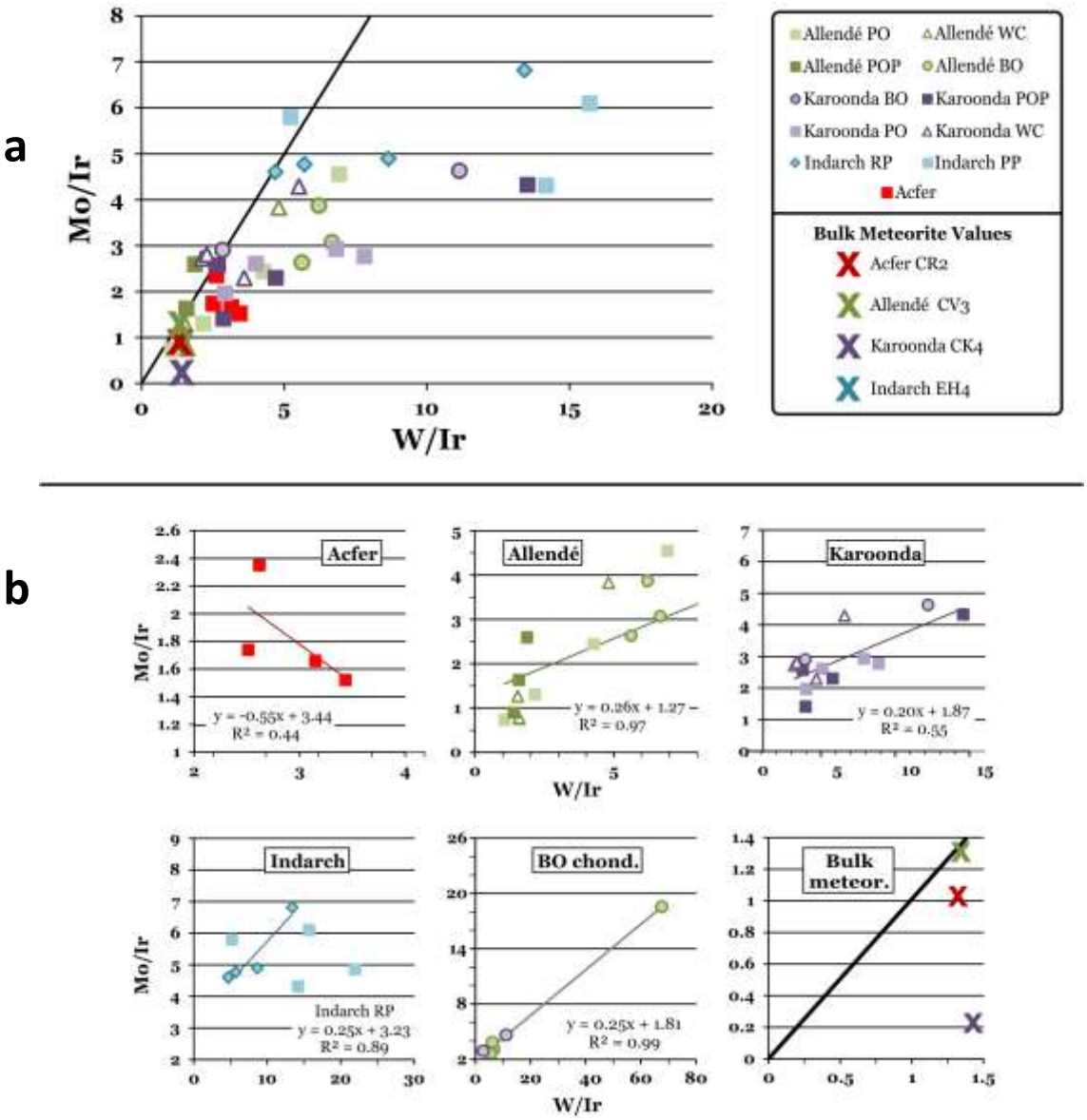

Figure 5.6 a) CI normalised plot for all chondrules and bulk meteorite values of Mo/Ir vs. W/Ir as an indicator of oxidation. Black diagonal is 1:1 with CI. Most chondrules plot off the 1:1 CI trend indicating fractionation of Mo relative to W due to oxidation. b) Individual plots for the studied meteorites. Acfer is the only sample that shows hints of metallic behaviour for both W and Mo. Allendé and Karoonda both show oxidized behaviour for the two elements. Indarch chondrules surprisingly do not show metallic behaviour of Mo and W, but might belinked to their extremely reduced mineralogy so that W and Mo occur in the same phase but not with Ir. Despite differences in bulk chondrule compositions, chondrules from Allendé and Karoonda (particularly the BO chondrules) plot on similar slopes and intercepts. Bulk meteorite data, however, show no correlation whatsoever between Mo/Ir vs. W/Ir, but this could be an analytical effect since both few and precise data are not readily available.

interesting to note that the BO chondrules of both meteorites have similar slopes, intercepts and compositional ranges. Surprisingly, Indarch RP and PP chondrules do not show negative trends. The PP chondrules have a very wide range in W/Ir values for a narrow range in Mo/Ir (i.e. essentially a zero slope) while the RP chondrules show a

positive correlation. For the PP chondrules it seems to rather be a case of variable W content since both Mo and Ir contents have fairly small ranges. The positive correlation of W and Mo in the RP chondrules may be an effect of the highly reduced mineralogy of the E chondrites. However, to produce a positive correlation it requires that W and Mo occur in the same phase but without Ir. Iron, Ni and Co are slightly less sensitive to redox conditions and particularly Ni and Co will remain together under most circumstances but can be fractionated from each other under oxidizing conditions (e.g. Kong & Ebihara, 1997 and refs. therein). A similar plot of Fe/Ir v Co/Ir (Figure 5.7) shows that for Allendé and Acfer, Fe and Co (and by inference Ni) are oxidized

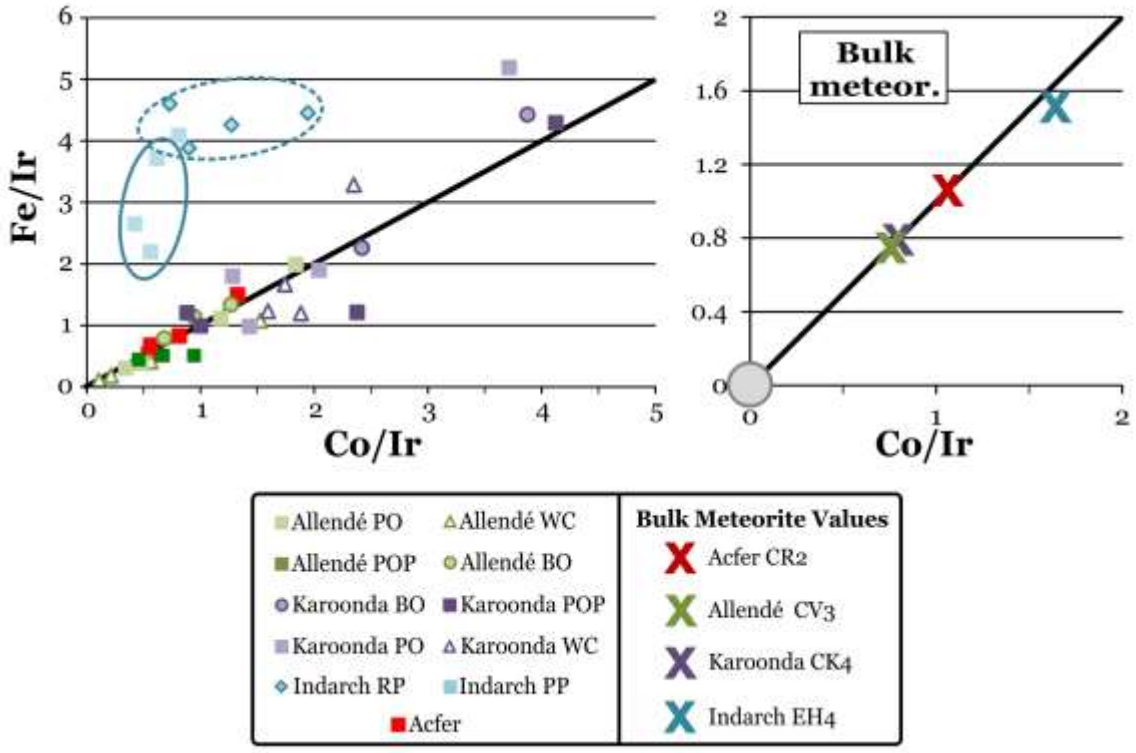

Figure 5.7 CI normalised plot of Fe/Ir vs. Co/Ir as additional measure of oxidation. All chondrules plot along a solar slope except Indarch. Karoonda chondrules show greater scatter than the other CCh chondrules. In contrast all bulk meteorite and average CAI values (gray circle) plot on the solar slope. Normalisation values are from Lodders (2003).

together so that the data plot along a solar trend. Karoonda shows a larger degree of scatter linked to its extremely oxidized state and reflects the differential partitioning of

Fe and Co (and Ni) into both silicate and sulfide phases. Indarch RP and PP chondrules, however, plot in a separate field off the solar trend and have essentially non-sloping trends. The former group have a large range in Co/Ir values while the latter have a large range in Fe/Ir. The bulk meteorite and CAI average all plot along a 1:1 slope.

5.3 Chalcophile elements

Where Ir is considered a proxy for metal components, Cu is a good measure for a sulfur component. Copper is the second most chalcophillic element after Pb (Luecke *et al.,* 2006; Stewart *et al.*, 2009), but Cu has a slightly higher $T_{C50\%}$ (1037 K vs. 727 K; Lodders, 2003) than Pb making it comparatively less susceptible to volatility processes. Zink potentially partitions into olivine and pyroxene (Lodders, 2003) and has a $T_{C50\%}$ similar to that of Pb, making it less suitable as a proxy. Even when Cu is not present as chalcopyrite ($CuFeS_2$) it still partitions into other sulfides such as pentlandite and troilite (Schrader *et al.*, 2008). A plot of Cu (ppm) vs. 1/Mg# (Figure 5.8) indicates the enrichment in sulfides relative to silicates and also the co-variation of Cu and Fe or Mg. Most of the CCh chondrules have Cu contents of <200ppm with the exception of three Karoonda chondrules (Kar-10 and 11 POP, Kar-12 WC; 200 ppm < Cu < 600 ppm). Indarch RP chondrules mostly overlap with the more enriched CCh chondrules, but the Indarch PP show large enrichment in Cu (up to ~720 ppm). The plot seems to be in general agreement with petrographic and binocular observations i.e. generally low sulfide contents in Acfer PO (I) and Allendé BO; higher average sulfide content in Karoonda compared to Allendé; increasing sulfide content in Allendé in the order BO<PO<POP; high average sulfide content in Indarch chondrules. On a plot of Cu/Mg# vs. Ir/Mg# (Figure 5.9) only the Karoonda chondrules, Allendé PO, PO and WC chondrules show a correlation between the two elements. Considering the lack of metal in these samples it suggests that both Cu and Ir behave as chalcophile elements in these chondrules. In both Acfer and Indarch these elements vary independently

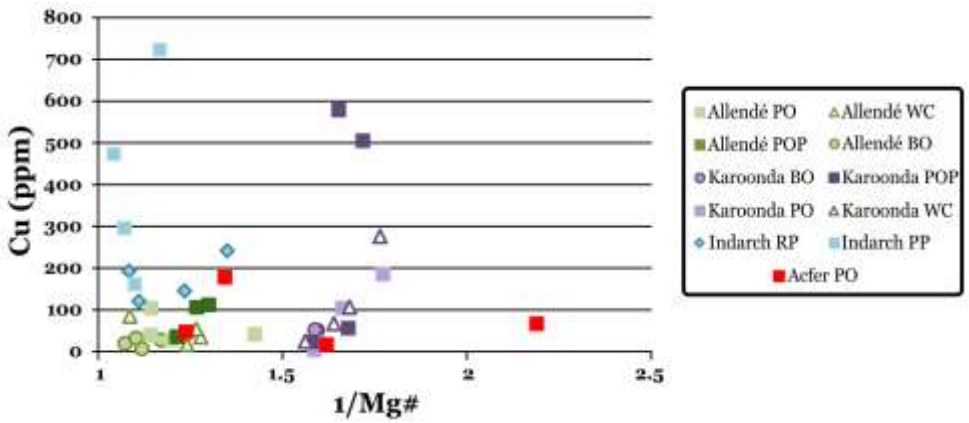

Figure 5.8 CI normalised values of Cu vs. 1/Mg# to illustrate enrichment in chalcophiles as well as the chalcophilic behaviour of Fe (see text for details). Normalisation values are from Lodders (2003).

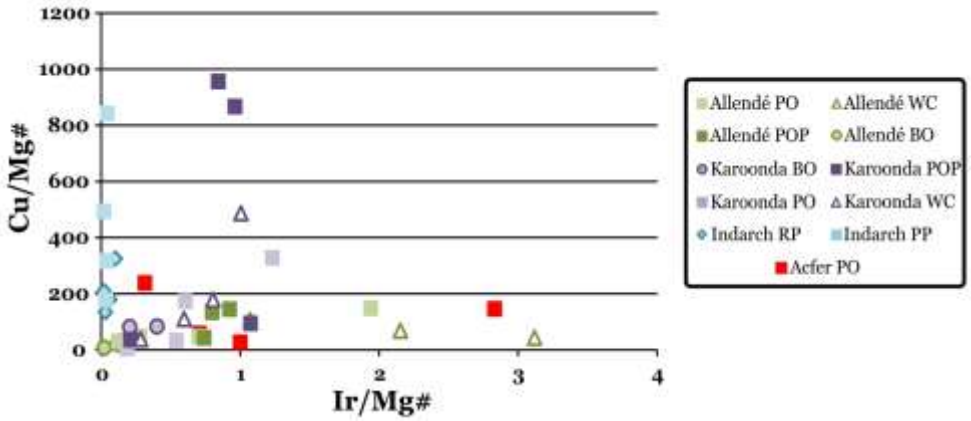

Figure 5.9 CI normalised values of Cu/Mg# vs. Ir/Mg# as a measure of oxidation and metal distribution (see text for details). Normalisation values are from Lodders (2003).

from each other, suggesting that they are located in separate phases and have been separated.

5.4 Formation

A big constraint on the formation of metal and sulfides in chondrules is the apparent difficulty with which liquid metal/sulfide or dust can be mixed into a liquid silicate droplet. Multiple layers of dust or immiscible liquids can be added to the surface of a chondrule, but unless a process is present that will mix the components up on a small scale just before chondrule crystallisation the general tendency will be for added

sulfide and metal to remain on the outside of a chondrule. Metal in the CR2 chondrules are thought to be either the result of direct condensation (e.g. Weisberg *et al.,* 2000; Campbell *et al.*, 2001) or reduction of FeO-rich silicates (e.g. Kallemeyn et al., 1994). Condensed metal is noted for its concentrically zoned structure (Grossman & Olsen, 1979; Weisberg *et al.*, 2000), although this is not observed in metal blebs inside CR2 chondrules (Kallemeyn, *et al.*, 1994). Despite the textural evidence suggesting that metal was present as an immiscible melt during growth of the silicates, it does not really preclude either scenario. Campbell *et al.* (2002) note that metal condensing from a gas will do so essentially independently from the silicate portion so that they form discreet phases. If a mixture of discreet condensed silicate and metal particles is mixed and then melted, a similar texture (i.e. unzoned metal blebs in silicates) might be observed compared to a molten chondrule that is actively being reduced to form an immiscible metal melt. The reduction could not take place at sub-solidus temperatures since the results would not match the observed textures in CR2 chondrules. For a metal condensing directly from a gas with solar proportions above 1500K, the siderophile elements should decrease according to volatility with W>Ir>Mo>Ni, Co>Fe (Campbell *et al.*, 2003). Below this temperature the siderophile elements up to Co are unlikely to be fractionated. Nickel and Co retain their chondritic ratio during condensation regardless of temperature, probably due to their very similar $T_{C50\%}$ and geochemical behaviour. Although there appears to be marginal volatility control on the siderophile elements in the chondrules, the overabundance of W and Mo relative to Ir is not easily explained by condensation from a gas, unless the W/Ir and Mo/Ir ratios were superchondritic. A superchondritic W/Ir ratio for the formation of CB_b metal has been proposed by Campbell *et al.*, (2002). Unless superchondritic W/Ir and Mo/Ir ratios are present in a large portion of the chondrite forming region, the variation of W and Mo relative to Ir and their overall ≥1 xCI enrichment in Mg-Fe-chondrules is easiest explained by oxidative enrichment in silicate phases, supported by Figure 5.6. Bulk meteorite values are not really adequate for estimating W/Ir and

Mo/Ir in the carbonaceous and enstatite chondrite region since often only single values or no data are available (see Appendix D, Table D-3). However, published data seem to suggest that W/Ir and Mo/Ir ratios might differ from solar values (Figure 5.6). Regardless, relative enrichment of W and Mo to Ir in the bulk meteorites is always less extreme than in the chondrules since bulk meteorites have higher Ir concentrations.

Since both sulfide and metal melts are sufficiently dense to move to the surface of a chondrule by surface tension effects, the separation of metal and sulfide phases in the Acfer and Indarch chondrules is interesting. Even if insufficient S is present to create a separate sulfide melt, the chalcophile elements will mostly remain in solid solution with the siderophile elements (Righter *et* al., 2010) and should be expelled simultaneously. In Acfer, sulfides are mostly found in type II chondrules, in the rims of type I chondrules and the matrix (this study; Schrader *et al.*, 2008). Connolly *et al.* (2008) and Schrader *et al.*, (2008) suggest that the sulfides originate from reworking of metal in a more oxidizing and S rich environment. While this is entirely plausible, it does not explain the non-correlation of Ir and Cu since both should partition into metal alloys at higher temperatures and reducing conditions (Lodders, 2003) and are likely to remain together under oxidizing and S-rich conditions. The latter effect is well demonstrated by the Allendé and Karoonda chondrules. Both suites of chondrules are more oxidized than Acfer (little or no free metal present) and as shown above, evidence strongly suggests that both Cu and Ir are present as sulfides. This is also typical behaviour for these elements in the Earth's mantle, which is significantly more oxidized than the CR2 meteorites. Volatility effects have been used to explain the enrichment in volatile metals in the rims surrounding CR2 type I chondrules (Kong & Palme, 1999; Connolly *et al.,* 2001). This could also account for the greater abundance of sulfides observed in the rims if S was too volatile to partake in the chondrule forming event at high temperatures i.e. >1783 K (Schrader *et al.*, 2008). However, Cu would have to behave similarly as a volatile chalcophile element and not partition into

the Fe-Ni alloy as calculated by Lodders (2003). Volatility separation of the elements cannot, however, explain the independent behaviour of siderophile and chalcophile elements in Indarch. Sulfides in the EC are known to form at high temperatures (e.g. T_C(CaS) = 1379 K, Lodders & Fegley, Jr., 1993) most likely simultaneously with metal alloys that condense around ~1357 K (Lodders, 2003). Chondrule textures in Indarch require that both metal and sulfide melts were present in the chondrules at the time of silicate crystallisation. Since Ir is highly siderophile, it will preferentially partition into the metal phase. Unless the metal phase was therefore preferentially expelled from the Indarch chondrules relative to the sulfides, it becomes difficult to separate them by liquid immiscibility.

Since the data represent whole chondrule compositions and not individual phases, they reflect the composition of the precursor material. A molten chondrule can react with the surrounding gas (e.g. Libourel *et al.*, 2006) or lose immiscible components (e.g. Acfer PO chondrules; Grossman & Wasson, 1985), but once it solidifies its bulk chemistry is set. The only subsolidus processes that can significantly alter the bulk chemistry of a chondrule are high temperature metamorphism, addition of rims or alteration. Since none of the chondrules present are extremely altered and none are above metamorphic grade 4, it is reasonably safe to assume that these processes have not extensively modified their chemistry. Addition of rims, although present, is fairly easily accounted for by analysis of multiple chondrules with varying amounts of rim and making careful petrographic observations.

Most if not all of the siderophile and chalcophile characteristics and textures of chondrules can be explained by establishing the local oxidation state before the chondrule solidified. From the data presented here the following sequences are suggested for the formation of metal and sulfides in the CCh and EC chondrules:

Acfer – Initial conditions in the CR formation region would have to have a sufficiently high fO_2 to allow W and Mo to partition into silicates. Simultaneously a metal (or sulfide) phase would have to exist to partition the Ir and remaining siderophile elements. Either the oxidation of W and Mo was not extreme or the extraction of Ir and the other siderophile elements to form a metal phase was not efficient since the depletion of Ir relative to W and Mo is not extreme. Simply creating a primary metal phase and mixing it into the silicates in varying proportion would not work since chondrules with large volumes of metal should show positive Ir anomalies relative to W and Mo. A major reduction episode of the silicates is then required to remove all the remaining siderophile elements, including W and Mo, into a metal phase. The initial metal phase would have to remain secluded since mixing it into the secondary metal phase would even out the relative depletions between the siderophile elements. Chondrule textures require that the reduction either took place just before or during a high temperature event so that the metal and silicates were molten together. Sulfur and the other chalcophile elements including Cu were only present in minor amounts in the chondrules, either due to their relative volatility or perhaps due to sequestration along with the primary Ir-rich phase. Expulsion of the metal and crystallisation of the silicates followed simultaneously. Sulfides could condense on the outside of the chondrules when the surroundings cooled down sufficiently.

Allendé – The chemistry of Allendé chondrules show an evolutionary trend in the order BO-PO-POP that is directly linked to the amount of pyroxene (which gradually becomes more FeO-rich), sulfides and rim present (this study; Cosarinsky *et al.,* 2008). The BO chondrules are suggested to represent the composition of the precursor material since they are pure olivine and contain little or no sulfides or a fine grained rim. As with Acfer, the precursor material for the Allendé chondrules requires a slightly oxidized formation region to enrich W and Mo in the silicate phase and a primary metal phase to sequester the siderophile elements. Formation of the metal phase appears to have

been more efficient for the Allendé chondrule precursor since the depletion of Ir relative to W and Mo is greater than that observed in Acfer. Crystallisation of the chondrules following a heating event produced liquid immiscibility due to sulfur saturation. The removal of the primary metal/sulfide phase from the formation region was probably not very efficient since the siderophile and chalcophile elements appear to be mixed back into the chondrules in the form of sulfides and FeO-rich silicates. This requires a gradual increase in fO_2 in the formation region so that the initially reduced M-S phase was oxidized over time. This would also allow a gradual increase in the amount of sulfides present as more elements became available from oxidation of the primary metal. The general effect would be for chondrule volatility patterns to approach the bulk meteorite pattern with increasing proportions of sulfides and fine grained rims, as is observed in Figure 5.5. An additional W,Ir-rich component appears to be present in the Allendé WC chondrules not observed elsewhere.

Karoonda – Data for Karoonda chondrules require that the precursor material for the Karoonda chondrules was already oxidized with all the Fe present in the 2+ state, and that both silicates and sulfides were present. Iridium would sequester into the sulfides with Fe, Ni and Co partitioning between both but mostly into the silicates. The presence of dusty olivine cores surrounded by clear olivine and a change from having the opaques as small, elongate crystallographically orientated inclusions to larger random rounded inclusions seems to imply a multistage process prior to chondrule formation. It is also pertinent that there appears to be some degree of agreement between the shape of the dusty core and the outer grain (Figure 5.3a, b). These features suggest that the already FeO-rich olivine was further oxidized to such an extent that its structure could not hold the Fe^{3+} and magnetite was exsolved. The growths of clear olivine may imply that the dusty grains were dissolved and a new layer grew, allowing the exsolved magnetite to coalesce and form larger immiscible blebs. A mixture of a sulfide-oxide melt and silicate mush (crystals plus melt) could explain the

observed chondrule texture. The large degree of similarity in siderophile and chalcophile elements between the Karoonda chondrules and bulk meteorite suggest that the sulfide component was either remixed thoroughly with the silicates after separation, or that separation of the silicates and sulfides not very effective.

Indarch – The tendency of the RP and PP chondrules in Indarch to have separate trends that converge on a single composition for all except the most chemically similar elements suggests the same source but different evolutionary histories. Figures 4.4 and 4.6 highlight the tendency of the sample Ind-7 PP to plot with the RP chondrules for all the chalcophile and lithophile elements. The theory pursued here is that the RP chondrules were formed after a major reduction event while the PP chondrules were already there prior to this and carry inherited chemical signatures from their own more oxidized formation environment. The RP chondrules display strong positive correlations between elements that have similar geochemical behaviour under reducing conditions as observed in the enstatite chondrites e.g. both Ti and Fe (chalcophile) and Fe and P, where Fe is siderophile and P occurs as phosphide (Figures 5.10). Such behaviour agrees with measurement of phases in the EC (Rambaldi & Cendales, 1980; Easton, 1985). The PP chondrules in contrast show essentially no correlation between either Ti and Fe or Fe and P. The PP chondrules, however, show good correlation between normally lithophile elements such as Hf and Lu (Figure 5.11), while these elements show no correlation in the RP chondrules. These correlations support the formation of the PP chondrules in a more oxidizing environment compared to the RP chondrules. As mentioned earlier, the general tendency of the compositions of Indarch PP and RP chondrules to converge to a single composition suggests that the PP and RP chondrules had a similar source, or (the favoured theory) that the PP chondrules were in fact the precursor material for the RP chondrules. Formation of the RP chondrules occurred under extremely reducing conditions to produce the chalcophilic behaviour of the REE (Lodders & Fegley, 1993) while Hf remained lithophile. In order to maintain

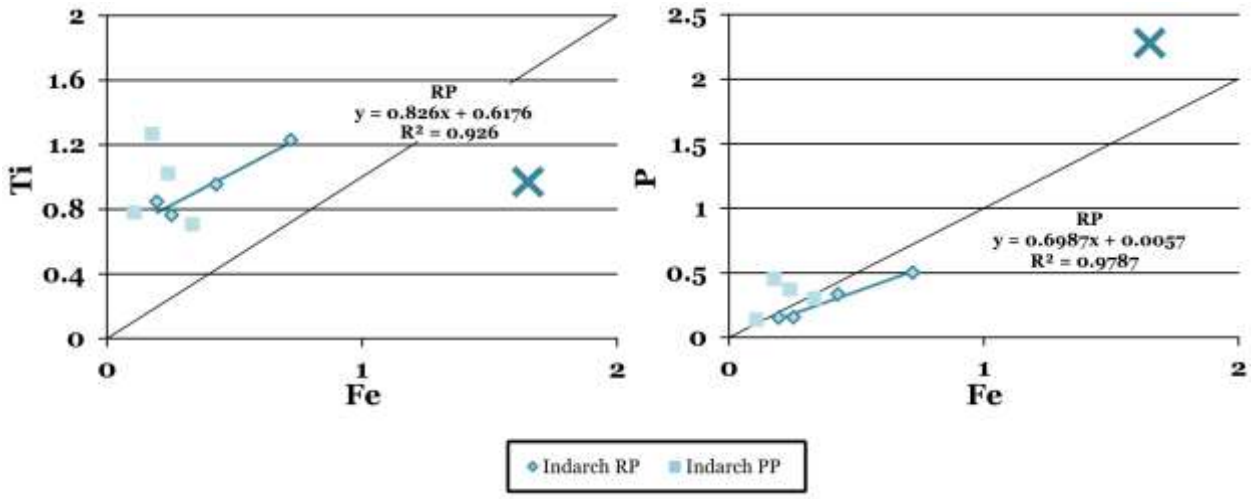

Figure 5.10 CI normalised plot of Ti vs. Fe and P vs. Fe for Indarch EH4. Correlating behaviour between the elements, as is expected for the extremely reducing conditions found in the EC, is only observed in the RP chondrules. Bulk meteorite values are plotted as a cross. 1:1 (CI) ratio is indicated by the diagonal black line.

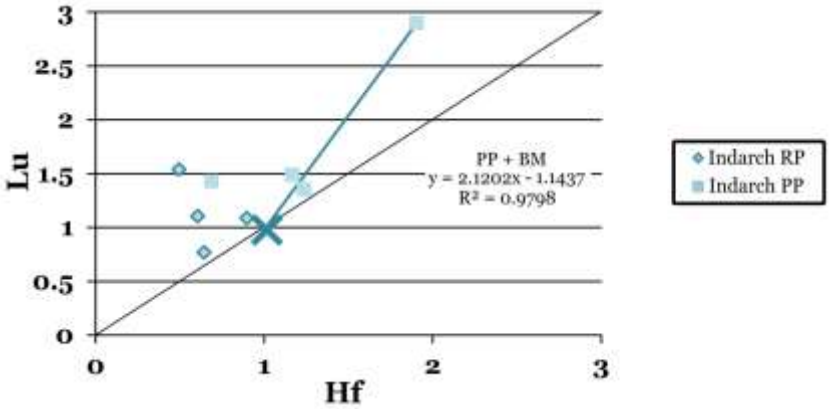

Figure 5.11 CI normalised plot of Lu vs. Hf for Indarch chondrules. PP chondrules (except Ind-7 PP) maintain lithophile behaviour for both elements, indicated by a stong positive correlation intercepting the bulk meteorite composition. Deviation from a 1:1 (CI) ratio (black diagonal) is probably due to the presence of small amounts of REE-enriched reduced sulphides. RP chondrules show a poorly correlated negative trend between Lu and Hf.

some of the original lithophile+oxidized characteristics in the PP chondrule, this theory requires that the PP chondrules were reduced in situ with inefficient redistribution of the elements, which has also been proposed by Berlin *et al.* (2007). The sequence for the Indarch chondrules therefore starts with the formation of FeO-rich porphyritic chondrules, possibly similar to the FeO-rich type II chondrules found in Allendé or Acfer. Conditions had to be slightly oxidizing to allow W, Mo and Fe to partition into the silicates while Ir, Co and Ni were extracted into a separate phase.

Reduction took place extracting all the siderophile elements from the PP chondrules. It should be mentioned that while Mo and Ir have the same ratios in both the PP and RP chondrules, W and Ir do not. The PP chondrules have higher concentration of W in comparison to the RP chondrules, which is also consistent with formation in a more oxidized environment. A heating event followed, which created the silicate melts for the RP chondrules. The nature of the heating event would have to allow at least some of the silicates from the PP chondrules to retain the chemical signatures from their more oxidized history.

5.5 Summary Chapter 5

Relative proportions of the siderophile elements to one another suggest that chondrule precursor material in Acfer, Allendé and Indarch were more oxidized than the current silicate composition suggests. This allowed W and Mo to be readily sequestered into the silicates while Ir and various proportions of the remaining siderophile elements formed a metal or sulfide phase. All three meteorites later experienced a reduction event to various extents (Indarch > Acfer >> Allendé) that stripped part or all of the remaining siderophile elements from their silicate host. The reduction event is suggested to have taken place either prior to or simultaneously with the high temperature event that melted the silicates. The exact nature of the host phase of the siderophile elements would have to be determined by the local conditions, so that Allendé would have all of the siderophile elements partitioning into sulfides whereas in Acfer the dominant host would be native metal. The absence of sulfides from the interiors of Acfer type I PO(P) chondrules is suggested to be the result of lower regional pressure ($\leq 10^{-4}$ bar) compared to Indarch and Allendé, so that the sulfides remained in the gas phase until they condensed at lower temperatures around the outside of the chondrules. In contrast to this, Allendé and Indarch chondrules had sulfides (and metal in Indarch) co-existing simultaneously with silicate. Indarch RP chondrules are thought to be derived from the melting and recrystallization of pre-existing PP

chondrules. During the melting process the normally lithophile elements still observed in the PP chondrules were totally 'liberated', allowing them to partition into the unusual sulfide and metal phases of the enstatite chondrites.

Karoonda chondrules probably had similar oxidized precursors to Acfer, Allendé and Indarch but underwent a further oxidation process to produce Fe^{3+}. The oxidation process would initially have to have been at subsolidus temperatures to allow for the formation of crystallographically orientated microscale magnetite inclusions in olivine. This was followed by a sufficient increase in temperature to melt and recrystallize the olivine while liberating the magnetite inclusions. Iridium was sequestered to some extent prior to chondrule formation (probably into sulfides) but any siderophiles remaining in the silicates up to the melting event would partition either into co-existing oxide or sulfide melts. Since chondrules contain both dusty and clear olivine/pyroxene components (Figure 5.12a), it appears that the chondrule formation process already started prior to the heating event(s). However, clear and dusty olivine/pyroxene appear to be mostly randomly mixed in the Karoonda PO(P) chondrules (RP chondrules are dominantly composed of dusty pyroxene with a clear rim; Figure 5.12b), raising the question whether the heating event was simply limited in effectiveness or regionally restricted.

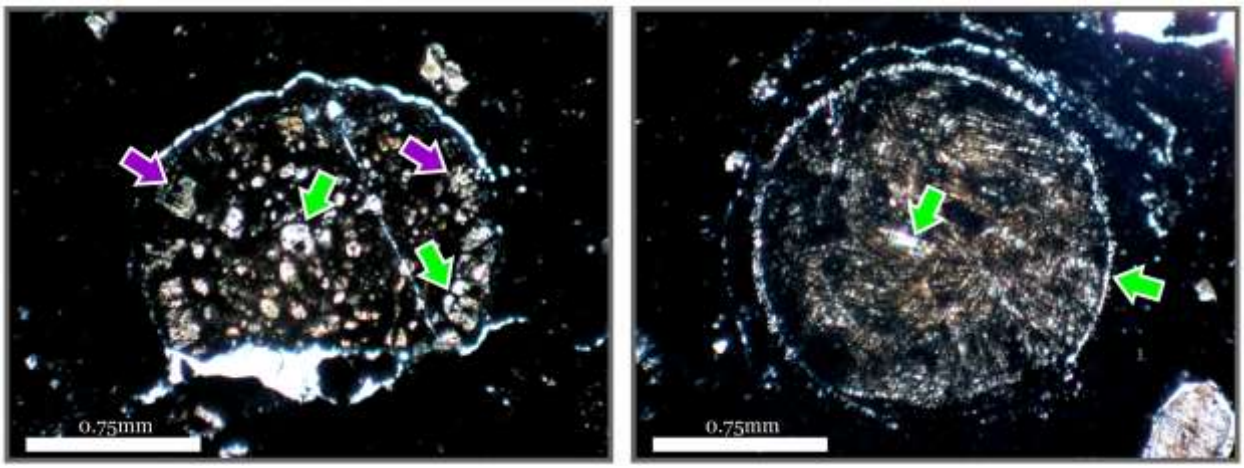

Figure 5.12 Photomicrographs of Karoonda CK4 chondrules showing presence of both dusty and clear olivine and pyroxene. a) PO(P) chondrules are mixtures of clear (green arrows) and dusty (purple arrows) olivine while RP chondrules (b) are dominated by dusty pyroxene with only few occurrences of clear grains (green arrows).

6 Planetary vs. Nebular origins

Several aspects of chondrule chemistry and petrography need to born in mind when discussing planetary and nebular settings for their origins: the refractory lithophile elements including the major oxides Al_2O_3, TiO_2 and CaO are largely unfractionated relative to each other and CI; siderophile and chalcophile elements are generally depleted relative to the lithophile elements; geochemical twins such as Sm-Nd and Ni-Co (usually) show the least variation of any element pairs; chondrules show a large degree of similarity in a single type of meteorite; chondrule compositions are strongly controlled by the bulk meteorite; all chondrules have oxidized precursors; some chondrule suites (e.g. RP and PP from Indarch) evolved from a common component.

6.1 Chondrule formation in a planetary environment

Creating chondrules in a planetary environment through impacts has several advantages such as abundant melts for chondrules as a likely products (Krot *et al.*, 2005); generation of a dense vapour-melt atmospheres that allows for the stability of sulfide melts at higher temperatures (~1380 K; Ebel & Grossman, 2000) and the direct condensation of silicate and metal liquids (Campbell *et al.*, 2002; Engler *et al.*, 2007); ^{26}Al is a potential heat source for self-insulating bodies that formed within <4.5 *Ma* of the Solar System (Lee *et al.*, 1976; Hevey & Sanders, 2006); gravitational settling of metal melts to form a core to explain the depletions of sidero- and chalcophile elements relative to the lithophile elements; fractional crystallisation can produce cumulate+melt mushes with typical chondrule minerals i.e. olivine, pyroxene and trace phases such as chromite and magnetite; igneous crystallisation process can produce zoned olivine grains with increases in FeO towards the rims.

A planetary origin has been invoked for the formation of CH/CB chondrules (e.g. Krot *et al.*, 2005, 2007) and also as a general solution by authors such as Asphaug *et al.* (2011). However, some restrictions on the planetary origin of chondrules as a model

includes the general lack of element fractionation amongst the HFSE, REE and major oxides Al_2O_3, TiO_2 and CaO found in this study. Igneous fractional crystallisation will initially act to enrich the incompatible elements in the residual melt and after a time start to produce element fractionations as more minerals are crystallised. For the scenario of colliding partially molten bodies this requires that both are chondritic in RLE elements and that no major silicate fractionation took place prior to the collision in order to maintain the flat REE patterns observed in Acfer and Allendé. For an impacting bolide-scenario it would require total melting of an impact site that was essentially chondritic in composition, at least in terms of RLE elements. However, as mentioned in Section 4.4, the REE patterns of Karoonda and Indarch chondrules are reminiscent of olivine and pyroxene crystallised from a melt. Conditions during olivine crystallisation would have to have been reducing (slightly for Karoonda, extremely for Indarch) in order to obtain observed negative Eu (and Yb in Indarch) anomalies (Figure 4.9). Such patterns cannot be established merely by internal partitioning in a chondrule of CI composition, since the whole chondrule will maintain its bulk chemistry. Fractionated REE patterns in whole chondrule data therefore require either that the complementary component was removed from the chondrule or, more likely, that the precursor was already fractionated. The extent of silicate fractionation could not have been extreme since the HFSE, Sm-Nd and refractory major elements for Karoonda chondrules do not deviate greatly from CI and the bulk meteorite. If the REE patterns in Karoonda and Indarch chondrules are, in fact, from fractional crystallisation it raises the possibility that the chondrules represent cumulate phases. Formation and segregation of immiscible sulfide and metal melts in a planetary body is most likely to occur in a partially or totally molten state, but core formation is inhibited by the tendency of metal droplets to stick to silicates until pressures exceeding 400 kbar are reached (Takafuji *et al.*, 2004) or shear forces are present (Rushmer *et al.*, 2005; McCoy *et al.*, 2006). Sulfide melts in contrast segregate more easily (Yoshino *et al.*, 2003). The presence of sulfides and metal in the chondrules

would therefor require that the immiscible melts did not exist at this point or were not segregated prior to impact or that the impact excavated and mixed already segregated silicate and metal. By having different oxidation states dominating each of the planetesimals prior to chondrule formation the siderophile elements can partition into the silicates accordingly and determine the presence or absence of metal. While this works as a general model, the studied samples each have special requirements: In Acfer reduction has to be included in the formation process since the chemistry requires oxidized precursors, and siderophile and lithophile elements show inverse correlations indicating varying amounts of metal. However, Acfer also requires an origin for its FeO-rich chondrules, which either need a different source or spatial variability in the reduction process. In contrast, the majority of Allendé chondrules contain only sulfides as the major non-silicate phase and become progressively more oxidized and SiO_2-rich towards the rims. While it is potentially possible to create a molten planetesimal with immiscible silicate and sulfide melts, the RLE patterns would require that the immiscibility threshold is achieved without any large degree of fractional crystallisation (this also holds for Acfer). The increase in FeO-content and pyroxene is not easily achieved by interaction with an evolved melt since this would change the REE and HFSE patterns. Interaction with the vapour from the collision is a possibility, but still requires that the vapour evolves without changing the REE and HFSE ratios. Karoonda probably best fits with a planetary origin where cumulus olivine and sulfide immiscibility have already been produced under oxidizing conditions followed by an episode of extreme oxidation just prior to chondrule formation. The second oxidation step could produce the observed immiscible oxide melts associated with the sulfides. A potential problem, however, is that any primary cumulate olivine is likely to have negligible REE contents compared to the bulk meteorite (Rollinson, 1993). Conversely large degrees of partial melting are likely to produce REE content similar to that of the bulk meteorite but this would most likely result in flat REE patterns (similar to terrestrial komatiites; Lesher & Arndt, 1995). Another factor to consider is that in

order to crystallize olivine with Mg# ~0.7 (chondrule olivine from Karoonda; Fitzgerald, 1979) from a magma, the equilibrium melt composition would have to be Mg# ~0.34 (Figure 6.1). Such low Mg# are never encountered in chondrules and only very seldom occur in matrix olivine (e.g. CV3 meteorites; Zolensky *et al.*, 1993). A CI composition melt with all the Fe as FeO has Mg# 0.55, which would yield an olivine

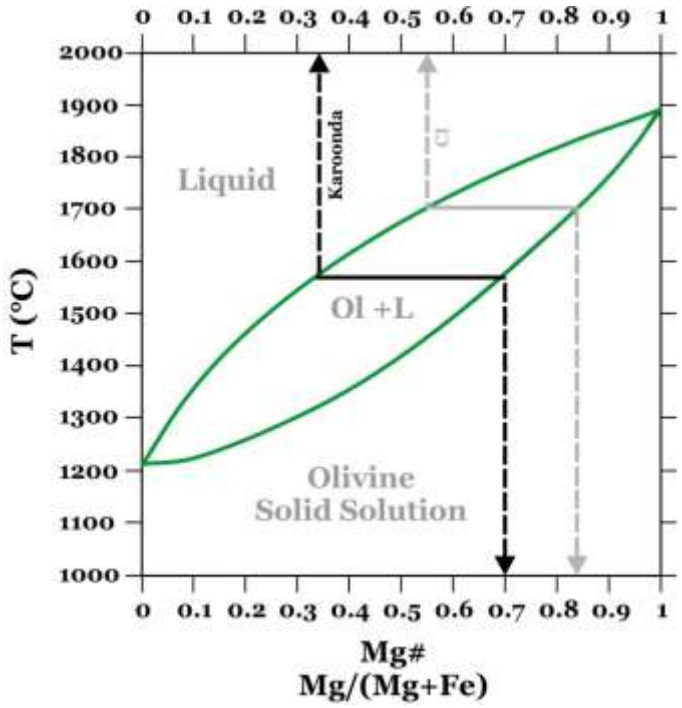

Figure 6.1 Olivine phase diagram at 1 atm. Black line indicates the composition of the liquid (Mg# ~0.35) that is required to be in equilibrium with the olivine in Karoonda chondrules (Mg# ~0.7). For comparison, the gray line indicates the composition of the solids (Mg# ~0.84) that would be in equilibrium with a CI composition melt (Mg# ~0.55). After Bowen & Schairer (1935).

composition of Mg# ~0.84. In addition, since textural evidence suggests that Karoonda olivine underwent subsolidus oxidization and possible oxide loss (see Section 5.1 and Figure 5.3) it suggests that the actual olivine composition may have originally been even more FeO-rich. The REE patterns for pyroxenes in Indarch RP chondrules are similar to a cumulate phase crystallised under extremely reducing conditions, although their textures refute that. However, the evidence that they share a common melt precursor with the PP chondrules opens an interesting possibility. The dominantly lithophile behaviour of e.g. Hf and Lu in the PP chondrules could originate

from their crystallisation as cumulate phases under more oxidizing conditions followed later by reduction. Since Lu and Hf retain their lithophile behaviour in the PP, it implies the REEs were not efficiently removed from the silicates during the reduction episode. If an impact occurred that melted some of the existing PP chondrules it would allow an REE 'free' silicate melt to form and equilibrate with the extremely reduced and REE enriched sulfide melt. If this silicate melt was cooled rapidly it could produce a new generation of RP chondrules with no remnant chemical signatures i.e. Lu would be concentrated exclusively in the sulfides to the exclusion of Hf. However, O-isotopes for the chondrules provide a very important constraint on theories of planetary origins for chondrules. Planetary processes such as fractional crystallisation will fractionate the O-isotopes according to mass to eventually produce a slope of 0.52, equivalent to that of the Terrestrial Fractionation line (White, 2007). Only the EC chondrules plot on a slope of ~0.5 while the CR and CV chondrules plot along the CCAM line with a slope of 1 (Clayton *et al.*, 1976; Krot *et al.*, 2006). While the details of O-isotope systematics are beyond the scope of this thesis, it seems likely that the kind of totally molten planetesimal impacts required to create the chemical patterns in Acfer and Allendé would produce a smaller, more homogenous spread in O-isotopes than observed. This is perhaps in part supported by the small range in O-isotope compositions observed for the cryptocrystalline chondrules from the CB_b chondrites (Krot *et al.*, 2006) that are thought to have originated through the impact of two totally molten bodies (Krot *et al.*, 2005, 2006). Karoonda chondrules plot on a slope of 0.82 (Clayton & Mayeda, 1999) but overlap to a great extent with the CV and CR chondrules. The slight shift in slope was attributed by the authors to metamorphism, but could conceivably also be from a degree of igneous evolution. It is also difficult to envisage a planetary setting that would produce both MgO-rich and FeO-rich chondrules from a single evolving magma without any form of element fractionation. Interestingly, Connolly *et al.* (2001) note that reduction of FeO to form native metal automatically enriches the silicate residue in SiO_2 to form orthopyroxene. This mechanism can be

directly applied to the EC chondrules and would explain the observed mineralogy to a great extent.

6.2 Chondrule formation in a nebular environment

On the other hand, chondrule formation by nebular processes also has distinct advantages. Observations of O-rich stars (e.g. Waters *et al.*, 1996) and planetary nebulæ (e.g. Waters *et al.*, 1998) show that O-rich stellar and nebular processes dominantly produce olivine, pyroxene, Fe-Mg amorphous silicates, Fe-metal (depending on the oxygen fugacity) and minor metal oxides such as Al_2O_3; nebular processes are known to transport non-equilibrium minerals from the cold outer disk to the hot inner disk where they equilibrate to the local conditions to create forsterite and Fe-Ni metal (e.g. Gail, 2004); turbulence in the solar system is known to transport material from the inner solar system outwards and from the midplane 'upwards' (e.g. Cuzzi *et al.*, 2003); silicate and metal phases may condensate simultaneously but separately (Campbell *et al.,* 2002); settling of particles to the midplane is strongly linked to mass/density (Alexander, 2008) and can act as a separation mechanism to produce siderophile and lithophile fractionation; REE patterns are unlikely to be changed by gas-solid reaction since it is likely that the REE will be already concentrated in the solid phase; nebular heating events can produce sufficient heat to melt but not vaporise chondrule precursor material (e.g. Desch *et al.*, 2005); nebular heating events such as shock fronts are repeatable (Boss & Durisen, 2005) as opposed to heating by radioactive nuclides such as ^{26}Al; high temperature interactions between ^{16}O-rich and –poor gases and solids are likely to plot on slopes greater than 0.52; several processes exist to regulate the local fO_2 state in a nebula, e.g. depletion of water stabilises sulfide phases (Pasek *et al.*, 2005); high density regions necessary for chondrule formation can be created by turbulent nebulæ (Boss & Durisen, 2005).

Maintaining CI ratios between the refractory elements and Ni-Co should be far simpler to achieve in a nebular environment than a planetary one if olivine (±metal) is the first

equilibrium high temperature phase as speculated in Section 4.4. At the temperature that forsterite is first stable in a canonical nebula (~1354 K; Lodders, 2003) REEs and the other RLE are proposed to uniformly condense into forsterite if no higher temperature phase is available. Assuming that this is feasible it would provide a ready source of forsterite for type I chondrules with slightly elevated RLE. In contrast, if the oxidized outer layers of stars are a source of primary olivine with a higher FeO content it could perhaps provide the precursor material for the type II chondrules as long as they are not entirely equilibrated under canonical conditions. This is thought to be in accordance with the observation that type II PO chondrules generally have larger olivine phenocrysts than type I (Hewins, 1997) if the type II precursor materials were not melted at such high temperatures or for so long. However, FeO-rich olivine produced in the outer oxidized shells of stars would have to have the zoned chemical profiles and euhedral shapes observed in type II olivine phenocrysts (e.g. Jones & Lofgren, 1993). Abreu & Brearley (2010) noted that the matrices of two pristine CR3 meteorites are dominated by amorphous FeO-rich silicates with minor olivine and pyroxene. This assemblage is similar to what might have been the primordial solar nebula prior to stellar ignition and would link in with the observations that the CR chondrites are extremely primitive in their chemical compositions (this study; Kong & Palme, 1999). The occurrence of both MgO-rich and FeO-rich chondrules in the same meteorite (e.g. Acfer 311 and Allendé) possibly requires that they were produced in different regions and mixed. However, considering the control of the bulk meteorite composition on the chondrules in this study, which are mostly MgO-rich, it needs to be investigated whether the same association holds for the FeO-rich chondrules. If it does, then the production of both type I and II chondrules from a specific meteorite a) has to occur within the same nebular region and b) has to be preceded by the chemical evolution of the formation region. Aluminium-Mg dating of chondrules from OC meteorites by Kurahashi *et al.* (2008) supports the idea of a single source region for both type I and II in a single meteorite. The authors suggest that the differences in

mineralogy are due to fluctuating oxidation states in the chondrule formation region. These can be plausibly linked to FU Orionis type outbursts that create advancing and retreating thermal fronts (e.g. Boley *et al.*, 2008) that could in turn influence the local oxidation states (e.g. Pasek *et al.*, 2005). An interesting aspect of having a more oxidized primordial solar nebula is the potential effect on the distribution of W and Mo relative to Ir since the former might both occur in silicates. Metal produced from reduction of such silicates during later re-equilibration of the solar system would potentially maintain the observed relationships i.e. Ir<W,Mo. Although olivine is commonly the dominant high temperature silicate in condensation models for the solar nebula, it is also possible to create pyroxene. Interaction with an evolved SiO_2-enriched gas (e.g. Libourel *et al.*, 2006) or direct condensation from a gas that has already been depleted in olivine (Engler *et al.*, 2007) are good candidates for producing textures observed in e.g. Allendé POP chondrules. However, these processes tend to produce pyroxene with flat REE patterns (Engler *et al.*, 2007), which is markedly different from the patterns observed in the EC chondrules. Formation of EC sulfides in a nebular setting has been linked to the primary condensation under extremely reducing conditions (C/O ~3x solar; Lodders & Fegley, 1993) and enhanced pressures (10^{-3} to 1 bar; Herndon & Suess, 1976; Lodders & Fegley, 1993). Gannoun *et al.* (2011), however, note that although oldhamite and orthopyroxene from the same EC meteorites have complementary REE patterns, the patterns for oldhamite do not agree with those predicted from thermodynamic calculations (Lodders & Fegley, 1993). According to the calculations of Lodders & Fegley, oldhamite condensing from a gas should have either flat REE patterns or otherwise depletions in the more volatile Eu and Yb. In contrast Gannoun *et al.* (2011) find that oldhamites commonly have positive Eu anomalies. However, under the extremely reducing conditions of the EC chondrites it is likely that both Eu and Yb will be in their +2 states (for examples of Yb^{2+}, see Amorello *et al.*, 2007), making them more compatible in the oldhamite structure and less compatible in that of enstatite. This suggests that either the exact condensation

sequence does not match the calculated order, or that another process is at work. There is also the question of the observed sloping REE patterns with negative Eu-anomalies in the Karoonda chondrules. The general enrichment in the Karoonda chondrule RLE in the studied chondrules conforms to the idea of a higher temperature condensate or evaporative residue. However, in order to produce the observed negative Eu-anomalies because of the higher volatility of Eu (i.e. similar to the negative Eu anomalies observed in CAIs), the olivine in Karoonda chondrules would have to condense at a temperature of >1400 K at 10^{-3} bars (Kornacki & Fegley, 1986). This is considered highly unlikely for Karoonda, since both 'normal' condensation sequences for the Solar System (e.g. Lodders, 2003) as well as shock heating (which have associated temperatures of ~1800 K; Desch *et al.*, 2005) predict the appearance of almost pure forsterite (Nahagara *et al.*, 1994). The latter authors produced a phase diagram for olivine evaporation for 10^{-4} bar (Figure 6.2). If the bulk Mg# for the CCh meteorites (Mg# ~0.57) is used as starting material and heated to 1750°C, it produces an olivine composition of Mg# 0.97. This agrees with published olivine compositions for Acfer and Allendé, but not for Karoonda (Figure 3.1). One possibility is to condense melilite in the Karoonda formation region prior to olivine formation since it has a preference for the LREE over the HREE and commonly has positive Eu-anomalies (e.g. Weber *et al.*, 1995). Although this provides a potential origin for the REE patterns and depletions in Ca, Ba and Sr (Figure 3.4, 3.5 and 3.7) the full effects of melilite condensation on the Karoonda bulk composition as well as a mechanism to separate melilite from olivine without losing the former from the bulk formation region would have to be further investigated.

6.3 Summary Chapter 6

Even with the large range of elements analysed in this study it is difficult to unambiguously distinguish between planetary and nebular formation environments for the CCh chondrules. However, the presented data and arguments appear to argue for a

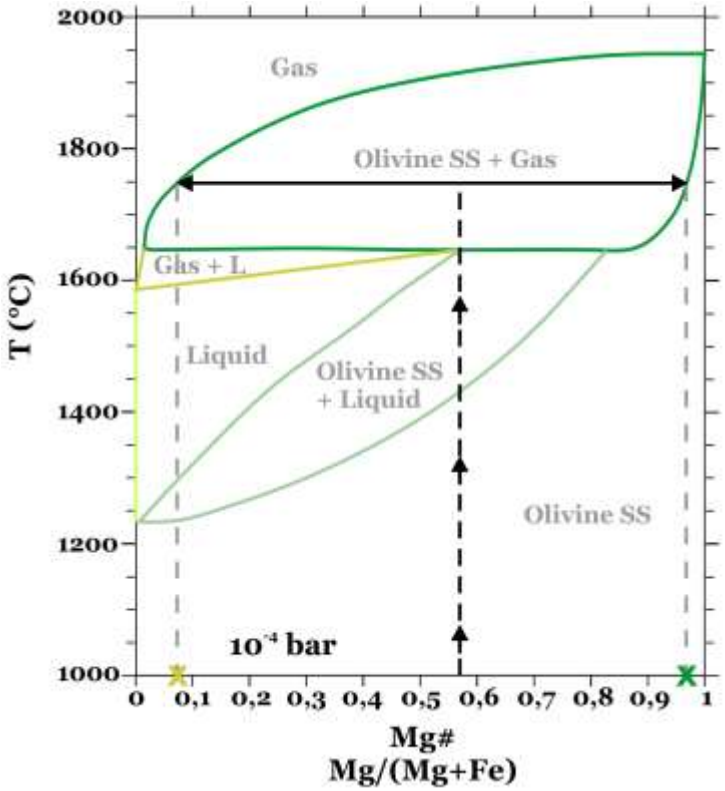

Figure 6.2 Phase diagram for olivine condensation from a solar composition gas at 10^{-4} bar (after Nagahara et al., 1994). If a starting material with a composition equal to the average bulk carbonaceous chondrites (Mg# ~0.57) is flash heated to ~1750°C, olivine with a composition of Mg# 0.97 would condense (green cross), which is similar to the olivine compositions in Acfer and Allendé chondrules studied here. The remaining gas (yellow cross) would be extremely enriched in Fe (Mg# 0.07).

nebular setting for formation of Acfer and Allendé chondrules, while Karoonda and Indarch require planetary settings to best explain the observed chemical trends. Producing olivine for the Acfer and Allendé chondrules by magmatic processes would require a parent liquid that is more Mg-rich than bulk CI since fractional crystallisation of a melt with Mg# ~0.55 will yield olivine with a lower Mg# than observed (i.e. ~0.85 vs. ~0.98 in Acfer and Allendé). However, creating the observed olivine compositions for Acfer and Allendé starting with a CI precursor and shock heating it under low ambient pressures (evaporation) is experimentally feasible (Figure 6.2) and the preferred formation mechanism. The extremely FeO-enriched gas produced as a by-product would most likely be unstable at typical Solar System conditions and is expected to decompose to stable products such as native metal and a more Mg-rich silicate phase. Chemically unfractionated precursors (i.e. relative to the Solar System)

for the Acfer and Allendé chondrules are proposed to have been abundant in the young Solar System since they are the likely major phases produced by the local stars that added their ejecta to the interstellar medium.

Both Karoonda and Indarch chondrules resemble to some extent cumulate phases, so that a planetary/fractional crystallisation environment is plausible. The chemical signatures for the REE patterns in particular are unlikely to be produced by nebular fractionation processes but are more typical for an igneous environment. The envisaged setting for formation of Karoonda and Indarch chondrules would require a parent body with pre-existing cumulate olivine and chondrules/pyroxene respectively which is hit by an impactor. At this point it is unclear whether or not the impacted surface on the Karoonda parent body would have been solid or a crystal+melt mush. Regardless of which, the parent body must necessarily have undergone a degree of fractional crystallisation to produce the observed REE patterns and may have experienced silicate-sulfide/oxide differentiation. The postulated scenario for Indarch is a bit more complex. Chemical differences between the Indarch RP and PP chondrules can be explained if the former were derived from the latter. It is unclear whether or not this requires that the PP chondrules already existed *per se*, or merely that cumulate pyroxene was available to form the chondrules. However, what does appear to be plausible from the data presented in Section 5, is that the PP chondrules (or their precursors) formed prior to the major reduction episode and did not equilibrate fully at subsolidus conditions with the reduced setting. The melt for the RP chondrules was derived from totally melting existing PP chondrules (or their precursors) under the extremely reducing conditions present allowing the RP chondrules to achieve equilibrium. The heat source for the melting is thought to be an impact since melt veins are present in thin section.

7 Timing and choices for suitable formation mechanisms

Based on the observations regarding the timing of the different growth stages of solar-type nebulæ and the ages of various Solar System events shown in Figure 1.3, we can estimate the likelihood of the nebular formation mechanisms in Table 1.2. As mentioned in Section 1.2.1, km-sized bodies are capable of being formed in 10^4 *a* (Scott, 2006 and refs. therein), potentially with some implications for nebular models of chondrule formation that require the presence of <mm size particles e.g. current sheets (Joung *et al.*, 2004). Electrical current sheets are thought to be possible only after several *Ma* of disk evolution when the dust:gas ratio in the midplane has been sufficiently enriched (Joung *et al.*, 2004). However, judging by the amount of planetary activity that was already present by 3 *Ma* (Figure 1.3) it is perhaps likely that too large a proportion of dust may already have been removed from the disk in the form of larger particles (>1 m) for the formation of current sheets to be effective. The latter requires small particles (~1 mm) and a dust:gas ratio of 50 (Joung *et al.*, 2004). Although the formation of current sheets potentially fits the chondrule formation window at 2-3 *Ma* (Figure 1.3 & 1.4), it might only operate on a 'local' scale where small patches of dust remain. Even assuming that only a small percentage of dust in the young Solar System was locked up in bodies of >1 km in diameter so that a dust-rich layer is created at the midplane, the creation of current sheets is still restricted to the thin upper layer of the midplane (several 10's of meters) exposed to cosmic and X-rays (Joung *et al.*, 2004). The amount of particles melted to become chondrules is then strongly dependent on turbulence within in the midplane bringing fresh material to the surface (Joung *et al.*, 2008), and how long the current sheets can be stably maintained. A further consideration is that melted grains in the outer margin of the midplane might not be sufficiently insulated to produce the observed porphyritic textures. Unless downward transport from the surface to a heated, insulated region is very fast, this would result in the production of a greater amount of rapidly cooled chondrules (BO,

RP, CC) than is observed in chondrites. Accretion shocks from the formation of the protodisk (Ruzmaikina & Ipp, 1994) are necessarily an early event, probably occurring before or overlapping with the release of gravitational energy from the nascent Sun. However, since the average size for interstellar medium particles is generally in the order of 1 μm or less (Pei, 1991; Kim *et al.*, 1994; Casuso & Beckmann, 2010), heating from accretionary shocks (frictional and UV; Ruzmaikina & Ipp, 1994) might evaporate a significant proportion of material rather than purely melting it. In this regard Ruzmainka & Ipp (1994) raise the possibility that interstellar medium (ISM) grains may already have coagulated to sizes ≥1mm, making their survival more likely. Release of gravitational energy as material is accumulated onto the nascent sun is in itself an efficient heating mechanism and will generate temperatures hot enough to melt silicates up to 3 AU within the first ~10^4 *a* (see Section 1.2.1; Cuzzi *et al.*, 2003). Flare heating (e.g. Shu *et al.*, 1996, 2001; Boley *et al.*, 2008) also provides a potential heat source for both CAIs and chondrules, but is restricted by the necessity for small (<several mm) particles. Assuming that >1km bodies are formed within 10^4 *a*, this requires that flare heating takes place in less time than this. However, observation-based models for Solar System evolution (Figure 1.3 and references therein) suggest that the Sun would not have reached a flaring-state for the first ~5 x 10^5 *a* after collapse of the nebular cloud, making flaring unlikely as a viable heat source. One shortcoming for flare heating, accretionary shock and gravitational energy release models is the lack of extremely young chondrule ages (<1 *Ma* after CAI), although the possibility exists that such young chondrules may have been reset during subsequent high temperature events. Planetesimal bow shocks (Miura *et al.*, 2010), shock fronts created by the formation of the gas planets (Boss & Durison, 2005) and planetesimal collisions or ablation (Krot *et al.*,, 2005, 2007; Asphaug *et al.*, 2011) on the other hand require the presence of planetesimals (>1 km) prior to the formation of chondrules. The overlap in ages for chondrules and differentiation of planetary bodies (Figure 1.3 and references therein) makes it likely that planetesimals directly or indirectly

contributed to chondrule formation. Shock fronts due to the formation of the gas planets potentially also provide a useful setting for the direct condensation of melts (Krot *et al.*, 2001; Engler *et al.*, 2007) since they are likely to turbulently concentrate dust/gas and provide heat sources for melting (Boss & Durisen, 2005). Impacts between planetesimals that are of sufficient magnitude to produce chondrules have already been documented for the CB/CH meteorites (Krot *et al.*, 2005, 2007) and overlap with the approximate formation time of the gas planets. Therefore it appears that formation mechanisms that either directly or indirectly involve planetesimals are temporally the most favourable. However, even if chondrule formation mechanisms are restricted to those that somehow involve planet formation, the time-window for chondrule formation is rather small. Assuming that all impacts that are sufficiently energetic to produce melt can potentially create chondrules, it seems remarkable that the CB chondrules appear to be the last recorded case of impact formation. The Moon-forming impact on Earth (e.g Yin *et al.*, 2002) suggests that highly energetic impacts were still occurring for at least another 7 *Ma* after the CB chondrites were formed (Figure 1.3). Either we have not yet sampled the youngest chondrules, or the end of the chondrule forming window at 7 *Ma* after CAI represents the start of a quiet, less-energetic Solar System and the Moon-forming impact was essentially a fluke.

The chemistry of Acfer and Allendé chondrules are interpreted in this work to require a nebular setting and only limited reworking (chapter 6). Although this hypothesis does not exclude the synchronous formation of Acfer and Allendé chondrules and the existence of planetesimals in the Solar System, it does exclude the contribution of planetesimals to the origin of these chondrules. The author favours a scenario of turbulent concentration, specifically the formation of eddies and related stagnant zones that could concentrate dust and gas. The presence of eddies in the young Solar System and their effect on dust and gas have been modeled on multiple occasions by authors such as Edgeworth (1949), Wood (1998) and Cuzzi *et al.* (2001). In the past, though,

turbulent concentration has mostly been viewed as a method to concentrate pre-existing chondrules. However, the writer feels that it might be worthwhile to consider the effects of frictional heating in such a setting since authors such as Wood (1984) have calculated temperatures for frictional heating within the melting range of silicates (i.e. 1500 to 2000 K; Wood, 1984). It might also be worth considering the effect of the likely presence of water adsorbed onto the surface of olivine grains (King *et al.*, 2010), probably in the form of ice (Wood, 1984 and references therein). On Earth, free water is accepted as an aid for melting in a number of scenarios, including migmatisation (e.g. Berger *et al.*, 2008) and arc magmatism (e.g. Rüpke *et al.*, 2004). If the postulated dust and gas concentration regions started off with fairly cold material (i.e. several hundred K) adsorbed water may have been present and able to assist in chondrule formation by lowering the solidus temperature for the dust. Alternatively regions of dust and gas concentration with large local densities could stabilise direct condensation of both silicate and metal or sulfide melts as proposed by Krot *et al.* (2001) and Engler *et al.* (2007). However, this requires that the region is heated to >1700 K in order to vaporise the dust and might require an external heat source such as flare heating. Regardless of a melting or condensation scenario, a dense 'atmosphere' in the concentration region will serve to insulate the molten material, allowing the development of porphyritic textures observed in most chondrules. The relationship between porphyritic and fine grained/rapidly grown chondrules (BO, CC, RP) can also be explained by this scenario. One possibility is that the fine grained chondrules originate in the poorly insulated outer layers of the chondrule forming region and essentially represent a chilled margin equivalent to those found in terrestrial plutonic rocks. However, the chemical evolution of the 'source' needs to be considered since the majority of fine grained chondrules appear to be pyroxene normative (Bridges *et al.*, 1998; Engler *et al.*, 2007). Condensation of olivine as the first stable phase will enrich the remaining gas in silica to produce pyroxene as suggested by Engler *et al.* (2007). However, this would restrict the formation of

pyroxene-normative fine grained chondrules to the later stages of chondrule formation parallel to the appearance of pyroxene in porphyritic chondrules, and raise the question of why more olivine-normative fine grained chondrules are not found. High local pressure in a turbulently concentrated area will stabilize metals and sulfides at higher temperatures (Lodders & Fegley, Jr., 1993; Krot *et al.*, 2007) making it possible that silicate-metal/sulfide immiscibility could occur simultaneously to heating. A complete review of turbulence within such a chondrule forming region is beyond the scope of this thesis, but it is strongly suspected that density separation of metals, sulfides and silicates will still take place providing a mechanism for producing the siderophile element depletion observed in chondrules.

Karoonda and Indarch RP chondrules are argued to represent material processed in a magmatic and asteroidal impact setting respectively. The necessity of a planetary setting is suggested to constrain the formation window of Karoonda and Indarch RP to a later epoch compared to Acfer and Allendé chondrules. This is also based on the I-Xe formation ages for chondrules from Qingzhen and Kota Kota EH3s (Figure 1.4; Whitby *et al.*, 2002), but needs to be confirmed for Indarch and Karoonda chondrules and also with alternative isotopic systems. However, the contemporaneous formation ages of the impact-produced CB chondrules (Krot *et al.*, 2005) with the EH3 chondrules of Whitby *et al.* (2002) lends some credence to the idea that planetary impacts may have been a common chondrule formation mechanism during this time. It is therefore suggested that chondrule formation can be roughly divided into two epochs, the first of which is dominated by nebular processes and the second by planetary processes, but with some overlap between the two as the relative amount of planetesimals and impacts increased over time. The window within which Karoonda and Indarch chondrules could be produced by impacts into (partially) molten bodies has to be restricted to a narrow time frame during the early history of the respective planetesimals. This is required to maintain the CI ratios amongst the RLE in Karoonda and Indarch

chondrules which would otherwise be disturbed by advanced differentiation or fractional crystallisation. Furthermore, if turbulent concentration of material is also considered as a potential planet formation mechanism (e.g. Avinash *et al.*, 2006; Cuzzi *et al.*, 2008; Chambers, 2010) for the Solar System in addition to oligarchic growth (see Chamber, 2004 and references therein), then the relationships between nebular and planetary-type chondrules needs to be considered. In the previous paragraphs turbulent concentration is emphasized as the author's choice for supplying suitable nebular conditions to create chondrules such as those found in Acfer and Allendé. If the same mechanism then carries on to form a planetesimal from the existing material in the turbulent region, the previously formed chondrules may either be melted by internal planetary processes or provide a 'soft target' depending on the nature of the planetesimal. If, however, a planetesimal is grown from oligarchic processes, it does not necessarily require the involvement of pre-existing nebular-type chondrules but can ultimately lead to the formation of chondrules through impacts.

However, at this point a last look at the available O-isotope data is warranted. The preferred nebular origin for the CV and CR chondrite chondrules based on chondrule chemistry data obtained in this study is in accordance with the generally accepted theories based on $\delta^{17}O$ and $\delta^{18}O$ data (Figure 1.2; Krot *et al.*, 2006a, b; Rudraswami *et al.*, 2011). As already mentioned, unaltered chondrules from these chondrites plot on or close to the CCAM line with slopes ~1 (as opposed to the TFL with slope ~0.52), which is accepted to be the result of the interaction of ^{16}O-rich precursor materials with a ^{16}O-poor gas or mixtures of components (e.g. Clayton *et al.*, 1993 and references therein; Krot *et al.*, 2006a, b; Rudraswami *et al.*, 2011; Weisberg *et al.*, 2001). The chondrules for CV and CR chondrites are further characterised by having internally homogenous O-isotopes (with the exception of relict grains; Krot *et al.*, 2006a, b; Rudraswami *et al.*, 2011) but show a spread in $\delta^{17}O$ and $\delta^{18}O$ values, suggesting little or no homogenisation of O-isotopes within the formation region. In contrast, O-isotope

data for the EC chondrules (Figure 1.2) show a large degree of homogenisation and plot as a small group overlapping with the TFL. Clayton & Mayeda (1985) interpreted this as an indication of almost complete equilibrium with the surrounding gas in terms of a nebular origin. However, in light of the data set presented in this study, which suggests a large degree of metal-sulfide melt extraction from the EC chondrules, we might also consider that the more or less homogeneous O-isotopes in EC chondrites are the result of an igneous origin in a mostly molten, well mixed parent body where mass-dependent fractionation is a dominant process. Oxygen isotope data for Karoonda, however, does not provide definitive support for the idea of an igneous origin for CK chondrules since, on a three isotope plot, they do not plot with a slope of ~0.5 and do not show extensive homogenisation. In Section 6.1 the suggestion is put forward that the slope of ~0.8 for unaltered CK chondrules should perhaps be considered as the result of the onset of fractional crystallisation, as opposed to the traditional view (Clayton & Mayeda, 1999) that the slope is the result of metamorphism of chondrules with a nebular origin. Although the data presented here suggest an igneous origin for the CK chondrules, more work, perhaps in the form of modeling of the simultaneous evolution of the REE and O-isotopes, is required to support (or refute) an origin by igneous crystallisation.

8 Summary

Liberating chondrules by Freeze-Thaw provides a powerful tool for analysing whole chondrules. The technique preserves structural information such as multi-layered rims as well as original mineralogy including metal and sulfides. Chondrules can be sorted based on relative proportions of minerals and textures observed with a binocular microscope and directly related back to common textures in thin sections. Whole chondrule observations also give the opportunity to analyse textures and mineral associations of chondrules (particularly of the surface) in 3D and compare them to models based on 2D thin section-based theories of formation. Chemical analysis of a whole chondrule essentially reports the composition of its precursor components plus the addition of rims. The effect of the added rims on the chemistry of the chondrule can be monitored by analysing chondrules with rims of varying thicknesses and making careful observations about accompanying changes in mineralogy. The sole drawback of the Freeze-Thaw method is its time consuming nature, but this can be partially optimised by disaggregating multiple samples simultaneously. Preparation of individual chondrules for dissolution and analysis is restricted to cleansing ultrasonic baths with ethanol and distilled acetone respectively, and a gentle tap with a pestle to increase the active surface. Powdering of the samples was avoided due to small sample sizes and high risk of contamination, but was shown to be unnecessary. Table top dissolution with mixtures of HF, HNO_3, HCl and $HClO_4$ proved effective in breaking down all mineral phases present in the analysed chondrules, avoiding time consuming and potentially high contamination-risk pressure dissolution procedures. Measurement of the chondrule solutions by ICP-OES and –MS yielded results with better than 3% RSD for most elements, allowing good comparison between chondrules. Plotting of CaO vs. FeO (wt%) in a fashion similar to the Sears *et al.* (1992) single mineral phase classification scheme for chondrules showed that these plots are also useful for whole chondrule data. Its usefulness in this case lies in the identification of

evolutionary trends in the entire chondrule caused by the addition of mew minerals through evolution of the source. Relationships amongst related chondrules that have a common source but different mineralogical histories are also identified by plotting CaO vs. FeO (wt%). Further discrimination ratios for distinguishing CCh chondrule suites are dominantly based on siderophile and chalcophile elements, some in combination with the moderately volatile lithophiles Mg and Fe since distinction using only the RLE+Mg+Fe did not prove effective. In contrast, the EC chondrule suites are effectively distinguished using several of the RLE and Cr, although it is interesting to note that all these elements behave as either siderophile or chalcophile elements in the EC.

Porphyritic and barred olivine chondrules from the carbonaceous chondrites Acfer 311 (CR2), Allendé (CV3) and Karoonda (CK4) have volatility arranged, CI-normalised patterns that decrease in abundance proportional to volatility for the moderately volatile and volatile elements. This is in contrast to the essentially flat pattern for chondrules from the enstatite chondrite Indarch (EH4). The composition of the analysed chondrules and bulk meteorites have ~1:1 relationships suggesting that the formation regions (bulk meteorite) control the chondrule compositions and were depleted in volatiles prior to the formation of chondrules. This implies that chondrule formation regions as a whole are likely to have behaved as closed systems, even if open system behaviour was experienced at the chondrule scale (Cohen *et al.*, 2004; Tsuchiyama *et al.*, 2004). The lack of volatile depletion in the Indarch bulk meteorite (and also in its chondrules) relative to the RLE elements stands in direct contradiction to the theory that the enstatite chondrites formed close to the Sun (Anders, 1971; Baedecker & Wasson, 1975; Shukolyukov & Lugmair, 2004) as indicated by their high temperature, reduced mineralogies and Mn-Cr data. If the depletion of volatile elements in the bulk meteorite is taken as an indicator for distance of the formation region from the Sun, the enstatite chondrites would therefore have to have formed at a

greater radial distance compared to the carbonaceous chondrites. Alternatively a mechanism has to be found either by which the entire EC formation region can be enriched in volatile elements or the volatile elements are locked in stable minerals at an early stage in the evolutionary history.

Likely precursor material for chondrules is pre-existing material from the source region for the Solar nebula rich in both olivine and FeO-rich amorphous material as well as metal oxides, the former most likely containing close to CI levels of refractory lithophile elements in solar proportions. Heating of this material at general Solar System conditions (10^{-4} bar; $H_2O/H_2=5.0 \times 10^{-4}$; Lodders, 2003) to ~1800K would produce the equilibrium components forsterite and metal (Nagahara *et al.,* 1994; Lodders, 2003) observed in most chondrules, while processing at lower temperatures or slightly different local conditions may have preserved the more FeO-rich precursor compositions. Chondrule formation processes appear to be unrelated to the formation of the refractory phases found in CAIs, nor were large amounts of CAI-type phases produced in the same region prior to the chondrules. Strong depletions in siderophile elements observed in chondrules are due to isolation of metal or sulfide phases prior to chondrule formation. The degree of siderophile element depletion as well as the degree of correlation between siderophile and chalcophile elements is directly linked to the oxidation state of the formation region, with a noticeable increase in the siderophile content of the silicates with increasing local oxidation. Evidence for later re-addition of the initially isolated metal/sulfide phase is observed in the evolution of chondrules in the order BO-PO-POP. Formation of immiscible silicate-metal or silicate-sulfide textures probably formed through both the heating of mixed silicate and metal or sulfide particles and through immiscibility produced by crystallisation of molten droplets. Refractory lithophile elements in Acfer and Allendé chondrules have primitive ratios and were sourced from the pre-existing primary nebular material. Apart from heating, the analysed chondrules do not show evidence that their

precursors experienced extensive processing and mineral/lithophile element fractionation. Compositions for the olivine found in Acfer and Allendé chondrules (Mg# ~0.97) are well approximated by the phase diagrams of Nagahara *et al.* (1994) for rapid heating of solar composition material (Mg# ~0.57) at 10^{-4} bar. Such high Mg# cannot be produced by simple fractional crystallisation of olivine (Bowen & Schairer, 1935) from a melt of solar composition. Rare Earth Element patterns for these chondrules further argue against a magmatic origin and require precursor material almost equivalent in RLE (and moderately volatile lithophile element) composition to that of the bulk meteorite with little or no mineral and related element fractionation. In short, the chemistry of Acfer and Allendé chondrules do not record a formation history linked to planetesimal evolution beyond alteration and metamorphism that would have occurred during formation of the CR and CV parent bodies. Formation of CR and CV chondrules is thought to have occurred in turbulent eddies or their related stagnation zones that concentrated dust and gas. The dominant heat source is speculated to be frictional heating, possibly assisted by H_2O ices adsorbed onto the surface of olivine that may have acted to lower the solidus of the dust particles. In contrast, chondrules from Karoonda and Indarch show evidence of reworking in a planetary setting despite also having RLE with solar relationships. Karoonda and Indarch chondrules have REE signatures that are similar to those of olivine and pyroxene crystallised from magmatic systems. Continuing with the hypothesis that the bulk meteorite formation region (Mg# ~0.55 ≈ CI) determines the composition of the chondrules and assuming that the Karoonda chondrules may have formed as a cumulate phase, then it requires an extremely FeO-rich parental melt (Mg# ~0.34) and raises the possibility that it was evolved from a CI-like magma by olivine crystallisation. Karoonda olivine may therefore represent a later stage of magmatic evolution, which also makes the coexistence of immiscible sulfide and oxide melts more likely. The similarity between Karoonda chondrules and the bulk meteorite composition also suggests that the planetesimal may have been either homogenously

mixed, or that the silicate and sulfide phases were not able to unmix, perhaps due to a too large degree of crystallinity. Pyroxene from Indarch has a more complex history compared to any of the analysed carbonaceous chondrules and most likely started with FeO-rich compositions. As with the CCh chondrules, origin of the precursor material for EC pyroxene is suggested to be primary solar nebular silicates. Indarch PP chondrules are suggested to represent the first phase of chondrule or cumulate formation in the EC formation region at higher fO_2 than is currently recorded in the enstatite chondrites. Extreme reduction of the oxidized EC PP chondrules probably occurred simultaneously to heating, but the latter was insufficient to completely melt and re-equilibrate the existing PP chondrules. This is shown by the common dusty appearance of PP pyroxene crystals as well as the apparently lithophile behaviour of such elements as Lu and Ti, which are known to behave as chalcophile elements in the EC. Indarch RP chondrules are suggested to represent a second generation of chondrules produced by an impact into the existing PP chondrules, which also produced metal-sulfide impact veins. The RP chondrules show complete re-equilibration of all elements under extremely reducing conditions.

9 Suggested research topics

- Modeling the evolution of liquids and solids produced by the magmatic crystallisation of a melt with a starting composition equivalent to bulk meteorite and not necessarily CI.
- Modeling of magmatic crystallisation in a highly reduced system (equivalent to EC) crystallising oldhamite and enstatite, using bulk EC meteorite as starting composition.
- Investigate processes that can produce the observed CI-equivalent composition of bulk E chondrites and compare the results to the generally accepted theory that E chondrites formed close to the Sun.
- Modeling the evolution of fO_2 conditions during turbulent concentration starting with both CI-like and bulk meteorite equivalent compositions, specifically related to the possible formation of extremely reducing environments.
- Acquisition of more detailed bulk meteorite data.
- Acquisition of whole chondrule data from (preferably) all chondrite meteorite groups.
- Investigate the contrasting behaviour of Co/Ir vs. Fe/Ir (Figure 5.7) in Indarch EH4 chondrules compared to the CCh chondrules, specifically focusing on the potential effects of metal (core) extraction from a CI-equivalent starting material, followed by magmatic evolution under oxidizing (fO_2 approx. equal to Acfer 311 initial conditions).
- Modeling the simultaneous evolution of O-isotopes and REE in a magmatic system with a starting material equivalent to bulk CK4 and O-isotopes plotting on the CCAM.
- Investigate how to produce an igneous parent melt with Mg# <0.3 without significant fractionation of the HFSE and RLE.
- Investigate the effectiveness of frictional heating in Solar System eddies.

- Investigate the effects of water adsorbed onto olivine during melting during chondrule formation, specifically focusing on possible effects on the solidus temperature and the effects of local pressure.
- Investigate the possibility of W inhomogeneity in the Solar System based on the apparent non-correlation of W to both the siderophile and lithophile elements in the precursor materials of the studied chondrules (e.g. Figures 3.3-3.5, 3.7, 5.5, 5.6).

Appendix A

Chondrule Catalogue

Acfer 311 CR2

Acfer-1 PO

Central chondrule

Other silicates: pyx
Mesostasis: 10%
Metal: minor
Oxides: lim, mgt, hmt
Sulfides: n/o
Remarks: Pyx increases towards chondrule rim; metal as interstitial blebs; anhedral ol

Rim

Present: Y
Silicates: pyx, ol, phyl
Metal: Y
Oxides: lim, mgt, hmt
Sulfides: n/o
Remarks: Rim is layered - inside is silicate + oxide layer, outside is metal/limonite layer

Acfer-2 PO

Central chondrule

Other silicates: N
Mesostasis: 10%
Metal: minor
Oxides: lim, mgt, hmt
Sulfides: n/o
Remarks: Metal as interstitial blebs; anhedral ol

Rim

Present: Y
Silicates: pyx, ol
Metal: Y
Oxides: lim, mgt, hmt
Sulfides: n/o
Remarks: Rim is layered - inside is silicate + oxide layer, outside is thin metal/limonite layer

Acfer-3 PO

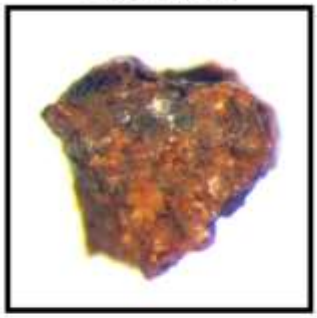

Central chondrule

Other silicates: ?
Mesostasis: 20%
Metal: minor
Oxides: lim, mgt, hmt
Sulfides: n/o
Remarks: Msts appears grayish from large volume small black oxides; anhedral ol

Rim

Present: Y
Silicates: N
Metal: n/o
Oxides: lim, mgt
Sulfides: n/o
Remarks: thin single layer rim

Acfer-4 PO

Central chondrule

Other silicates: pyx
Mesostasis: 15%
Metal: n/o
Oxides: lim, mgt, hmt
Sulfides: n/o
Remarks: Black and red oxides occur interstitially; anhedral ol with pyx laths

Rim

Present: Y
Silicates: pyx, ol,phyl
Metal: Y
Oxides: lim, mgt, hmt
Sulfides: n/o
Remarks: rim is layered - inside is thin fine grained black/red oxide+silicate mixture, middle is thick layer fine grained ol+pyx (?), outside is thick black oxide layer (after metal)

Acfer-5 PO

Central chondrule

Other silicates: pyx
Mesostasis: 15%
Metal: minor
Oxides: lim, mgt, hmt
Sulfides: n/o
Remarks: Black and red oxides occur interstitially; metal occurs as interstitial blebs; anhedral ol and pyx

Rim

Present: Y
Silicates: pyx, ol, phyl
Metal: Y
Oxides: lim, mgt, hmt
Sulfides: n/o
Remarks: single layer mixture of ol, pyx, oxides and limonite (after metal)

Allendé CV3

Allendé-1 WC

Central chondrule

Other silicates:
Mesostasis:
Metal:
Oxides:
Sulfides:
Remarks:

Surface

Silicates: pyx, ol
Metal: N
Oxides: mgt
Sulfides: n/o
Remarks: fine grained; continuous

Allendé-2 WC

Central chondrule

Other silicates:
Mesostasis:
Metal:
Oxides:
Sulfides:
Remarks:

Surface

Silicates: pyx, ol, phyl
Metal: N
Oxides: mgt
Sulfides: Y
Remarks: relatively large pyx poikilitically enclosing ol; sulf finely disseminated

Allendé-3 WC

Central chondrule

Other silicates:
Mesostasis:
Metal:
Oxides:
Sulfides:
Remarks:

Surface

Silicates: pyx, ol, phyl
Metal: N
Oxides: mgt
Sulfides: Y
Remarks: coarse grained ol with some poikilitic pyx; phyl only minor; sulf finely disseminated or small blebs

Allendé-4 WC

Central chondrule
Other silicates:
Mesostasis:
Metal:
Oxides:
Sulfides:
Remarks:

Surface
Silicates: pyx, ol, phyl
Metal: N
Oxides: mgt
Sulfides: Y
Remarks: coarse grained pyx both as subhedral laths and poikilitically enclosing small ol; sulf both as small blebs and finely disseminated; fine silicates minor

Allendé-5 BO

Central chondrule
Other silicates: N
Mesostasis: 40%
Metal: N
Oxides: mgt?
Sulfides: Y
Remarks: Sulf + ox occur at ol-msts interface; ol bars relatively thick; ol fairly pale green

Rim
Present: Y
Silicates: ol+(pyx, phyl)
Metal: N
Oxides: lim, mgt
Sulfides: N
Remarks: double rim - inside is discontinuous magmatic ol rim, possibly unrelated to central chondrule, outside is a thin fine grained silicate sulf layer

Allendé-6 BO

Central chondrule
Other silicates: N
Mesostasis: 50%
Metal: N
Oxides: mgt?
Sulfides: Y
Remarks: Ol bars relatively thin; ol dark green

Rim
Present: Y
Silicates: ol
Metal: N
Oxides: N
Sulfides: N
Remarks: continuous magmatic ol rim; ol pale green

Allendé-7 BO

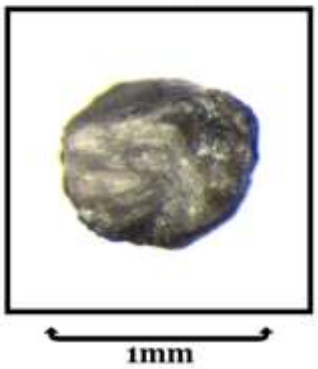

Central chondrule
Other silicates: N
Mesostasis: 50%
Metal: N
Oxides: N
Sulfides: N
Remarks: Ol bars relatively thin; interior has snowball-like structure; large volume of msts in center

Rim
Present: Y
Silicates: ol
Metal: N
Oxides: N
Sulfides: N
Remarks: double magmatic rim - inside is a thin continuous dark green ol rim, outside is a thicker fine grained of paler green ol

Allendé-15 BO

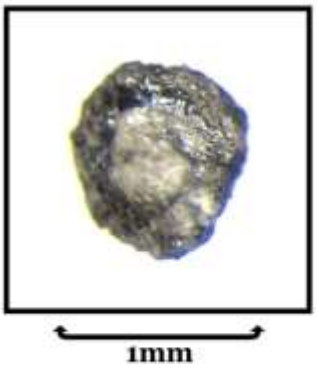

Central chondrule

Other silicates: N
Mesostasis: 70%
Metal: N
Oxides: N
Sulfides: N
Remarks: Ol bars are of intermediate thickness; pale green ol

Rim

Present: Y
Silicates: ol (+ fine silicates)
Metal: N
Oxides: N
Sulfides: Y
Remarks: double rim - inside is thick continuous magmatic rim of dark ol, outside is fine grained ol (plus other silicates?) + fine sulf

Allendé-8 PO

Central chondrule

Other silicates: N
Mesostasis: 20%
Metal: N
Oxides: mgt
Sulfides: Y
Remarks: Anhedral ol; sulf occurs as interstitial blebs; ox dissem through mesostasis

Rim

Present: Y
Silicates: pyx, phyl
Metal: N
Oxides: ?
Sulfides: Y
Remarks: fine grained

Allendé-9 PO

Central chondrule

Other silicates: N
Mesostasis: 5%
Metal: N
Oxides: mgt
Sulfides: Y
Remarks: Anhedral ol; msts only in central portion of chondrule; msts milky; ox+sulf blebs occur interstitially

Rim

Present: Y
Silicates: ol + (pyx, phyl)
Metal: N
Oxides: ?
Sulfides: Y
Remarks: double rim - inside have continuous thick magmatic ol rim, outside is fine grained silicate rim with sulf

Allendé-10 PO

Central chondrule

Other silicates: N
Mesostasis: ?
Metal: N
Oxides: N
Sulfides: N
Remarks: fragment, apparently dominated by ol

Rim

Present: Y - coating
Silicates: pyx, phyl
Metal: N
Oxides: N
Sulfides: Y
Remarks: thin layer of fine grained minerals; sulf occurring as small blebs or disseminated

Allendé-11 PO

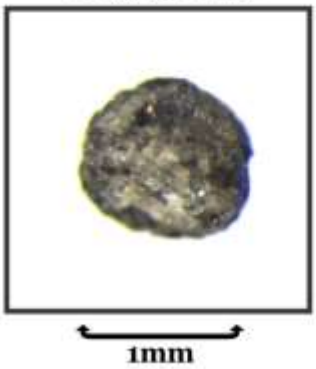

Central chondrule

Other silicates: pyx
Mesostasis: 25%
Metal: N
Oxides: mgt
Sulfides: Y
Remarks: anhedral ol; pyx occuring towards rim and poikilitically enclosing ol; ox occur in milky gray msts

Rim

Present: Y
Silicates: ol + (ol, pyx)
Metal: N
Oxides: N
Sulfides: Y
Remarks: double rim - inside is continuous magmatic rim of dark ol, outside is fine grained ol (plus other silicates?) + fine sulph

Allendé-12 POP-PP

Central chondrule

Other silicates: ?
Mesostasis: ?
Metal: N
Oxides: ?
Sulfides: ?
Remarks: Fragment; features obscured by fine grained coating

Rim

Present: Y - coating
Silicates: pyx, phyl, plag, ol
Metal: N
Oxides: mgt
Sulfides: Y
Remarks: fine grained; pyx poikilitically enclosing ol

Allendé-13 POP

Central chondrule

Other silicates: N
Mesostasis: <10%
Metal: N
Oxides: mgt
Sulfides: Y
Remarks: Sulf occur as interstitial blebs; central chondrule entirely of ol + sulf ; pyx poikilitically encloses ol; pyx + sulf + ox increase towards the rim; msts not obvious

Rim

Present: Y
Silicates: pyx, phyllo
Metal: N
Oxides: mgt
Sulfides: Y
Remarks: fine grained

Allendé-14 POP-PP

Central chondrule

Other silicates: N
Mesostasis: ?
Metal: N
Oxides: mgt
Sulfides: Y
Remarks: Pyx both as anhedral xls and subhedral laths poikilitically enclosing ol; ox+sulf blebs occur interstitially; msts (?) contains many ox inclusions

Rim

Present: Y
Silicates: ol
Metal: N
Oxides: N
Sulfides: N
Remarks: thin rim appears to be magmatic - solid layer of dark olivine

Karoonda CK4

Karoonda-2 BO

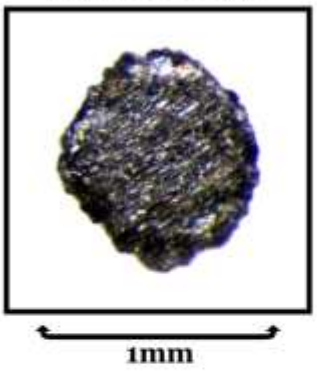

Central chondrule

Other silicates: N
Mesostasis: 40%
Metal: N
Oxides: likely
Sulfides: Y
Remarks: ol bars are relatively thick; msts cloudy, probably due to ox

Rim

Present: Y
Silicates: ol
Metal: N
Oxides: N
Sulfides: Y
Remarks: thick magmatic rim; sharp interface with barred section; sulf occur as blebs

Karoonda-3 BO

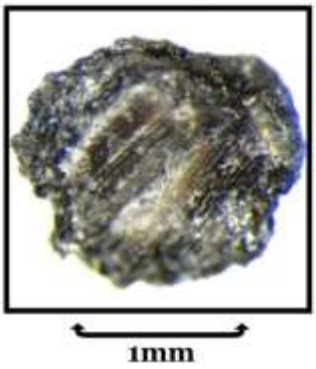

Central chondrule

Other silicates: N
Mesostasis: 30%
Metal: N
Oxides: N
Sulfides: N
Remarks: relatively thin brown ol bars; multiple sectors; ol bars curve in places

Rim

Present: Y
Silicates: ol
Metal: N
Oxides: N
Sulfides: Y
Remarks: thick magmatic rim; sharp interface with barred section; black ol; sulf occur as blebs

Karoonda-4 PO

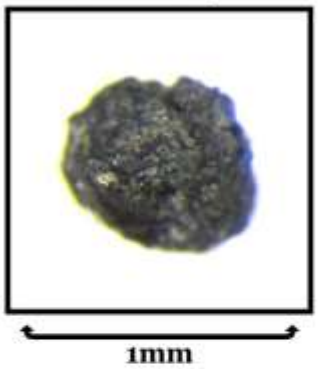

Central chondrule

Other silicates: pyx?
Mesostasis: 10%
Metal: N
Oxides: mgt
Sulfides: Y
Remarks: anhedral ol; minor black pyx laths (?); sulf as small interstitial blebs; msts dark

Rim

Present: Y
Silicates: fine silicates
Metal: N
Oxides: mgt
Sulfides: Y
Remarks: sulf occur as larger blebs

Karoonda-5 PO

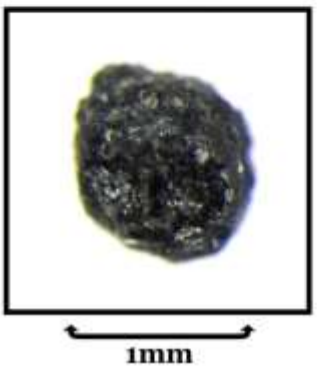

Central chondrule

Other silicates: N
Mesostasis: 7%
Metal: N
Oxides: mgt
Sulfides: Y
Remarks: anhedral ol; sulf as interstitial blebs; msts dark

Rim

Present: Y
Silicates: ol
Metal: N
Oxides: N
Sulfides: N
Remarks: fine grained

Karoonda-6 PO

Central chondrule

Other silicates: N
Mesostasis: ?
Metal: N
Oxides: likely
Sulfides: N
Remarks: dark brown to black, almost massive ol

Rim

Present: Y
Silicates: ol
Metal: N
Oxides: N
Sulfides: Y
Remarks: fine grained, sulf disseminated

Karoonda-7 PO

Central chondrule

Other silicates: N
Mesostasis: <5%
Metal: N
Oxides: mgt
Sulfides: N
Remarks: sulf + mgt occur as interstitial blebs

Rim

Present: Y
Silicates: ol
Metal: N
Oxides: N
Sulfides: Y
Remarks: fine grained; sulf dissem

Karoonda-8 POP

Central chondrule

Other silicates: plag?
Mesostasis: ?
Metal: N
Oxides: mgt
Sulfides: N
Remarks: presence of pyx not entirely clear; voids filled with white/colourless mineral - shows cleavage, possibly plag?

Rim

Present: Y
Silicates: ol
Metal: N
Oxides: mgt
Sulfides: Y
Remarks: fine grained; sulf disseminated

Karoonda-9 POP

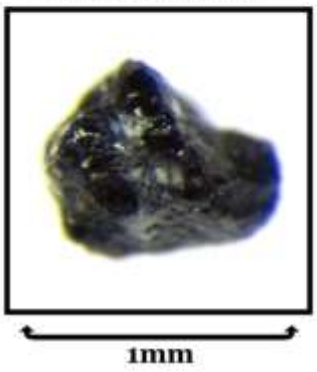

Central chondrule

Other silicates: N
Mesostasis: ?
Metal: N
Oxides: mgt
Sulfides: N
Remarks: fragment; presence of pyx not entirely clear; voids filled with white/colourless mineral - shows cleavage, possibly plag?

Rim

Present: N
Silicates:
Metal:
Oxides:
Sulfides:
Remarks:

Karoonda-10 POP

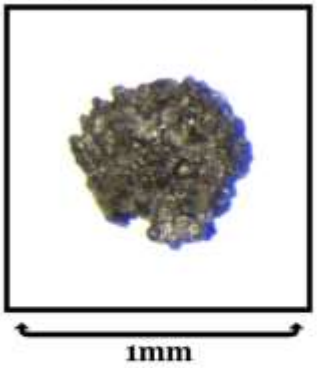

Central chondrule

Other silicates: N
Mesostasis: 5%
Metal: N
Oxides: likely
Sulfides: Y
Remarks: pyx increases towards rim; sulf occurs as interstitial blebs

Rim

Present: Y
Silicates: ol, pyx, plag?
Metal: N
Oxides: N
Sulfides: Y
Remarks: fine grained; sulf disseminated

Karoonda-11 POP

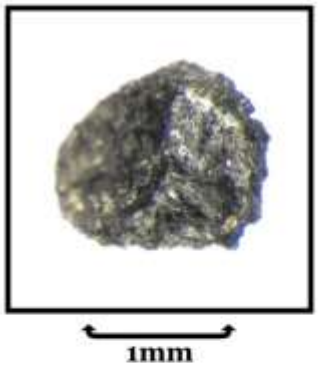

Central chondrule

Other silicates: N
Mesostasis: N
Metal: N
Oxides: (mgt)
Sulfides: N
Remarks: massive ol

Rim

Present: Y
Silicates: plag?, sulf + (ol, pyx, sulph, mgt)
Metal: N
Oxides: Y
Sulfides: Y
Remarks: double rim - inside is colourless plag(?) + small sulf blebs, outside is fine grained silicates + sulf + ox; patches of pyx(?) visible on surface

Karoonda-12 WC

Central chondrule

Other silicates:
Mesostasis:
Metal:
Oxides:
Sulfides:
Remarks:

Surface

Silicates: ol+pyx>plag(?)
Metal: N
Oxides: mgt
Sulfides: Y
Remarks: fine grained; sulf as unevenly distributed patches interstitial to silicates

Karoonda-13 WC

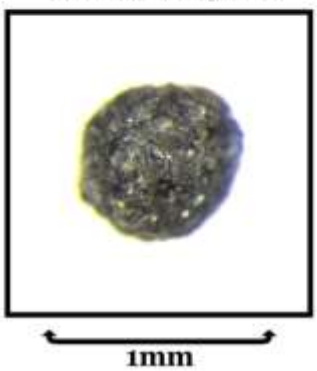

Central chondrule

Other silicates:
Mesostasis:
Metal:
Oxides:
Sulfides:
Remarks:

Surface

Silicates: ol>pyx+plag(?)
Metal: N
Oxides: mgt
Sulfides: Y
Remarks: relatively coarse grained; anhedral ol + pyx laths (poikilitic?) with interstitial plag(?) and sulf blebs

Karoonda-14 WC

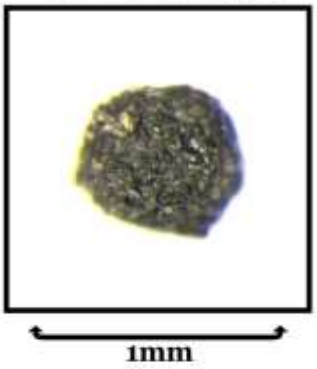

Central chondrule
- Other silicates:
- Mesostasis:
- Metal:
- Oxides:
- Sulfides:
- Remarks:

Surface
- Silicates: ol>pyx
- Metal: N
- Oxides: mgt
- Sulfides: Y
- Remarks: medium grained; sulf ides occur as large interstitial blebs

Karoonda-15 WC

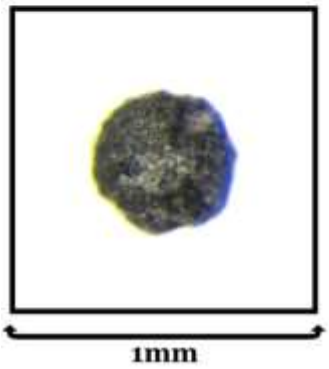

Central chondrule
- Other silicates:
- Mesostasis:
- Metal:
- Oxides:
- Sulfides:
- Remarks:

Surface
- Silicates: ol>pyx+plag(?)
- Metal: N
- Oxides: mgt
- Sulfides: Y
- Remarks: coarse grained ol; sulph as small interstitial blebs; also some fine grained silicate coating

Indarch EH4

Indarch-1 RP

Central chondrule
- Other silicates: N
- Mesostasis: <5%
- Metal: Y
- Oxides: N
- Sulfides: Y
- Remarks: fragment; multiple growth zones

Rim
- Present: Y
- Silicates: pyx, plag?
- Metal: Y
- Oxides: N
- Sulfides: Y
- Remarks: thin magmatic rim; colourless mineral present (plag?)

Indarch-2 RP

Central chondrule
- Other silicates: N
- Mesostasis: N
- Metal: n/o
- Oxides: N
- Sulfides: n/o
- Remarks: multiple growth zones

Rim
- Present: Y
- Silicates: pyx
- Metal: n/o
- Oxides: N
- Sulfides: n/o
- Remarks: semi-smooth thin magmatic rim; colourless mineral present (plag?)

Indarch-3 RP

Central chondrule

Other silicates: N
Mesostasis: N
Metal: Y
Oxides: N
Sulfides: Y
Remarks: multiple growth zones; sulf + metal located along planes between growth zones

Rim

Present: Y
Silicates: pyx
Metal: n/o
Oxides: N
Sulfides: n/o
Remarks: semi-smooth mag - matic rim

Indarch-4 RP

Central chondrule

Other silicates: N
Mesostasis: <5%
Metal: n/o
Oxides: N
Sulfides: n/o
Remarks: sulf + metal finely disseminated, located between pyx laths

Rim

Present: Y
Silicates: pyx
Metal: Y
Oxides: N
Sulfides: Y
Remarks: semi-smooth mag - matic rim with small blebs of sulf/metal

Indarch-5 PP

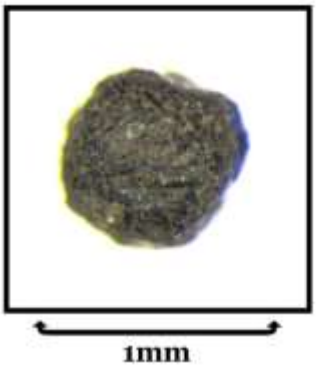

Central chondrule

Other silicates: N
Mesostasis: N
Metal: Y
Oxides: N
Sulfides: Y
Remarks: coarse grained; sulf + metal blebs interstitial

Rim

Present: N
Silicates:
Metal:
Oxides:
Sulfides:
Remarks:

Indarch-6 PP

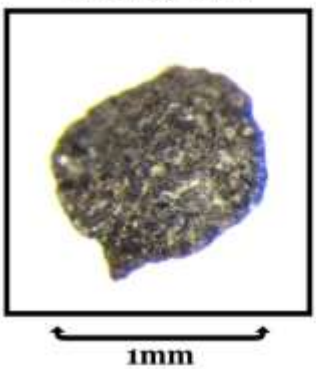

Central chondrule

Other silicates: N
Mesostasis: 10%
Metal: Y
Oxides: N
Sulfides: Y
Remarks: Colourless msts; sulf + metal blebs interstitial

Rim

Present: N
Silicates:
Metal:
Oxides:
Sulfides:
Remarks:

Indarch-7 PP

Central chondrule

- Other silicates: N
- Mesostasis: ?
- Metal: Y
- Oxides: N
- Sulfides: Y
- Remarks: Large amount of fine grained material obscuring surface

Rim

- Present: N
- Silicates:
- Metal:
- Oxides:
- Sulfides:
- Remarks:

Indarch-8 PP

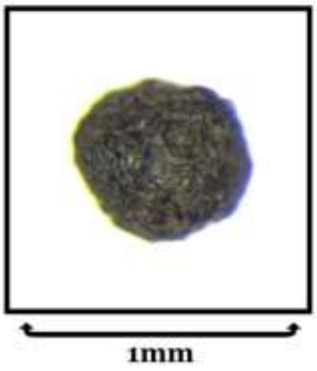

Central chondrule

- Other silicates: N
- Mesostasis: N
- Metal: n/o
- Oxides: N
- Sulfides: n/o
- Remarks: Sulf + metal as inter-stitial blebs

Rim

- Present: N
- Silicates:
- Metal:
- Oxides:
- Sulfides:
- Remarks:

Appendix B

Test- and Procedural-blanks

- All suspect blanks are highlighted in ***bold italics***

Table B-1 Blanks

	L.O.D.	Blank Deppe	Blank Gilbert	Blank 3	Blank UW 4	Blank 1	Blank 2	Blank 3	Blank 4	Blank 5	Blank 6	*max. blank*	min. sample	ave. sample
ICP-MS														
W	**0.01**	0.004	0.001	0.007	0.004	***0.008***	***0.008***	0.005	0.004	0.003	0.002	***0.008***	***0.03***	***0.24***
Zr	**0.1**	0.001	0.003	0.014	0.001	0.038	0.006	0.005	0.003	0.003	0.002	0.038	1.42	8.42
Hf	**0.01**	0.000	0.000	0.001	0.000	0.002	0.001	0.001	0.001	0.000	0.000	0.002	0.057	0.232
Sc	**0.1**	0.005	0.008	0.02	0.005	0.018	0.013	0.014	0.014	0.006	0.005	0.018	4.33	13.4
Y	**0.04**	0.000	0.000	0.000	0.000	0.001	0.000	0.000	0.000	0.000	0.000	0.001	0.97	3.47
Gd	**0.01**	0.000	0.000	0.001	0.000	0.001	0.001	0.001	0.001	0.000	0.000	0.001	0.12	0.45
Tb	**0.002**	0.000	0.000	0.000	0.000	0.000	0.000	0.000	0.000	0.000	0.000	0.000	0.024	0.087
Dy	**0.01**	0.000	0.000	0.000	0.000	0.001	0.001	0.001	0.001	0.000	0.000	0.001	0.15	0.59
Ho	**0.002**	0.000	0.000	0.000	0.000	0.000	0.000	0.000	0.000	0.000	0.000	0.000	0.036	0.126
Er	**0.01**	0.000	0.000	0.000	0.000	0.001	0.001	0.001	0.001	0.000	0.000	0.001	0.10	0.35
Tm	**0.002**	0.000	0.000	0.000	0.000	0.000	0.000	0.000	0.000	0.000	0.000	0.000	0.017	0.058
Lu	**0.002**	0.000	0.000	0.000	0.000	0.000	0.000	0.000	0.000	0.000	0.000	0.000	0.018	0.058
Nd	**0.01**	0.001	0.000	0.001	0.000	0.001	0.001	0.001	0.001	0.001	0.001	0.001	0.20	1.05
Sm	**0.01**	0.000	0.000	0.000	0.000	0.001	0.001	0.001	0.001	0.000	0.001	0.001	0.078	0.354
Pr	**0.002**	0.000	0.000	0.000	0.000	0.000	0.000	0.000	0.000	0.000	0.000	0.000	0.037	0.209
La	**0.02**	0.000	0.000	0.001	0.000	0.001	0.001	0.000	0.000	0.000	0.001	0.001	0.094	0.529
Yb	**0.01**	0.000	0.000	0.000	0.000	0.001	0.001	0.001	0.001	0.000	0.000	0.001	0.067	0.386
Ce	**0.02**	0.000	0.000	0.001	0.000	0.002	0.001	0.001	0.000	0.000	0.001	0.002	0.23	1.36
Eu	**0.005**	0.000	0.000	0.000	0.000	0.000	0.000	0.000	0.000	0.000	0.000	0.000	0.01	0.11
Th	**0.002**	0.000	0.000	0.000	0.000	0.001	0.000	0.000	0.000	0.000	0.004	0.004	0.029	0.065
U	**0.002**	0.000	0.000	0.000	0.000	***0.001***	0.000	0.000	0.000	0.000	0.000	***0.001***	***0.008***	***0.025***
Ir	**0.005**	0.000	0.000	0.000	0.000	0.001	0.001	0.001	0.001	0.000	0.000	0.001	0.019	0.428
Mo	**0.01**	0.008	0.007	0.015	0.022	***0.027***	0.023	0.015	0.013	0.009	0.012	***0.027***	***0.85***	***1.65***
Ta	**0.002**	0.000	0.000	***0.004***	0.000	0.003	0.002	0.001	0.001	0.001	0.001	***0.004***	***0.009***	***0.037***
Nb	**0.005**	0.000	0.000	0.003	0.002	0.004	0.002	0.001	0.001	0.001	0.001	0.004	0.048	0.560
Sr	**0.3**	0.014	0.002	0.033	0.015	0.034	0.021	0.005	0.017	0.011	***0.085***	***0.085***	***0.76***	***17.69***
Ba	**0.1**	0.004	0.001	0.010	0.004	0.013	0.021	0.004	0.005	0.009	0.008	0.021	0.60	9.3
V	**1**	0.006	0.004	0.009	0.005	0.035	0.050	0.045	0.045	0.020	0.052	0.052	20	103
Ni	**1**	0.005	0.004	0.042	0.014	0.061	0.023	0.015	0.017	0.020	0.016	0.061	249	7622
Co	**0.3**	0.001	0.001	0.002	0.001	0.007	0.004	0.010	0.003	0.001	0.001	0.010	8	405
Cr	**3**	0.382	0.195	0.297	0.299	1.249	0.484	0.472	0.470	0.220	0.199	1.2	143	3508
Li	**0.3**	0.111	0.004	0.005	0.004	0.012	0.010	0.010	0.011	0.004	0.004	0.012	0.47	1.71
Cu	**0.5**	0.013	0.011	0.041	0.016	0.084	0.084	0.066	0.060	0.015	0.014	0.084	3	127
Ga	**0.05**	0.010	0.000	0.000	0.000	0.001	0.001	0.001	0.001	0.000	0.000	0.001	0.33	2.45
Rb	**0.1**	0.001	0.002	0.002	0.001	0.006	0.004	0.003	0.003	0.001	0.002	0.006	0.20	2.21
Pb	**0.04**	0.003	0.002	0.008	0.005	0.008	0.007	0.005	0.005	0.006	0.012	0.012	0.12	0.67
Zn	**0.5**	0.448	0.088	1.579	1.302	1.500	1.594	0.309	0.430	0.562	**2**	**2**	***11***	***69***
ICP-OES														
Al_2O_3	**0.009**			0.002	0.002	0.001	0.001	0.001	0.001	0.001	0.001	0.002	1.1	3.0
Fe_2O_3T	**0.012**			0.006	0.007	0.003	0.003	0.003	0.003	0.003	0.003	0.007	2	21
MnO	**0.00031**			0.000	0.000	0.000	0.000	0.000	0.000	0.000	0.000	<0.001	0.053	0.174
MgO	**0.023**			0.007	0.007	0.004	0.003	0.004	0.004	0.004	0.004	0.007	20	30
CaO	**0.010**			0.005	0.005	0.003	0.003	0.003	0.003	0.003	0.003	0.005	0.36	2.18
Na_2O	**0.023**			***0.013***	***0.013***	0.006	0.006	0.006	0.006	0.006	0.006	***0.013***	***0.07***	***0.73***
K_2O	**0.007**			0.002	***0.003***	0.001	0.001	0.002	0.002	0.001	0.001	***0.003***	***0.011***	***0.047***
TiO_2	**0.00297**			0.001	0.001	0.001	0.001	0.001	0.001	0.001	0.001	0.001	0.052	0.163
P_2O_5	**0.011**			***0.003***	***0.003***	0.001	0.002	0.002	0.001	0.002	0.001	***0.003***	***0.029***	***0.157***

Appendix C

Raw data – Terrestrial Standards

- All data reported as ppm, except oxides (wt%)
- Δ% = difference between the average of the measured standards and the preferred value, expressed as a percentage of the preferred values

$$\Delta\% = \frac{\left(\frac{\sum_{i=1}^{n}}{n}\right) - C}{C} * 100$$ where C = Preferred Value

- Data in gray are previous repeat analyses of the standards (no ICP-OES data available)
- FeO* recalculated from Fe_2O_3
- $Mg\# = \frac{Mg_{mol}}{Mg_{mol}+Fe_{mol}}$
- $Co\# = \left(\frac{Co_{mol}}{Co_{mol}+Fe_{mol}}\right) * 10^4$

Table C-1 BIR-1 Basalt

	BIR-1 Schumann auf 10 mL	BIR-1 Schumann auf 2.5 mL	BIR-1 Petersen auf 10 mL	BIR-1 Petersen auf 2.5 mL	BIR-1 Petersen auf 10 mL	BIR-1 Gerber auf 2.5 mL	BIR-1 (A)	BIR-1 (B)	Ave.	%RSD	*BIR-1 PREFERRED*	Δ%
W	0.082	0.088	0.074	0.076	0.056	0.071	0.076	0.083	**0.077**	6.2	*0.07*	*9.7*
Zr	14.2	13.9	14.4	14.3	15.4	14.4	13.2	14.2	**13.9**	3.7	*15.50*	*-10.2*
Hf	0.59	0.57	0.60	0.59	0.59	0.59	0.52	0.54	**0.55**	5.6	*0.60*	*-8.6*
Sc	45.5	45.0	46.3	45.5	46.7	47.9	38.3	43.3	**43.2**	9.1	*44.00*	*-1.9*
Y	15.5	15.1	15.6	15.4	16.0	15.8	13.6	14.8	**14.7**	6.0	*16.00*	*-7.9*
Gd	1.80	1.76	1.81	1.79	1.75	1.81	1.53	1.63	**1.66**	6.9	*1.85*	*-10.4*
Tb	0.36	0.35	0.36	0.36	0.36	0.37	0.31	0.33	**0.34**	6.9	*0.36*	*-6.7*
Dy	2.59	2.52	2.61	2.58	2.56	2.64	2.22	2.40	**2.42**	7.0	*2.50*	*-3.2*
Ho	0.57	0.56	0.58	0.57	0.57	0.58	0.49	0.53	**0.53**	7.0	*0.57*	*-6.3*
Er	1.64	1.59	1.65	1.62	1.61	1.66	1.40	1.50	**1.52**	7.0	*1.70*	*-10.4*
Tm	0.25	0.24	0.25	0.25	0.25	0.25	0.21	0.23	**0.23**	6.7	*0.26*	*-11.0*
Lu	0.25	0.24	0.25	0.25	0.25	0.25	0.21	0.23	**0.23**	6.7	*0.26*	*-11.2*
Nd	2.41	2.38	2.45	2.42	2.42	2.44	2.08	2.21	**2.24**	6.6	*2.50*	*-10.3*
Sm	1.12	1.09	1.12	1.12	1.10	1.13	0.96	1.01	**1.03**	6.7	*1.10*	*-5.9*
Pr	0.38	0.37	0.38	0.38	0.38	0.38	0.33	0.34	**0.35**	6.3	*0.38*	*-8.3*
La	0.61	0.60	0.62	0.62	0.62	1.29	0.53	0.55	**0.79**	44.6	*0.62*	*27.2*
Yb	1.65	1.61	1.66	1.64	1.64	1.67	1.44	1.53	**1.55**	6.1	*1.65*	*-6.1*
Ce	1.90	1.86	1.92	1.90	1.91	1.90	1.64	1.73	**1.76**	6.1	*1.95*	*-9.9*
Eu	0.53	0.52	0.53	0.53	0.52	0.53	0.45	0.48	**0.49**	7.2	*0.54*	*-9.8*
Th	0.031	0.030	0.032	0.031	0.029	0.032	0.028	0.028	**0.029**	5.2	*0.03*	*-1.8*
Al_2O_3						15.0	14.0	14.9	**14.6**	3.1	*15.35*	*-4.7*
U	0.013	0.013	0.014	0.014	0.013	0.012	0.013	0.013	**0.013**	1.8	*0.010*	*26.5*
Ir	0.007	0.007	0.007	0.007	0.008	0.006	0.010	0.010	**0.009**	23.8	*0.0002*	*5714.6*
Mo	0.07	0.16	0.08	0.09	0.08	0.09	0.13	0.20	**0.14**	31.9	*0.50*	*-71.7*
TiO_2						0.93	0.86	0.94	**0.91**	3.7	*0.96*	*-4.9*
Ta	0.043	0.042	0.041	0.041	0.041	0.043	0.035	0.038	**0.039**	7.8	*0.04*	*-3.1*
Nb	0.52	0.51	0.52	0.52	0.55	0.52	0.47	0.52	**0.50**	4.4	*0.60*	*-16.2*
CaO						12.6	11.5	12.6	**12.2**	4.3	*13.24*	*-7.6*
Sr	110	108	111	111	115	110	99	104	**104**	4.2	*108.00*	*-3.3*
Ba	6.6	6.5	6.5	6.8	6.6	6.5	5.8	6.0	**6.1**	4.9	*7.00*	*-13.1*
V	354	352	359	354	369	366	317	335	**339**	5.9	*313*	*8.4*
Ni	171	169	173	171	189	175	166	174	**172**	2.4	*166*	*3.6*
Co	55.2	54.5	55.9	54.7	60.4	56.5	51.5	54.5	**54.2**	3.8	*51*	*5.4*
MgO						9.7	8.6	9.5	**9.3**	4.9	*9.68*	*-4.2*
FeO*						10.3	9.4	10.0	**9.9**	3.9	*10.13*	*-2.5*
Cr	413	410	341	330	343	448	323	398	**390**	13.2	*382*	*2.0*
P_2O_5						0.045	0.048	0.043	**0.045**	4.5	*0.02*	*114.5*
MnO						0.17	0.16	0.17	**0.17**	3.8	*0.17*	*-3.1*
Li	3.4	3.3	3.5	3.4	3.4	3.5	2.9	3.1	**3.1**	7.6	*3.40*	*-7.8*
Cu	126	126	126	128	131	125	114	121	**120**	4.0	*126.00*	*-4.6*
K_2O						0.009	0.005	0.006	**0.006**	25.1	*0.03*	*-76.6*
Ga	15.9	15.5	15.9	15.9	16.0	15.9	13.8	14.5	**14.7**	5.9	*16.00*	*-8.0*
Na_2O						1.9	1.7	1.8	**1.8**	4.2	*1.75*	*3.0*
Rb	0.213	0.222	0.213	0.215	0.212	0.213	0.222	0.216	**0.217**	1.7	*0.25*	*-13.2*
Pb	3.70	3.64	3.32	3.37	3.30	2.47	2.25	2.20	**2.31**	5.2	*3.00*	*-23.1*
Zn	69	71	70	77	70	71	68	71	**70**	1.9	*71.00*	*-1.2*
Mg#						**0.63**	**0.62**	**0.63**	**0.626**		**0.63**	*-0.39*
Co#						**7**	**7**	**7**	**6.684**		**6**	*7.8*

Table C-1 UB-N Serpentinite

	-N Duggen auf 10 mL	-N Duggen auf 2.5 mL	B-N Petersen auf 10 mL	B-N Petersen auf 2.5 mL	B-N Petersen auf 10 mL	B-N Petersen	UB-N Gerber	*UB-N REFERRED*	Δ%
W	21.1	20.6	24.8	24.4	32.0	32.6	20.3	*20*	*1.5*
Zr	3.37	3.28	3.65	3.57	3.89	3.99	3.46	*4.00*	*-13.6*
Hf	0.13	0.12	0.13	0.13	0.13	0.13	0.14	*0.10*	*35.6*
Sc	13.2	12.7	13.5	13.2	13.0	13.8	13.9	*13.00*	*7.2*
Y	2.55	2.48	2.61	2.55	2.69	2.75	2.64	*2.50*	*5.7*
Gd	0.31	0.30	0.32	0.31	0.31	0.32	0.33	*0.30*	*11.2*
Tb	0.060	0.059	0.062	0.061	0.062	0.062	0.064	*0.06*	*7.3*
Dy	0.42	0.42	0.44	0.43	0.44	0.44	0.45	*0.38*	*18.2*
Ho	0.095	0.092	0.097	0.095	0.097	0.098	0.100	*0.09*	*11.2*
Er	0.28	0.27	0.28	0.28	0.28	0.29	0.29	*0.28*	*4.4*
Tm	0.04	0.04	0.04	0.04	0.04	0.04	0.05	*0.045*	*4.3*
Lu	0.046	0.045	0.047	0.047	0.047	0.048	0.051	*0.045*	*12.4*
Nd	0.61	0.58	0.63	0.61	0.62	0.63	0.64	*0.60*	*7.1*
Sm	0.22	0.21	0.23	0.22	0.22	0.23	0.24	*0.20*	*19.9*
Pr	0.12	0.11	0.12	0.12	0.12	0.12	0.12	*0.12*	*0.7*
La	0.31	0.30	0.32	0.32	0.32	0.33	0.32	*0.35*	*-7.6*
Yb	0.30	0.29	0.30	0.30	0.30	0.31	0.32	*0.28*	*12.7*
Ce	0.77	0.75	0.80	0.79	0.81	0.82	0.79	*0.80*	*-1.2*
Eu	0.082	0.079	0.084	0.082	0.081	0.085	0.088	*0.080*	*10.3*
Th	0.063	0.061	0.061	0.060	0.061	0.060	0.055	*0.070*	*-21.5*
Al_2O_3							2.93	*2.90*	*1.2*
U	0.055	0.053	0.060	0.058	0.060	0.060	0.051	*0.070*	*-27.7*
Ir	0.005	0.005	0.004	0.004	0.004	0.004	0.010	*0.003*	*196.9*
Mo	0.51	0.49	0.55	0.54	0.55	0.56	0.62	*0.550*	*13.3*
TiO_2							0.10	*0.11*	*-8.4*
Ta	0.017	0.017	0.017	0.016	0.017	0.017	0.023	*0.020*	*13.0*
Nb	0.050	0.048	0.055	0.053	0.055	0.057	0.054	*0.05*	*7.8*
CaO							1.20	*1.20*	*0.1*
Sr	7.4	7.3	7.7	7.6	8.0	8.4	7.8	*9.00*	*-13.6*
Ba	21.7	21.0	27.2	26.7	27.7	28.2	24.6	*27.00*	*-8.9*
V	71.2	68.2	72.7	70.6	70.0	74.7	73.4	*75*	*-2.2*
Ni	1806	1752	1853	1790	1937	2017	2028	*2000*	*1.4*
Co	100	98	103	100	107	112	112	*100*	*11.9*
MgO							35.1	*35.2*	*-0.2*
FeO*							7.57	*7.50*	*0.9*
Cr	2445	2337	2491	2403	2389	2540	2590	*2300*	*12.6*
P_2O_5							0.023	*0.04*	*-41.7*
MnO							0.12	*0.12*	*5.0*
Li	29.0	28.0	28.9	28.5	28.7	29.1	29.5	*27.00*	*9.2*
Cu	25.4	24.7	25.6	25.0	25.6	26.4	33.2	*28*	*18.5*
K_2O							0.0003	*0.02*	*-98.6*
Ga	2.7	2.6	2.7	2.6	2.6	2.7	2.8	*3*	*-5.7*
Na_2O							0.072	*0.10*	*-28.1*
Rb	3.31	3.22	3.43	3.35	3.47	3.59	3.48	*4.00*	*-13.0*
Pb	11.4	11.1	12.5	12.3	12.4	12.7	13.5	*13.00*	*3.5*
Zn	78	77	82	82	81	90	92	*85*	*8.0*
Mg#							**0.89**	***0.90***	*-0.34*
Co#							**18**	***17***	*7.46*

Table C-1 NIM-D Dunite

	M-D auf 2.5 mL	NIM-D (A)	NIM-D (B)	Ave.	%RSD	*NIM-D PREFERRED*	Δ%
W	0.10	0.41	0.15	**0.22**	61.1		
Zr	1.3	2.1	2.2	**1.8**	22.2	*2*	*1.1*
Hf	0.036	0.049	0.049	**0.045**	13.2	*0.050*	*-10.5*
Sc	2.4	4.6	4.1	**3.7**	24.9	*7*	*-46.9*
Y	0.08	0.14	0.13	**0.12**	24.61	*0.157*	*-25.4*
Gd	0.020	0.024	0.018	**0.021**	11.9	*0.015*	*37.1*
Tb	0.003	0.004	0.003	**0.004**	11.4	*0.003*	*30.3*
Dy	0.019	0.024	0.020	**0.021**	10.3	*0.019*	*7.8*
Ho	0.005	0.007	0.005	**0.006**	13.5	*0.005*	*11.8*
Er	0.017	0.025	0.020	**0.021**	16.1	*0.022*	*-5.3*
Tm	0.005	0.006	0.005	**0.005**	13.0	*0.004*	*31.2*
Lu	0.007	0.009	0.008	**0.008**	14.2	*0.008*	*0.6*
Nd	0.039	0.058	0.050	**0.049**	15.9	*0.049*	*-0.3*
Sm	0.021	0.024	0.017	**0.021**	12.4	*0.011*	*88.2*
Pr	0.009	0.015	0.015	**0.013**	19.5	*0.014*	*-5.0*
La	0.044	0.078	0.076	**0.066**	23.6	*0.07*	*-8.7*
Yb	0.032	0.047	0.039	**0.039**	15.3	*0.042*	*-7.2*
Ce	0.072	0.126	0.133	**0.110**	24.8	*0.13*	*-15.2*
Eu	0.006	0.007	0.005	**0.006**	14.4	*0.003*	*100.2*
Th	0.015	0.021	0.020	**0.019**	12.4		
Al_2O_3	0.17	0.21	0.25	**0.21**	16.0	*0.30*	*-30.6*
U	0.057	0.081	0.082	**0.073**	15.5	*0.030*	*144.5*
Ir	0.007	0.010	0.007	**0.008**	14.9	*0.000*	*1685.6*
Mo	0.6	1.4	1.7	**1.2**	38.6	*4*	*-68.9*
TiO_2	0.02	0.03	0.02	**0.02**	27.3	*0.02*	*10.8*
Ta	0.012	0.025	0.010	**0.016**	42.3		
Nb	0.14	0.33	0.17	**0.21**	39.4		
CaO	0.16	0.29	0.25	**0.23**	22.3	*0.28*	*-16.5*
Sr	1.6	3.4	2.8	**2.6**	27.8	*3.00*	*-13.3*
Ba	0.8	1.6	1.5	**1.3**	27.3	*1.92*	*-31.5*
V	28	35	40	**35**	14.4	*40*	*-13.6*
Ni	935	1950	1718	**1535**	28.3	*2050*	*-25.1*
Co	106	215	192	**171**	27.6	*210*	*-18.6*
MgO	22.4	38.2	36.4	**32.3**	21.9	*43.51*	*-25.7*
FeO*	8.0	13.9	13.1	**11.7**	22.3	*15.26*	*-23.5*
Cr	1853	1925	2250	**2009**	8.6	*2900*	*-30.7*
P_2O_5	0.03	0.04	0.02	**0.03**	30.1	*0.01*	*176.3*
MnO	0.11	0.20	0.19	**0.16**	22.4	*0.22*	*-25.2*
Li	1.8	3.5	3.1	**2.8**	26.0	*4*	*-30.7*
Cu	3.0	4.6	5.9	**4.5**	26.2	*10*	*-54.8*
K_2O	0.01	0.02	0.01	**0.01**	45.5	*0.01*	*24.0*
Ga	0.47	0.56	0.63	**0.55**	12.0		
Na_2O	0.06	0.12	0.05	**0.08**	36.9	*0.04*	*91.3*
Rb	0.12	0.28	0.21	**0.21**	31.6	*0.316*	*-34.3*
Pb	0.37	0.74	0.70	**0.60**	27.5	*1*	*-50.3*
Zn	49	81	77	**69**	20.7	*90*	*-23.6*
Mg#	**0.83**	**0.83**	**0.83**	**0.83**		***0.77***	*7.46*
Co#	**16**	**19**	**18**	**18**		***13***	*32.84*

Table C-1 NIM-P Pyroxenite

	NIM-P	NIM-P (A)	NIM-P (B)	Ave.	%RSD	*NIM-P PREFERRED*	*Δ%*
W	0.17	0.95	0.36	**0.49**	67.4		
Zr	6.0	5.5	5.1	**5.5**	7.0	*9*	*-37.4*
Hf	0.19	0.17	0.16	**0.17**	5.4	*0.30*	*-42.1*
Sc	26	24	23	**24**	5.0	*29*	*-16.1*
Y	3.0	2.7	2.5	**2.7**	7.3	*3*	*-12.5*
Gd	0.43	0.39	0.36	**0.40**	7.1	*0.461*	*-14.0*
Tb	0.075	0.068	0.063	**0.068**	7.3	*0.076*	*-10.0*
Dy	0.48	0.43	0.41	**0.44**	6.4	*0.500*	*-11.4*
Ho	0.11	0.10	0.09	**0.10**	6.3	*0.110*	*-11.9*
Er	0.31	0.28	0.28	**0.29**	5.5	*0.351*	*-16.8*
Tm	0.051	0.046	0.045	**0.047**	5.4	*0.051*	*-7.7*
Lu	0.059	0.054	0.052	**0.055**	5.3	*0.065*	*-15.6*
Nd	1.76	1.60	1.46	**1.61**	7.6	*1.860*	*-13.5*
Sm	0.39	0.36	0.33	**0.36**	7.0	*0.427*	*-15.0*
Pr	0.44	0.39	0.35	**0.39**	9.5	*0.497*	*-21.1*
La	1.82	1.48	1.39	**1.56**	11.9	*2*	*-17.1*
Yb	0.36	0.33	0.33	**0.34**	4.7	*0.390*	*-12.6*
Ce	3.6	3.1	2.9	**3.2**	10.2	*3.39*	*-5.6*
Eu	0.12	0.11	0.10	**0.11**	7.9	*0.131*	*-15.9*
Th	0.30	0.25	0.20	**0.25**	15.4	*0*	*-4.6*
Al_2O_3	4.2	3.6	3.2	**3.7**	11.3	*4.18*	*-12.3*
U	0.17	0.15	0.13	**0.15**	12.1	*0.28*	*-45.4*
Ir	0.010	0.012	0.013	**0.012**	8.7	*0.0078*	*49.1*
Mo	0.31	0.42	0.49	**0.41**	18.2		
TiO_2	0.18	0.16	0.16	**0.17**	6.3	*0.20*	*-16.6*
Ta	0.031	0.024	0.029	**0.028**	10.2		
Nb	0.40	0.34	0.33	**0.35**	8.6		
CaO	2.5	2.2	2.0	**2.2**	9.9	*2.66*	*-16.6*
Sr	34	28	25	**29**	12.6	*32*	*-8.4*
Ba	33	27	30	**30**	8.1	*31*	*-3.7*
V	254	229	233	**239**	4.5	*230*	*3.7*
Ni	524	492	490	**502**	3.1	*560*	*-10.4*
Co	109	101	100	**103**	4.2	*110*	*-6.2*
MgO	24.1	21.9	20.5	**22.2**	6.6	*25-33*	*-12.5*
FeO*	10.3	9.4	10.0	**9.9**	3.9	*11.48*	*-14.0*
Cr	21535	18549	19393	**19826**	6.3	*24000*	*-17.4*
P_2O_5	0.03	0.03	0.05	**0.04**	29.5	*0.02*	*85.3*
MnO	0.21	0.19	0.18	**0.19**	7.4	*0.22*	*-11.8*
Li	4.1	3.7	3.6	**3.8**	5.7		
Cu	14	12	21	**15**	24.3	*18*	*-14.5*
K_2O	0.09	0.06	0.04	**0.06**	30.7	*0.09*	
Ga	6.8	5.9	5.9	**6.2**	6.8	*8*	*-22.3*
Na_2O	0.33	0.24	0.15	**0.24**	31.9	*0.37*	*-35.9*
Rb	2.7	2.3	2.0	**2.4**	11.8	*3*	*-16.0*
Pb	0.80	0.70	0.64	**0.71**	9.6	*1*	*-49.9*
Zn	112	99	105	**105**	4.9	*100*	*5.4*
Mg#	**0.81**	**0.81**	**0.78**	**0.80**		***0.80***	*0.36*
Co#	**13**	**13**	**12**	**13**		***12***	*9.45*

Table C-1 PCC-1 Peridotite

	PCC-1 Gerber	PCC-1 (A)	PCC-1 (B)	Ave.	%RSD	*PCC-1 PREFERRED*	Δ%
W	0.034	0.073	0.093	**0.067**	37.0	*0.020*	233.3
Zr	0.17	0.15	0.16	**0.16**	3.6	*0.15*	5.8
Hf	0.008	0.014	0.009	**0.010**	27.3	*0.008*	25.7
Sc	9.4	6.5	7.1	**7.6**	16.3	*8.400*	-9.0
Y	0.088	0.061	0.070	**0.073**	15.4	*0.077*	-5.0
Gd	0.011	0.018	0.012	**0.014**	23.3	*0.006*	147.3
Tb	0.002	0.003	0.002	**0.002**	23.8	*0.001*	128.8
Dy	0.013	0.018	0.013	**0.015**	17.7	*0.010*	54.8
Ho	0.004	0.004	0.003	**0.004**	12.1	*0.003*	46.3
Er	0.014	0.015	0.013	**0.014**	8.7	*0.012*	21.4
Tm	0.003	0.004	0.004	**0.004**	11.0	*0.002*	56.5
Lu	0.006	0.006	0.006	**0.006**	5.3	*0.005*	31.9
Nd	0.034	0.037	0.032	**0.034**	6.7	*0.027*	27.0
Sm	0.011	0.019	0.012	**0.014**	26.8	*0.006*	135.3
Pr	0.009	0.007	0.008	**0.008**	7.3	*0.008*	4.6
La	0.035	0.026	0.028	**0.030**	12.8	*0.029*	2.7
Yb	0.028	0.029	0.025	**0.027**	6.3	*0.021*	32.4
Ce	0.067	0.047	0.054	**0.056**	15.0	*0.053*	5.3
Eu	0.003	0.006	0.003	**0.004**	38.1	*0.001*	266.3
Th	0.012	0.012	0.011	**0.012**	3.9	*0.013*	-10.1
Al_2O_3	0.67	0.49	0.64	**0.60**	13.2	*0.68*	-11.3
U	0.005	0.009	0.006	**0.007**	22.7	*0.0045*	48.2
Ir	0.006	0.012	0.007	**0.008**	32.0	*0.005*	72.5
Mo	0.28	0.33	0.55	**0.39**	30.5		#DIV/0!
TiO_2	0.01	0.01	0.02	**0.01**	18.4	*0.01*	-0.9
Ta	0.032	0.009	0.024	**0.022**	43.0	*0.020*	7.6
Nb	0.033	0.016	0.041	**0.030**	35.1		#DIV/0!
CaO	0.53	0.46	0.48	**0.49**	6.6	*0.52*	-6.2
Sr	0.42	0.49	0.51	**0.48**	7.7	*0.400*	18.8
Ba	0.92	0.70	0.79	**0.80**	11.3	*1*	-4.2
V	36	27	34	**32**	12.5	*31*	3.9
Ni	2300	1877	2042		8.4	*2380*	-12.9
Co	121	96	105	**108**	9.7	*112*	-4.0
MgO	42.4	33.2	38.5	**38.1**	10.0	*43.43*	-12.4
FeO*	7.4	5.8	6.8	**6.7**	10.1	*7.42*	-10.1
Cr	2960	1744	2673	**2459**	21.1	*2730*	-9.9
P_2O_5	0.01	0.02	0.02	**0.02**	20.2	*0.00*	664.1
MnO	0.12	0.09	0.11	**0.10**	10.4	*0.12*	-13.4
Li	1.2	0.89	1.0	**1.0**	13.6	*1.60*	-35.2
Cu	7.4	5.4	6.3	**6.4**	12.5	*10*	-36.4
K_2O	0.01	0.01	0.02	**0.01**	49.1	*0.01*	75.7
Ga	0.69	0.46	0.59	**0.58**	15.8	*0.700*	-17.1
Na_2O	0.03	0.06	0.08	**0.06**	34.2	*0.03*	99.4
Rb	0.069	0.073	0.058	**0.067**	9.1	*0.066*	1.0
Pb	9.0	6.0	6.9	**7.3**	17.5	*10.00*	-26.8
Zn	46	37	44	**42**	8.6	*42*	1.0
Mg#	**0.91**	**0.91**	**0.91**	**0.91**		***0.91***	-0.21
Co#	**20**	**20**	**19**	**20**		***18***	7.10

Appendix D

Raw data – Preferred CI/Solar values[1], samples and published bulk meteorite values[2]

- All data reported as ppm, except oxides (wt%)
- [1] Lodders (2003)
- [2] See tables for references
- FeO* recalculated from Fe_2O_3
- $Mg\# = \frac{Mg_{mol}}{Mg_{mol}+Fe_{mol}}$
- $Co\# = \left(\frac{Co_{mol}}{Co_{mol}+Fe_{mol}}\right) * 10^4$

Table D-1
CI/Solar Composition

	L.O.D.	50% T C (from 1)	conc. (from 1)
W	**0.010**	1789	0.089
Zr	**0.100**	1741	3.96
Hf	**0.010**	1684	0.115
Sc	**0.100**	1659	5.83
Y	**0.040**	1659	1.53
Gd	**0.010**	1659	0.198
Tb	**0.002**	1659	0.036
Dy	**0.010**	1659	0.238
Ho	**0.002**	1659	0.056
Er	**0.010**	1659	0.162
Tm	**0.002**	1659	0.024
Lu	**0.002**	1659	0.024
Nd	**0.010**	1602	0.457
Sm	**0.010**	1590	0.145
Pr	**0.002**	1582	0.093
La	**0.020**	1578	0.232
Yb	**0.010**	1487	0.163
Ce	**0.020**	1478	0.632
Eu	**0.005**	1356	0.055
Th	**0.002**	1659	0.031
Al_2O_3	**0.009**	1653	1.61
U	**0.002**	1610	0.008
Ir	**0.005**	1603	0.47
Mo	**0.010**	1590	1.02
TiO_2	**0.003**	1582	0.073
Ta	**0.002**	1573	0.014
Nb	**0.005**	1559	0.265
CaO	**0.010**	1517	1.27
Sr	**0.300**	1464	7.74
Ba	**0.100**	1455	2.31
V	**1.000**	1429	56
Ni	**1.000**	1353	10640
Co	**0.300**	1352	502
MgO	**0.023**	1336	16
FeO*	**0.012**	1334	24
Cr	**3.000**	1296	2590
P_2O_5	**0.011**	1229	0.211
MnO	**0.000**	1158	0.247
Li	**0.300**	1142	1.46
Cu	**0.500**	1037	127
K_2O	**0.007**	1006	0.064
Ga	**0.050**	968	9.51
Na_2O	**0.023**	958	0.675
Rb	**0.100**	800	2.13
Pb	**0.040**	727	2.56
Zn	**0.500**	726	310
Mg#			**0.55**
Co#			**26**

Table D-2 Chondrules - Acfer 311 CR2

	AC-1	AC-2	AC-3	AC-4	AC-5
W	0.12	0.77	0.12	0.37	0.29
Zr	5.4	2.6	7.2	8.5	4.8
Hf	0.15	0.08	0.21	0.22	0.14
Sc	9.2	4.8	11.8	15.6	8.8
Y	2.1	1.0	2.8	3.3	1.9
Gd	0.27	0.15	0.41	0.44	0.27
Tb	0.05	0.03	0.08	0.08	0.05
Dy	0.34	0.18	0.51	0.56	0.33
Ho	0.07	0.04	0.11	0.12	0.07
Er	0.21	0.11	0.31	0.33	0.21
Tm	0.034	0.018	0.051	0.058	0.035
Lu	0.034	0.018	0.051	0.054	0.035
Nd	0.67	0.36	0.94	1.10	0.64
Sm	0.21	0.12	0.31	0.35	0.22
Pr	0.14	0.07	0.18	0.22	0.13
La	0.39	0.19	0.46	0.57	0.31
Yb	0.23	0.12	0.34	0.38	0.24
Ce	0.96	0.50	1.18	1.41	0.82
Eu	0.08	0.04	0.11	0.13	0.08
Th	0.06	0.03	0.06	0.07	0.04
Al_2O_3	2.4	1.3	**n.d.**	3.7	2.0
U	0.047	0.062	0.064	0.041	0.056
Ir	0.24	1.29	0.05	0.57	0.62
Mo	1.2	4.7	0.4	1.9	2.3
TiO_2	0.11	0.07	**n.d.**	0.17	0.10
Ta	0.022	0.015	0.051	0.035	0.027
Nb	0.44	0.21	0.57	0.66	0.39
CaO	2.9	1.1	**n.d.**	2.9	1.4
Sr	62	25	31	48	43
Ba	36	57	41	25	39
V	91	64	115	141	91
Ni	6467	15496	1009	6666	10541
Co	333	778	69	333	536
MgO	29	21	**n.d.**	36	23
FeO*	20	49	**n.d.**	17	28
Cr	4306	3530	5592	3750	4762
P_2O_5	0.24	0.30	**n.d.**	0.12	0.15
MnO	0.40	0.22	**n.d.**	0.20	0.16
Li	5.1	2.0	2.2	2.9	6.9
Cu	178	67	8	47	16
K_2O	0.029	0.055	**n.d.**	0.021	0.049
Ga	2.2	2.2	0.3	1.3	0.7
Na_2O	0.091	0.091	**n.d.**	0.070	**b.d.**
Rb	0.96	1.25	0.43	0.46	1.87
Pb	0.37	0.13	0.15	0.17	0.13
Zn	85	23	11	17	30
Mg#	**0.74**	**0.46**		**0.81**	**0.62**
Co#	**23**	**22**		**27**	**25**

Table D-2 Chondrules- Indarch EH4

	In 1 RP	In 2 RP	In 3 RP	In 4 RP	In 5 PP	In 6 PP	In 7 PP	In 8 PP
W	0.046	0.056	0.051	0.068	0.057	0.103	0.030	0.158
Zr	1.9	2.1	1.4	2.8	3.6	8.3	1.9	2.7
Hf	0.057	0.070	0.074	0.103	0.142	0.219	0.079	0.134
Sc	6.1	4.3	5.9	6.0	8.8	10.6	5.4	8.8
Y	2.3	1.6	1.0	1.6	1.9	4.4	1.9	2.1
Gd	0.30	0.21	0.13	0.21	0.24	0.61	0.25	0.27
Tb	0.054	0.040	0.024	0.039	0.047	0.112	0.051	0.053
Dy	0.37	0.27	0.16	0.26	0.31	0.76	0.34	0.35
Ho	0.080	0.057	0.036	0.056	0.069	0.156	0.077	0.078
Er	0.23	0.16	0.11	0.16	0.20	0.44	0.21	0.22
Tm	0.035	0.025	0.017	0.025	0.031	0.069	0.032	0.033
Lu	0.036	0.026	0.018	0.026	0.032	0.069	0.034	0.035
Nd	0.66	0.50	0.20	0.51	0.55	1.41	0.57	0.64
Sm	0.23	0.17	0.08	0.14	0.19	0.48	0.19	0.18
Pr	0.13	0.10	0.04	0.10	0.11	0.28	0.11	0.13
La	0.32	0.25	0.09	0.27	0.26	0.70	0.24	0.35
Yb	0.23	0.18	0.07	0.15	0.19	0.50	0.17	0.18
Ce	0.83	0.66	0.23	0.70	0.69	1.82	0.68	0.87
Eu	0.068	0.045	0.013	0.062	0.059	0.147	0.044	0.077
Th	0.042	0.034	0.035	0.031	0.033	0.081	0.032	0.035
Al_2O_3	2.4	1.9	2.5	2.3	2.5	2.8	2.7	2.7
U	0.013	0.011	0.008	0.010	0.012	0.026	0.011	0.012
Ir	0.028	0.052	0.020	0.076	0.019	0.038	0.030	0.038
Mo	0.30	0.54	0.30	0.76	0.25	0.36	0.38	0.40
TiO_2	0.056	0.070	0.062	0.090	0.057	0.052	0.075	0.093
Ta	0.009	0.013	0.016	0.018	0.030	0.025	0.009	0.012
Nb	0.15	0.23	0.15	0.34	0.05	0.13	0.12	0.10
CaO	1.10	0.98	0.37	1.26	1.07	3.19	0.83	1.33
Sr	4	3	1	20	11	7	2	28
Ba	1.0	0.9	0.6	3.1	2.8	1.2	0.7	5.0
V	71	69	51	87	25	20	56	45
Ni	799	1246	353	3303	249	791	461	480
Co	38	50	16	158	9	33	20	23
MgO	30	24	31	27	34	26	32	33
FeO*	7	11	5	19	3	9	6	5
Cr	2802	3699	2368	4796	1414	1997	2505	1798
P_2O_5	0.033	0.070	0.032	0.105	0.029	0.064	0.078	0.095
MnO	0.10	0.15	0.18	0.22	0.31	0.50	0.17	0.18
Li	2.1	1.4	1.3	2.0	2.3	2.4	1.7	2.4
Cu	120	145	192	241	473	722	161	295
K_2O	**b.d.**	**b.d.**	**b.d.**	0.02	**b.d.**	0.01	0.02	0.03
Ga	0.84	1.09	0.53	2.93	0.92	2.34	0.74	0.98
Na_2O	1.2	1.2	1.5	1.1	1.4	1.9	1.6	1.0
Rb	0.39	0.64	0.50	1.40	0.61	0.98	0.48	0.79
Pb	1.7	1.7	0.6	1.5	2.1	4.8	1.7	1.7
Zn	30	31	30	55	110	239	44	65
Mg#	**0.90**	**0.81**	**0.92**	**0.74**	**0.96**	**0.86**	**0.91**	**0.93**
Co#	**8**	**6**	**4**	**11**	**4**	**5**	**4**	**7**

Table D-2 Chondrules - Allendé $CV3_{OX-A}$

	All-1 WC	All-2 WC	All-3 WC	All-4 WC	All-5 BO	All 15 BO	All 6 BO	All 7 BO	All-8 PO	All-9 PO	All 10 PO	All 11 PO	All-12 PP-POP	All-13 PP-POP	All-14 PP-POP
W	0.77	0.51	0.25	0.11	0.14	0.19	0.26	0.19	0.19	0.25	0.27	0.14	0.25	0.19	0.16
Zr	22.4	16.0	9.7	7.3	23.3	8.1	19.6	9.9	13.4	5.1	16.6	6.1	10.1	10.3	9.9
Hf	0.58	0.43	0.27	0.20	0.60	0.22	0.55	0.22	0.35	0.14	0.45	0.16	0.27	0.34	0.27
Sc	33	23	14	14	30	10	27	14	20	9	22	11	13	20	16
Y	8.5	6.3	3.8	2.9	8.8	3.2	7.6	3.2	5.2	2.0	6.3	2.4	3.8	4.1	4.1
Gd	1.06	0.86	0.48	0.38	1.12	0.42	1.02	0.50	0.67	0.27	0.79	0.33	0.50	0.64	0.52
Tb	0.20	0.16	0.09	0.07	0.21	0.08	0.20	0.09	0.13	0.05	0.15	0.06	0.09	0.13	0.10
Dy	1.4	1.1	0.6	0.5	1.4	0.5	1.3	0.6	0.9	0.3	1.0	0.4	0.6	1.0	0.7
Ho	0.30	0.22	0.14	0.10	0.30	0.11	0.29	0.12	0.18	0.07	0.22	0.09	0.14	0.19	0.15
Er	0.84	0.65	0.39	0.30	0.86	0.32	0.84	0.33	0.52	0.21	0.63	0.25	0.39	0.42	0.41
Tm	0.13	0.11	0.06	0.05	0.14	0.05	0.13	0.05	0.08	0.04	0.10	0.04	0.06	0.05	0.07
Lu	0.13	0.10	0.06	0.05	0.14	0.05	0.13	0.05	0.08	0.03	0.10	0.04	0.06	0.09	0.07
Nd	2.5	2.0	1.1	0.9	2.7	1.0	2.5	1.7	1.6	0.6	1.8	0.8	1.2	0.9	1.2
Sm	0.82	0.66	0.38	0.30	0.88	0.33	0.83	0.48	0.52	0.22	0.59	0.27	0.38	0.30	0.41
Pr	0.49	0.38	0.22	0.18	0.53	0.19	0.50	0.38	0.31	0.13	0.35	0.15	0.23	0.18	0.25
La	1.26	1.00	0.57	0.46	1.39	0.50	1.25	0.86	0.80	0.33	0.88	0.39	0.59	0.45	0.64
Yb	0.93	0.75	0.41	0.33	0.95	0.35	0.90	0.37	0.57	0.24	0.65	0.31	0.42	0.34	0.46
Ce	3.2	2.5	1.4	1.2	3.6	1.3	3.2	2.6	2.1	0.8	2.2	1.0	1.5	1.2	1.6
Eu	0.29	0.26	0.13	0.11	0.32	0.11	0.26	0.21	0.18	0.07	0.21	0.09	0.14	0.10	0.14
Th	0.14	0.11	0.07	0.05	0.16	0.06	0.14	0.09	0.09	0.04	0.11	0.05	0.07	0.07	0.07
Al_2O_3	7.2	5.6	3.1	2.8	8.2	2.5	6.0	3.7	4.3	2.2	5.0	2.1	3.7	3.0	3.3
U	0.032	0.030	0.020	0.017	0.047	0.018	0.041	0.031	0.028	0.013	0.026	0.018	0.020	0.017	0.020
Ir	2.51	1.68	0.85	0.12	0.11	0.16	0.02	0.18	0.23	0.62	1.36	0.11	0.71	0.63	0.61
Mo	4.13	2.82	2.32	0.97	0.74	1.37	0.82	1.00	1.23	1.74	2.16	1.07	4.00	2.23	1.18
TiO_2	0.39	0.28	0.16	0.15	0.37	0.13	0.39	0.28	0.24	0.11	0.28	0.13	0.16	0.15	0.17
Ta	0.077	0.063	0.041	0.030	0.092	0.040	0.074	0.048	0.050	0.024	0.069	0.027	0.037	0.034	0.035
Nb	1.74	1.08	0.70	0.39	1.50	0.51	1.00	1.22	0.78	0.40	0.86	0.43	0.58	0.58	0.63
CaO	4.5	4.2	1.9	2.0	5.9	1.4	3.1	3.0	2.6	1.6	3.0	1.1	2.7	2.5	1.8
Sr	37	47	17	14	43	12	18	14	16	11	27	8	19	12	9
Ba	9	9	5	4	16	4	7	4	5	2	6	4	5	5	5
V	332	171	156	105	97	105	157	169	145	120	171	130	112	115	110
Ni	5777	7894	10331	3723	1619	4415	555	3681	5441	6477	9958	3951	15118	9144	5494
Co	290	384	509	190	80	222	41	178	292	315	498	212	719	452	298
MgO	31	31	37	41	33	43	37	33	37	46	28	42	34	34	36
FeO*	15.0	16.9	19.4	7.0	4.8	12.2	8.8	11.2	14.4	13.0	23.2	12.0	20.2	18.0	15.1
Cr	3006	3775	3913	3526	3663	3428	3336	3120	3836	2032	4273	3877	4512	5631	4053
P_2O_5	0.15	0.19	0.19	0.10	0.04	0.13	0.05	0.11	0.15	0.15	0.27	0.10	0.35	0.18	0.16
MnO	0.09	0.12	0.13	0.08	0.06	0.10	0.19	0.07	0.13	0.05	0.17	0.09	0.09	0.21	0.10
Li	1.5	1.7	1.1	2.2	0.9	1.3	0.9	0.6	1.9	0.6	2.1	1.3	1.2	3.3	2.6
Cu	35	54	84	28	19	32	6	27	40	42	104	26	112	106	35
K_2O	0.14	0.06	0.06	0.04	0.05	0.04	0.13	0.10	0.10	0.02	0.09	0.04	**b.d.**	0.02	0.04
Ga	4.0	4.1	3.0	1.0	0.4	1.8	2.1	1.7	3.3	1.0	5.3	2.2	2.6	2.3	3.2
Na_2O	1.73	0.97	0.66	0.54	1.29	0.80	2.23	0.90	1.40	0.20	1.28	0.54	0.31	0.28	0.79
Rb	4.1	2.4	2.2	3.3	1.9	2.3	5.8	5.1	3.2	0.9	3.1	2.5	0.5	1.7	1.6
Pb	0.36	0.44	0.33	0.17	0.66	0.22	0.20	0.46	0.27	0.22	0.63	0.20	0.35	0.25	0.25
Zn	80	79	58	26	45	38	50	46	66	54	104	48	43	47	62
Mg#	**0.81**	**0.78**	**0.79**	**0.92**	**0.93**	**0.89**	**0.85**	**0.83**	**0.88**	**0.70**	**0.87**	**0.77**	**0.79**	**0.82**	**0.87**
Co#	**26**	**31**	**35**	**37**	**22**	**6**	**21**	**27**	**33**	**29**	**24**	**48**	**34**	**27**	**25**

Table D-2 Chondrules - Karoonda CK4

	Kar 2 BO	Kar 3 BO	Kar 4 PO	Kar 5 PO	Kar 6 PO	Kar 7 PO	Kar 8 POP	Kar 9 POP	Kar 10 POP	Kar 11 POP	Kar 12 WC	Kar 13 WC	Kar 14 WC	Kar 15 WC
W	0.27	0.14	0.50	0.15	0.28	0.38	0.35	0.35	0.45	0.28	0.23	0.25	0.21	0.19
Zr	10.5	11.2	5.5	9.1	6.3	8.6	9.0	5.2	7.3	9.8	7.1	8.9	12.3	5.8
Hf	0.27	0.28	0.12	0.23	0.16	0.24	0.25	0.13	0.22	0.26	0.19	0.23	0.33	0.15
Sc	11	17	8	15	10	16	13	11	11	16	12	14	18	14
Y	4.7	4.5	1.7	2.8	2.1	4.2	3.3	2.0	2.5	4.0	3.1	3.7	5.4	2.9
Gd	0.59	0.57	0.22	0.37	0.28	0.57	0.45	0.24	0.36	0.50	0.42	0.43	0.69	0.29
Tb	0.11	0.11	0.04	0.07	0.05	0.11	0.08	0.05	0.07	0.09	0.08	0.08	0.13	0.07
Dy	0.77	0.74	0.30	0.47	0.38	0.71	0.54	0.31	0.46	0.65	0.53	0.59	0.92	0.49
Ho	0.16	0.16	0.07	0.10	0.08	0.15	0.12	0.07	0.10	0.14	0.11	0.13	0.19	0.11
Er	0.45	0.45	0.20	0.29	0.23	0.41	0.33	0.21	0.28	0.40	0.31	0.38	0.53	0.34
Tm	0.071	0.074	0.037	0.050	0.043	0.071	0.054	0.037	0.047	0.066	0.058	0.064	0.085	0.059
Lu	0.063	0.070	0.039	0.051	0.037	0.064	0.052	0.042	0.044	0.065	0.049	0.063	0.071	0.061
Nd	1.4	1.3	0.5	0.7	0.7	1.3	1.0	0.6	0.8	1.2	1.0	0.9	1.5	0.6
Sm	0.47	0.44	0.18	0.26	0.23	0.44	0.35	0.19	0.29	0.39	0.34	0.32	0.53	0.22
Pr	0.27	0.26	0.10	0.14	0.14	0.24	0.19	0.11	0.17	0.22	0.19	0.18	0.29	0.10
La	0.69	0.67	0.25	0.37	0.33	0.60	0.51	0.30	0.43	0.55	0.46	0.45	0.71	0.23
Yb	0.43	0.50	0.25	0.33	0.28	0.47	0.35	0.27	0.30	0.41	0.36	0.43	0.52	0.39
Ce	1.8	1.7	0.7	0.9	0.9	1.5	1.2	0.7	1.1	1.4	1.2	1.1	1.8	0.6
Eu	0.089	0.154	0.054	0.048	0.092	0.087	0.090	0.050	0.101	0.088	0.095	0.110	0.112	0.051
Th	0.075	0.072	0.030	0.067	0.032	0.069	0.070	0.037	0.065	0.072	0.055	0.059	0.093	0.040
Al_2O_3	2.9	4.3	1.4	2.1	1.2	2.1	2.7	1.7	2.6	1.6	2.1	3.1	3.5	1.2
U	0.023	0.023	0.012	0.018	0.013	0.023	0.022	0.012	0.020	0.020	0.018	0.016	0.025	0.011
Ir	0.13	0.25	0.34	0.12	0.37	0.70	0.64	0.14	0.51	0.56	0.57	0.37	0.48	0.18
Mo	1.3	1.6	2.0	0.7	2.1	3.0	2.0	1.3	2.5	3.1	3.4	1.8	2.9	1.7
TiO_2	0.20	0.23	0.09	0.15	0.14	0.18	0.15	0.11	0.17	0.17	0.16	0.14	0.20	0.14
Ta	0.047	0.042	0.015	0.029	0.025	0.077	0.039	0.025	0.030	0.036	0.029	0.036	0.054	0.020
Nb	0.74	0.79	0.34	0.41	0.48	0.78	0.63	0.30	0.50	0.55	0.53	0.50	0.78	0.26
CaO	1.5	3.4	1.2	2.4	1.3	2.0	1.9	1.5	3.1	2.1	2.1	2.5	3.2	1.4
Sr	24	24	6	6	4	7	10	8	12	6	8	15	9	4
Ba	7.7	6.4	1.7	3.2	1.4	4.6	5.4	3.6	2.9	3.3	3.2	6.1	8.5	2.0
V	60	94	58	71	95	122	104	71	86	93	116	85	92	49
Ni	6581	12079	6184	4922	15412	22150	11995	8080	8682	27034	28006	12232	16007	5937
Co	536	655	467	469	797	1063	684	595	480	1423	1148	680	815	459
MgO	27	27	29	29	29	25	26	28	26	26	25	27	24	30
FeO*	32	32	34	34	39	38	35	32	34	38	38	34	33	33
Cr	2248	2797	1703	4160	3298	4725	3924	2447	3023	3480	4663	3558	3781	2189
P_2O_5	0.15	0.14	0.17	0.06	0.33	0.27	0.20	0.09	0.43	0.21	0.22	0.21	0.16	0.17
MnO	0.19	0.18	0.20	0.21	0.20	0.18	0.19	0.20	0.19	0.19	0.18	0.19	0.17	0.21
Li	0.52	0.47	0.50	0.71	1.14	1.98	1.12	0.59	1.15	1.36	1.47	1.62	0.54	0.89
Cu	51	52	21	3	104	185	56	23	579	505	276	67	106	24
K_2O	0.022	**b.d.**	0.021	**b.d.**	**b.d.**	**b.d.**	0.017	**b.d.**	0.074	**b.d.**	0.011	0.013	0.016	0.048
Ga	2.5	2.8	2.4	3.2	4.2	5.3	4.7	1.8	4.1	3.9	5.0	3.8	4.2	2.2
Na_2O	0.40	0.26	**b.d.**	0.21	**b.d.**	0.13	0.34	0.16	0.22	0.14	0.16	0.24	0.42	0.14
Rb	20.7	1.0	0.2	1.0	0.2	1.7	3.1	3.1	0.5	0.7	1.5	0.5	8.0	0.8
Pb	0.60	0.45	0.30	0.27	0.34	0.66	0.59	0.30	0.90	0.56	0.70	0.52	0.69	0.27
Zn	91	84	90	98	105	104	102	96	95	86	98	99	98	94
Mg#	**0.63**	**0.63**	**0.63**	**0.63**	**0.60**	**0.56**	**0.60**	**0.63**	**0.61**	**0.58**	**0.57**	**0.61**	**0.59**	**0.64**
Co#	**23**	**28**	**19**	**19**	**28**	**38**	**26**	**25**	**19**	**51**	**41**	**27**	**34**	**19**

Table D-3 Published data - CR2 Bulk Meteorite

	Bischoff et al. (1993)			Dreibus et al. (1993)		Dreibus et al. (1995)	Kallemeyn et al. (1994)			Kong et al. (1999)		Weisberg et al. (1995)	Spettel et al. (1992)
W	0.16	0.12	0.16										
Zr													
Hf	0.16	0.18	0.19										
Sc	8.63	8.54	8.34				7.74	8.48	8.04	9.57	8.05		8.5
Y													
Gd													
Tb	0.046	0.055	0.05										
Dy	0.39	0.34	0.22										
Ho	0.087	0.103	0.096										
Er													
Tm													
Lu	0.033	0.037	0.038				0.042	0.034	0.028	0.04	0.025		
Nd	0.58		0.93										
Sm	0.245	0.24	0.264				0.21	0.229	0.22	0.325	0.265		0.26
Pr													
La	0.44	0.42	0.633				0.372	0.399	0.4	0.755	0.686		
Yb	0.26	0.24	0.24				0.24	0.233	0.255	0.318	0.291		
Ce	0.84	0.75	1.09										
Eu	0.09	0.09	0.088				0.09	0.086	0.087				
Th													
Al_2O_3	2.34	2.40	1.87				2.21	2.38	2.40	2.61	2.57	2.06	
U	0.13	0.15	0.15										
Ir	0.682	0.6	0.627				0.6	0.578	0.53	0.535	0.537		
Mo	1.12	1.2	1.6										
TiO_2												0.12	
Ta		0.045											
Nb													
CaO	1.74	2.01	1.54				1.96	2.28	1.93	2.94	2.46	1.96	
Sr													
Ba	90	156	83.7										
V	66.8	74.2	66.8				73	75	78	83.3	76.9		
Ni	1430	1470	1470	14300	13900	14700	14800	12600	12800	1480	1590		14600
Co	632	658	671				725	615	642	650	730		
MgO	24.71	23.21	18.90				21.89	22.22	22.38	24.37	23.54	22.70	
FeO*	30.49	31.90	32.81				32.68	28.56	29.85	28.43	32.68	31.58	31.71
Cr	3790	3750	3520				3530	3590	3520	3540	3560	3733	
P_2O_5												0.24	
MnO	0.23	0.21	0.20				0.22	0.22	0.22	0.22	0.22	0.24	0.22
Li													
Cu	80	86	74									12233	
K_2O	0.06	0.06	0.07				0.06	0.06	0.07	0.07	0.07	0.04	
Ga	4.1	4.18	4.7				4.2	4.2	4.2	4.63	3.97		
Na_2O	0.16	0.15	0.16	0.16		0.15	0.13	1.40	0.17	0.16	0.20	0.49	0.16
Rb													
Pb													
Zn	60	89	63				64	60	52	53.3	40.6		61
Mg#	**0.59**	**0.56**	**0.51**				**0.54**	**0.58**	**0.57**	**0.60**	**0.56**	**0.56**	
Co#	**25**	**25**	**60**										

Table D-3 Published data - CV3 Bulk Meteorite

	Jarosewich et al. (1987)	Shinotsuka et al. (1995)	Showalter et al. (1987)	Rubin et al. (1985)		Paul & Lipshutz	Rhodes & Fulton	Rocholl & Jobhum	Muir et al. (1987)	Murty et al. (1983)	(Metbase)			
W	0.22										0.2			0.25
Zr	9						7.6	7.77	6.4		11	11		
Hf	0.21							0.22	0.21		0.2	0.19		0.23
Sc	11		12	10.5	13.4						10		11.9	11.9
Y	3.1	2.47	3				2.8	3.22	2.7			3.1		
Gd	0.42	0.394	0.44					0.37	0.38			0.42		
Tb	0.081	0.069	0.081						0.07		0.1	0.076		0.083
Dy	0.42	0.466	0.44					0.42	0.46			0.41		0.36
Ho	0.1	0.0954	0.113					0.12	0.1		0.1	0.12		0.09
Er	0.29	0.288	0.3					0.34	0.28			0.28		
Tm	0.055	0.0496	0.055						0.061					
Lu	0.052	0.0456	0.049						0.06		0.06			0.052
Nd	0.99	0.977	1.05					0.91	1			0.93		
Sm	0.34	0.318	0.347	0.264	0.312			0.28	0.31		0.35	0.36		0.33
Pr	0.21	0.197	0.21					0.19	0.2			0.22		
La	0.52	0.503	0.5	0.463	0.519			0.49	0.53			0.56		0.47
Yb	0.3	0.311	0.3					0.3	0.3			0.3		0.24
Ce	1.33	1.26	1.39					1.49	1.44		1	1.2		1.26
Eu	0.11	0.108	0.116	0.146	0.198			0.1	0.11		0.1	0.1		0.16
Th	0.065	0.061						0.054	0.063					
Al_2O_3	3.29		3.25	3.31	4.55		3.23				3.59		3.25	3.38
U	0.016	0.0154						0.0206						
Ir	0.74			0.664	1.107									0.78
Mo	2.5													
TiO_2	0.15						0.15				0.15		0.14	0.15
Ta														
Nb	0.62								0.51			0.74		
CaO	2.57		2.52	2.18	2.67		2.38				2.66		2.63	2.66
Sr	12						15	15.5				27		
Ba	4							5.29	5.4			12		
V	92		112	102	102		105				89	83	84.4	95
Ni	14200			13100	13800		14000						14315	14800
Co	600		738	652	662	615						610		694
MgO	24.59			22.38	23.21		24.19				23.21		24.84	24.87
FeO*	30.32		33.83	29.59	30.36		31.21				30.23		30.28	28.56
Cr	3600		4230	3400	3500		3700				3500		3400	3650
P_2O_5	0.23						0.25							
MnO	0.19		0.18	0.19	0.18		0.21				0.19		0.19	0.19
Li	3									1.74		1.3		
Cu	119										230		111.2	
K_2O	0.04		0.03	0.03	0.03		0.04				0.04		0.04	0.04
Ga	6					5.97	11				5			5.3
Na_2O	0.46		0.44	0.50	0.51						0.47		0.46	0.46
Rb	1.2					1.11	1.6	1				1.4		0.82
Pb	1.39								1.53			1.3		
Zn	110			86	112	119					100		70.4	92
Mg#	**0.59**			**0.57**	**0.58**		**0.58**				**0.58**		**0.59**	**0.61**
Co#														

Table D-3 Published data - CV3 Bulk Meteorite (cont.)

	Lovering & Keays (1987)	Kong et al. (1999)		Heier et al. (1987)	Jochum et al. (2000)	Kleine et al. (2004)	Newsome (1995)
W						0.1678	0.19
Zr				9.2	7.04		8.3
Hf						0.1866	0.194
Sc		10.4	11				11.4
Y				3	2.99		2.4
Gd							0.415
Tb							0.065
Dy							0.475
Ho							0.11
Er							0.315
Tm							0.045
Lu		0.056	0.052				0.048
Nd							0.99
Sm		0.292	0.337				0.295
Pr							0.2
La		0.54	0.552				0.486
Yb		0.3	0.286				0.322
Ce							1.29
Eu							0.113
Th							0.06
Al_2O_3		3.17	3.23				3.31
U							0.017
Ir	0.77	0.832	0.816				0.76
Mo							2.1
TiO_2							0.16
Ta					0.027		
Nb					0.452		
CaO		2.67	2.43				2.66
Sr				15.5			15.3
Ba				5.3			4.9
V		91.2	96				96
Ni		14300	14300				13400
Co		680	706				655
MgO		24.87	24.54				24.04
FeO*							30.23
Cr		3570	3690				3600
P_2O_5							0.23
MnO		0.19	0.19				0.19
Li							1.24
Cu							100
K_2O			0.04				0.04
Ga		6.1	6.3				6
Na_2O		0.47	0.46				0.44
Rb							1.25
Pb							1.4
Zn		112	119				116
Mg#							**0.59**
Co#							

Table D-3 Published data - CK4 Bulk Meteorite

	Evensen et al. (1978)	Patchett et al. (2004)	Pack et al. (2007)	Yates et al. (1968)	Palme & Rammensee (1981)	Fischer-Goedde et al. (2010)	Nichiporuk et al	Ehmann & Rabagay (1970)	Takahashi et al. (1978)	Seitz et al. (2007)	Matza & Lippschutz (1977)	Rocholl & Jochum (1993)	Knab (1981)	Kallemeyn et al. (1990)
W													0.223	
Zr								9.5					7.72	
Hf		0.19						0.29					0.183	
Sc														11.1
Y			3.2705											
Gd	0.404												0.468	
Tb														
Dy	0.479												0.495	
Ho			0.1253											
Er	0.348													
Tm														
Lu		0.0474												0.046
Nd	0.935	0.932											1.13	
Sm	0.304	0.301											0.342	0.275
Pr														
La	0.472													0.45
Yb	0.321												0.346	0.312
Ce	1.27													
Eu	0.112												0.111	0.109
Th												0.0561		
Al_2O_3														3.14
U									0.0137			0.014		
Ir					0.76	0.712			0.794					0.853
Mo					0.38									
TiO_2														
Ta														
Nb														
CaO							2.34							2.43
Sr													14.8	
Ba													5.29	
V														99
Ni							13900		13300					13600
Co							640				636			682
MgO														25.04
FeO*							31.36							30.88
Cr				3800			3200							3750
P_2O_5														
MnO				0.15			0.18							0.18
Li										1				
Cu													113	
K_2O														0.04
Ga											5.36		5.93	5.2
Na_2O														0.42
Rb									0.64					
Pb													1.62	
Zn									92.5		102			92
Mg#														**0.59**
Co#														

Table D-3 Published data - CK4 Bulk Meteorite (cont.)

	Jochum et al. (2000)	Fitzgerald (1979)	Hirota et al. (2002)	Morgan & Lovering (19..)	Nichiporuk & Bingham (1970)	Kleine et al. (2004)	Mason & Wiik (1962)
W						0.1987	
Zr	8.15						
Hf						0.1877	
Sc							
Y	3.74						
Gd			0.380				
Tb							
Dy			0.459				
Ho							
Er			0.290				
Tm							
Lu			0.044				
Nd			0.898				
Sm			0.287				
Pr							
La			0.483				
Yb							
Ce			1.156				
Eu			0.106				
Th				0.057			
Al_2O_3		2.97	0.00				2.78
U				0.014			
Ir							
Mo							
TiO_2		0.17					0.22
Ta							
Nb	0.538						
CaO		2.39	2.46				2.10
Sr			12.65				
Ba			3.767				
V					84		160
Ni		15000					14000
Co							620
MgO		24.06	23.25				25.27
FeO*		30.70	29.13				32.87
Cr		3000					4240
P_2O_5		0.23					0.10
MnO		0.19					0.19
Li							
Cu					135		101
K_2O		0.05	0.05				0.03
Ga							
Na_2O		0.53					0.71
Rb			1.142				
Pb							
Zn							
Mg#		**0.58**	**0.59**				**0.58**
Co#							

Table D-3 Published data - EH4 Bulk Meteorite

	Baedecker & Wasson (1975)	Binz et al. (1974)	Crocket et al. (1967)	Ebihara (1984)	Ehmann et al. (1970)	Ehmann et al. (1979)	Evensen et al. (1978)	Garrison et al. (2000)	Horan & Walker (2000)	Kallemeyn & Wasson (1986)	Laul et al. (1972)	Manhes & Allegre (1978)	McDonald & Russell (2001)	Michealise et al. (1969)	Nakamura & Masuda (1973)
W															
Zr						5.1								6	
Hf						0.102									
Sc	5.6					5.8				5.53					
Y															
Gd				0.188			0.227								0.179
Tb				0.026											
Dy							0.275								0.223
Ho															
Er							0.188								0.149
Tm				0.023											
Lu				0.023						0.023					0.023
Nd				0.403			0.567								0.399
Sm				0.138			0.183			0.126					0.129
Pr															
La				0.198			0.318			0.229					0.209
Yb				0.145			0.195			0.153					0.147
Ce				0.503			0.776								0.54
Eu				0.046			0.072			0.0525					0.051
Th															
Al_2O_3	1.51									1.47				1.47	
U												0.0083			
Ir	0.56		0.25		0.58				0.567	0.541			0.52		
Mo															
TiO_2														0.07	
Ta															
Nb															
CaO								1.08		1.20				1.13	
Sr														8	
Ba															2.3
V	57									52.7					
Ni	18900									16300					
Co	910	1100				988				805					
MgO										17.41				18.27	
FeO*	39.24					40.40				35.64				39.12	
Cr	3100					3290				3030					
P_2O_5														0.48	
MnO	0.32									0.31				0.28	
Li															
Cu		225													
K_2O								0.09		0.11				0.10	
Ga	16.2	17								16					
Na_2O	1.12									0.98				0.00	
Rb											2.4			3.9	
Pb												2.319			
Zn		430								305	490				
Mg#										**0.47**				**0.45**	
Co#															

Table D-3 Published data - EH4 Bulk Meteorite (cont.)

	Nichiporuk & Moore (1970)	Schmitt et al. (1972)	Wiik (1956)	Lee & Halliday (2000)	Morgan & Lovering (19..)	Newsome (1995)
W				0.124		
Zr						4.9
Hf				0.109		0.14
Sc		6.25				5.7
Y						1.3
Gd						0.214
Tb						0.035
Dy						0.24
Ho						0.05
Er						0.166
Tm						0.025
Lu						0.024
Nd						0.46
Sm						0.14
Pr						0.094
La						0.235
Yb						0.16
Ce						0.66
Eu						0.054
Th					0.029	0.03
Al_2O_3		1.45	1.45			1.53
U					0.011	0.009
Ir						0.565
Mo						
TiO_2			0.07			0.08
Ta						
Nb						
CaO			1.25			1.19
Sr						7.2
Ba						2.6
V						54
Ni			18300			17500
Co		835	800			840
MgO			17.48			
FeO*		37.44	42.65			37.31
Cr		3150	2300			3150
P_2O_5			0.50			0.46
MnO		0.29	0.25			0.28
Li	1.8					2.1
Cu		183				185
K_2O			0.11			0.10
Ga						16
Na_2O		1.00	1.01			0.92
Rb						2.6
Pb						1.1
Zn						250
Mg#			**0.42**			
Co#						

Appendix E

Raw data – Published UOC whole chondrule and CAI values

- All data reported as ppm, except oxides (wt%)
- See tables for references
- FeO* recalculated from Fe_2O_3
- $Mg\# = \frac{Mg_{mol}}{Mg_{mol}+Fe_{mol}}$
- $Co\# = \left(\frac{Co_{mol}}{Co_{mol}+Fe_{mol}}\right) * 10^4$

Table E-1 Published data - UOC RP/CC

	Engler et al. (2007)														
W		0.02	0.03	0.07	0.06	0.01	0.1	0.04		0.06	0.06	0.09	0.03		0.05
Zr	5.2	5.19	3.29	6.22	1.62	1.97	13.81	4.57	8.14	6.40	4.85	5.77	3.08	5.49	3.88
Hf	0.15	0.14	0.09	0.16	0.24	0.19	0.61	0.14	0.24	0.18	0.12	0.15	0.08	0.16	0.10
Sc	8.85	10.74	6.14	10.71	7.05	8.51	35.74		10.6	10.51	9.63	9.62	6.70	9.60	8.74
Y	2.16	2.14	1.33	2.29	2.07	1.82	8.43	1.92	3.25	2.61	1.90	2.38	1.26	2.22	1.52
Gd	0.31	0.31	0.18	0.29	0.49	0.34	1.3	0.26	0.47	0.35	0.24	0.38	0.16	0.31	0.20
Tb	0.05	0.05	0.03	0.05	0.09	0.06	0.24	0.04	0.09	0.07	0.04	0.06	0.03	0.05	0.03
Dy	0.36	0.37	0.21	0.4	0.61	0.43	1.62	0.33	0.57	0.43	0.32	0.39	0.21	0.39	0.27
Ho	0.08	0.09	0.05	0.09	0.16	0.1	0.36	0.07	0.12	0.09	0.07	0.10	0.05	0.08	0.05
Er	0.23	0.24	0.15	0.28	0.4	0.27	1.02	0.18	0.34	0.29	0.21	0.25	0.14	0.27	0.17
Tm	0.03	0.03	0.02	0.04	0.07	0.04	0.18	0.03	0.05	0.04	0.03	0.04	0.02	0.04	0.02
Lu	0.04	0.04	0.02	0.04	0.07	0.05	0.17	0.04	0.06	0.04	0.03	0.04	0.02	0.05	0.03
Nd	0.68	0.66	0.38	0.73	0.73	0.58	2.94	0.33	1.02	0.78	0.62	0.67	0.36	0.68	0.44
Sm	0.23	0.21	0.13	.24.	0.38	0.23	1.04	0.16	0.33	0.23	0.18	0.25	0.14	0.21	0.14
Pr	0.13	0.13	0.07	0.15	0.22	0.15	0.71	0.11	0.21	0.16	0.12	0.16	0.07	0.14	0.09
La	0.35	0.35	0.21	0.4	0.39	0.31	1.59	0.29	0.53	0.43	0.29	0.41	0.20	0.37	0.26
Yb	0.26	0.25	0.15	0.27	0.37	0.32	1.04	0.19	0.33	0.33	0.23	0.28	0.14	0.27	0.18
Ce	0.93	1.01	0.57	1.25	0.82	0.69	4.51	0.74	1.52	1.10	0.82	1.15	0.50	0.96	0.68
Eu	0.08	0.06	0.05	0.13	0.14	0.04	0.38	0.04	0.03	0.11	0.06	0.10	0.04	0.03	0.05
Th	0.04	0.04	0.03	0.05	0.07	0.05	0.26	0.03	0.07	0.05	0.04	0.05	0.05	0.04	0.03
Al_2O_3	2.9	3.1	1.9	2.1	1.7	2	12	2.08	4	3.04	1.80	3.10	1.87	2.44	0.89
U	0.02	0.03	0.01	0.03	0.03	0.02	0.1	0.01	0.02	0.01	0.01	0.01	0.01	0.01	0.01
Ir															
Mo															
TiO_2	0.13	0.2	0.3	0.2	0.3	0.3	0.4	0.09	0.2	0.14		0.15	0.08	0.12	0.07
Ta	0.02	0.02	0.01	0.03	0.04	0.02	0.1	0.01	0.03	0.03	0.02	0.03	0.01	0.02	0.01
Nb	0.49	0.51	0.29	0.61	0.68	0.51	1.84	0.38	0.65	0.54	0.42	0.48	0.27	0.47	0.37
CaO	1.7	1.71	1.4	1.9	1.7	1.8	7.7	1.4	2.2	1.80	1.60	2.10	1.45	1.74	1.30
Sr	6.8	4	7.4	17.3	1.05	0.24	36.3	5	5.3	11.50	9.10	12.50	2.20	6.30	6.30
Ba	3.3	3.1	2.7	3.8	0.22	0.05	8.1	1.6	1.6	3.90	3.20	4.60	1.40	2.80	1.80
V	71.9	85.3	60.1	95.6	10.8	17.9	42.3	59.4	88.2	81.1	82.7	83.1	53.8	79.0	62.5
Ni									0.51	0.15			0.03		0.05
Co															
MgO	26.3	23.4	21	30.4	18.5	23.8	24.2	21.7	30.3	26.0	26.5	31.5	18.6	25.4	22.3
FeO*	4.1	7.1	19.9	6.4	18.8	12.2	4.7	16.6	8.2	12.4	7.9	11.5	17.4	16.7	17.1
Cr	0.78	1	0.9	0.5	0.7	0.9	0.2	0.63	1	0.69	1.10	0.72	0.58	0.76	0.69
P_2O_5			0.1	0.1	0.2	0.1	0.2	0.1		0.05			0.06	0.09	0.03
MnO	0.85	1.1	0.8	0.2	0.8	0.9	0.2	0.62	0.6	0.61	0.70	0.43	0.65	0.71	0.84
Li															
Cu															
K_2O	0.43	0.2	0.3	0.1	0.3	0.1	0.3	0.14	0.3	0.22	0.00	0.18	0.20	0.06	0.06
Ga															
Na_2O	1.27	0.5	0.1	0.3	0.2	0.2	2.8	0.67	2.5	1.58	2.90	1.46	1.11	0.87	0.50
Rb	17.48	4.1	9.33	4.6	4.6	0.49	0.39	4.27	6.15	2.75	4.45	7.43	5.93	1.23	4.09
Pb															
Zn															
Mg#	**0.92**	**0.85**	**0.65**	**0.89**	**0.64**	**0.78**	**0.90**	**0.70**	**0.87**	**0.79**	**0.86**	**0.83**	**0.66**	**0.73**	**0.70**
Co#															

Table E-1 Published data - UOC Type I

	Jones (1994)								
W									
Zr									
Hf									
Sc									
Y									
Gd									
Tb									
Dy									
Ho									
Er									
Tm									
Lu									
Nd									
Sm									
Pr									
La									
Yb									
Ce									
Eu									
Th									
Al_2O_3	3.1	2.2	1.8	3.2	2.1	2.9	1.1	1.9	3.1
U									
Ir									
Mo									
TiO_2	0.14	0.90	0.90	0.13	0.10	0.11	0.05	0.11	0.15
Ta									
Nb									
CaO	2.7	1.3	1.2	2.3	1.6	2.1	0.5	1.6	2.3
Sr									
Ba									
V									
Ni									
Co									
MgO	30.4	33.8	35.9	30.7	31.2	34.9	36.1	37.3	33.1
FeO*	4.4	1.7	2.2	4.3	6.4	2.2	2.6	2.1	2.6
Cr	0.64	0.56	0.56	0.65	0.61	0.58	0.45	0.55	0.62
P_2O_5									
MnO	0.28	0.31	0.26	0.47	0.45	0.34	0.22	0.29	0.44
Li									
Cu									
K_2O	0.06	0.07	0.03	0.09	0.08	0.05	0.06	0.03	0.03
Ga									
Na_2O	0.62	0.55	0.20	0.84	0.89	0.56	0.38	0.31	0.39
Rb									
Pb									
Zn									
Mg#	**0.92**	**0.97**	**0.97**	**0.93**	**0.90**	**0.97**	**0.96**	**0.97**	**0.96**
Co#									

Table E-1 Published data - UOC Type II

	Jones (1990)										
W											
Zr											
Hf											
Sc											
Y											
Gd											
Tb											
Dy											
Ho											
Er											
Tm											
Lu											
Nd											
Sm											
Pr											
La											
Yb											
Ce											
Eu											
Th											
Al_2O_3	2.72	3.02	3.01	2.07	2.73	1.80	2.37	3.47	1.89	3.15	3.23
U											
Ir											
Mo											
TiO_2		0.11						0.14			0.12
Ta											
Nb											
CaO	1.77	1.91	1.82	1.76	2.17	1.29	1.64	2.25	1.66	2.17	2.32
Sr											
Ba											
V											
Ni											
Co											
MgO	30.0	29.8	28.5	33.2	33.2	36.1	35.5	28.0	31.0	27.8	30.8
FeO*	15.6	13.9	15.8	15.9	14.1	15.7	14.0	11.9	17.1	17.1	12.3
Cr	0.45	0.53	0.63	0.52	0.42	0.54	0.46	0.59	0.42	0.50	0.42
P_2O_5	0.69	0.11	0.52	0.06	0.93		0.10	0.25	0.38	0.57	0.12
MnO	0.45	0.45	0.40	0.42	0.27	0.43	0.36	0.41	0.34	0.36	0.40
Li											
Cu											
K_2O	0.24	0.23	0.19	0.13	0.20	0.05	0.06	0.26	0.11	0.22	0.23
Ga											
Na_2O	1.69	1.68	1.74	1.35	1.83	1.13	1.37	2.12	1.14	1.98	2.17
Rb											
Pb											
Zn											
Mg#	**0.77**	**0.79**	**0.76**	**0.79**	**0.81**	**0.80**	**0.82**	**0.81**	**0.76**	**0.74**	**0.82**
Co#											

Table E-2 Published data - Melilite CAI

	Sylvester et al. (1993)										Mao et al. (1990)		Kornacki & Fegley (1986)				
W	1.36	7.5	1.53	1.26	2.47	2.38	0.85	5.25	1.22								
Zr	131	87.5	53.6	54.8	68.8	42.2	180	86.9	55.2				63	101	106	5.5	3.6
Hf	4.77	5.6	3.2	1.62	2.17	1.04	4.48	3.01	1.89	0.017	0.56	0.975	1.7	2.9	2.4	0.2	0.12
Sc	240.17	122.31	179.04	90.39	104.39	54.34	294.4	124.82	128.31	91.06	52.75	46.62	107	142	143	22	23
Y													28	36	38	2.3	1.6
Gd													3.5	4.8	4.6	2.8	2.2
Tb	0.896	0.803	0.745	0.435	0.617	0.441	0.599	0.714	0.511	2.25	1.1	0.384	0.63	0.89	1.1	0.39	0.4
Dy	5.98	5.31	4.79	2.73	4.46	2.89	4.06	4.93	3.28	12.2	8.43	2.76	4.5	6.4	7.8	2	2
Ho	1.45	1.21	1.13	0.696	0.943	0.69	0.875	1.16	0.784	0.847			1	1.3	2	0.2	0.13
Er													3.3	4.2	5.4	0.5	0.17
Tm	0.673	0.578	0.453	0.373	0.385	0.302	0.395	0.492	0.305	1.96	0.704	0.267	0.43	0.61	0.76	0.79	0.63
Lu	0.65	0.569	0.443	0.37	0.392	0.317	0.397	0.477	0.312	0.0049	0.706	0.0673	0.48	0.72		0.11	0.019
Nd													8	10	10	18	12
Sm	3.16	3.23	2.73	1.734	2.476	1.75	2.392	2.86	2.259	15.23	4.49	1.69	2.4	3.6	5	4.1	4.2
Pr													1.7	1.9	2.2	3.5	2.9
La	5.09	5.08	4.49	2.83	4.38	3.2	3.65	4.5	4.04	28.9	6.57	2.3	4.2	5.5	8.4	7.2	6.9
Yb	4.72	3.84	3.45	2.5	2.69	2.2	2.61	3.46	2.11	0.324	2.45	1.25	2.8	2.9	1.3	1.4	0.68
Ce	11.7	13.2	11.5	7.43	11.2	8.02	9.89	12.2	10.02	64.6	15.7	5.44	12	15	20	20	18
Eu	1.54	1.23	1.411	1.309	1.507	1.449	1.27	1.275	1.226	0.312	0.785	0.487	1.1	0.76	0.36	0.65	0.31
Th	0.643		0.534	0.313	0.515	0.65	0.468	0.497	0.507	2.11	0.196		0.5	0.7	0.71	0.72	0.45
Al2O3	35.8	32.7	34.7	33.2	35.3	29.9	34.7	36.5	25.3	47.4	38.9	66.6					
U		0.134	0.116										0.09	0.08	0.09	0.076	0.04
Ir	10.15	50.22	11.42	6.66	10.42	54.73	6.57	21.04	8.64	0.0057	0.0655	17.02	7.5	14		0.3	0.45
Mo	10.7	17.4	21.9	11.9	15.1	10.6	14.3	37.8	19.9								
TiO2	2.19	1.68	1.79	0.94	0.82	0.61	2.14	1.69	1.18	0.47	0.86	0.93					
Ta	0.249	0.363	0.235	0.161	0.204	0.162	0.157	0.224	0.185	1.15	0.168	0.119	0.24	0.41	0.72	0.3	0.36
Nb													4.3	3.7	5.5	2.2	1.3
CaO	39.3	25.1	34.2	37.8	32.8	41.3	30.7	26.1	31.1	12.9	20.8	15.2					
Sr	207	198	190	168	211	253	165	174	193	41.2	144	88.7	130	84	36	125	28
Ba												129	49	38	16	41	13
V	407	702	834	445	895	191	1370	886	807	548	157	2510	637	180		802	66
Ni	183	32.2	667	406	562	222	1772	4070	687	101		138					
Co	7.01	0.684	38.42	16.45	19.18	8.63	89.4	203.1	30.85	6.71	9.9	8.8					
MgO	5.00	10.60	7.76	6.90	4.13	4.66	8.66	11.80	12.20	14.60	3.96	10.30					
FeO	0.06	0.14	0.70	0.22	0.17	0.29	1.45	3.59	0.64	0.42	2.06	0.44					
Cr	112	446	327	275	161	62.7	320	501	343	1258	185	286					
P																	
Mn	7.67	9.61	44.7	6.46	12	22.9	11.6	26.6	16.7	21.1	175	27.2					
Li																	
Cu																	
K	31.7	47.4	18.4	23.4	11.3		41.3	86	20.4	30.5							
Ga																	
Na	168	864	187	263	197	344	258	2020	1540	641	9199	477					
Rb																	
Pb																	
Zn		42				13.2	18.6	71	22.2		330	561					
Mg#	**0.99**	**0.99**	**0.95**	**0.98**	**0.98**	**0.97**	**0.91**	**0.85**	**0.97**	**0.98**	**0.77**	**0.98**					
Co#	**149**	**6**	**159**														

Table E-2 Published data - Spinel-hibonite CAI

	Ireland et al. (1991)			MacPherson & Davis (1994)								
W												
Zr	92	83	18.9	9.8	25.6	43.8	5-3	10.8	15.8	8.6	3.93	4.04
Hf	1.2	0.72	0.26									
Sc	39	42	27	31.5	39.2	28.3	67.8	34.4	59.1	19.7	118	72.9
Y	17	28	3.2	7.7	11.9	19.8	1.03	2.91	4.44	1.97	1.67	1.96
Gd	4.6	3	0.43	0.98		1.23	1.43	1.88		0.74	2.01	4.55
Tb	0.89	0.61	0.1	0.167		0.54	0.303	0.44	0.2		0.51	0.9
Dy	5.9	4.5	0.65	1.35	1.83	2.44	1.62	4.04	2.9	0.97	3.16	4.95
Ho	0.97	1	0.16	0.29	0.34	0.54		0.25	0.12		0.25	0.41
Er	2.6	4.3	0.46	1.05	1.2	1.57	0.32	0.31	0.63		0.3	0.76
Tm	0.42	0.75	0.29	0.207	0.244	0.362	0.227	1.18	1	0.308	0.742	1.153
Lu	0.14	0.88	0.07	0.17	0.302	0.156		0.106	0.168	0.163		
Nd	14	5	0.67	3.35	4.22	3.29	3.56	15.7	25.7	12.7	22.4	19.6
Sm	4.5	1.9	0.72	0.94	1.12	1.58	1.16	6.24	8.66	3.95	5.56	7.07
Pr	2.7	0.92	0.16	0.82	0.99	0.62	0.6	3.76	6.66	2.75	3.41	4.74
La	6.92			2.13	2.64	1.5	1.6	7.93	12.5	6.02	12.7	10.3
Yb	2.7	5.8	2.6	1.47	1.85	0.99	1.17	5.63	6.41	3.06	1.33	0.99
Ce	19	6	1.3	5.54	7.07	5.14	4.46	22.3	33.7	17.9	30.3	27.9
Eu	0.48	0.65	0.28	0.59	0.359	0.103		0.521	1.54	0.533	0.174	0.058
Th				0.36	0.069	0.5	0.249	0.54	0.7	0.58	1.13	1.08
Al2O3	35.10	28.9	47	62.7	70.0	65.2	41.2	62.8	39.4	66.2	34.0	49.1
U				0.155	0.069	0.148		0.165	0.131	0.071	0.142	0.121
Ir												
Mo												
TiO2	1.7	1.8	2.6	0.60	0.84	1.09	0.61	4.01	4.01	2.56	0.46	0.58
Ta	6.9	2	0.24									
Nb	5.9	8.8	7.5	3.98	4.55	7.03	1.81	6.67	13.5	3.25	2.45	2.4
CaO	23.8	22.6	17.9	1.02	0.74	2.94	6.91	4.12	21.30	1.94	1.68	1.37
Sr	72	37	30	10.2	6.08	8.77	13	26.7	63	22.1	3.65	3.2
Ba	15	0.61	6.3	9.5	5.14	4.9	4.92	2.83	9.1	2.82	2.03	1.92
V	557	852	850	3433	3778	2266	1095	2616	1559	2747	811	1552
Ni												
Co												
MgO	6.3	7.2	5.3	21.5	22.9	23.3	19.8	22.0	17.8	23.1	19.0	23.7
FeO				6.86	2.26	0.91	11.40	2.65	8.28	2.35	25.30	10.70
Cr				971	794	2761	2854	1409	2085	1324	1346	1576
P												
Mn				552	251	52	571	178	705	190	1653	946
Li												
Cu												
K				762	311	112	339	813	1195	485	836	528
Ga												
Na				5105	1794	829	3438	3470	4888	2249	2598	1700
Rb				1.43	0.5	0.74			2.37			2.62
Pb												
Zn												
Mg#				**0.85**	**0.95**	**0.98**	**0.76**	**0.94**	**0.79**	**0.95**	**0.57**	**0.80**
Co#												

References

Abreu, N.M. & Brearley, A.J. (2010): Early Solar System processes recorded in matrices of two highly pristine CR3 carbonaceous chondrites, MET 00426 and QUE 99177; *GCA*, **74**, p. 1146-1171.

Alexander, C.M.O'D., Grossman, J.N., Ebel, D.S. & Ciesla, F.J. (2008): The formation conditions of chondrules and chondrites; *Science*, **320**, p. 1617-1619.

Alexander, R. (2008): From discs to planetesimals: Evolution of gas and dust discs; *New Astron. Rev.*, **52**, p. 60-77.

Amelin, Y., Krot, A.N., Hutcheon, I.D. & Ulyanov, A.A. (2002): Lead isotopic ages of chondrules and Calcium-Aluminium-rich Inclusions; *Science*, **297**, p. 1678-1683.

Amorello, D., Romano, V. & Zingales, R. (2007): The Formal Redox Potential of the Yb(III, II) Couple at 0 °C in 3.22 Molal NaCl Medium; *An. di Chimica*, **94 (3)**, p. 113-122.

Anders, E. (1971): Meteorites and the early solar system; *Ann. Rev. Astron. Astrophys.* **9**, p. 1-34.

Asphaug, E., Jutzi, M. & Moshovitz, N. (2011): Chondrule formation during planet accretion; *EPSL*, **308**, p. 369-379.

Avinash, K., Eliasson, B. & Shukla, P.K. (2006): Dynamics of self-gravitating dust clouds and the formation of planetesimals; *Phys. Letters A*, **353**, p. 105-108.

Baedecker, P.A. & Wasson, J.T. (1975): Element fractionations amongst entstatite chondrites; *GCA*, **39**, p. 735-765.

Becker H., Horan M.F., Walker R.J., Gao S., Lorand J.-P., Rudnick R.L. (2006): Highly siderophile element composition of the Earth's primitive upper mantle: Constraints from new data on peridotite massifs and xenoliths; *GCA*, **70**, p. 4528-4550.

Bédard, J.H. (2005): Partitioning coefficients between olivine and silicate melts; *Lithos,* **83**, p. 394-419.

Berger, A., Burri, T., Alt-Epping, P. & Engi, M. (2008): Tectonically controlled fluid flow and water-assisted melting in the middle crust: An example from the Central Alps; *Lithos*, **102**, p. 598-615.

Berlin, J., Jones, R.H. & Brearley, A.J. (2007): A common origin for FeO-rich silicates in Kakangari and enstatite chondrite chondrules? *70th Annual Meteoritical Society Meeting, abstract volume*, no. 5272.

Berthet, S., Malavergne, V., Righter, K., Corgne, A. & Combes, R. (2006): The evolution of the EH4 chondrite Indarch at high pressure and temperature: the first experimental results; *LPS XXXVII abstract volume,* **2026**.

Bischoff, A., Palme, H. & Spettel, B. (1989): Al-rich chondrules from the Ybbsitz H4-chondrite: evidence for formation by collision and splashing; *EPSL*, **93**, p. 170-180.

Bischoff, A., Palme, H., Ash, R.D., Clayton, R.N., Schultz, L., Herpers, U., Stöffler, D., Grady, M.M., Pillinger, C.T., Spettel, B., Weber, H., Grund, T., Endreß, M. & Weber, D. (1992): Paired Renazzo-type (CR) carbonaceous chondrites from the Sahara; *GC A,* **57**, p. 1587-1603.

Bizarro, M., Baker., J.A. & Haack, H. (2004): Mg isotope evidence for contemporaneous formation of chondrules and refractory inclusions: *Nature*, **431**, p. 275-278.

Bland, P.A., Alard, O., Benedix, G.K., Kearsley, A.T., Menzies, O.N., Watt, L.E. & Rogers, N.W. (2005): Volatile fractionation in the early solar system and chondrule-matrix complementarity; *PNAS*, **102 (39)**, p. 13755–13760.

Blander, M. & Fuchs, L.H. (1975): Calcium-Aluminium-rich inclusions in the Allendé meteorite: evidence for a liquid origin; *GCA*, **39**, p. 1605-1619.

Bockelée-Morvan, D., Gautier, D., Hersant, F., Huré, J.-M. & Robert, F. (2002): Turbulent radial mixing in the solar nebular as the source of crystalline silicates in comets; *The Origin of Stars and Planets: The VLT View*; ESO Astrophysics Symposia, 445-452,

Boley, A.C. & Durisen, R.H. (2008): Gravitational instabilities, chondrule formation and the FU Orionis phenomenon; *Astrophys. J.,* **685**, p. 1193-1209.

Boss, A.P. (2004): Evolution of the solar nebula. VI. Mixing and transport of isotopic heterogeneity; *Astrophys. J.*, **616**, p. 1265-1277.

Boss, A.P. & Durisen, R.H. (2005): Chondrule-forming shock fronts in the solar nebula: A possible unified scenario for planet and chondrite formation; *Astrophys. J.*, **621**, p. L137–L140.

Bouvier, A., Blichert-Toft, J., Moynier, F., Vervoort, J.D. & Albaréde, F. (2007): Pb–Pb dating constraints on the accretion and cooling history of chondrites; *GCA*, **71**, p. 1583–1604.

Bowen, N. L. & Schairer, J.F. (1935): The system, MgO-FeO-SiO2; *Am. J. Sci.*, 29, p. 151-217.

Boynton, W.V. (1975): Fractionation in the solar nebula: Condensation of yttrium and the rare earth elements; *GCA,* **39**, p. 569-584.

Bridges, J.C., Franchi, I.A., Hutchison, R., Sexton, A.S., & Pillinger, C.T. (1998): Correlated mineralogy, chemical compositions, oxygen isotopic compositions and size of chondrules; *EPSL*, **155**, p. 183–196.

Burkhardt, C., Kleine, T., Bourdon, B., Palme, H., Zipfel, J., Friedrich, J.M. & Ebel, D.S. (2008): Hf-W mineral isochron for Ca,Al-rich inclusions: Age of the Solar System and the timing of core formation in planetesimals; *GCA*, **72**, p. 6177-6197.

Campbell, A.J., Humayun, M., Meibom, A., Krot, A.N. & Keil, K. (2001): Origin of zoned metal grains in the QUE94411 chondrite; *GCA*, **65 (1)**, p. 163-180.

Campbell, A.J., Humayun, M. & Weisberg, M.K. (2002): Siderophile element constraints on the formation of metal in the metal-rich chondrites Bencubbin, Weatherford and Gujba; *GCA*, **66 (4)**, p. 647-660.

Campbell, A.J., Simon, S.B., Humayun, M. & Grossman, L. (2003): Chemical evolution of metal in refractory inclusions in CV3 chondrites; *GCA*, **67 (17)**, 3119-3134.

Cassen, P. (1996): Models for the fractionation of moderately volatile elements in solar nebula; *MPS,* **31**, p. 793-806.

Casuso, E. & Beckman, J.E. (2010): Explaining the galactic interstellar dust grain size distribution function; *Astrophys. J.*, **139**, p. 1406-1412.

Chambers, J.E. (2004): Planetary accretion in the inner Solar System; *EPSL*, **223**, p. 241-252.

Chambers, J.E. (2010): Planetesimal formation by turbulent concentration; *Icarus*, **208**, p. 505-517.

Ciesla, F.J. (2009): Two-dimensional transport of solids in viscous protoplanetary disks; *Icarus*, **200 (2)**, 655-671.

Ciesla, F.J. & Charnley S. (2006): The Physics and Chemistry of Nebular Evolution; from *Meteorites and the Early Solar System II*, Eds. D. Lauretta and H. McSween, University of Arizona Press, 209 pp.

Clayton, R.N. (1993): Oxygen isotopes in meteorites; *Annu. Rev. Earth Planet. Sci.*, **21**, p. 115-149.

Clayton, R.N. & Mayeda, T.K. (1985): Oxygen isotopes in chondrules from enstatite chondrites: possible identification of a major nebular reservoirs; *LPS XVI abstract volume*, p. 142–143.

Clayton, R.N. & Mayeda, T.K. (1999): Oxygen isotope studies of carbonaceous chondrites; *GCA*, **63 (13/14)**, p. 2089-2104.

Clayton, R.N., Onuma, N. & Mayeda, T.K. (1976): A classification of meteorites based on oxygen isotopes; *EPSL*, **30**, p. 10-18.

Cohen, B.A., Hewins, R.H. & Alexander, C.M.O'D. (2004): The formation of chondrules by open-system melting of nebular condensates; *GCA*, **68 (7)**, p. 1661-1675.

Connolly, Jr., H.C. & Bizarro, M. (2008): Pb–Pb dating of chondrules from CV chondrites by progressive dissolution; *Chem. Geol.,* **259**, p. 143-151.

Connolly, Jr., H.C. & Hewins, R.H. (1991): The influence of bulk compositions and dynamic melting conditions on olivine chondrule textures; *GCA*, **55**, p. 2943-2950.

Connolly, Jr., H.C., Hewins, R.H., Ash, R.D., Zanda, B., Lofgren, G.E. & Bourot-Denise, M. (1994): Carbon and the formation of reduced chondrules; *Nature,* **371**, 136-139.

Connolly, Jr., H.C., Huss, G.R. & Wasserburg, G.J. (2001): On the formation of Fe-Ni metal in Renazzo-like carbonaceous chondrites; *GCA,* **65 (24)**, p. 4567–4588.

Connolly, Jr., H.C., Huss, G.R., Nagashima, K., Weisberg, M.K., Ash, R.D., Ebel, D.S., Schrader, D.L. & Lauretta, D.S. (2008): Oxygen isotopes and the nature and origins of type-II chondrules in CR2 chondrites; *LPS XXXIX abstract volume,* **1675**.

Cosarinsky, M., Leshin, L.A., MacPherson, G.J., Guan, Y. & Krot, A.N. (2008): Chemical and oxygen isotopic compositions of accretionary rim and matrix olivine in CV chondrites: Constraints on the evolution of nebular dust; *GCA*, **72**, p. 1887-1913.

Cuzzi, J. N., Hogan, R. C., Paque, J. M. & Dobrovolskis, A. R. (2001): Size-selective concentration of chondrules and other small particles in protoplanetary nebula turbulence; *Astrophys. J., 546*, p. 496–508.

Cuzzi, J.N., Davis, S.S. & Dobrovolskis, A.R. (2003): Blowing in the wind. II. Creation and redistribution of refractory inclusions in a turbulent protoplanetary nebula; *Icarus*, **166**, p. 385-402.

Cuzzi, J.N. & Alexander, C.M.O'D. (2006): Chondrule formation in particle-rich nebular regions at least hundreds of kilometres across; *Nature,* **441**, p. 483-485.

Cuzzi, J.N., Hogan, R.C. & Shariff, K. (2008): Towards planetesimals: dense chondrule clumps in the protoplanetary nebula; *Astrophys. J.*, **687**, p. 1432-1447.

Day, K.L. (1976): Further measurements of amorphous silicates; *Astrophys. J.,* **210**, p. 614-617.

Desch, S.J., Ciesla, F.J., Hood, L.L. & Nakamoto, T. (2005): Heating of chondritic material in solar nebula shocks; in *Chondrites and the Protoplanetary Disk (Eds. Krot, Scott & Reipurth)*, ASP conference series, **341**, p. 849-872.

Dulski, P. (2001): Reference Materials for Geochemical Studies:New analytical data by ICP-MS and critical discussion of reference values; *Geostand. Newsletter,* **25 (1)**, p. 87-125.

Easton, A.J. (1985): E-chondrites: Significance of the partition of elements between 'silicate' and 'sulfide'; *Meteoritics,* **20 (1)**, p. 89-101.

Ebel, D.S. & Grossman, L. (2000): Condensation in dust-enriched systems; *GCA*, **64 (2)**, p. 339-366.

Edgeworth, K.E. (1949): *Monthly Notices, Royal Astron. Soc.*, **109**, p. 600-609

Eggins, S.M., Woodhead, J.D., Kinsley, L.P.J., Mortimer, G.E., Sylvester, P., McCulloch, M.T., Hergt, J.M. & Handler, M.R. (1997): A simple method for the precise determination of > 40 trace elements in geological samples by ICPMS using enriched isotope internal standardization; *Chem. Geol.*, **134**, p. 311-326.

Ehlers, K., Grover, T.L., Sisson, T.W., Recca, S.I. & Zervas, D.A. (1992): The effect of oxygen fugacity on the partitioning of nickel and cobalt between olivine, silicate melt, and metal; *GCA,* **56**, p. 3733-3743.

El Goresy, A., Zinner, E., Matsunami, S., Palme, H., Spettel, B., Lin, Y. & Nazarov, M. (2002): Efremovka 101.1: A CAI with ultrarefractory REE patterns and enormous enrichments of Sc, Zr, and Y in Fassaite and Perovskite; *GCA,* **66 (8)**, p. 1459–1491.

Ehmann, W.D. & Rebagay, T.V. (1970): Zirconium and hafnium in meteorites by activation analysis; *GCA,* **34**, p. 649-658.

Engler, A., Varela, M.E., Kurat, G., Ebel, D. & Sylvester, P. (2007): The origin of non-porphyritic pyroxene chondrules in UOCs: Liquid solar nebula condensates? *Icarus*, **192**, p. 248-286.

Evensen, N.M., Hamilton, P.J. & O'Nions, R.K. (1978): Rare-earth abundances in chondritic meteorites; *GCA,* **42**, p. 1199-1212.

Fagan, T.J., Krot, A.N. & Keil, K. (1999): FeO-rich silicates in EH3 and EL3 chondrites: Evidence for variations in redox; *LPS XXX abstract volume*, **1523**.

Fischer-Gödde, M., Becker, H. & Wombacher, F. (2010): Rhodium, gold and other highly siderophile element abundances in chondritic meteorites; *GCA,* **74**, p. 356-379.

Fitzgerald, M.J. (1979): The chemical composition and classification of the Karoonda meteorite; *Meteoritics*, 1**4 (1)**, p. 109-115.

Foley, C.N., Wadhwa, M., Borg, L.E., Janney, P.E., Hines, R. & Grove, T.L. (2005): The early differentiation history of Mars from ^{182}W-^{142}Nd isotope systematics in the SNC meteorites; *GCA,* **68 (18)**, p. 4557-4571.

Gail, H.-P. (2004): Radial mixing in protoplanetary accretion disks: IV. Metamorphosis of the silicate dust complex; *Astr. Astrophys.*, **413**, p. 571-591.

Gannoun, A., Boyet, M., El Goresy, A. & Devouard, B. (2011): REE and actinide microdistribution in Sahara 97072 and ALHA 77295 EH3 chondrites: A combines cosmochemical and petrologic investigation; *GCA*, **75**, p. 3269-3289.

Garbe-Schönberg, C-D. (1993): Simultaneous determination of 37 trace elements in 28 international rock standards by ICP-MS; *Geostandards Newsletter*, **17**, p. 81-93

Geiger, T. & Bischoff, A. (1995): Formation of opaque minerals in CK chondrites; *Planet. Space Sci.,* **43 (3/4)**, p. 485-498.

Genge, M.J. (2000): Chondrule formation by ablation of small planetesimals; *Met. Planet. Sci.*, **35**, p. 1143-1150.

Gooding, J.L. & Keil, K. (1981): Relative abundances of chondrules primary textural types in ordinary chondrites and their bearings on the conditions of chondrule formation; *Meteoritics*, **16 (1)**, p. 17-43.

Govindaraju, K. (1989): Compilation of working values and sample description for 272 geostandards; *Geostandards Newsletter*, **13** (Special Issue), p. 1-113.

Govindaraju, K. (1994): Compilation of working values and sample description for 383 geostandards; *Geost. Newsletter*, **18**, P. 1-158.

Grossman, L. & Ganapathy, R. (1975): Trace elements in the Allendé meteorite: II. Fine-grained, Ca-rich inclusions; *GCA,* **40**, p. 967-977.

Grossman, L. & Wasson, J.T. (1985): The origin and history of metal and sulfide components of chondrules; *GCA*, **49**, p. 925-939.

Grossman, J.N., Rubin, A.E., Rambaldi, E.R., Rajan, R.S. & Wasson, J.T. (1985): Chondrules in the Qingzhen type-3 enstatite chondrite: Possible precursor components and comparison to ordinary chondrite chondrules; *GCA*, **49**, p. 1781-1795.

Herndon, J.M, & Suess, H.E. (1976): Can enstatite meteorites form from a nebula of solar composition; *GCA*, **40**, p. 395-399.

Hevey, P.J. & Sanders, S. (2006): A model for planetesimal meltdown by ^{26}Al and its implications for meteorite parent bodies; *MPS*, **41 (1)**, p. 95-106.

Hewins, R.H. (1997): Chondrules; *Annu. Rev. Earth Planet. Sci.,* **25**, p.61–83.

Hewins, R.H. & Fox, G.E. (2004): Chondrule textures and precursor grain size: an experimental study; *GCA*, **68 (4)**, p. 917-926.

Hewins, R.H. & Herzberg, C.T. (1996): Nebular turbulence, chondrule formation, and the composition of the Earth; *EPSL*, **144**, p. 1-7.

Hezel, D.C. & Palme, H. (2008): Constraints for chondrule formation from Ca-Al distribution in carbonaceous chondrites; *EPSL*, **265**, p. 716-725.

Hezel, D.C. & Palme, H. (2010): The chemical relationship between chondrules and matrix and the chondrule-matrix complementarity; *EPSL*, **294**, p. 85-93.

Hirota, Y., Tamaki, M. & Nakamura, N. (2002): Rare earth element abundances in the CK chondrites including the Kobe meteorite; *Geochem. J.,* **36**, p. 309-322.

Hirschmann, M.M. & Ghiorso, M.S. (1994): Activities of nickel, cobalt, and manganese silicates in magmatic liquids and applications to olivine /liquid and to silicate /metal partitioning; *GCA,* **58 (19)**, p. 4109-4126.

Holzheid, A. (2010): Separation of sulfide melt droplets in sulfur saturated silicate liquids; *Chem. Geol.,* **274**, p. 127-135.

Hutcheon, I.D., Marhas, K.K., Krot, A.N., Goswami, J.N. & Jones, R.H. (2010): ^{26}Al in plagioclase-rich chondrules in carbonaceous chondrites: Evidence of extended duration of chondrule formation; *GCA*, **73**, p. 5080-5099.

Hutchison, R. (2004): Meteorites: A petrologic, chemical and isotopic synthesis; *Cambridge University Press*, pp. 506.

Ireland, T.F., Fahey, A.J. & Zinner, E.K. (1991): Hibonite-bearing microspherules: A new type of refractory inclusions with large isotopic anomalies; *GCA,* **55**, p. 367-379.

Ireland, T.F. & Fegley Jr. B. (2000): The Solar System's Earliest Chemistry: Systematics of Refractory Inclusions; *Int. Geol. Rev.*, **42 (10)**, p. 865-894.

Itoh, S. & Yurimoto, H (2003): Contemporaneous formation of chondrules and refractory inclusions in the early Solar System: *Nature,* **423**, p. 728–731.

Jochum, K.P., Stolz, A.J. & McOrist, G. (2000): Niobium and tantalum in carbonaceous chondrites: Constraints on the solar system and primitive mantle niobium/tantalum, zirconium/niobium, and niobium/uranium ratios; *MPS*, **35**, p. 229-235.

Jones, R.H. (1990): Petrology and mineralogy of Type II, FeO-rich chondrules in Semarkona (LL3.0): Origin by closed-system fractional crystallization, with evidence for supercooling; *GCA*, **54**, p. 1785-1802.

Jones, R.H. (1994): Petrology of FeO-poor, porphyritic pyroxene chondrules in the Semarkona chondrite; *GCA*, **58 (23)**, p. 5325-5340.

Jones, R.H. & Lofgren, G.E. (1993): A comparison of FeO-rich, porphyritic olivine chondrules in unequilibrated chondrites and experimental analogues; *Meteoritics*, **28**, p. 213-221.

Joung, M.K.R., Low, M.M.M. & Ebel, D.S. (2004): Chondrule formation and planetary disk heating by current sheets in non-ideal magnetohydrodynamic turbulence; *Astrophys. J.*, **606**, p. 532-541.

Kallemeyn, G.W. & Wasson, J.T. (1982): The compositional classification of chondrites: III. Ungrouped carbonaceous chondrites; *GCA*, **46**, p. 2217-2228.

Kallemeyn, G.W., Rubin, A.E. & Wasson, J.T. (1990): The compositional classification of chondrites: V. The Karoonda (CK) group of carbonaceous chondrites; *GCA*, **55**, p. 881-892.

Kallemeyn, G.W., Rubin, A.E. & Wasson, J.T. (1994): The compositional classification of chondrites: VI. The CR carbonaceous chondrite group; *GCA*, **58 (13)**, p. 2873-2888.

Kogiso T., Suzuki Katsuhiko, Suzuki T., Shinotsuka K., Uesugi K., Takeuchi A., Suzuki Y. (2008): Detecting micrometer-scale platinum-group minerals in mantle peridotite with microbeam synchrotron radiation X-ray fluorescence analysis; *Geochem. Geophys. Geosyst.,* **9 (3)**

Kennedy, A.K., Lofgren, G.E. & Wasserburg, G.J. (1993): An experimental study of trace element partitioning between olivine, orthopyroxene and melt in chondrules: equilibrium values and kinetic effects; *EPSL,* **115**, p. 177-195.

Kim, S-H., Martin, P.G. & Hendry, P.D. (1994): The size distribution of interstellar dust particles as determined from extinction; *Astrophys. J.*, **422**, p. 164-175.

King, H.E., Stimpf, M., Deymier, P., Drake, M.J., Catlow, C.R.A., Putnis, A. & de Leeuw, N.H. (2010): Computer simulations of water interactions with low-coordinated forsterite surfacesites: Implications for the origin of water in the inner solar system; *EPSL*, **300**, p. 11-18.

Kita, N.T., Nagahara, H., Togashi, S. & Morishita, Y. (2000): A short duration of chondrule formation in the solar nebula: Evidence from ^{26}Al in Semarkona ferromagnesian chondrules; *GCA*, **64 (22)**, p. 3913–3922.

Kleine, T., Münker, C., Mezger, K. & Palme, H. (2002): Rapid accretion and early core formation on asteroids and the terrestrial planets from Hf–W chronometry; *Nature*, **418**, p. 952-955.

Kleine, T., Mezger, K., Münker, C., Palme, H & Bischoff, A. (2004): 182Hf-182W isotope systematics of chondrites, eucrites, and Martian meteorites: Chronology of core formation and early mantle differentiation in Vesta and Mars

Kleine, T., Mezger, K., Palme, H., Scherer, E. & Münker, C. (2005): Early core formation in asteroids and late accretion of chondrite parent bodies: Evidence from ^{182}Hf-^{182}W in CAIs, metal-rich chondrites, and iron meteorites; *GCA,* **69 (24)**, p. 5805-5818.

Knab, H.-J. (1981): The distribution of trace elements in carbonaceous chondrites; *GCA,* **45**, p. 1563-1572.

Kominani, J. & Shigeru, I. (2004): Formation of terrestrial planets in a dissipating gas disk with Jupiter and Saturn; *Icarus*, **167**, p. 231-243.

Kong, P. & Ebihara, M. (1997): The origin and nebular history of the metal phase of ordinary chondrites; *GCA,* **61 (11)**, p. 2317-2329.

Kong, P. & Palme, H. (1999): Compositional and genetic relationship between chondrules, chondrule rims, metal, and matrix in the Renazzo chondrite; *GCA*, **63 (21)**, p. 3673-3682.

Kong, P. & Ebihara, M. & Palme, H. (1999): Distribution of siderophile elements in CR chondrites: Evidence for evaporation and recondensation during chondrule formation; *GCA*, **63 (17)**, p. 2637–2652.

Kornacki, A.S. & Fegley, Jr. B. (1986): The abundance and relative volatility of refractory trace elements in Allende Ca, Al-rich inclusions: implications for chemical and physical processes in the solar nebula; *EPSL,* **79**, p. 217-234.

Korotev R.L. (1996): A Self-Consistent compilation of elemental concentration data for 93 geochemical reference samples; *Geostand. Newsletter,* **20 (2),** p. 217-245

Krot, A.N., Meibom, A., Russell, S.S., Alexander, C.M.O'D., Jeffries, T.E. & Keil, K. (2001): A new astrophysical setting for chondrule formation; *Science*, **291**, p. 1776-1779.

Krot, A.N., Hutcheon, I.D. & Keil, K. (2002): Plagioclase-rich chondrules in the reduced CV chondrites: Evidence for complex formation history and genetic links between calcium-aluminium-rich inclusions and ferromagnesian chondrules; *MPS,* **37**, p. 155-182.

Krot, A.N., Yurimoto, H., Hutcheon, I.D. & MacPherson, G.J. (2005a): Chronology of the early Solar System from chondrule bearing calcium-aluminium-rich inclusions; *Nature*, 434, p. 998-1001.

Krot, A.N., Amelin, Y., Cassen, P. & Meibom, A. (2005b): Young chondrules in CB chondrites from a giant impact in the early Solar System; *Nature*, **436**, p. 989-992.

Krot, A.N., Libourel, G. & Chaussidon, M. (2006a): Oxygen isotope compositions of chondrules in CR chondrites; *GCA*, **70**, p. 767-779.

Krot, A.N., Yurimoto, H., McKeegan, K.D. and coworkers (2006b): Oxygen isotopic compositions of chondrules: Implications for evolution of oxygen isotopic reservoirs in the inner solar nebula; *Chem. Erde*, 249–276.

Krot, A.N., Ivanova, M.A. & Ulyanov, A.A. (2007): Chondrules in the CB/CH-like carbonaceous chondrite Isheyevo: Evidence for various chondrule-forming mechanisms and multiple chondrule generations; *Chemie der Erde,* **67**, p. 283-300.

Kunihiro, T., Rubin, A.E., McKeegan, K.D. & Wasson, J.T. (2004): Initial $^{26}Al/^{27}Al$ in carbonaceous-chondrite chondrules: Too little ^{26}Al to melt asteroids; *GCA*, **68 (13)**, p. 2947–2957.

Kurahashi, E., Kita, N.T., Nagahara, H. & Morishita, Y. (2008): ^{26}Al–^{26}Mg systematics of chondrules in a primitive CO chondrite; *GCA*, **72**, p. 3865-3882.

Lee, D.-C. & Halliday, A.N. (2000): Accretion of Primitive Planetesimals: Hf-W Isotopic Evidence from Enstatite Chondrites; *Science*, **288**, p. 1629-1631.

Lee, T., Papanastassiou, D. A. & Wasserburg, G. J.: The Presence of ^{26}Al in the Early Solar Nebula; *Bullet. Am. Astron. Soc.*, **8**, p.457

Leitch, C.A., Smith, J.V., Smith, M.R. & Schmitt, R.A. (1982): Microscopic properties and the bulk chemistry of individual chondrules of the Indarch enstatite chondrite; *Meteoritics*, **17**, p. 243.

Lesher, C.M. & Arndt, N.T. (1995): REE and Nd isotope geochemistry, petrogenesis and volcanic evolution of contaminated komatiites at Kambalda, Western Australia; *Lithos,* **34**, p. 127-157.

Libourel, G., Krot, A.N. & Tissandier, L. (2006): Role of gas-melt interaction during chondrule formation; *EPSL*, **251**, p. 232-240.

Lodders, K. (2003): Solar System abundances and condensation temperatures of the elements; *Astrophys. J.*, 591 (2), p. 1220-1247.

Lodders, K. & Amari, S. (2005): Presolar grains from meteorites: Remnants from the early times of the Solar System; *Chemie der Erde*, 65, p. 63-166.

Lodders, K. & Fegley Jr., B. (1993): Lanthanide and actinide chemistry at high C/O ratios in the solar nebula; *EPSL,* **117**, p. 125-145.

Lofgren, G. (1989): Dynamic crystallisation of chondrules melts of porphyritic olivine composition: Textures experimental and natural; *GCA*, **53**, p. 461-470.

Lofgren, G. & Russell, W.J. (1986): Dynamic crystallisation of chondrule melts of porphyritic and radial pyroxene composition; *GCA*, **50**, p. 1715-1726.

Luecke, W., Muszynski, A. & Berner, Z. (2006): Trace element partitioning in the Morasko meteorite from Poznan, Poland; *Chem. Erde,* **66 (4)**, p. 315-318.

MacPherson, G.J. & Davis, A.M. (1994): Refractory inclusions in the prototypical CM chondrite, Mighei; *GCA,* **58 (24)**, 5599-5625.

Mao, X.-Y., Ward, B.J., Grossman, L. & MacPherson, G.J. (1990): Chemical compositions of refractory inclusions from the Vigarano and Leoville carbonaceous chondrites; *GCA,* **54**, p. 2121-2132.

Markowski, A., Leya, I., Quitté, G., Ammon, K., Halliday, A.N. & Wieler, R. (2006): Correlated helium-3 and W isotopes in iron meteorites: quantitative cosmogenic corrections and planetesimal formation times; *EPSL*, **250**, p. 104-115.

Markowski, A., Quitté, G., Kleine, T., Halliday, A.N., Bizarro, M. & Irving, A.J. (2007): Hafnium-tungsten chronometry of angrites and the earliest evolution of planetary objects; *EPSL*, **262**, p. 214-229.

Mason, B. & Wiik, H.B. (1962): Descriptions of Two Meteorites: Karoonda and Erakot; *American Museum Novitates,* **2115**.

Matza, S.D. & Lipschutz, M.E. (1977): Volatile/mobile trace elements in Karoonda (C4) chondrite; *GCA*, **41**, p. 1398-1401.

McCoy, T.J., Carlson, W.D., Nittler, L.R., Stroud, R.M., Bogard, D.D. & Garrison, D.H. (2006): Graves Nunataks 95209: A snapshot of metal segregation and core formation; *GCA,* **70**, p. 516–531.

McSween, Jr., H.Y. (1977): Chemical and petrographic constraints on the origins of chondrules and inclusions in carbonaceous chondrites; *GCA*, **41**, p. 1843-1860.

Meisel T., Moser J. (2004): Platinum-group element and Rhenium concentrations in low abundance reference materials; *Geostand. Geoanalyt. Res.,* **28 (2)**, p.233-250.

Meixner, M., Ueta, T., Borrowsky, M. & Speck, A. (2002): Two subclasses of proto-planetary nebulæ: Model calculations; *Astrophys. J.*, **571**, p. 936-946.

Miura, H., Tanaka, K.K., Yamamoto, T., Nakamoto, T., Yamada, J., Tsukamoto, K. & Nozawa, J. (2010): Formation of cosmic crystals in highly supersaturated silicate vapor produced by planetesimal bow shocks; *Astrophys. J.,* **719**, p. 642-654.

Morgan. J.W. & Lovering, J.F. (1968): Uranium and Thorium abundances in chondrite meteorites; *Talanta*, **15**, p. 1079-1095.

Moynier, F., Bouvier, A., Blichert-Toft, J., Telouk, P., Gasperini, D. & Alberède, F. (2006): Europium isotopic variations in Allende CAIs and the nature of mass-dependent fractionation in the solar nebula; *GCA*, **70**, p. 4287-4294.

Nahagara, H., Kushiro, I. & Mysen, B.O. (1994): Evaporation of olivine: Lower pressure phase relations of the olivine system and its implications for the origins of chondritic components in the solar nebula; *GCA*, **58 (8)**, p. 1951-1963.

Newsom, H.E. (1995): Composition of the Solar System, Planets, Meteorites, and Major Terrestrial Reservoirs; *Global Earth Physics: A Handbook of Physical Constants,* p. 159-189.

Nichiporuk, W. & Bingham, E. (1970): Vanadium and copper in chondrites; *Meteoritics,* **5 (3)**, p. 115-130.

O'Brian, D.P., Morbidelli, A. & Levison, H.F. (2006): Terrestrial planet formation with strong dynamical friction; *Icarus,* **184**, p. 39-58.

O'Neill, H.S.T. & Palme, H. (1998): Composition of the silicate Earth: Implications for accretion and core formation; in *The Earth's Mantle: Composition, Structure and Evolution (Ed. Ian Jackson)*, Cambridge University Press, pp. 567.

Pack, A., Russell, S.S., Shelley, M.G. & Van Zuilen, M. (2007): Geo- and cosmochemistry of the twin elements yttrium and holmium; *GCA,* **71**, p. 4592-4608.

Palme, H. & Rammensee, W. (1981): The cosmic abundance of molybdenum; *EPSL,* **55**, p. 356-362.

Pasek, M.A., Milsom, J.A., Ciesla, F.J., Lauretta, D.S., Sharp, C.M. & Lunine, J.I. (2005): Sulfur chemistry with time-varying oxygen abundance during Solar System formation; *Icarus,* **175**, p. 1-14.

Patchett, P.J., Vervoort, J.D., Söderlund, U. & Salter, V.J.M. (2004): Lu–Hf and Sm–Nd isotopic systematics in chondrites and their constraints on the Lu–Hf properties of the Earth; *EPSL,* **222**, p. 29-41.

Pei, Y.C. (1992): Interstellar dust from the Milky Way to the Magellanic Clouds; *Astrophys. J.*, **395**, p. 130-139.

Petitat, M., Kleine, T., Touboul, M., Bourdon, B. & Wieler, R. (2008): Hf-W chronometry of aubrites and the evolution of the planetary bodies; *LPS XXXIX abstract volume*, **2164**.

Planner, H.N. (1983): Phase separation in a chondrule fragment from the Piancaldoli (LL3) chondrite; in *Chondrules and their Origins (Ed. E.A. King)*, The Lunar and Planetary Institute, pp. 377.

Plessen H.-G., Erzinger J. (1998): Determination of the platinum-group elements and gold in twenty rock reference materials by inductively coupled plasma-mass spectrometry (ICP-MS) after pre-concentration by nickel sulfide fire assay; *Geostand. Newsletter*, **22 (2)**, p. 187-194

Puchtel I.S., Humayun M., Walker R.J. (2007): Os-Pb-Nd isotope and highly siderophile and lithophile trace element systematics of komatiitic rocks from the Volotsk suite, SE Baltic Shield; *Precamb. Res.*, **158**, p.119-137.

Puchtel I.S., Walker R.J., James O.B., Kring D.A. (2008): Osmium isotope and highly siderophile element systematics of lunar impact melt breccias: Implications for the late accretion history of the Moon and Earth; *GCA*, **72**, p. 3022-3042

Rambaldi, E.R. & Cendales, M. (1980): Siderophile element fractionation in enstatite chondrites; *EPSL,* **48**, p. 325-334.

Raymond, S.N., O'Brian, D.P., Morbidelli, A. & Kaib, N.A. (2009): Building the terrestrial planets: Constrained accretion in the inner Solar System; *Icarus*, **203**, 644-662.

Rietmeijer, F.J.M. (2002): The Earliest Chemical Dust Evolution in the Solar Nebula; *Chem. Erde,* **62**, 1-45.

Righter, K. & Neff, K.E. (2007): Temperature and oxygen fugacity constraints on CK and R chondrites and implications for water and oxidation in the early solar system; *Polar Science I*, p. 25-44.

Righter, K., Pando, K.M., Danielson, L. & Lee, C.-T. (2010): Partitioning of Mo, P and other siderophile elements (Cu, Ga, Sn, Ni, Co, Cr, Mn, V, and W) between metal and silicate melt as a function of temperature and silicate melt composition; *EPSL*, **291**, p. 1-9.

Rocholl, A. & Jochum, K.P. (1993): Th, U and other trace elements in carbonaceous chondrites: Implications for the terrestrial and solar-system Th/U ratios; *EPSL,* **117**, p. 265-278.

Rollinson, H. (1993): Using geochemical data: Evaluation, presentation, interpretation; *Prentice Hall*, pp. 352.

Rubin, A.E. (1984): Coarse-grained chondrules rim in type 3 chondrites; *GCA*, **48**, p. 1779-1789.

Rubin, A.E. (2000): Petrologic, geochemical and experimental constraints on models of chondrule formation; *Earth-Sci. Rev.*, **50**, p. 3-27.

Rubin, A.E., Scott, E.R.D. & Keil, K. (1997): Shock metamorphism in enstatite chondrites; *GCA*, **61 (4)**, p. 847-858.

Rubin, A.E., Wasson, J.T., Clayton, R.N. & Mayeda, T.K. (1990): Oxygen isotopes in chondrules and coarse-grained chondrule rims from the Allendé meteorite; *EPSL*, **96**, p. 247-255.

Rudraswami, N.G., Goswami, J.N., Chattopadhyay, B., Sengupta, S.K. & Thapliyal, A.P. (2008): ^{26}Al records in chondrules from unequilibrated ordinary chondrules: II. Duration of chondrule formation and parent body thermal metamorphism; *EPSL*, **274**, p. 93-102.

Rudraswami, N.G., Ushikubo, T., Nakashima, D. & Kita, N.T. (2011): Oxygen isotope systematics of chondrules in the Allende CV3 chondrite: High precision ion microprobe studies; *GCA*, **75**, P. 7596-7611.

Rüpke, L.H., Morgan, J.P., Hort, M. & Connolly, J.A.D. (2004): Serpentine and the subduction zone water cycle; *EPSL*, **223**, p. 17-34.

Rushmer, T., Petford, N., Humayun, M. & Campbell, A.J. (2005): Fe-liquid segregation in deforming planetesimals: Coupling Core-Forming compositions with transport phenomena; *EPSL,* **239**, p. 185–202.

Ruzmaikina, T.V. & Ip, W.H. (1994): Chondrule formation in radiative shock; *LPS XXV abstract volume*, p. 1173-1174.

Schrader, D.L., Connolly Jr., H.C. & Lauretta, D.S. (2008): Opaque phases in type-II chondrules from CR2 chondrites: Implications for CR parent body formation; *GCA,* **72**, p. 6124–6140.

Sears, D.W.G., Lu, J., Benoit, P.H., DeHart, J.M., Lofgren, G.E. (1992): A compositional classification scheme for meteoritic chondrules; *Nature*, **357**, pp. 207–211

Seitz, H.-M., Brey, G.P., Zipfel, J., Ott, U., Weyer, S., Durali, S. & Weinbruch, S. (2007): Lithium isotope composition of ordinary and carbonaceous chondrites, and differentiated planetary bodies: Bulk solar system and solar reservoirs; *EPSL,* **260**, p. 582-596.

Shu, F.H., Shang, H., Gounelle, M., Glassgold, A.E. & Lee, T. (2001): The origin of chondrules and refractory inclusions in chondritic meteorites; *Astrophys. J.,* **548**, p. 1029-1050.

Shukolyukov, A. & Lugmair, G.W. (2004): Manganese-chromium isotope systematics of enstatite meteorites; *GCA,* **68 (13)**, p. 2875-2888.

Scott, E.R.D. (2006): Meteoritical and dynamical constraints on the growth mechanisms and formation times of asteroids and Jupiter; *Icarus*, **185**, p. 72-82.

Scott, E.R.D. & Krot, A.N. (2007): Chondrites and their components; in *The Treatise on Geochemistry,* Holland & Turekian (Eds.), Chpt. 1.07, 72 pp.

Scott, E.R.D. & Taylor, G.J. (1985): Petrology of types 4-6 Carbonaceous Chondrites; *J. Geophys. Res.,* **90**, p. C699-C709

Shu, F.H., Shang, H. & Lee, T. (1996): Toward an astrophysical theory of chondrites; *Science,* **271 (5255)**, p. 1545-1522.

Shu, F.H., Shang, H., Gounelle, M., Glassgold, A.E. & Lee, T. (2001): The origin of chondrules and refractory inclusions in chondritic meteorites; *Astrophys. J.*, **548**, p. 1029-1050.

Smith D.B.: USGS Certificate of Analysis Icelandic Basalt, BIR-1: http://crustal.usgs.gov/geochemical_reference_standards/icelandic.html

Stewart, A.J., Van Westrenen, W., Schmidt, M.W. & Günther, D. (2009): Minor element partitioning between fcc Fe metal and Fe–S liquid at high pressure: The role of crystal lattice strain; *EPSL,* **284**, p. 302-309.

Stöffler, D., Keil, K. & Scott, E.R.D. (1991): Shock metamorphism of ordinary chondrites; *GCA*, **55**, p. 3845-3867.

Sylvester, P.J., Simon S.B. & Grossman, L. (1993): Refractory inclusions from the Leoville, Efremovka, and Vigarano C3V chondrites: Major element differences between Types A and B, and extraordinary refractory siderophile element compositions; *GCA,* **57**, p. 3763-3784.

Takafuji, N., Hirose, K., Ono, S., Xu, F., Mitome, M. & Bando, Y. (2004): Segregation of core melts by permeable flow in the lower mantle; *EPSL*, **224**, p. 249– 257.

Takahashi, H., Gros, J., Higuchi, H., Morgan, J.W. & Anders, E. (1978): Volatile elements in chondrites: metamorphism or nebular fractionation?; *GCA,* **42**, p. 1959-1969.

Tizard, J., Lyon, I. & Henkel, T. (2005): The gentle separation of presolar SiC grains from meteorites; *Met. Plan. Sci.*, **40 (3)**, 335-342.

Tolstikhin, I.N. & Kramers, J.D. (2008): The Evolution of Matter: From the Big Bang to the Present Day; *Cambridge University Press*, 522 pp.

Toppani, A., Libourel, G., Robert, F. & Ghanbaja, J. (2006): Laboratory condensation of refractory dust in protosolar and circumstellar conditions; *GCA*, **70**, p. 5035-5060.

Touboul, M., Kleine, T. & Bourdon, B. (2008): Hf-W systematics of cumulate eucrites and the chronology of the eucrite parent body; *LPS XXXIX abstract volume,* **2336**.

Tsuchiyama, A., Nagahara, H. & Kushiro, I. (1980): Experimental reproduction of textures of chondrules; *EPSL*, **48**, p. 155-165.

Tsuchiyama, A., Osada, Y., Nakano, T. & Uesugi, K. (2004): Experimental reproduction of classic barred olivine chondrules: Open-system behavior of chondrule formation; *GCA*, **68 (3)**, p. 653-672.

Van Boekel, R., Min, M., Leinert, C. and coworkers (2004): The building blocks of planets within the 'terrestrial' region of protoplanetary disks; *Nature,* **432**, p. 479-482.

Van Schmus, W.R. & Wood, J.A. (1967): A chemical-petrologic classification for the chondritic meteorites; *GCA*, **31**, p. 747-765.

Villeneuve, J., Chaussidon, M. & Libourel, G. (2011): Magnesium isotopes constraints on the origin of Mg-rich olivines from the Allende chondrite: Nebular versus planetary?; *EPSL*, **301**, p. 107-116.

Wasson, J.T. & Rubin, A.E. (2003): Ubiquitous low-FeO relict grains in Type II chondrules and limited overgrowths on phenocrysts following the final melting event; *GCA*, **67 (12)**, p. 2239-2250.

Wasson, J.T. & Rubin, A.E. (2010): Metal in CR chondrites; *GCA*, **74**, p. 2212-2230.

Waters, L.B.F.M., Molster, F.J., de Jong, T. and others (1996): Mineralogy of oxygen-rich dust shells; *Astron. Astrophys.* **315**, p. L361-L364.

Waters, L.B.F.M., Beintema, D.A., Zijlstra, A.A. and other (1998): Crystalline silicates in Planetary Nebulae with [WC] central stars; *Astron. Astrophys. Letters,* **331**, L61.

Weber, D., Zinner, E. & Bischoff, A. (1995): Trace element abundances and calcium, magnesium, and titanium isotopic composition of grossite containing inclusions from the carbonaceous chondrite Acfer 182; *GCA,* **59 (4)**, p. 803-823.

Weisberg, M.K., Prinz, M. & Fogel, R.A. (1994): The evolution of enstatite and chondrules in unequilibrated enstatite chondrites: Evidence from iron-rich pyroxene; *Meteoritics*, **29**, p. 362-373.

Weisberg, M.K., Prinz, M., Clayton, R.N. & Mayeda, T.K. (1995): The CR (Renazzo-type) carbonaceous chondrite group and its implications; *GCA,* **57**, p. 1567-1586.

Weisberg, M.K., Prinz, M., Humayun, M. & Campbell, A.J. (2000): Origin of metal in the CB (Bencubbinite) chondrites; *LPS XXXI abstract volume*, **1466**.

Weisberg, M.K., Ebel, D.S., Connolly, Jr., H.C., Kita, N.T. & Ushikubo, T. (2011): Petrology and oxygen isotope compositions of chondrules in E3 chondrites; *GCA*, p. **75**, p. 6556-6569.

Whattam, S.A. & Hewins, R.H. (2009): Granoblastic olivine aggregates as precursors of Type I chondrules: an experimental test; *GCA,* **73**, p. 5460-5482.

Whitby, J.A., Gilmour, J.D., Turner, G., Prinz, M. & Ash, R.D. (2002): Iodine-xenon dating of chondrules from the Qingzhen and Kota Kota enstatite chondrites; *GCA*, **66 (2)**, p. 347-359.

White, W.M. (2007): Stable isotope geochemistry; in *Geochemistry* (http://www.imwa.info/white-geochemistry.html).

Wlotzka, F. (1993): A weathering scale for ordinary chondrites; *Meteoritics*, **28 (3)**, p. 460-460.

Wood, J.A. (1984): On the formation of meteoritic chondrules by aerodynamic drag heating in the solar nebula; *EPSL*, **70**, p. 11-26.

Wood, J.A. (1998): Meteoritic evidence for the infall of large instertellar dust aggregates during the formation of the Solar System; *Astrophys. J.*, **503**, p. L101-104.

Wood, J.A. (2004): Formation of chondritic refractory inclusions: the astrophysical setting; *GCA*, **68 (19)**, p. 4007-4021.

Wurm, G. & Krauss, O. (2006): Concentration and sorting of chondrules and CAIs in the late solar nebula; *Icarus*, **180**, p. 487-495.

Yates, A.M., Tackett, S.L. & Moore, C.B. (1968); Chromium and manganese in chondrites; *Chem. Geol.,* **3**, p. 313-322.

Yang Jing-sui, Jiang S.Y., Brügmann G. (2001): Precise determination of the platinum-group elements and Os isotopic ratios in low-level rock samples; *Acta Petrol. Sinicia,* **17 (2)**, p. 325-331

Yin, Q., Jacobsen, S.B., Yamashita, K., Blichert-Toft, J., Télouk, P. & Albarède, F. (2002): A short timescale for planet formation from Hf-W chronometry of meteorites; *Nature,* **418**, p. 949-951.

Yin *et al.* (2007)

Yoshino, T., Walter, M.J. & Tomoo, K. (2003): Core formation in planetesimals triggered by permeable flow; *Nature,* **422**, p. 154-157.

Yu, Y. & Hewins, R.H. (1998): Transient heating and chondrule formation: Evidence from sodium loss in flash heating simulation experiments; *GCA*, **62 (1)**, p. 159-172.

Yurimoto, H. & Wasson, J.T. (2002): Extremely rapid cooling of a carbonaceous-chondrite chondrule containing very ^{16}O-rich olivine and a ^{26}Mg-excess; *GCA*, **66 (24)**, p. 4355-4363.

Zanda, B. (2004): Chondrules; *EPSL*, **224**, p. 1-17.

Zinner, E. (2007): Presolar Grains; in *Treatise On Geochemistry*, Holland & Turekian (Eds.), Chpt. 1.02, 33 pp.

Zolensky, M., Barrett, R. & Browning, L. (1993): Mineralogy and composition of matrix and chondrule rims in carbonaceous chondrites; *GCA,* **57**, p. 3123-3148.

Curriculum Vitæ

(not available for online publication)